Signature of the 2005 Flood Event in the Sediments of Lake Brienz: Implications for Flood Reconstruction

Master's Thesis

Faculty of Science, University of Bern

presented by

Danae Motta

Oeschger Centre for Climate Change Research OCCR

2016

Supervisor:

Prof. Flavio Anselmetti

Institute of Geology and Oeschger Centre for Climate Change Research

Abstract

In August 2005, an extreme precipitation event lead to episodes of erosion, flooding, landslides and debris flows over Switzerland. Strong rainfall initiated on the 20th of August, peaking on August 22 and finally decreasing on the 23rd of August. Between 20-23rd of August, more than 300 mm of rain fell in some regions. Lake Brienz (Bernese Oberland) is considered to be the one of the most representative examples of the destructive power of the event. In the night between the 22nd and 23rd of August, two debris flows from two mountain torrents (Trachtbach and Glyssibach) hit the villages of Brienz and Schwanden bei Brienz, damaging and partly destroying the area and causing the death of two inhabitants. During the event, flooding was also observed for the two main tributaries of the lake, Lütschine and Aare, with discharges increasing by an order of magnitude of 3-4 compared to normal levels.

The present study focuses on a sedimentological and hydrological analysis of the 2005 flood event in Lake Brienz. The 2005 layer was identified in the sediment record and the contribution of the different inflows during the event was assessed based on sedimentary differences within the layers and the geochemical composition of the sediments. Geochemical analysis provided insights on the two main controlling factors of the sediments, such as lithology and grain size. The lithological signal allowed to differentiate the contribution of Aare and Lütschine inflows, which present a different catchment geology and lithology. Cores presenting a Lütschine signal show a carbonate and siliciclastic composition, while cores reflecting the Aare signal mainly present a siliciclastic composition. Calcium was therefore used as proxy for the distinction of Aare and Lütschine input. Grain size and carbon content analysis were also applied to better differentiate the different riverine contributions, as well as to identify the two debris flows within the sediment record. Trachtbach and Glyssibach presented a higher carbonate content in respect to the two major inflows due to sedimentary composition of the two catchments, and their related debris flows were identified in two cores. The extent of the different riverine contributions during the flood was assessed, however missing layers in the depocentre precluded a complete reconstruction of the extent of the turbidic plumes deriving from the event. Missing layers have been interpreted to be a result of erosion or unsuccessful core recovery due to very coarse and thick material accumulated in the centre of the lake. Discharge and precipitation time series were also analysed in order to reconstruct the succession of events during the 2005 flood. Finally, an estimation of the volume of sediments transported and accumulated in the lake basin was presented for all the studied inflows. It was estimated that around 1 Mio m^3 of material deposited during the event.

Overall, Lake Brienz provided valuable insights on sedimentary processes characterizing the flood of August 2005 in the area, allowing to extend the flood record in the Holocene and to better interpret climatic conditions of floods triggered by extreme precipitation events.

Table of Contents

List of Figures

Appendix

List of Tables

Annex

Acknowledgements

I have the feeling that this project would have not came to an end without the help and support of many people. First, I would love to thank Lea, because without her I simply don't know where I would be right now. Steph, your commitment to everything you do (as well as your BI) is and will always be an inspiration for me. To my incredible roommate Mandy, thank you for always being there for me. To all my friends at home and around Switzerland, thank you for your support (and for the holidays pictures posted throughout the whole summer on every possible online platform). There is no need to explain why I should be thankful to my family: grazie di esserci, semplicemente. I would also like to thank Moritzeli for helping me enjoy the summer despite the work, and for the refreshing jumps in the Aare.

I am further indebted to Prof. Dr. Martin Grosjean, who gave me the incredible opportunity to work at the Paleolimnology labs and therefore to get to know all the amazing people who work there every day. Thus, I would love to thank from the bottom of my heart all the Paleolimn guys: Tobi, Ivan and Christoph D. To Christoph B., thank you so much for your everyday support…and for your driving skills around Brienz during a very busy and stressful day. To Daniela Fischer, thank you for your kindness and patience towards my chaotic knowledge of the labs. Another powerful woman I would love to thank is Julijana Krbanjevic, for her constant support throughout many (many) carbon content measurements. From the Geology Institute, I would also thank Hendrik Vogel, Marina Morlock and Valentin Nigg, for always taking the time to help me and to answer all my questions.

I am also indebted with EAWAG, and especially with Nathalie Dubois, for giving me the opportunity to work with one of their boats and to enjoy the company of Wisi and Michael while coring.

Last but not least, I would love to thank my supervisor, Prof. Flavio Anselmetti, for his support and endless positivity throughout this entire past year, and for giving me the opportunity to learn so much about something I care, such as natural hazards in Switzerland.

1 Introduction

1.1 Research Motivation

Flood events represent one of the most common and disruptive natural hazards, leading to extensive and costly damage and therefore representing a major threat for human lives, infrastructure, economy and natural ecosystems (Münich, 2014; Barredo, 2007; IPCC, 2012). In the last few decades, Europe has been struck by several major floods. An example of such catastrophic events is the massive flooding in the catchments of Danube and Elbe in August 2002. This event caused 38 casualties and more than 18 billion Euros worth of damage. During this episode, Germany alone registered a financial damage amounting to 11,6 billion Euros. In 2007, extreme precipitation in Great Britain lead to several flood events and lead to 14 fatalities and to a financial damage of about 5,4 billion Euros (Hilker, Badoux, & Hegg, 2009).

Mountainous regions, specifically, are one of the most sensitive ecosystems to such events. Atmospheric patterns such as temperature and precipitation, as well as specific micro-climates and geomorphological characteristics of the area, highly influence the initiation of floods in Alpine regions (Weingartner et al., 2003; Viviroli & Weingartner, 2004). Because of their high elevation, mountainous areas are characterized by higher rainfall compared to lowlands (Viviroli et al., 2010). However, vegetation cover, topographic relief, soil type and runoff characteristics of the area strongly determine a rapid or slow conversion of precipitation into runoff (Weingartner et al., 2003; Viviroli & Weingartner, 2004; Viviroli et al., 2010). For this reason, a change in atmospheric variables will largely influence hydrological processes, especially in sensitive regions such as the Alps. As projected from the IPCC, temperature and precipitation patterns will be subjected to seasonal and regional changes (IPCC, 2012), which will in turn affect seasonal runoff and discharge. Therefore, there is a need of improve the understanding of processes related to the initiation and development of flood events, especially in complex and important regions such as mountains. It is thus important to study past events in order to have a more comprehensive understanding about triggers, magnitudes and frequency of floods in the last hundreds (or thousands) of years. Lake sediments provide valuable, continuous, long-term and highly-resolved records of processes influencing the area surrounding the lake throughout time (Schillereff et al., 2014). Flood events can be identified in the sediment records based on different depositional processes and other specific characteristics, such as thickness, geochemistry and lithology (Gilli et al., 2003).

In this project, lake sediments will be used to study a specific flood event. In August 2005, a particular low-pressure system triggered a large-scale heavy rainfall over Switzerland, Southern Germany and partly Eastern Europe. Central Switzerland, especially on the northern flanks of the Alps, has been strongly affected by the torrential rainfalls, which registered up to 300 mm in three days (Bezzola & Hegg, 2007). This exceptional water discharge lead to soil saturation, massive erosion, floods, landslides and debris flows in many regions of Switzerland, causing up to 3 billion CHF damage and leading to six casualties. Overall, the flood of August 2005 has been described as the most destructive event that has ever been registered in Switzerland since 1972, when the systematic recording of storm damages began (Bezzola & Hegg, 2007). Specifically, the Canton of Bern has been one of the most affected areas, accounting for 25% of the total damages (Bezzola & Hegg, 2007). In particular, the region of Lake Brienz in the Bernese Oberland is one of the most representative examples of the destructive power of the event. During the night between the 22nd and the 23rd of August, two large debris flows hit the village of Brienz and Schwanden b. Brienz, causing the destruction of several buildings and leading to two casualties (Bezzola & Hegg, 2007; Müller, 2007).

As far as reviewed literature has shown, no publications to date have focused on the sedimentological aspects of the 2005 event, rather they directed their attention on the causes and predisposition of the event, as well as on the singular inflows and related flooding (Zimmermann, 2006a, 2006b; Müller & Loew, 2009). For this reason, this thesis will focus on the reconstruction and understanding of the event from a sedimentary point of view. The sedimentary record of the lake will be analysed through a series of visual, physical, geochemical and particle-size analyses in order to retrieve information about the different catchments' contribution to the event. The discharges from the main inflows will be also analysed in order to investigate the succession of events during the flood, and an estimation of the sediments transported into the lake by individual inflows will be presented.

1.2 Floods

The Special Report from the IPCC (2012), defines floods as "*the overflowing of the normal confines of a stream or other body of water or the accumulation of water over areas that are not normally submerged. Floods include river (fluvial) floods, flash floods, urban floods, pluvial floods, sewere floods, coastal floods and glacial lake outburst floods".* River floods, which this thesis will focus on, are usually related to an increase in stream discharge. This often rapid increase in water-flow causes overbanking with subsequent flooding of the surrounding area (Støren, 2011). The damages associated to such events depend on the intensity of the flood (the speed and the volume of transported water), as well as on the suspended load carried during the event (Kundzewicz et al., 2014). The magnitude defines the return period (or recurrence interval) between two floods of a specific size (e.g. 100-, 200-, 300-year flood) (Støren, 2011). High magnitude floods can be defined as extreme events, which are defined from the IPCC (2012) as *"[…] a value of a weather or climate variable above a threshold value near the upper ends of the range of observed values of the variable"*. Statistically speaking, extremes are events, which deviate from the mean and are as rare or rarer than the 90th percentile (IPCC, 2012). Such events are usually of short duration and with a large return period (Støren, 2011).

1.2.1 Floods in Switzerland

In the last decades Switzerland experienced several natural events, which caused serious damage. Figure 1.1, for example, shows the result of a study conducted by Hilker et al. (2009), in which a flood and landslide damage database was created for Switzerland for the time period between 1972 and 2007.

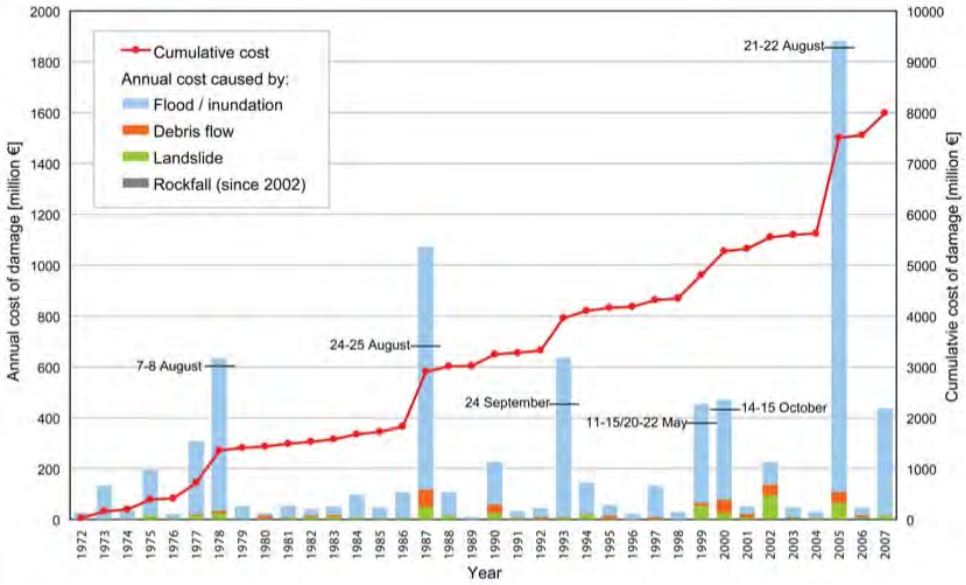

Fig. 1.1 Flood and landslide damage in Switzerland from 1972 to 2007 (Hilker et al. 2009). Bars represents annual costs (in million Euros) due to natural hazards. Blue bars are indicative for flood and inundations, red bars for debris flows, green bars for landslides and grey bars for rockfalls. The red dotted line indicates the cumulative cost for the studied period (in million Euros).

Figure 1.1 shows the cumulative cost of damage deriving from floods and/or inundations, debris flows, landslides and rockfalls. Six major events are clearly visible: August 1978, August 1987, September 1993, March 1999, October 2000 and August 2005. From the period of 1972 to 2007, natural events caused around 8 billion Euros worth of damage in Switzerland. The six events mentioned before totalled 56% of the overall damage. 89% of the total costs (7110 million Euros) were caused by floods and inundations, while debris flows covered only 4% (340 million Euros). Landslide and rockfall events caused 6% (520 million Euros) and less than 1% (15 million Euros) of the total cost, respectively. The study also shows that 75% (6000 million Euros) of the total losses were caused by an event triggered by high-duration rainfall, while thunderstorms were accountable for just 23%, representing 1850 million Euros. Most significantly, the six major disasters were all reported to be caused by long-lasting rainfall. Regarding the temporal distribution of flooding, the study showed that most of the events (72%) occurred from June to August, with August recording the highest number of flood events. The likelihood to have flood events in summertime shows quite a stable pattern concerning timing of discharge on a mountain catchment, as it will be presented in the next section 1.2.2.

1.2.2 Floods in Mountain Regions

Mountain regions play a significant role concerning hydrological processes. Covering around a quarter of the Earth's surface (Weingartner et al., 2003), they differ from the lowlands in terms of micro-climate, elevation, evaporation, temperature and precipitation patterns, providing higher rainfall and discharge and therefore supplying the lowlands in terms of water demand (Viviroli & Weingartner, 2004). The Swiss Alps, in particular, play a major role for production and transport of water surplus to the surrounding lowlands (Weingartner et al., 2003). Situated in Central Europe, the Alps are influenced by three different humid areas - the Mediterranean, the Atlantic and the Northern Sea (Viviroli & Weingartner, 2004) - and can therefore rely on constant sources of humidity (Viviroli & Weingartner, 2004). The higher precipitation occurring in mountainous environments (in the form of rain in the summer and stored as snow and ice in the winter), as well as reduced evapotranspiration, lower net radiation, higher snow cover and a more opened vegetation cover leads to a high storage of water in

such regions (Viviroli et al., 2010). For this reason, the Swiss Alps are defined as "the water tower of Europe" (Mountain Agenda, 1998). Characterized by one of the densest hydrological network, the Swiss Alps constantly distribute their water surplus not only to the Swiss lowlands, but also to Western and Central Europe, as well as to the Mediterranean Sea (Weingartner et al., 2003; Viviroli & Weingartner, 2004; Beniston, 2010). While in many regions of the planet there is minimal usage of mountains for human settlements, the surrounding lowlands are usually characterized by a higher density of settlements, industries and agricultural areas (Viviroli & Weingartner, 2004). Mountain discharge as such has a great importance concerning the population living in the lowlands, which uses the incoming water for land use, energy production, and human development. However, the role of mountain-water supply comes with dangers, namely the highly destructive potential of mountain discharge, usually experienced in form of floods (Weingartner et al., 2003). It is therefore of great importance to understand the complexity behind such events in Alpine regions.

In mountainous areas, the initiation of floods is mainly determined by the hydrological and geomorphological characteristics of the catchment. These characteristics are twofold: the ones connected with altitude, such as precipitation, temperature, soil development and vegetation, and the elements connected with the surrounding relief, such as wind and slope (Weingartner et al., 2003). Altitude is an important characteristic for floods triggered in Alpine regions. Catchments located between 1000 and 2000 meters above sea level (m a.s.l.) are the most vulnerable. Characterized by steep slopes, thin soils, a poor vegetation cover and high precipitation intensity, such catchments often respond very rapidly to weather events. A further element, which contributes to this vulnerability, is the dense river network, which characterizes most of the Alpine catchments and contributes to a rapid conversion of precipitation into surface runoff (Weingartner et al., 2003). By contrast, catchments situated both in lowlands and higher up in the Alpine area (lower 1000 m a.s.l or above 2000 m a.s.l) are characterized by lower runoff coefficients and are less likely to trigger a flood event (Weingartner et al., 2003).

1.2.3 Precipitation

Precipitation is a major trigger for floods in alpine regions (Froidevaux & Martius, 2016; Weingartner et al., 2003). Acting as a physical barrier, the Alps are characterized by convective and advective weather systems, which are not able to cross the mountain chain resulting in higher rates of precipitation with increasing elevation (Viviroli et al., 2010). This, along with a catchment's other characteristics (shallow soils, steep slopes, open vegetation), contributes to the rapid conversion of precipitation into runoff (Viviroli et al., 2010).

1.2.3.1 Precipitation in Alpine Regions

There are two major atmospheric precursors, which lead to rainfall: (1) there must be strong and continuous moisture in a region, which is transported towards Switzerland, and (2) this moist air must ascent towards the Alps (Froidevaux & Martius, 2016). Concerning the transport of moist air masses, atmospheric rivers (ARs) play a crucial role. ARs are weather systems, which can be defined as corridors transporting water vapour (Stucki et al., 2012). These corridors are usually related to tropical and moist air masses, which get transported further inland (Froidevaux & Martius, 2016). Once transported towards the Alps, the second atmospheric precursor comes into play. The ascension of moist and warm air is caused by two main processes: convective systems (Fig. 1.2a) and orographic uplift (Fig. 1.2b). Also known as Mesoscale Convective Systems (MSC), these convective systems are characterized by several thunderstorms clustered and acting as a single system (NSSL, n.d). In meteorology, a convective

process refers to an upward movement and a subsequent heating up of the air mass caused by a warm surface. The warmer air mass becomes less dense and therefore rises up in the atmosphere, leading to formation of clouds and instabilities as shown in Fig. 1.2a (WW2010, n.d). At high altitude, the mass cools and its water holding capacity decreases, therefore leading to rainfall. Usually related to intense and short-lasting rainfall in summer, these systems have a major role controlling precipitation events over the European Alps, especially in the Alpine foothills (Weingartner et al., 2003).

Orographic uplift is another type of advection process that largely affects the Alps. For this process, air masses coming from the surrounding regions encounter mountainous relief and are therefore forced to rise. The large evaporation from the warm sea surface, combined with low-pressure systems on the Mediterranean, cause the transport of humid air masses towards the Alps, where the uplifting process takes place. This causes precipitation events, which affect especially the southern Alps, causing long-lasting flood events in spring and autumn (Weingartner et al., 2003). In general, however, the Alpine chain acts as an obstacle towards atmospheric flows coming from different directions, which releases heavy precipitation only on one side of the mountain, while the opposite side is characterized by lower precipitation (Fig. 1.2b) (Viviroli et al., 2010).

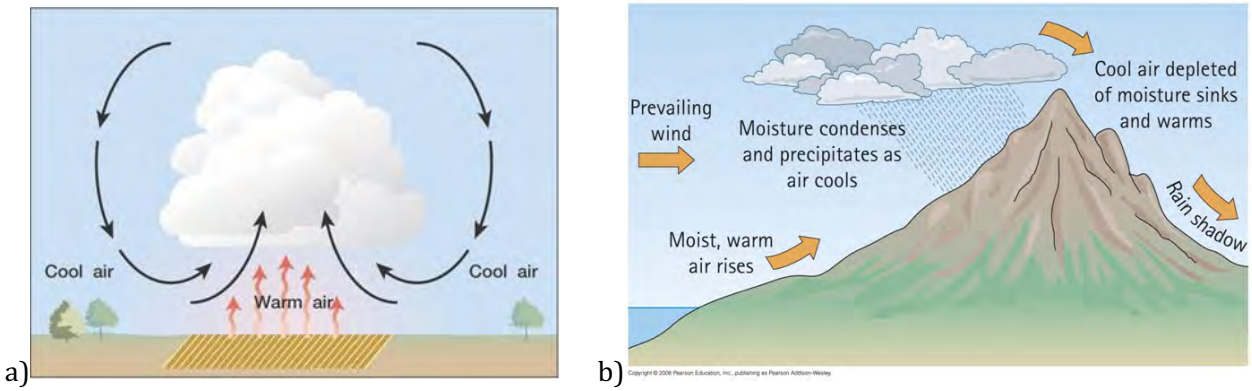

Fig. 1.2 Schemes of convective (a) and orographic (b) systems (from Hegg, 2013)

Despite the multitude of atmospheric processes, which can trigger natural hazards, there are particular weather patterns, which are related to flood events. For example, as the study by Stucki et al. (2012) indicates, the major floods of the last 120 years were caused by similar weather systems such as the Potential Velocity (PV) "cut-off" (PCO), PV streamers and/or zonal flow. *PCO, for instance, was the weather system related to the 2005 flood event.* In section 1.7.1., related to the August 2005 flood event, this synoptic system will be presented more in details.

Finally, precipitation can have either a solid or liquid form. Thus far liquid precipitation has been described. Solid precipitation, such as snow, hail and ice, play an important role in temporary storing water on the Alpine chain, and therefore contributing to the water balance in Alpine catchments (Viviroli et al., 2010).

1.2.4 Vegetation

Vegetation is an important parameter for flood events and, more specifically, for a catchment's response to precipitation. It influences soil conditions, as well as the micro-climatic conditions of the region and acts as interceptor of rainfall (Weingartner et al., 2003). Forested areas located in the Eastern Alps, for example, intercept around 20-30% of yearly precipitation, which therefore does not contribute to runoff (Viviroli et al., 2010). Moreover, through a dense network of roots, such areas improve the stability of

soils, and thus the stability of slopes, which as a result acts as a better protection against such events (Daniel Viviroli et al., 2010). As stated before areas located above 1000 m a.s.l. are more sensitive to flood events (Weingartner et al.; 2013). This statement can also be explained through soil cover: catchments situated above this altitude provide much less vegetation cover, which in turn leads to a less stable and less water-retaining soil covered by rocks and debris. Such soils are more prone to surface runoff (Viviroli et al., 2010).

1.2.5 Topographic Relief

Topographic relief plays a key role concerning flood generation. In mountain areas, catchments are usually characterized by steep slopes, which accelerate the discharge during a rainfall event and create high-energy conditions, leading in turn to stronger erosion and mobilization of material (Weingartner et al., 2003).

1.2.6 Soil

With the ability to absorb and retain water, soils influence the occurrence of the catchment's discharge and the consequent runoff during extreme precipitation events (Weingartner, 2003).

1.2.7 Runoff

Interacting between each other, all previously mentioned processes and catchment's characteristics play a major role in the creation of discharge. The magnitude of such discharge also highly depends on the basin characteristics. Here, not only topography, altitude, soil and vegetation are taken into consideration, but also the geology of the catchment and the land-use of the region (Daniel Viviroli et al., 2010). As a result of the afore mentioned Alpine and basin characteristics, discharge is higher at higher altitudes. Concerning the timing of runoff, seasonality plays a major role. In Alpine catchments, winter runoff is largely influenced by snow and ice accumulation, while spring and early summer runoff is characterized by snowmelt. Summer discharge in Alpine catchment is largely influenced by the presence of glaciers and their relative melting processes, as well as by the weather pattern described in section 1.3.1.1 (Weingartner et al., 2003; Daniel Viviroli et al., 2010; Froidevaux & Martius, 2016).

Floods are extremely complex events, accounting for a multitude of different triggers and dependent not only on global atmospheric circulation, but also on the regional and local characteristics of the region and of the studied catchment. In addition, there are limitations in the understanding of hydrological processes in Alpine regions resulting from the inadequacy of measuring networks tackling the high spatial and temporal variability of hydrological processes (Viviroli & Weingartner, 2004). Weingartner et al. (2003) show that, despite the relatively dense measurement network in the Swiss Alpine area (on average one station per 120 km^2), because of the complexity concerning precipitation patterns and topography, the network is still poorly represented. The study shows that just 18% of the stations are located above 1312 m a.s.l., with a density of measuring networks at high altitude of just one station every 350 km^2. As the area between 1000 and 2000 m a.s.l. is the most sensitive to flood events, it is implied that there is a lack of measurement stations in the most responsive region of Switzerland.

1.3 Floods and Climate

Future behaviour of flood events largely depends on the changes within the climate system (Messerli et al., 2004). Changes in climate will impact the sensitive hydrological cycle (IPCC, 2012; Schillereff, Chiverrell, Macdonald, & Hooke, 2014). Temperature and precipitation patterns are therefore important variables whose future changes need to be understood in order to predict changes in the intensity and frequency of flood events. In general, it is expected that in the future an increase in moisture in the atmosphere of 7% approximately per degree of warming will occur, following the Clausius-Clapeyron relation (Frei et al., 2000). A warmer and more humid atmosphere will lead to an intensification not only of evaporation, but of the entire hydrological cycle (Frei et al., 2000).

In Europe, large-scale warming is expected during all four seasons, with a larger increase in winter temperatures over Northern Europe and an increase in summer temperatures over Southern Europe (CH2011, 2011). Precipitation patterns will most likely experience a change as well, with an increase in precipitation over Northern Europe and a decrease over Southern Europe (CH2011, 2011; IPCC, 2012). Europe will, in general, experience a shift in mean precipitation, with a decrease in summer and an increase in winter months. Consistent with European patterns, Switzerland will most likely experience an increase in temperature. Temperatures are expected to rise, especially during the summer months, with a higher increase in the southern part of Switzerland (CH2011). The amplitude of the change in temperature varies depending on the climate scenario. On the other hand**,** precipitation changes are more uncertain for Switzerland. As Switzerland is located in the transition zone between the two above-mentioned European projected precipitation patterns, there is more uncertainty about changes in future precipitation. However, there is a general consensus that precipitation will follow an increase in winter and spring (Beniston, 2006).

1.4 Floods in the Future

In Alpine catchments, changes in hydrological processes due to an increase in temperature and changes in precipitation will mainly affect the melting of glaciers and snow, and therefore strongly influencing seasonal river discharge (CH2014, 2014). A change in such atmospheric variables will lead to a change in the ratio of liquid and solid precipitation for the winter and spring season. This modification in seasonal storage will therefore be followed by a change in seasonal discharge patterns (Viviroli et al., 2010; Köplin et al., 2014). The interaction between temperature, precipitation and atmospheric processes is complex and there are uncertainties on how and to which extent they will interact together, as well as on the role they will have for flood patterns in the future (CH2011, 2011). In the literature there are conflicting opinions on the range of changes in flood events in the future. Most studies focus on changes in future seasonality rather than flood frequency or intensity. As stated from the IPCC 5th Assessment Report *"[…] there continues to be a lack of evidence and this low confidence regarding the sign of trend in the magnitude and/or frequency floods on a global scale".*

A study from Birsan et al. (2005) focused on the detection and identification of Alpine runoff trends from 1931 to 2000, a period during which changes in the climate were observed. The study performed an analysis of precipitation and discharge, as well as of a wide range of catchment's characteristics (basin area, mean altitude, mean slope, soil depth, geology, rock and glacier coverage) for 48 basins located throughout Switzerland. The results showed that for the study period, a general increase in annual discharge was recorded for all basins. A stronger increase has been found especially in winter and spring, while the detection of a summer trend was more complex and less consistent. Other studies focused on a longer time-scale (e.g. Schmocker-Fackel & Naef, 2010; Wirth et al., 2013), showing that

flood frequency in Switzerland was high during the second half the 19th century and decreased during the beginning of the 20th century until 1975. After this date, is was shown that the frequency of flood events increased again. Specifically, between 1882 and 1976, Switzerland has been affected by only a few natural disasters (Pfister, 2009). Such "disaster gap" lead to a decrease in consciousness and awareness of the destructive power of flood events. Therefore, time series spanning along the 20th century in Switzerland recorded the "disaster gap", and can therefore be misleading for what concerns trends of floods and other natural hazards, showing a strong increase in frequency despite of the fact that the 19th century recorded many flood events.

Beniston (2010) followed an approach more focused on the future. This study shows that projections for Alpine discharge in 2100 indicate that a first peak runoff will be recorded two or three months earlier in the year, followed by a second peak in summer. According to the author, the volume of the summer peak will strongly depend on the volume of the upstream glaciers, which is expected to decline under a warmer climate. Therefore, the runoff peak in summer is expected to be much more modest compared to spring due to the smaller availability of snow-pack and glaciers. Further, the study states that heavy precipitation events will occur in early spring and winter (melting seasons), and that such events will have a cumulative effect on water release. Catchments will not be able to absorb the excess of water, which will result in an increase discharge and thus an increase in flood risk.

Yet precise projections on future mountain discharge patterns under a changing climate are difficult to draw, especially considering the difficulty and uncertainty that global circulation models (GCMs) and regional climatic forecasts have in projecting climatic change on a regional and local level (Messerli et al., 2004). Hydrological models are extremely complex and as such are difficult to apply to higher altitudes and snow-covered areas (Messerli et al., 2004). To conclude this section, flood occurrences are likely to change in a future climate. However, the understanding of the extent of this change has still to be improved.

1.5 Lake Sediments as Archives

The understanding of flood processes and their related future changes in frequency and intensity is of great value in a mountainous area like Switzerland. The damage potential of such events must not be underestimated, and in order to infer some information about the future it is important to look into the past. Instrumental and historical records, however, do not cover a long enough time span. In order to acquire a comprehensive understanding of past processes and their relation with and variability to changes in climate, long-term records (on a centennial to millennial scale) are required (Schillereff et al., 2014). In the inner Alps, for example, systematic instrumental measurement of hydrological parameters has been collected only for the past 100 years (L. Schulte, Peña, et al., 2015). For this reason, an increasing number of scientific studies are focusing on reconstructing past flood events in various locations of the planet using lake sediments (Amann et al., 2015). Wirth et al. (2013), for example, used lake sediments to study flood frequency spanning throughout the last 10'000 years, covering a much longer time-span compared to instrumental measurements.

Depending on the characteristics of an Alpine region, catchments can be more or less prone to erosive processes and mobilization of material. Clastic, allochtonous material coming from the catchment, the surrounding area or from the atmosphere is continuously transported into the basin by the catchment's hydrological network (Gilli et al., 2003; Schillereff et al., 2014). Once the transported material reaches the lake, it settles on the lake basin and becomes incorporated into the sediment. Normal 'vertical' sedimentation refers to background sedimentation, which is a low and continuous sedimentation rate

(Gilli et al., 2003). This vertical or pelagic-type 'endogenic' sedimentation contrasts to 'lateral' sedimentation where various forms of flows transport and redistribute detrital constituents through the lake. The process of incorporation and sedimentation of transported material occurs since the formation of the lake, providing information about past conditions surrounding the water basin. Lakes, therefore, provide highly-resolved, long and continuous records of processes and variables influencing the formation of the lake and its history, such as past climate, vegetation, tectonic activity, bedrock composition, anthropogenic impacts (Cohen, 2003), as well as information on lake conditions and their surroundings (Gilli et al., 2003). Thus lakes can act as archives, recording palaeoenvironmental conditions. Lake sediments therefore provide ideal archives for the investigation of changes in past sedimentation rates, which can provide insight on palaeofloods or debris flood events. In order to reconstruct flood events a more specific focus on the sedimentation processes of a river flume are required.

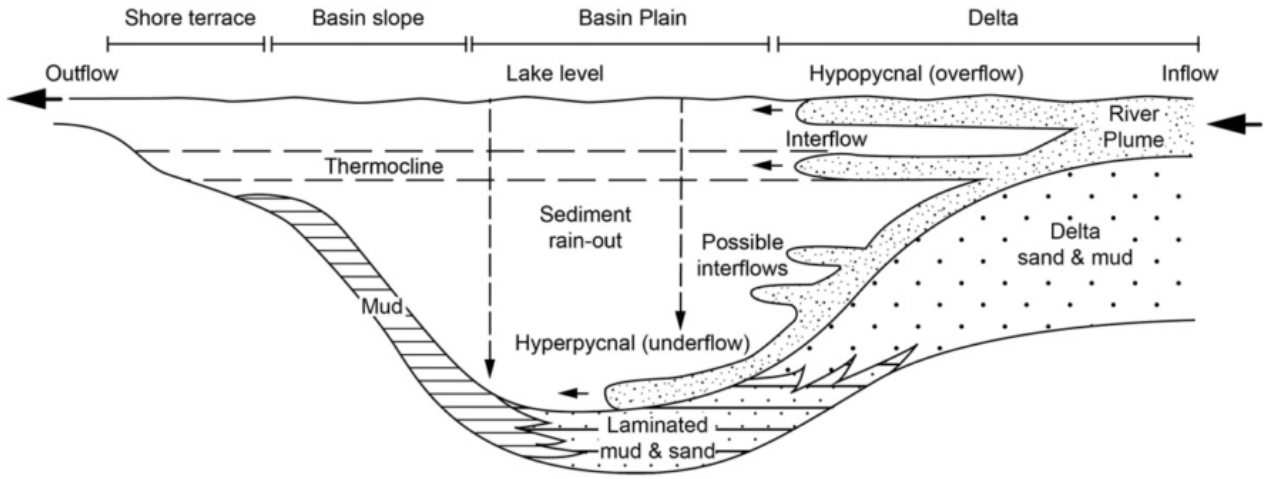

Fig. 1.3 Sedimentation scheme for a clastic lake, as proposed by Sturm and Matter (1978) and modified by Schillereff et al. (2014)

Figure 1.3 represents a scheme of sedimentation processes and their relative deposits in a lake. The scheme was produced for a study for Lake Brienz (Sturm & Matter, 1978), and can therefore be applied to lakes characterized by a major input of clastic material. Figure 1.3 shows the sedimentary processes involved when a river plume enters a lake. Such a plume can develop into three types of flows: hypopycnal (or overflow), interflow and hyperpycnal (or underflow). Differences in density between the water body of a lake and the incoming water flow determine the distribution of the transported sediment load into one of the three afore-mentioned flow types (Schillereff et al., 2014). If the incoming streamflow is characterized by a lower density than that of the lake basin (such as for normal discharge), it will enter the lake as overflow. Interflows are located at the boundary between warm and less dense lake surface waters (epilimnion) and the deep, cold and dense waters (hypolimnion). This boundary is referred as thermocline, which represents a thermal stratification between the surface and deep waters (Cohen, 2003). Interflow occurs in stratified lakes when the density of the river discharge is lower than the hypolimnion but higher than the epilimnion (Sturm & Matter, 1978). For both inter- and overflows, the material is then transported in suspension and slowly integrated into the sedimentary record as it settles, forming laminations.

Underflows, or hyperpycnal flows, occur when sedimentation within a lake is largely dependent on sediment supply (Gilli et al., 2003). Extreme events, such as floods or debris-flows, increase erosive processes in the catchment, therefore mobilizing large volumes of particles, which are transported along stream channels and floodplains. In contrasts to the normal sedimentation process described in Figure

1.3, water flows containing large amounts of suspended material are much denser than lake waters. Such high-density flows will therefore enter the lake as underflows (also called turbiditic underflow) (Gilli et al., 2013) moving along the deepest region of the basin. There, flow velocity decreases and the underflow spreads on the lake bed and is deposited as a distinct detrital layer (Gilli et al., 2013). These detrital layers will be here forth be referred to as turbidites. Turbidites differ from the background sedimentation in a wide range of characteristics, which are detectable through sedimentological and geochemical analyses. The following list contains the main characteristics of a turbidite:

- **THICKNESS**: flood events mobilize a large amount of material, which is transported to the lake in a short period of time and therefore leaves a distinct thicker sediment layer.

- **LITHOLOGY AND COMPOSITION**: flood-related turbidites usually have a different mineralogical composition, in line with the surrounding catchment composition, and are commonly characterized by a low organic content (Gilli et al., 2003). Such differences are visible in the sediment layering, for example, if the background sedimentation is characterized by authigenic material (light colour, such as for Lake Brienz), the turbidite will present a darker colour. On the contrary, if the sedimentation within the lake consists of organic material (dark colour), the detrital layer will be characterized by a lighter colour (Gilli et al., 2003). This characteristic allows for a first, visual differentiation of the flood layer.

- **SEDIMENTOLOGY AND DEPOSITIONAL PROCESSES***:* differing from background sedimentation, turbidites are characterized by a different sedimentation processes which reflect flood dynamics (Gilli et al., 2003). The depositional characteristics of turbidites, especially their grain size, are dependent on flow energy and velocity (Mulder et al., 2001; Mulder et al., 2003). During a flood event, while the coarser and heavier fraction may not leave the catchment (depositing rather on alluvial fans), the finer particles stay in suspension in the water flow, and are transported longer distances to the lake basin. For this reason, turbidites are usually characterized by an upward grading of grain size. Depending on the magnitude of the event, turbidites can be characterized by normal or inversely graded sections (Wirth et al., 2011). While normally graded sections show a fining upward of grain size, with coarser material at the bottom and finer at the top, inversely graded sections show a coarsening up of grain size towards the top (Mulder et al., 2003). The first deposit is characteristic for the initial peak discharge, which is followed by a decline in flow energy. Inversely graded turbidites mirror an increase in flow velocity during the flood event (Wirth et al., 2011).

- **GEOCHEMISTRY**: geochemical analysis are common techniques for the identification and differentiation of turbidites and detrital layers along a sediment core. Elements, which are characteristics of turbidites are, for example, aluminium (Al), silicon (Si), iron (Fe), potassium (K) and titanium (Ti) (Croudace et al., 2006; Ian W Croudace & Rothwell, 2015; Gilli et al., 2003).

1.6 August 2005 Flood Event

In August 2005, Europe was hit by a major flood event. The major affected areas were located in southern Bavaria, Germany, Salzburg, Austria, Switzerland, Romania and Bulgaria (Bezzola & Hegg, 2007). During the event, Switzerland was severely impacted and the event caused damages costing 3 billion CHF (Bezzola & Hegg, 2007).

1.6.1 Meteorological Situation

The August 2005 flood event was triggered by a particular cyclonic system, the so-called PCO (Pivoting cut-off). The term pivoting refers to the path of the cyclonic system, which in this case "cuts off" and surrounds the Alps, moving from the Mediterranean across northern Italy (Stucki et al., 2012). This synoptic weather system moves following the pattern of the classic Van Bebber cyclone track (Vb), which is known to have high potential for triggering summer floods (Stucki et al., 2012; Messmer et al., 2015). Despite cyclonic systems often develop during summer season, the reason the event caused such a high degree of damage is explained by a succession of weather events and processes, which lead up to the main flooding event. In the days prior to the event a low-pressure system, situated over Great Britain, moved towards France, bringing with it humid air masses. The eastern side of this low-pressure system reached central Switzerland on the 18th of August causing heavy storms. Already leading up to the 18th of August, central and eastern Switzerland registered 75% more rainfall than usually experienced for the month of August (Bezzola & Hegg, 2007). While such precipitation events are not uncommon in the summer season, the succeeding stages and development of the system played a crucial role in the triggering of the flood event. On the 19th of August, a low-pressure system characterized by cyclonic activity developed over the Netherlands, moving towards Benelux. During this day, Switzerland registered between 20 and 40 mm of rain over its territory. This cyclonic system subsequently moved to northern Italy on the 20th of August, where at the same time a further surface low-pressure system developed over the Gulf of Genoa. The associated humid air mass slowly moved from the Mediterranean across northern Italy and towards Switzerland. There, such masses shifted their main North-South axis towards a much more horizontal orientation, pivoting around the Alps from the East, following in an anti-clockwise direction During this phase, Switzerland experienced north-easterly winds caused by the convective character of the system, which caused long-lasting and intense precipitation on both sides of the Swiss Alps. The 21st of August was characterized by an intensification of the low-pressure system south of the Alps. The system increased its power, and a large area of rainfall developed over central Switzerland, with a specific focus on the Bernese Oberland, where the highest rainfall intensities were registered in Switzerland (Bezzola & Hegg, 2007). During the morning of the 22nd, the low-pressure system reached its maximum and the entire system moved eastwards (concentrically) towards the northern Adriatic. Upper winds turned north of the Alps, with the northern flanks of the Alpine chain experiencing the majority of heavy precipitation. All of Switzerland was consequently impacted by precipitation, significantly so in Central and Eastern Switzerland. During the 22nd of August the highest daily sums of the entire precipitation event were registered, with rainfall registered for the entire 24 hour day. On the 23rd of August, the wet air masses moved over Hungary, relieving Switzerland and converging on Bavaria and Austria. Figure 1.4 shows the evolution of precipitation in Switzerland during the event.

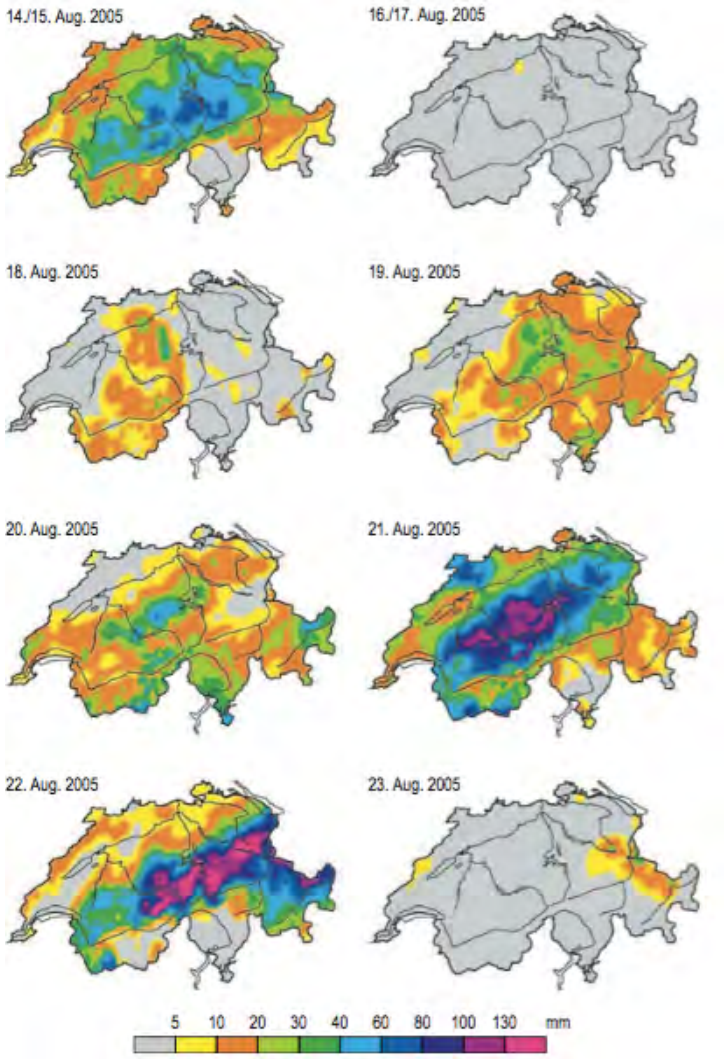

Fig. 1.4 Evolution of total daily precipitation over Switzerland from the 14th to the 23rd of August (Bezzola & Hegg, 2007). The first two images (14/15th of August and 16/17th of August present total precipitation over 2 days)

The PCO characterizing the August 2005 flood event was reported to have caused the most extreme flood event of the 20th century in Switzerland in terms of precipitation rates, hydrological discharge and damage (Stucki et al., 2012). Stucki et al. (2012) reported in their work that the 2005 event was one of the highest episodes of precipitation, lasting 42 hours over the Alps. Heavy precipitation was observed from the 19th to the 22nd of August, with a maximum intensity reached on the 21-22nd of August. The total amount of rain, which fell during those two days exceeded 200 mm in 48 hours, with a maximum of 350 mm of precipitation falling from the 20th to the 23rd of August (Bezzola & Hegg, 2007; Jaeggi, 2007). Following the exceptional amount of rain fall over the territory, high runoff occurred in many streams with peak discharges exceeding a 100-year flood in many basins across Switzerland (Jaeggi, 2007). As a consequence of both long-lasting, intense precipitation and elevated discharge, several regions experienced strong erosive processes. Those, in turn, lead to a destabilization of slopes and river banks and a subsequent transport of material. The instability and transport of material lead to a number of landslides and debris flows, as well as flood events, caused both from instability or strong depositional processes due to mobilized material (Rickenmann & Koschni, 2010). Figure 1.5 shows some examples of processes triggered by the August 2005 event in Switzerland.

Fig. 1.5 Natural hazards triggered by the August 2005 event. In pictures, (a) Flood in Sarnen (SRF, 2014) (b) highly swollen River Aare in Bern (BE) (Müller, 2007) (c) Flooding in the streets of Oey (BE) (MySwitzerland.com, n.d) and (d) Flooding in the mountainous region of Klosters (GR) (Schweizer Luftwaffe, 2005)

Although the entire Swiss territory was affected by the event, major damages occurred mostly in Central Switzerland, from the Bernese Oberland to the St-Gallen Rhine Valley, as it can be observed from Figure 1.6.

The total amount of damage caused by the August 2005 flood event is ~3 billion CHF for the entire territory of Switzerland, with the recorded damage mainly results from the long duration of heavy rainfall rather than its peak intensity (Jaeggi, 2007). The 2005 event has been described as "the most catastrophic event of the last century" (Bezzola & Hegg, 2007; Stucki et al., 2012). Despite being referred to as "the event of the century", it has been revealed that, when considering the entire event in Europe, the return period on a local scale is of about 80 years (Roger Müller & Loew, 2009). This would therefore classify the August 2005 flood event was "rare but not exceptional".

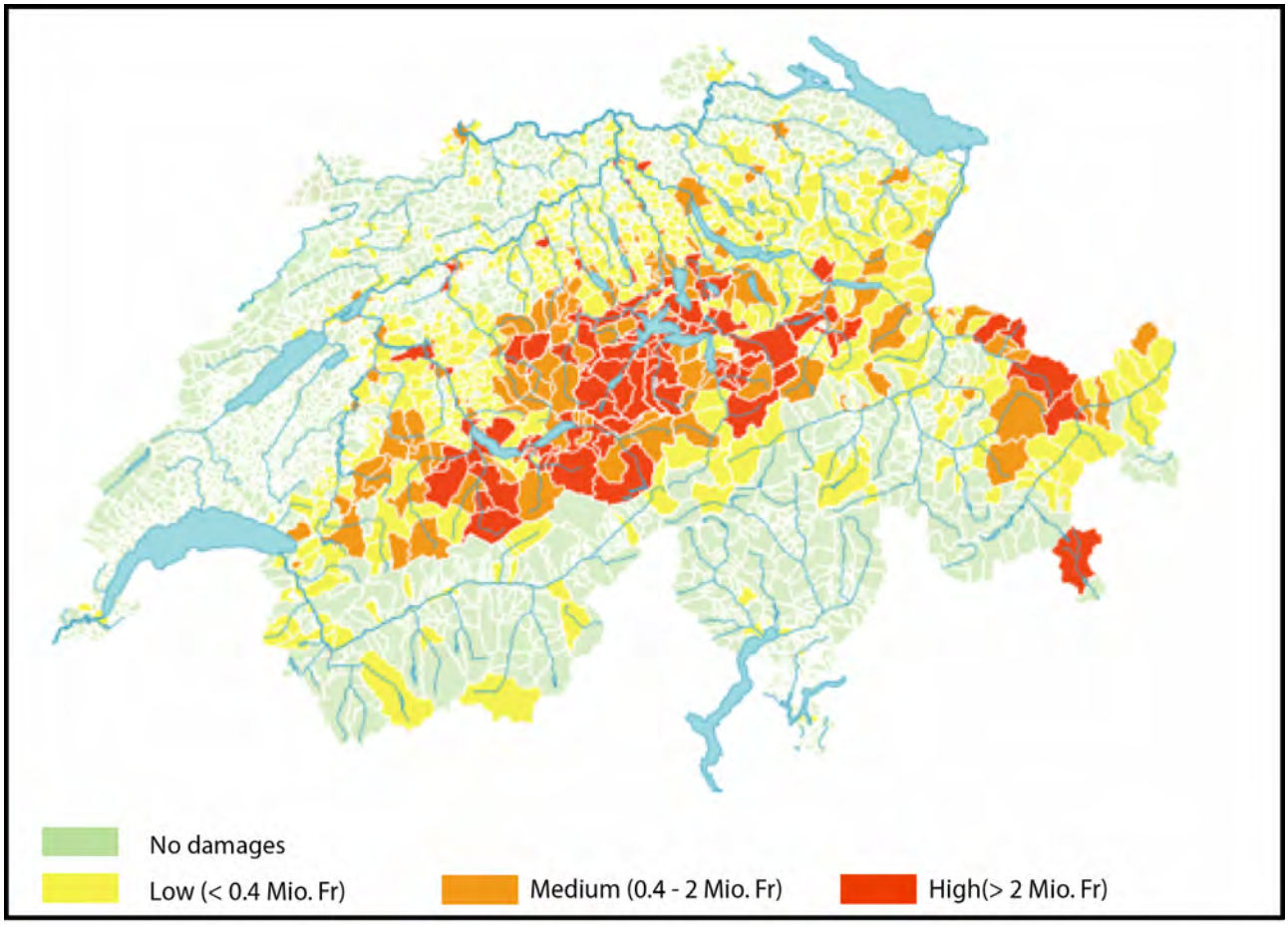

Fig. 1.6 Total damages per municipalities during the event, in million CHF. Colour green characterizes municipalities not affected in terms of damages, yellow corresponds to municipalities, which experienced low damages (< 0.4 millions CHF). Orange areas experienced medium damages (0.4-2 Mio CHF) and red areas show municipalities characterized by high damages (> 2 millions CHF). Modified from Rickenmann & Koschni (2010) .

1.6.2 Lake Brienz

Lake Brienz can be described as the most representative example of the devastating power of the 2005 event. Strong rain fall in the area began on the 20th of August and peaked on the 22nd of August, reaching 215 mm in Brienz and 307 mm at higher altitudes (Roger Müller & Loew, 2009). Figure 1.7 shows the rate of daily precipitation in Brienz throughout the year 2005 and, as clearly indicated, the observed precipitation amount during the 2005 August event is outstanding. While on the 22nd of August the observed amount of precipitation reached 73 mm, the wettest day was the 23rd of August, during which 98 mm of rainfall fell in one day.

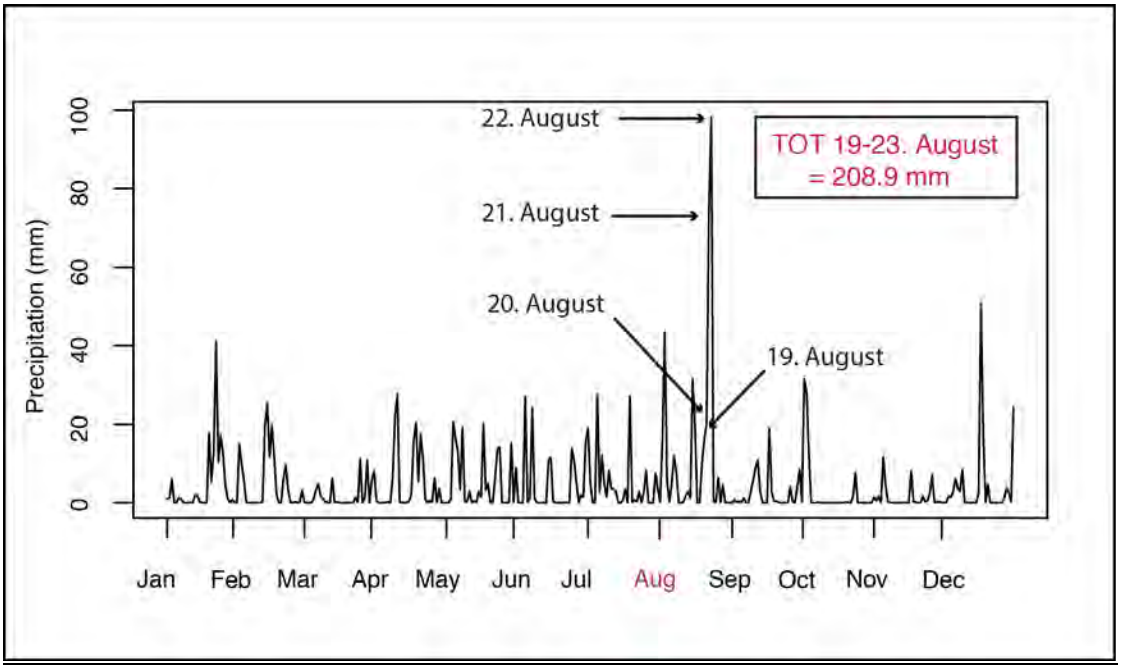

Fig. 1.7 Daily precipitation (in mm) at Brienz for the year 2005 (data from MeteoSchweiz)

The days prior the event experienced some rainfall (31 mm fell on the 15th of August and 19 mm on the 16th). Subsequently, no precipitation was recorded for the 17th and 18th, with the main precipitation event beginning only on the 19th of August with an increasing quantity of precipitation falling during the following days. Maximum rainfall was recorded on the 22nd, thereafter an abrupt discontinuation of precipitation was recorded with only 0.4 mm on the 23th of August. Such intense precipitation facilitated strong erosion on the steeper slopes surrounding the catchment, with many roads, railways lines and bridges destroyed as a result of bank collapses. Lower areas experienced rapid accumulation of material, which in turn caused flooding and overflows (Jaeggi, 2007). The river and streams of the Brienz catchment experienced a rapid increase in discharge: similarly to precipitation, discharge during the August 2005 flood event was also outstanding when compared to the runoff throughout the year (Figure 1.8).

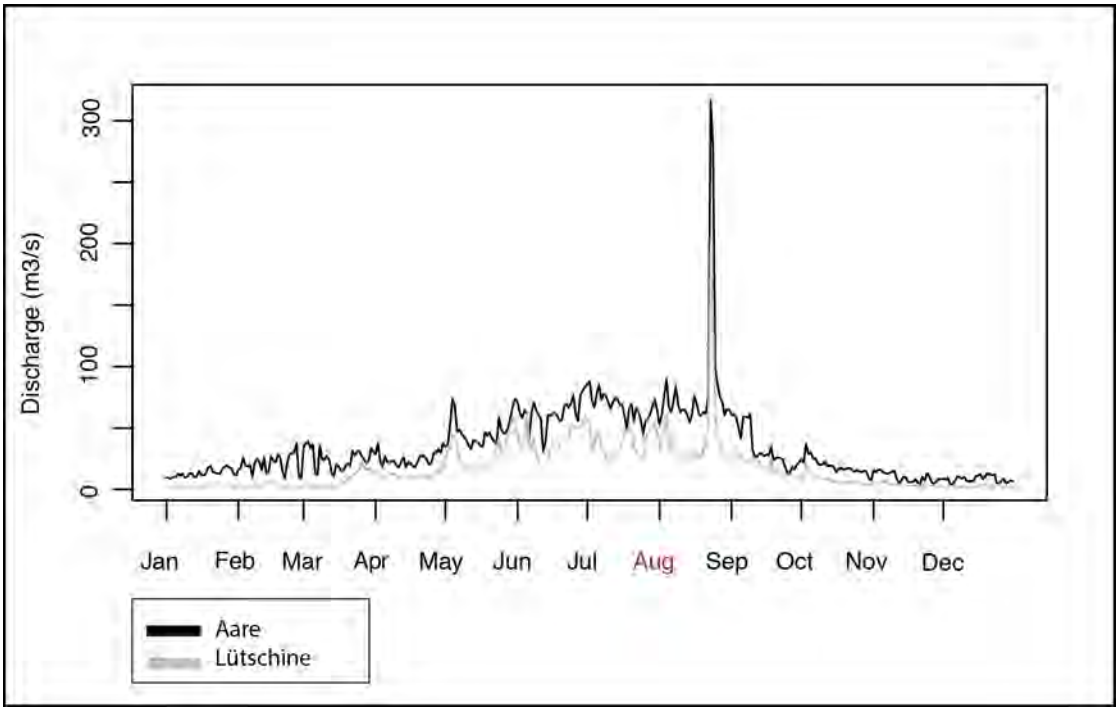

Fig. 1.8 Daily discharge (in m3/s) for Aare and Lütschine river for the year 2005, as recorded at the gauging stations of Lütschine-Gsteig and Aare-Brienzwiler

Figure 1.8 shows daily discharge for the year 2005 for both Aare (black) and Lütschine (grey). The highest discharge was reached on the 23rd of August for both tributaries, with a mean discharge reaching 204 m^3/s and 316 m^3/s for Lütschine and Aare, respectively. In contrast to the gradually increasing precipitation development in the catchment, discharge prior to the 23rd of August was not particularly high, with discharge values for both rivers prior to the event in line with usual discharge. Concerning the Aare discharge, an important contributor during the event was the hydropower network located upstream. In section 2.6**,** a more detailed explanation is given for the four hydropower stations in the region of the Grimsel Pass. Nevertheless, during the August 2005 event, the hydropower dams contributed to a reduction in the discharge of the river and accumulated water upstream. In total, 21.5% of the water mass characterizing the flood (from the Aare) was retained in such reservoirs (Bezzola & Hegg, 2007). During the event, the Lütschine, which has a channelized entrance into Lake Brienz and is surrounded by levees, experienced a rapid increase of water-flow. The gauging station of Lütschine Gsteig stopped measuring discharge when 227 m^3/s was reached, with an estimated peak occurring at above 250 m^3/s (Jaeggi, 2007). Prior to the 2005 event, a 100-year flood was estimated at 195 m^3/s, while a 200-year flood at 208 m^3/s. The channelized river therefore exceeded the expected discharge, overtopping and destroying the surrounding levees (Jaeggi, 2007). In total, about half a million cubic meters of water outflowed the banks, flooding a surface of 2 km^2 in the area of Bönigen and Interlaken (Tiefbauamt des Kantons Bern, 2007).

It was reported by the report from Bezzola & Hegg (2007) that the estimated sediment loads transported by Lütschine and Aare were of 250'000 m^3 and 350'000 m^3, respectively. These volumes are an order of magnitude of 3 (Lütschine-Gsteig) and 4.5 (Aare-Brienzwiler) times higher than the average annual loads. However, a report from the Tiefbauamt des Kantons Bern (2007) estimated that the volume of sediments transported into Lake Brienz from Lütschine was ca. 20'000 m^3**,** while the rest of the material accumulated in the flood plain due to low inclination. For Aare, no further information on the exact volume of transported sediments in the lake was available.

Fig. 1.9 The Brienz area after the 2005 flood event. Fig. a) Lütschine flood in Bönigen (Hunziker, 2014); Aare flood near Brienz (Jungfrau Zeitung, 2005); c) Glyssibach debris flow in Schwanden b. Brienz (Protection forest, Loat BWG, 2005); d) Cars destroyed by Trachtbach debris flow (Jungfrau Zeitung, 2005)

Despite both the Aare and the Lütschine rivers flooding and causing damages to the surrounding areas, the major, and most devastating, contributors to the 2005 event were the Trachtbach and Glyssibach torrents. These two mountain torrents are located in the region above Brienz and Schwanden b. Brienz, on the eastern flank of the lake. The intense precipitation, which fell in the catchment during the event (more than 300 mm in three days) triggered two landslides from the Trachtbach and Glyssibach torrents. The subsequent development of such landslides (moderately deep, between 2 and 10 m depth) into debris flows caused major damage in the villages of Brienz and Schwanden b. Brienz (Müller, 2009).

1.6.2.1 Trachtbach & Glyssibach Debris Flows

Müller and Loew (2009) showed through geological mapping and historical records that this area has been subject to a number of moderately deep (>2 m) and large (between 100 m^3 and several 10'000 m^3) landslides in the past. Such landslides often developed into debris flows, which in turn caused damage in the piedmont area of Brienz and consequently flowed into the lake. The explanation behind this is related to the geomorphology and geology of the catchments of Trachtbach and Glyssibach. In this area (mid-slope, 700-1400 m a.s.l.), mean slope gradients are on a range between 30° and 45° (Roger Müller & Loew, 2009) and are prone to erosion, instability and mass-movements. Geologically, the area comprise Jurassic and Cretaceous sediments from the Wildhorn nappe (R. Müller, 2007). From a geological and stratigraphical point of view, this area has been proven to be unstable, as will be described below in more detail. Figure 1.10 shows the geographical setting of the two catchments, prior to the 2005 event.

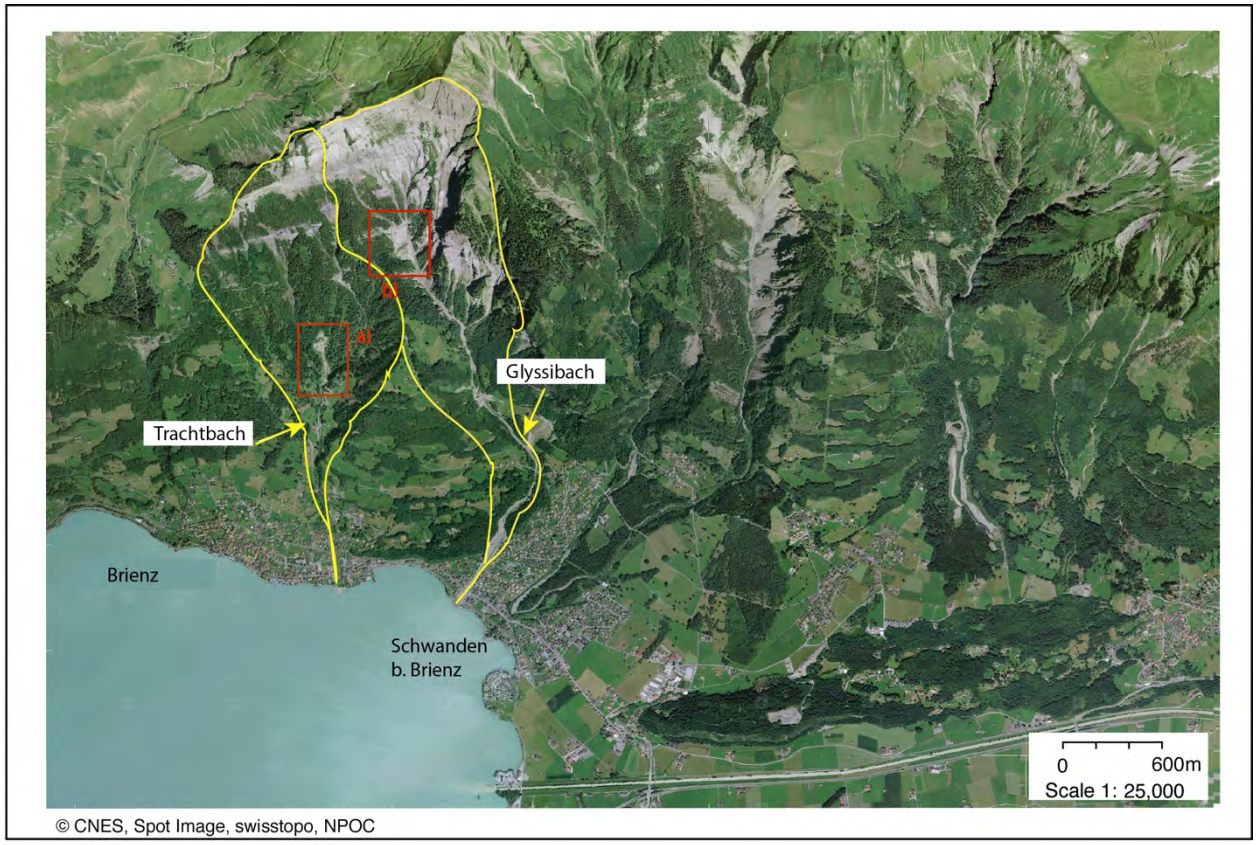

Fig. 1.10 Location of Brienz and its surroundings. Trachtbach and Glyssibach torrents are indicated with white arrows. A) Location of Trachtbach landslide and b) location of Glyssibach landslide. The two catchments are indicated in yellow. Modified after Swisstopo.ch

Trachtbach Landslide

During the 2005 event, a landslide was triggered in the Ritzwald forest situated above Brienz. The weathered rock and soil composed by an unstable geological formation of Cretaceous Marls from the Wildhorn nappe. The Cretaceous series is faulted, folded and detached from the Wildhorn nappe. The detachment is due to a sequence of incompetent, soft shales and marls (Palfris Formation) forming a sliding surface between Cretaceous sediments and the Wildhorn nappe (Müllet & Loew, 2009). Thus, the area is characterized by a highly unstable alternation of Valanginian Marls from the Cretaceous. The sequence is composed by hard limestones and soft marls and shales, and through weathering of the bedrock such alternation leads to a low-permeability structure overlaid by a more permeable surface soil (Müller & Loew, 2009). During the 2005 event, such weathered and unstable formation failed, creating a sliding surface. The estimated volume of the displaced material caused by such a failure amounts to ~57'000 m^3, while the estimated sediment load, which reached the lake is ~10'000 m^3 (Müller & Loew, 2009; Rickenmann & Koschni, 2010). The exact time at which the landslide occurred is still unknown. As reported by Müller (2009), *"a first, highly viscose debris flow was observed at Rauenhag (750 m asl) on August 22, at 10 pm. At 10.15 and 10.20 two subsequent low-viscosity debris flows reached Lake Brienz without leaving the Trachtbach canal. The following surges overtopped the dams of the canal and inundated about 76'000 m^2 of land with debris in the central part of the village of Brienz".* The Trachtbach landslide was a reactivation of an historical slide, which occurred in 1978. Brienz is located precisely on the alluvial fan of this historical landslide, and consequently the 2005 Trachtbach landslide caused the destruction of 20 habitations (Zimmermann, 2006a,b)

Glyssibach Landslide

During the August 2005 flood event, the major damage was caused by the landslide triggered in the Glyssibach catchment, located above the village of Schwanden. As with the Trachtbach landslide, the unstable geological alternation of marls and limestones failed, creating a sliding surface. The total volume of the initially mobilized material was ~80'000 m^3 of material, of which ~30'000 m^3 remained in the rupture (Müller and Loew 2009). The remaining material subsequently slid into the headwater channel. In contact with water, the landslide developed into a rapid debris-flow (6-10 m/s) of ~70'000 m^3, composed of both debris and large boulders of a diameter of more than 4 m. The material is expected to have been transported to the village in two, separate phases (Zimmermann, 2006b). The main debris flow hit the village of Schwanden b. Brienz at around 2am, causing the death of two inhabitants and the destruction of 28 houses.

1.7 Project Aim

The presented Master Thesis Project will focus on reconstructing the August 2005 flood event from a sedimentological perspective. The chosen study site is the basin of Lake Brienz, which as presented in section 1.7, is the most representative example concerning the magnitude and destructive power of the event. This thesis will analyse the basinal sediments of the lake from a visual, physical and geochemical perspective, with the goal of answering the following research questions:

1. Can we distinguish the **individual flood layers** from the respective inflows?

2. Can we distinguish the **2005 event** layer in the sediment record?

3. Can we distinguish the **extent of the contribution of the different catchments** during the 2005 event as recorded in the sediments of Lake Brienz?

4. How much sediment was **transported** to the lake from the different catchments?

5. What was the **temporal succession** of extreme runoffs and can that be reconstructed using the set of sediment cores?

1.8 Project Design:

In order to answer the above-mentioned research questions, this MSc thesis project was designed as followed:

- **SAMPLING**: Sediment cores and riverine samples were collected from Lake Brienz and its tributaries between July 2015 and July 2016. Cores were sampled along the Western-Eastern transect of the lake using a ETH gravity corer with a 6 cm diameter PVC tube.

- **LOGGING AND SCANNING TECHNIQUES:** Physical properties of the cores were analysed through logging and analysis of bulk density and magnetic susceptibility. The geochemical characteristics of the sediments were analysed via micro X-ray fluorescence core-scanning.

- **LABORATORY ANALYSIS:** Laboratory analysis of grain size, carbon content (TIC and TOC) and smear slide analysis were be performed on the 2005-layers along the cores.

- **STATISTICS:** Correlation Analysis and Principal Component Analysis were performed on the elemental profiles derived from micro X-ray fluorescence analysis

- **INTERPRETATION OF RESULTS**: The results were interpreted in order to answer the research questions presented in section 1.7

2 Study Site

2.1 Geography

The site of interest, Lake Brienz, is one of the numerous peri-alpine lakes situated on the front range of the Swiss Alps, in the Bernese Oberland, Central Switzerland. Lying at an altitude of 564 m a.s.l., the lake basin occupies an area of 29.8 km^2 along a deep, longitudinal valley formed by erosion of the Aare glacier during the last Ice Ages. The retreat of the glacier, at first, lead to the formation of a single lake called Wendelsee, which extended from Meiringen to Thun (Adams et al., 2001; Liechti, 1994). Through transport and accumulation of sediments from the Lütschine and Lombach rivers throughout time, a fan delta was built up where Interlaken lies today, dividing the basin in two and therefore shaping the present-day landscape characterized by the two distinct lakes of Thun and Brienz (Liechti, 1994; Schulte et al., 2009).

Today, the surrounding geomorphology of the 1134 km^2 Brienz catchment shown in Fig. 2.1 (Finger, 2006) is characteristic of an alpine area, with about a half of the area situated above 2000 m a.s.l and with a maximum elevation of 4,272 m a.s.l. (Finger, 2006; Girardclos et al., 2007; Schulte et al., 2015). Modelled by the movement of past glaciers, the catchment is characterized by a wide variety of formations, such as glacier forefields, cirques, scree slopes and moraines, as well as debris and alluvial cones, deltas and glacial lakes (Schulte et al., 2015). About 56% of the catchment is characterized by unproductive areas, of which around 19% is glaciated (Girardclos et al., 2007; Schulte et al., 2015). The rest of the catchment is occupied by forested (21 %) and agricultural (21%) areas, with the rest 2% inhabited (Finger, 2006; Wüest et al., 2007). The large catchment is composed by several sub-catchments, of which the two most important concerning size and sediment contribution are the Aare and Lütschine drainage systems (Fig. 2.1). The Aare catchment (Fig. 2.1a) extends over an area of 596 km^2 (Schulte et al., 2015), and it is delimited by the Grimsel on its southern side, and from a range of mountains on the eastern and western sides, such as the the Titlis and the Finsteraarhorn, respectively. The mean altitude of the catchment lies at 2150 m a.s.l. (Finger, 2006), with a maximum altitude of 4262 m a.s.l. (Schulte et al., 2015). The Lütschine catchment (Fig. 2.1b) lies at a mean altitude of 2050 m a.s.l and with a maximum elevation of 4158 m a.sl. (Finger, 2006; Schulte et al., 2009), occupies an area of 379 km^2 (Schulte et al., 2009). The catchment extends from the Lauterbrunnen Valley on the West, to the Jungfrau on the south and to the Wetterhorn to the east. In this project, two other sub-catchments will be taken into consideration, those of Glyssibach (Fig. 2.1c) and Trachtbach (Fig. 2.1d). Located on the area above the village of Brienz, their catchments occupy an area of 2.02 km^2 and 1.55 km^2, respectively (Rickenmann & Koschni, 2010).

The main settlements present in the vicinity of the lake are the homonymous town of Brienz, on the NE side of the lake, and Interlaken and Bönigen on the SW side. The area nearby the Lütschine delta counts the higher population, with 5659 inhabitants at Interlaken and 2520 at Bönigen in 2014 (Swiss Statistics). Brienz, on the other hand, in 2014 counted 2998 inhabitants.

2.2 Geology and Catchment Lithology

Geologically, the basin of Brienz lies entirely within the Helvetic zone (Hänni & Pfiffner, 2001), which forms a folded and thrust area along the northern flank of the central Swiss Alpine chain (Pfiffner, 2011). This nappe system originates from the southern margin of the Eurasian plate, and is characterized by

Mesozoic and (to a minor degree) Cenozoic sediments (Pfiffner, 2011). To the east, it extends into the Austrian Eastern Alps, while to the west continues to the French Chaînes subalpines. The northern and southern limit of the Helvetic zone is determined by the tectonically underlying Subalpine Molasse and by the overlying Penninic nappes (Pfiffner, 2011).

The Helvetic Zone, in turn, is composed by two separated zones, the Helvetic nappes and the underlying Infrahelvetic complex (Pfiffner, 2011). The Helvetic nappes can still be divided into several single nappes. As shown in Fig. 2.1, Lake Brienz lies parallel to two of those structures, the Wildhorn thrust on the north and the Axen thrust on the south (Pfiffner, 2011). While the lithology of the Wildhorn Nappe is mainly characterized by Cretaceous and Cenozoic beds composed by sedimentary rocks such as marls and limestone (Swisstopo; Sturm, 1976), the Axen Nappe is defined by Jurassic carbonate rocks such as limestone, calcareous sandstone, marl and phyllite (Schulte et al., 2015). Acting as a separation between the Axen thrust and the Aare Massif lies a narrow band of the Infrahelvetic Nappe, whose base is defined by pre-Triassic crystalline rocks and its cover consists in Mesozoic and Cenozoic sedimentary rocks (flysh, marls, limestones and sandstone-rich formations) (Pfiffner, 2011; Schulte et al., 2009, 2015).

South of the Axen nappe and the Infrahelvetic, the lake's catchment partially lies on the Aare massif: the Aare drainage system is in fact partly located on the typical units of the Northern Aare Massif, the Para-Mesozoic and Late Paleozoic, which are composed by crystalline rocks such as granite, diorite and quartz (Schulte et al., 2015). On the other hand, the southern area of the Lütschine catchment is only partly characterized by the above-mentioned typical units of the Aare massif: while the latter formations of the Northern Aare Massif mainly characterize the southern area of the Aare catchment, the southern side of the Lütschine drainage system is composed by the crystalline rocks of the Aare Massif on its upper altitudinal region, while at lower elevation is composed by Mesozoic sedimentary rocks (limestones) from the Doldenhorn Nappe (Swisstopo; Schulte et al., 2009, 2015; Hänni & Pfiffner, 2001.

The difference of the two catchments of the Aare and Lütschine is therefore visible from both a geological and lithological point of view, with the Lütschine draining three times more carbonate from its catchment (Matter & Sturm, 1982). This difference is visible in the sediments of Lake Brienz, in which higher carbonate content can be found along the southern shore (Matter & Sturm, 1982).

As specific interest for this study project, the geology of the area around the settlement of Brienz plays an important role concerning landslides and debris-flow formations such as in the case of the 2005 event. In a Diploma Thesis from (Müller, 2007) it is in fact shown that the surrounding area is characterized, under soil layer of a few meters depth, by weathered Valanginian Marls belonging to a sedimentary sequence defined by an alternation of hard marls and soft layers of limestones. This bedding sequence is highly unstable and prone to weathering, which lead in the past (in 2005 for instance) to sliding processes subsequently turning into landslides.

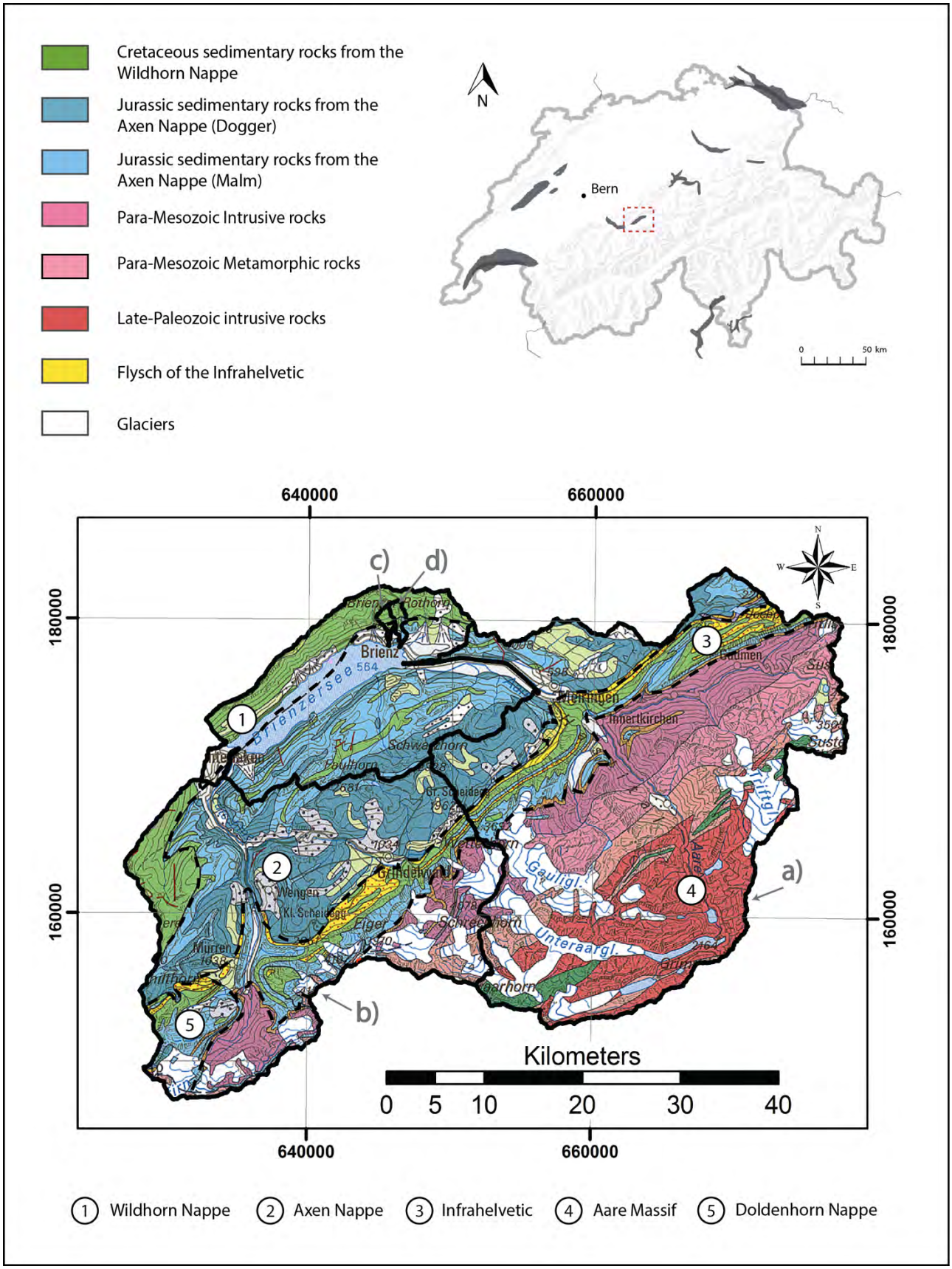

Fig. 2.1 Site location and geology of the catchment. Black lines indicate Aare (a), Lütschine(b), Glyssibach (c) and Trachtbach(d) catchments. Black dotted lines indicate the different tectonic units: Wildhorn Nappe (1), Axen Nappe (2), Infrahelvetic (3), Aare Massif (4) and Doldenhorn Nappe (5). Map of Switzerland (top right) modified after Myswitzerland.com

2.3 Climate

As specified in the previous sections, Lake Brienz is located on the northern flank of the Swiss Alps. Climatologically, the Alps are located in a transition area between different climatic zones such as continental and oceanic regimes, as well as Mediterranean and North-Atlantic climates (Beniston, 2006; Wanner, Rickli, & Salvisberg, 1997). The climatic conditions of the Alps are also strongly conditioned by the North Atlantic Oscillation (NAO), and specifically by its positive and negative phases, which reflects lower precipitation and milder temperatures for NAO+ and higher precipitation and colder temperatures during NAO- phases (Beniston, 2006). The particular location of the alpine range, with different climatic influences on the region, makes the Alpine range very sensitive to extreme precipitation events and therefore to flood triggers (Wanner et al., 1997).

The Alpine region is also strongly influenced by regional climate, which is in turn dependent on the complex topography of the region: orographic precipitation, downslope winds are for instance characteristic features and processes of an Alpine climate (Wanner et al., 1997). Regarding climate in Lake Brienz, precipitation is recorded to be around 1175 mm/yr at Interlaken, reaching up to 2800 mm/yr at the summit of the Aare sub-catchment (Schulte et al., 2015). The wettest season is summer, with precipitation varying between 120-150 mm in the months from May to August at Interlaken (Meteonews). The precipitation pattern of the studied area is 40% higher than the regional average, which is characteristic for a typical climatic situation for Alpine regions (Finger, 2006). Temperatures at Interlaken vary between -4°C (min T in January) to 24°C (max T in August) (Meteonews). Fig. 2.2 shows, for instance, daily precipitation in Brienz from 1990 to present-day. As it can be observed, there is no clear trend and precipitation varies from a minimum of 0 mm per day to almost 100 mm per day in 1990, 1992 and 2005. Fig. 2.3 shows the seasonal pattern of precipitation through boxplots, calculated on the period 1990-2015.

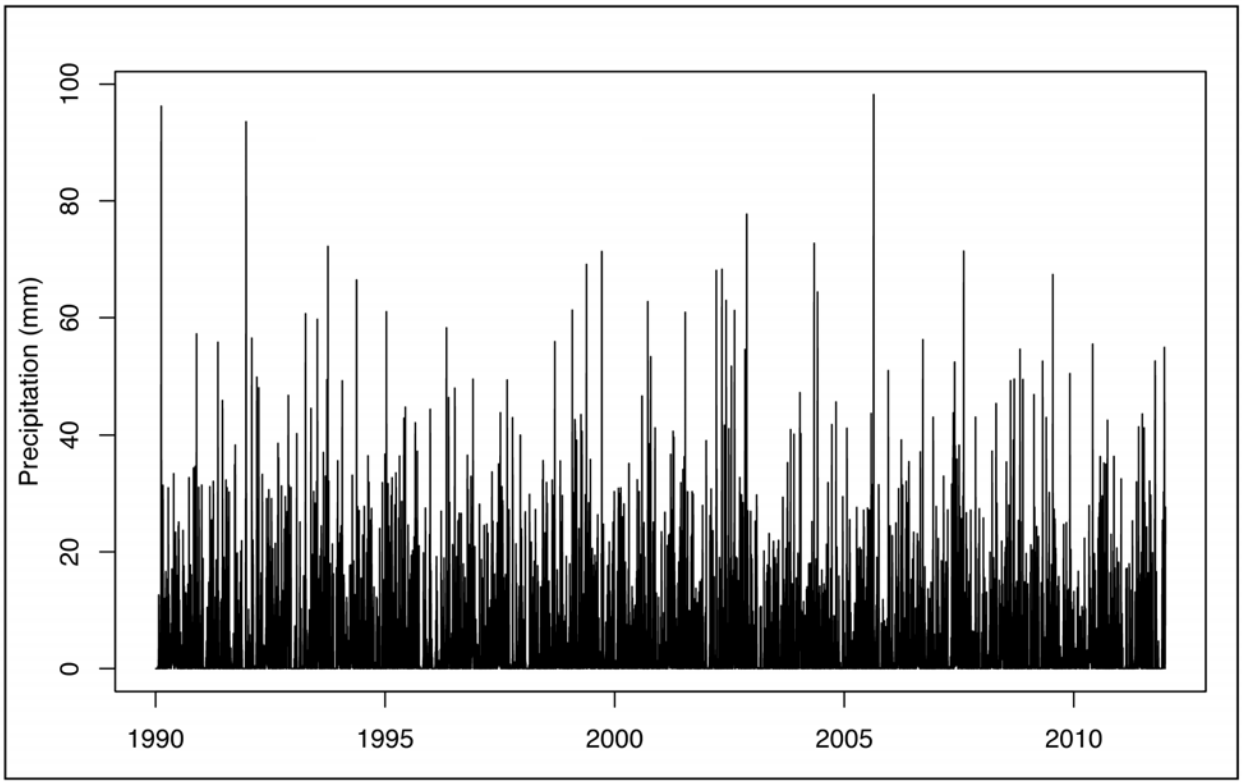

Fig 2.2 Daily Precipitation (in mm) in Brienz for the period of 1990-2015. Data from MeteoSchweiz

The boxplot shows monthly distribution of precipitation throughout the entire study period. As it can be observed, the months from May to August are characterized by highest amounts of precipitation, with May as the most variable month concerning precipitation distribution. The median of such months varies between 150 to 200 mm of rain, with a maximum value of around 380 mm reached in August. The lowest precipitation distribution is characteristic of the winter months (December to February), with the median located around 100 mm. In spite of this distribution, minimum precipitation are reached in October (around 0 mm), while maximum precipitation are given by an outlier event in November, which reached more than 400 mm of precipitation in a month.

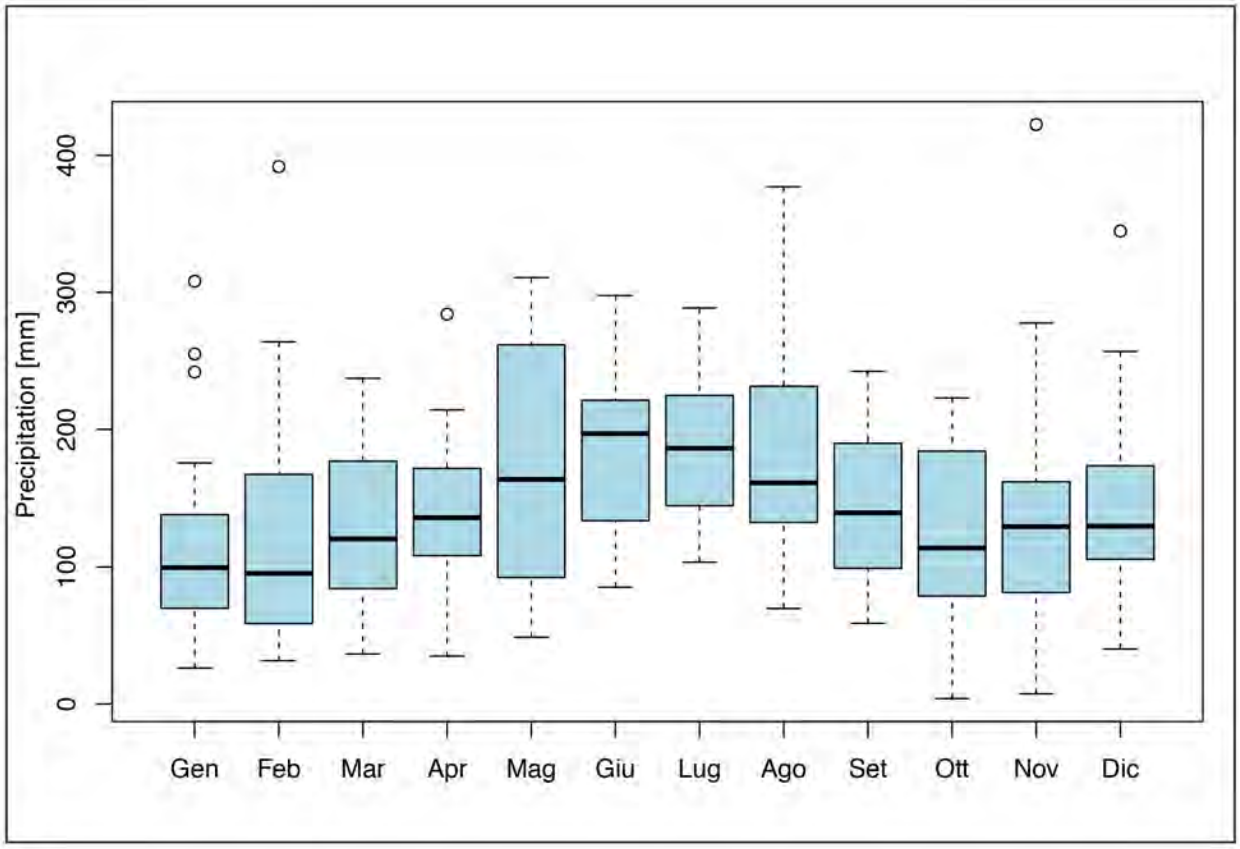

Fig. 2.3 Boxplot of monthly distribution of precipitation (in mm) of the period between 1990-2015 in Brienz. In the boxplot, the Median is shown by the black, thick line. Blue boxes indicate the distribution between the Lower Quartile (25th Percentile) and the Upper Quartile (75th Percentile). Dotted lines represent the Whisker, which is indicative for the variability outside the lower and upper quartiles. The lines at the end of the Whisker represent minimum and maximum values, while the circles are indicative for outliers or single data point outside the normal distribution.

Finally, Lake Brienz is also characterized by a specific type of wind, the Foehn, which blows from the Alpine range through the the lake and it is one of the strongest wind system present in the Alps (Adams et al., 2001).

2.4 Vegetation and Soil

As presented in section 2.1, the catchment around Lake Brienz is covered by 21% of forested area (Wüest et al., 2007). More specifically, the vegetation around the lake is mainly coniferous on its southern side and deciduous on the northern slopes (Swisstopo). The upper reaches (above 1400 m a.s.l) on the northern slopes are characterized a high erosive potential (around 500 t/ha/yr, Swisstopo),

with landslides, rockfalls and avalanches detaching and therefore affecting the stability of lower regions (Müller, 2007). Middle reaches are mainly forested, and are dominated by toppling, sliding and creep processes as well as from a network of channelized water system Finally, the lower reaches are mainly influenced by debris flow processes, with scree-slopes deltas and debris fans forming along the shores (Müller, 2007). In general, landslides around the Brienz settlement are relatively common events, recorded in both geological and historic records (Müller, 2007) since it is situated on debris fans of the Trachtbach and Glyssibach active catchments. The instability of the soil is also given by the geological structure.

2.5 Hydrology and Lake System

Lake Brienz is an open system, characterized by two main tributaries, the Aare and the Lütschine rivers, as well as by several lateral torrents. While the Aare and the Lütschine are responsible for the majority of the sediment load, drained by their large catchments, the role the lateral streams have on sediment input and therefore on sedimentation is neglectable (Sturm & Matter, 1978).

The lake occupies a volume of 5.17 km^3, is 14 km long and 3 km wide and is characterized by a flat, smooth and deep central basin, with a maximum depth of 260 m. Steep slopes (>30°) at the flanks of the lake cause a shallow, littoral zone (Sturm & Matter, 1978). The eastern and western ends of the basin are characterized by the two deltas formed by the Aare and the Lütschine, respectively (Matter & Sturm, 1982). Because of their high erosive force, the two tributaries created gullies, channels and levees in their deltas, which can reach 30 m deep and 200 m wide in the case of the Aare delta (Matter & Sturm, 1982). The lateral torrents, in turn, drain small, secondary catchments around the lake, therefore building narrow and steep alluvial fans at the lateral shores of the lake (Sturm, 1976).

Lake Brienz is an oligotrophic lake with an extremely low nutrient input caused by a small densely populated area and the scarce agricultural activities in the region (Finger, 2006; R. Müller, 2007). The dominant role of the two main tributaries in the sediment input can be observed from the large extent of their two deltas (Matter & Sturm, 1982). The Aare and Lütschine rivers transport the majority of the sediments from the glaciers located in the upper areas of their sub-catchments, with highest discharge in summer and spring (Sturm & Matter 1978) and lowest water-flow in winter, when the temperature in the catchments decreases below the freezing point (Finger, 2006). This massive input of clastic material gives the characteristic milky-grey colour of the water in the lake (Finger, 2006). Discharge pattern is characterized by a strong seasonality, as it is visible in Fig. 2.4, showing daily discharge for Aare river during 1990-2015.

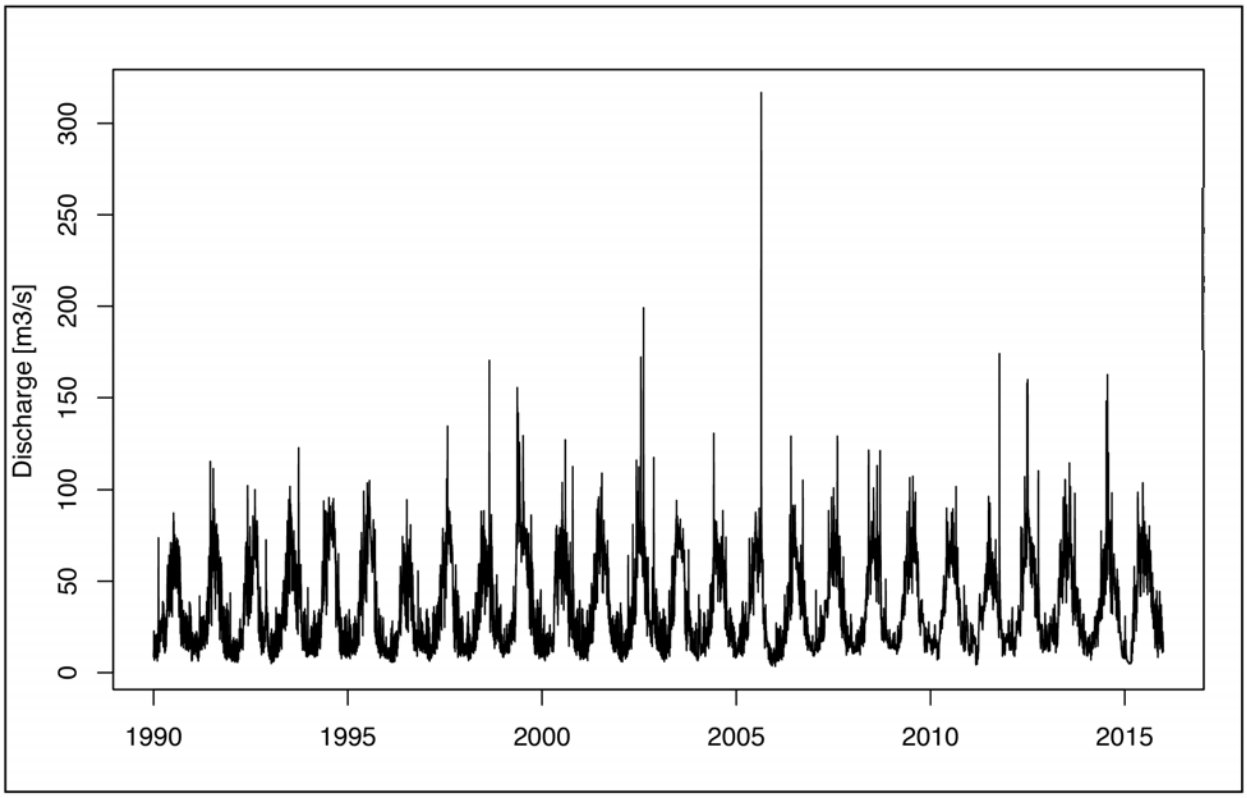

Fig. 2.4 Daily discharge (in m^3/s) for Aare river during 1990-2015. The plot clearly shows a high seasonal pattern, with higher discharge in the summer season and lower during winter months.

The following Fig. 2.5 highlights the seasonal character of Aare discharge. From the figure, the seasonal pattern is clear, with highest discharge (in blue) for the months from June to August. The lowest discharge (orange-red) is on the contrary characteristic for the winter months. As it can be observed from the colour, the maximum discharges were reached during the studied period in August 1995, May 1999, August 2005, and June July 2012. Interestingly, the highest discharge was not recorded in August 2005, but in May 1999. Lütschine shows a very similar discharge pattern as that shown in Fig. 2.4 and Fig. 2.5**,** only with lower discharge values.

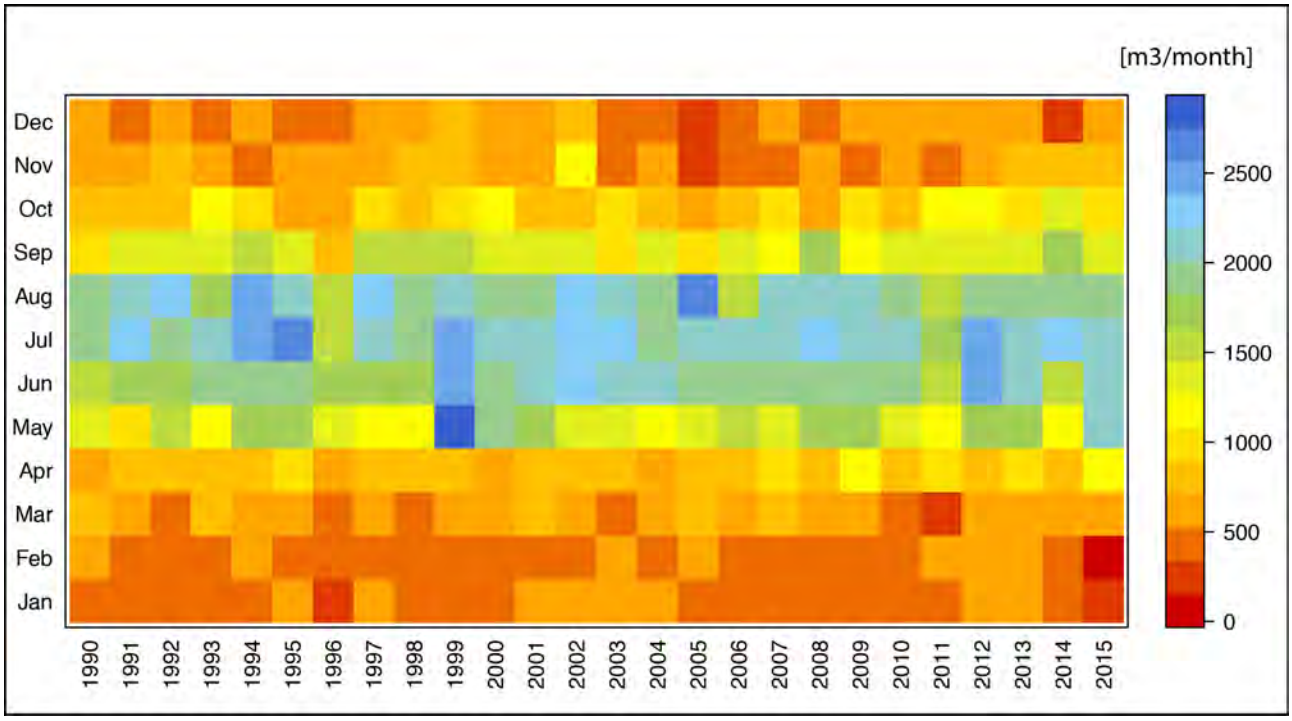

Fig. 2.5 Monthly distribution of discharge (in m^3/month) for Aare river, as recorded at Aare-Brienzwiler gauging station, for the period 1990-2015. Red-orange colours indicate lower discharge, while blue-greenish colours indicate higher discharge.

As stated before, the two main tributaries play a dominant role in the sediment input of the lake. With both catchments characterized with a nival-glacial regime given from the large percentage of glaciated areas (Finger, 2006), they differ however in the type of drained material. While the Aare river drains mostly crystalline material coming from the glaciers located in its upper catchment on the Aare Massif, the Lütschine river drains relatively small amounts of crystalline material, with a sediment input of sedimentary origin, and the material entering the lake is therefore composed by a large carbonate fraction (Sturm & Matter, 1978). Because of their geologically different catchments, the two tributaries are characterized by different lithological and mineralogical signatures (Sturm & Matter, 1978). The Aare and Lütschine differ also in term of discharge: the mean annual discharge of the Aare river lies around 35 m^3/s, with a maximum reached on the 22nd of August 2005 of about 444 m^3/s (Schulte et al., 2015). The Lütschine river, in turn, has a mean discharge of 18.8 m^3/s, with also a maximum reached on the 22nd of August 2005, when the discharge went up to more than 250 m^3/s (Schulte et al., 2009).

The lake is characterized as holomictic, with a thermal stratification occurring from April to October with a counter-clockwise movement of the water mass mainly driven by the continuous and powerful input of the Aare and the Lütschine, as well as by the Coriolis force (Nydegger, 1967). The pelagic sedimentation within the lake is largely influenced by density differences in the water column. The water density of the river is usually higher than the one of the basin, and therefore the waterflow will enter the lake as underflow (Sturm & Matter, 1987). However, if the water density and the suspended load transported by the rivers cause the water to be less dense than the lake basin, the river water will enter the lake as interflow or overflow (Sturm & Matter, 1987). This, in turn, causes the presence of a turbid layer / current to move along or above the thermocline. Turbidity currents are, as presented in the study from Sturm & Matter (1987), rare sedimentological events in the lake. When they occur, they flow on the bottom of the lake as underflow because of their higher density, and they are usually related to erosive processes.

2.6 Anthropogenic Impact on Lake Brienz

The area surrounding Lake Brienz is characterized by a low density population, with only 2% of the catchment inhabitated (Wüest, 2010). Despite the relative marginality of Lake Brienz, compared for instance to other alpine lakes such as lake Thun or lake Biel, the lake has been indirectly heavily impacted by anthropogenic activities throughout the last few decades.

Firstly, between 1866 and 1855 the Aare river was channelized, shifted south its natural flow and inflow (Sturm & Matter, 1978) and formed a new delta. Between 1929 and 1953, three dams were built for hydropower generation and water exchange in the upper Aare basin, specifically in Grimsel area: the Grimselsee, the Räterichsbodensee and the Obserarsee (Anselmetti et al., 2007), as shown in Fig. 2.6. The three basins, lying at an altitude of 1909, 1767 and 2303 m a.s.l, respectively (Thevenon et al., 2013), are connected by a network of pipelines (Anselmetti et al., 2007). Because the three reservoirs are fed directly from the Unteraar- and Oberaar Glaciers, the basins register low water level in winter and high water level in summer, analogous to the melting of the glacier (Anselmetti et al., 2007).

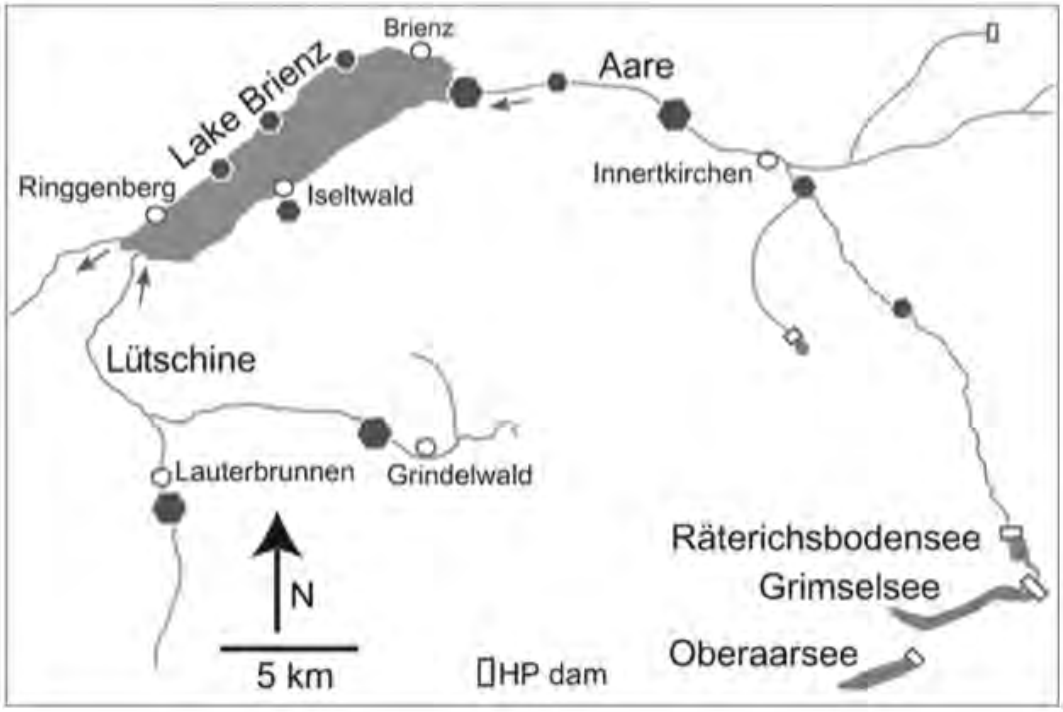

Fig. 2.6 The three hydropower stations (rectangles) and sewage treatment plants (exagon) in the area of Brienz. Modified after Wüest et al. (2007).

As presented from several studies in the area (Finger, 2006; Anselmetti et al., 2007) this extensive damming in the upstream region of Lake Brienz caused the retention of large amounts of sediments – more specifically the coarse fraction, with only 3% of fine particles (< 4 μm diameter) retained in the three basins. This, in turn, had important consequences on the sediment supply of the lake from the glaciers located in the area, drained by the Aare river. One of the consequences of this damming procedure is that the overall sediment input from the Aare was reduced by two thirds (Thevenon et al., 2013), with 232 kt/yr of material trapped in the three upstream basins (Anselmetti et al., 2007). As a consequence, despite the Aare discharge being twice as the Lütschine's discharge, the suspended annual sediment load coming from the Aare river is 26% lower than the ones transported from the Lütschine catchment, with 128 kt/yr against 174 kt/yr, respectively (Finger, 2006). The same study from Finger

(2006) showed that, in a hypothetical no-dams situation, the mean suspended particle load would be annually 2.8 times higher (360 kt/yr) than today (128 kt/yr). The decrease in particle concentration of the Aare, if combined with the low salinity (0.0069 g/kg, Finger, 2006) caused by the crystalline composition of its catchment, also lead to a lowering of the water density compared to the Lütschine (Finger, 2006). This, in turn, causes an annual particle input in the upper water column of the lake being dominated by the Aare riverflow (92.8 kt/yr vs 64.7 kt/yr for Lütschine, Anselmetti et al, 2007). Damming had consequences not only on sedimentation processes, but it caused an alteration of the seasonality of the Aare flow as well, with a shift of 17% of the annual water flow from summer season to winter (Finger, 2006; Anselmetti et al., 2007). As a result, winter season experienced an increase in turbidity, which in turn increased light attenuation in winter and decreased it in summer (Finger, 2006).

Another anthropogenic influence on Lake Brienz is determined by the construction in the 70s of sewage water treatment plants (Fig. 2.6), which strongly reduced phosphate concentration back to natural levels (Finger, 2006). This, combined with the light attenuation effect mentioned above, lead to a decrease in algae production which in turn caused a zooplankton and fishing yield decline (Finger, 2006). In 1999, for instance, fishermen registered a sharp decline in the local whitefish (*Coregonus* sp.) (Wüest et al., 2007).

As a conclusion Lake Brienz, despite its alpine characterization and marginal location, it is not absent from the consequences human activities have in the surrounding area.

3 Materials and Methods

3.1 Fieldwork

Two separated field campaigns for the sampling of cores from Lake Brienz took place in July and November 2015. Another excursion to the field was done in July 2016 in order to retrieve the fine sediment fraction from the different tributaries of the lake. During fieldwork, seventeen cores between 30 cm and 1 m length were taken along a W-E transect of the lake using an ETH gravity corer with PVC tubes of ~6 cm diameter. The cores were then stored and further analysed at the laboratories of the Geology and Geography Institutes at the University of Bern. Specific core locations and the bathymetric map of Lake Brienz are shown in Fig 3.1 and Tables 3.1 – 3.2.

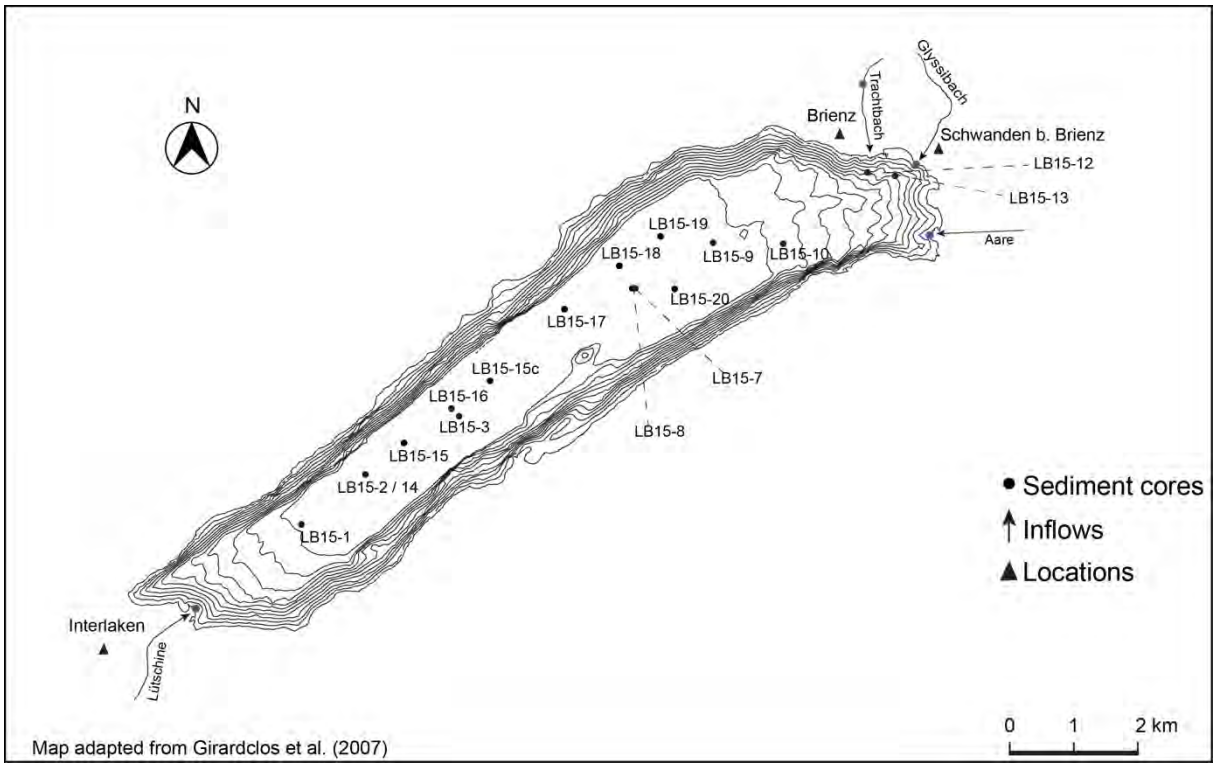

Fig. 3.1 Bathymetric map of Lake Brienz with sampling sites. Black dots represent sediment cores locations, blue dots represent fluvial sediments locations. Black triangles show the major settlements, while black arrows indicate the four inflows Aare, Lütschine, Trachtbach and Glyssibach. Map adapted from Girardclos et al. (2007).

Table 3.1 Name, coordinates and length of the cores. Coordinates are in CH1903 format

Core Name	Coordinates (CH1903)	Core Length (cm)
LB15-1	636776,172504	77.5
LB15-2	637766,173272	30.1
LB15-3	639216,174191	81.9
LB15-7	641945,176147	36
LB15-8	641913,176134	40.6
LB15-9	643148,176848	73.5
LB15-10	644234,176827	44.1
LB15-12	645539,177934	29.2
LB15-13	645965,177882	64
LB15-14	637766,173272	72.1
LB15-15	638360,173750	67.9
LB15-15c	639696,174720	105.4
LB15-16	639097,174273	45.9
LB15-17	640852,175824	80.5
LB15-18	641696,176489	87.3
LB15-19	642326,176936	57.4
LB15-20	642548,176132	32.4

Table 3.2 Name and coordinates of the rivers from which fine fraction samples were retrieved

River	Coordinates
Aare	2646516, 1177009
Lütschine	2635199, 117191
Trachtbach	2645489,1179209
Glyssibach	2646318, 1178115

3.2 Core Opening and Description

The whole-round unopened cores were first scanned with a Multisensor Core Logger at the Geology Institute of the University of Bern. The procedure is described in section 3.4.3. Subsequently, the cores were opened, wrapped in protective plastic film and stored in a core fridge at a temperature of 4°C in order to avoid biological contamination and oxidation.

3.2.1 Multi-Sensor Core Logger (MSCL)

In order to collect preliminary information about the physical properties of Lake Brienz, full cores were measured with a Geotek Multi-Sensor Core Logger (MSCL-S) at the Institute of Geological Sciences of the University of Bern (Fig. 3.2). The automated multi-sensor core logger (MSCL) is a widely used technique for the analysis of lacustrine and marine sediments, offering a continuous, rapid, non-destructive and highly-resolved measurement of their physical properties (Rothwell & Rack, 2006; Schultheiss & Weaver, 1992).

Fig. 3.2 A Geotek Multi-Sensor Core Logger (Geotek, n.d)

The apparatus measures a wide range of parameters, such as p-wave velocity and attenuation, gamma density, magnetic susceptibility, and line-scan imaging. Other sensors can be added separately. Following, a short description of the parameters used for this project:

3.2.1.1 Gamma Density

In order to measure bulk density, a gamma-ray source (^{137}Cs beam) emits photons across the core, which are then detected on the opposite side. The result of the measurement, which is the degree of scattering or the attenuation of photons through the core, provides indications on the density of the material, as well as of porosity changes along the cores (Geotek, n.d)

3.2.1.2 P-wave Velocity

This parameter can also be an indicator of porosity, lithology and pore-fluid content (Schultheiss & Weaver, 1992). It is also useful for the identification of grain-size variation following variations in acoustic properties (Croudace & Rothwell, 2015).

3.2.1.3 Magnetic Susceptibility

Per definition, magnetic susceptibility is "*the degree of magnetization of a material in response to an applied magnetic field*" (Geotek, n.d), and mirrors the concentration of magnetite and magnetically susceptible minerals in the cores (Schultheiss & Weaver, 1992). In lake sediments, variations in magnetic susceptibility usually represent changes in the amount of allochtonous, inorganic material in the sediments (Thompson et al., 1975). This parameter is therefore used as an indicator for turbidites, as well as for correlation between cores (Croudace & Rothwell, 2015).

3.2.1.4 Linescan Imaging

In this project, all the un-opened cores were scanned, and the parameters described above were measured at a resolution of 0.5 cm along the entire length of the cores. Shortly after the opening of the sediment cores, the Geotek's MSCL-S was used again in order to obtain a visual record of the split

sections through the *Linescan Imaging* sensor. The sensor provides 48-bit RGB images and profile data of the core-halves (Geotek, n.d). If the cores are scanned shorter after the opening, the images produced by the Geotek apparatus provide visual information about oxidation states of the core and help defining lithological units (Croudace & Rothwell, 2015). Data retrieved from MSCL scan are presented in the Annex (Tables A.1.1-A.1.6)

3.2.2 Core Description

Once opened, the cores were analysed and described in order to retrieve a catalogue of the different sediment types present in the lake and to distinguish between flood layers and background sedimentation. For this purpose, a sedimentological and lithological description was conducted on all the split cores, with a focus on two representative cores for the Aare (LB15-8) and the Lütschine (LB15-14) signal.
The analysis was performed following the procedure defined by Schnurrenberger et al. (2003). A first step consisted of a macroscopic observation of the sediments. For this purpose, the following characteristics were taken into consideration:

- **SEDIMENT COLOUR AND TEXTURE**: sediment colour was described using a Munsell Colour Chart, while texture was determined rubbing small amounts of sediments between the fingers. Smear slides were also used in order to determine roundness and sorting of the sediment particles

- **SEDIMENTARY STRUCTURES:** differences in sedimentation throughout the cores were described in order to distinguish between event layers and the background sedimentation

- **LAMINATION AND THICNKESS:** thickness of the different bedding structures was visually observed and described, and laminations were identified along the cores

- **BEDDING PLANES:** the contacts separating different lithological units were determined in order to distinguish between erosive contact (caused by higher sedimentation processes) and constant deposition, which could help identify event layers

- **CORE DISTURBANCES**: finally, the cores were observed in order to determine the presence of disturbances caused by the coring process, such as deformation of beds and gas expansion

3.3 Flood Layer Correlation

In order to further proceed with targeted analyses on the 2005 event, a visual core correlation and flood layer identification was firstly carried out. The highly-resolved core images were arranged following the SE-NW transect of the lake, and the sediment description was used to visually compare and distinguish between event layers and background sedimentation. In order to identify the 2005 event, studies from Anselmetti et al. (2007) and Wirth et al. (2011) were used and the cores compared to the ones of the present study. This, combined with the previous core descriptions, allowed the author to being able to identify with a high degree of confidence the 2005 flood event on nine cores, which were then used for further analyses described in the following sections.

3.4 Micro X-ray Fluorescence (μXRF)

3.4.1 Introduction to μXRF

X-ray fluorescence (XRF) core scanning is a non destructive technique which, provides high-resolution records of the elemental (geochemical) composition of terrestrial, marine and lacustrine sediments (Jansen et al., 1998; Croudace et al., 2006). The technique of X-ray fluorescence spectrometry consists in the bombardment of the material with high-energy gamma rays. When gamma rays are absorbed by atoms, an electron is ejected from the inner shell (K shell), causing the atom to be in an excited state. The resulting vacancy is then filled by another electron falling from an outer shell. The energy difference between the outer and inner shells is then emitted in the form of secondary electromagnetic (fluorescent) radiation (Richter et al., 2006). Since the wavelengths of emitted X-rays are characteristics for each element, X-ray fluorescence can provide information on the elemental composition of sediments (Richter et al., 2006).

Modern scanners allow rapid and continuous measurement and analysis on split sediment cores, reporting variations in elemental and sediment properties throughout the core, and therefore providing information on textural and geochemical characteristics of the studied sediments (Croudace et al., 2006). For this reason, XRF core scanning has several applications, such as stratigraphic interpretations, investigation of terrigenous allochtonous input provenance and patterns and the identification of sedimentological events and their lithologies (Richter et al., 2006; Rothwell et al., 2006). In this project, the technique is in particular useful for the identification of turbidites along the core as it has been shown on previous studies (Richter et al., 2006; Moreno et al.,2008; Czymzik et al., 2013;). This technique is widely used for correlation studies of specific events, and can provide bases for further analyses on the studied samples (Croudace et al., 2006; Richter et a., 2006).

In this project, an ITRAX core scanner at the Institute of Geology of the University of Bern was used to perform the analysis (Fig. 3.3). The unique characteristic of this scanner is that it allows, through a micro-X-ray beam, a micro-XRF analysis at higher resolution (Croudace et al., 2006). With this apparatus, an optical camera system generates digital images of the sediment surface before the x-ray scan (similar to the line scan of the MSCL scanner described above). Depending on the chosen range of analysis, a Molibdenum (Mo), Rhodium (Rh) or Chromium (Cr) tube is used to generate X-rays, which focus on a 20 x 0.22 mm rectangular beam (Croudace & Rothwell, 2015). The ITRAX core scanner provides, for each scan, a RGB digital image, a highly-resolved micro-radiographic image (up to 200 micrometer spatial resolution) and a micro-X-ray elemental profile for the sediment core (Croudace, 2006; Kylander et al., 2011). The scan detects a wide range of elements, from Si to U (Rothwell et al., 2006). For each measurement point, which is given in number of counts, peak areas are calculated and their amplitude is given as proportional to the concentration (in ppm) of elements in the sediment (Croudace et al., 2006; Cuven et al., 2010). However, peak area can also be influenced by the sediment matrix, which implies that X-ray fluorescence analysis does not provide absolute concentration values for the studied elements. Therefore, geochemical data have to be considered as semi-quantitative results (Cuven et al., 2010).

Compared to conventional systems such as Wavelenght dispersive X-Ray fluorescence (WD-XRF), the ITRAX core scanner provides a non-destructive, highly resolved and faster analysis of split sediment cores, and it is therefore a preferable and reliable procedure.

Fig. 3.3 An ITRAX XRF Core scanner (Cox Analytical System, n.d)

3.4.2 Procedure

In the present study, a 40 kV voltage and 20mA current molybdenum tube has been used for the analysis of the cores. A high-resolution scan has been performed on the 2005 event layers of nine cores, with a selected step size of 0.5 mm, and a count time of 20s for each step. Aside from the high-resolution procedure, a low-resolution scan (2.5 mm every 20 s) was performed on representative cores for the Aare and Lütschine signal. For the Lütschine signal, LB15-14 was scanned along its entire length. Concerning the Aare signal, a composite section from LB15-18 and LB15-8 was used in order to obtain a full-length scan.

The cores' surfaces were first cleaned with a glass slide in order to smooth the surface and avoid irregularities, and pieces of paper were used to cover air-induced holes in the core. A thin protective film (4 μm thickness) was then placed on the split cores' surfaces to protect the sensor from possible contamination. The machine provided concentrations for 48 elements.

Between the wide range of elements which were analysed by the ITRAX core scanner, a further selection of specific elements was applied. This was done in order to differentiate the different turbidites present in the core, and specifically the 2005 event layer, from the background sedimentation. A particular focus was also given to elements, which could be representative for the two catchments of the Aare and Lütschine. A detailed research in the literature provided information about elemental proxies for turbidites and grain size, as well as for the Aare and Lütschine signal. In Table 3.3, the chosen elements are listed.

Table 3.3 Elemental proxies for detrital layers, grain size changes, Aare and Lütschine signal as retrieved from the literature.

Proxy	Elements	Reference
Detrital layers	Al, K, Rb, Mn, Si, Ti, Zr	Croudace et al., 2015 Cuven et al., 2010
Grain size changes	Sand, coarse fraction: Zr, Si Silt: Ti Clay (Fine fraction): Rb, K Zr/Rb, Zr/K	Croudace et al., 2015 Cuven et al., 2010
Aare signal	Phyllosilicates: Fe, Al, Ti, Mn, Fe Granites (crystalline): Zr Others: Rb,K K/Ti Rb/Sr	Schulte et al., 2015
Lütschine signal	Alluminosilcates: Al, Si, Fe, Ca Phyllosilicates : Fe, Ti, K, Mg Ca/Rb	Schulte et al., 2009

All the different element profiles were plotted and studied, in order to retrieve representative elements and elemental ratios for the two catchment's fingerprints.

3.4.3 Statistical Analysis of XRF Dataset

3.4.3.1 Dataset Compilation

From the range of elements listed in section 3.4.2, two datasets were created for further data processing and statistical analysis. The first dataset contains the potential characteristic elements for Aare and Lütschine signal, while the second dataset is characterized by elemental ratios representative for grain size, Aare and Lütschine signal (Table 3.4).

Table 3.4 Dataset 1 and 2, containing representative elements for Aare, Lütschine and grain size (1) as well as representative ratios (2)

Dataset 1	Dataset 2
Mg, Al, K, Ca, Ti, Mn, Cu, Fe, Rb, Sr, Zr, Si	Zr/Rb, Zr/K, K/Ti, Ca/Ti, Ca/Rb, Rb/Sr

3.4.3.2 Data Visualization

Elemental profiles of the two datasets D1 and D2 were plotted for each core using R software with the aim of obtaining a visual representation of the most suitable elements characterizing the catchment's fingerprints.

3.4.3.3 Statistical Analysis of the Dataset

Exploratory analyses were carried out on the dataset D1 in order to reduce its dimensions and therefore to identify and assess characteristic elemental profiles for Aare and Lütschine. The dataset was first

standardized in order to obtain a mean equal to 0 and a standard deviation of 1. A test for normality was performed on the dataset, which resulted to be non-linear. Following, a correlation analysis and a Principal Component Analysis (PCA) analysis on the standardized dataset was performed for all the 9 cores.

The aim of the correlation analysis was the identification of associations between the different variables and the assessment of the strength of their relation. For this analysis, a Spearman rank correlation was performed on the dataset. The choice of Spearmans' method was determined by the non-linearity character of the dataset. Spearman's correlation is applicable to trace and major elements and it is measured on a rank scale (Rollinson, 2013). Correlation analysis allows to retrieve a correlation coefficient (r_s) between to variables (Rollinson, 2013). The correlation can be either positive or negative: a positive correlation indicates that high levels of a variable x is followed by high values of variable y, while a negative correlation indicates the opposite. The correlation coefficients vary between +1 and -1, representing the strength of the correlation between variable x and y, with higher (positive or negative) values indicating a higher relation. Values equal to zero indicates no correlation between variables. In this project, the correlation analysis was performed in order to retrieve groups of elements related to each other and representing therefore the lithological composition of the catchments.

The Principal Component Analysis was performed on the dataset D1 as exploratory analysis, with the aim of further reducing the dimensionality of the data, allowing to highlight the elements characterizing the catchments' fingerprints. Because PCA performs the analysis without assuming a structure in the dataset, it is usually performed on geochemical data in order to detect and differentiate between different geomorphic processes, as well as for sediment source identification (Rollinson, 2013; Rothwell & Croudace, 2015). The broken stick method was used in the analysis in order to identify the number of relevant principal components. The principal for each core were finally listed, as well as their loadings.

3.5 Smear Slides

3.5.1 Introduction to Smear Slides

Smear-slides analysis is an analytical tool often used in sedimentological studies as their observation provides information about sedimentary components and lithologies, facilitating the characterization of the major components of the sedimentary matrix within a basin and providing further information on past depositional environments, ecology and geochemistry (Rothwell, 1989; Myrbo, 2007). This type of analysis is often used to semi-quantitatively determine, for instance, the mineralogy, the grain-size distribution and the abundance of organic matter, providing not only information for core description, but also the basis for interpreting instrumental data generated from further or previous sedimentological analysis such as (micro-)XRF and grain size (Myrbo, 2007).

3.5.2 Procedure

To perform smear-slide analysis, the expected 2005 event was sub-sampled at 2.5 mm intervals for all the nine cores. For each sample, a very small quantity of sediment was sampled using a toothpick and put on a standard microscope glass slide. A drop of distilled water was then added to the sample, which was subsequently homogeneously smeared on the slide with the toothpick. The slide was then let to dry until the distilled water was completely evaporated. A drop of Norland 61 optical adhesive was then added in the middle of the smear slide, and a cover glass was placed on the adhesive. The samples were

then transferred under a UV-light for 2-3 minutes for hardening. Other samples were also taken from different lithotypes present along the cores.

Smear slides were analysed with an Olympus BX 41 microscope at the Institute of Geology. A cross-polarized filter was applied in order to better detect the crystal structure of the samples and to identify carbonates.

3.6 Grain Size Analysis

3.6.1 Introduction to Grain Size Analysis

Grain-size distribution (or particle-size distribution, PSD), representing the percentage of total dry weight of particles of a determined size fraction (Di Stefano et al., 2010) is an important physical property of sediment. It influences pore distribution, water conductivity, water retention, and other thermal and sorption properties of the sediment (Ryzak & Bieganowski, 2011). In sedimentology, particle-size distribution is a property of great interest, often used in palaeoflood studies as proxy for such events, with coarse-grained layers representing higher discharge and sediment input (Sperazza et al., 2004; Cockburn & Lamoureux, 2008; Schillereff et al., 2014). The mean, median and the degree of sorting of particle size in event layers is also often used to distinguish between river floods, snow avalanches and mass-movement deposits (Arnaud et al., 2002; Czymzik et al., 2010; Vasskog et al., 2011).

In order to measure PSD, several sedimentation methods can be used. Traditional methods include sieve, pipette and hydrometer as most common ones, as well as electrozone sensing and X-ray absorption (Sperazza et al., 2004). However, these techniques have the disadvantage of being time consuming and imprecise, with reported errors going up to 40% for the sieve and pipette methods (Sperazza et al., 2004).

In this project, particle size was analysed with the laser diffraction method (LDM). This method has been increasingly implemented in the last few decades (Sperazza et al., 2004), and it is now recognized as a standard sedimentological analysis (Sperazza et al., 2004). Laser diffraction is a much more reliable, faster and precise technique than the classic methods (Ozer & Orhan, 2015). Moreover, LDM covers a wide range of grain sizes, determining PSD in the size range between 0.2 and 2000 micrometres (Ozer & Orhan, 2015). Finally, it requires small amount of samples (between 100-200 mg of material for the analysis, therefore being more suitable for a rapid and accurate analysis of large amounts of sediment samples (Bauselinck et al., 1998). The laser diffraction method is based on the principle that particles of different sizes scatter light through different angles (Di Stefano et al., 2010), and the angle at which the light is scattered is inversely proportional to the particle size (Ryzak & Bieganowski, 2011). Laser scattering systems emit a laser beam of known wavelength through the material, and measure the intensity and angular distribution of the diffracted light by the particles in suspension in the material (Sperazza et al., 2004; Ryzak & Bieganowski, 2011). The scattering pattern read by the detectors represents the sum of the scattering pattern of all individual particles (Escubed Ltd, n.d). An important parameter, which has to be taken into consideration while using the laser diffraction method, is the obscuration. Per definition, the obscuration is "*the degree to which the light from the laser beam is obscured by the particles being measured*" (Ryzak & Bieganowski, 2011), whose value is recommended to be between 10-20% (Ryzak & Bieganowski, 2011). If the value is situated below 10% and above 20%,

no reliable results will be obtained because the number of particles in the sample would be too small or too large (and therefore the risk of a secondary refraction increases), respectively.

3.6.2 Procedure

In this project, a Malvern Mastersizer 2000 laser diffractor apparatus with Hydro Mu adapter from the Geography Institute of the University of Bern was used (Fig. 3.4). The machine uses two different sources of light, red and blue, with wavelengths of 633 and 466 nm, respectively (Sperazza et al., 2004; Di Stefano et al., 2010; Ryzak & Bieganowski, 2011) and it records the diffracted beam into 52 detectors (Sperazza et al., 2004).

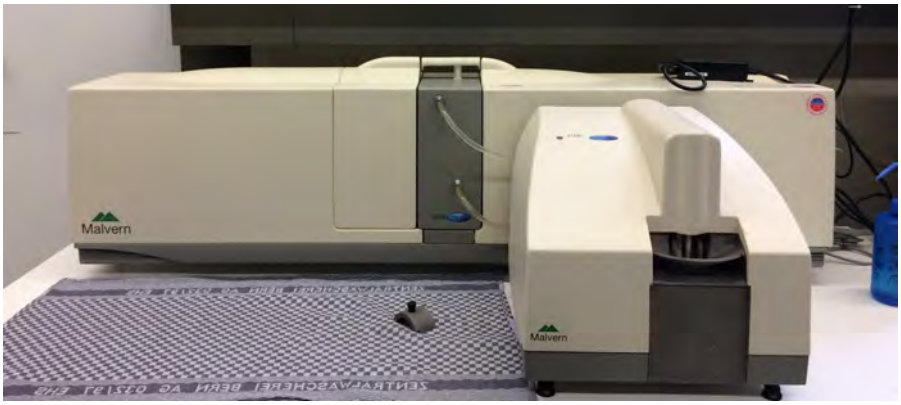

Fig. 3.4 Malvern Mastersizer, University of Bern (D. Motta, 2016)

Concerning the sampling, the 2005 layer in the 9 cores was sub-sampled at 2.5 mm intervals, resulting in a total of 90 samples. All the sub-samples were then freeze-dried for 25 hours at 0.053 mbar and -54°C. The dried sub-samples were then gently crushed, weighted and stored.
In order to determine particle-size distribution, sediment aggregates need to be dispersed: if insufficiently broken up aggregates disintegrate during the measurement, they most likely will change the properties of the sample (Ryzak & Bieganowski, 2011). In order to avoid aggregation and flocculation, which lead to instability and lack of data reproducibility, these natural aggregations have to be broken down before the measurement starts (Ryzak & Bieganowski, 2011). For this purpose, a chemical dispersion method was carried out, which consisted in the application of 500 ml of a dispersion solution on the samples. The dispersion solution is obtained adding 16.5 g of Sodium-hexametaphosphate $(NaPO_3)_6$ to 3.5 g of Sodium Carbonate (Na_2CO_3). The mixture is then filled up to 500 ml with milli-Q water. A magnetic steering-tool was used to homogenise the solution.
In order to assess the optimal sample amount readable from the laser diffractor, a test run was carried out on two samples. Because of the two different fingerprints of the two main inflows Aare and Lütschine, the two samples of 400 mg each were taken from two different cores (LB20, LB14) representing the Aare and the Lütschine signal, respectively. In order to get representative sub-samples for both clay and sand, for LB14 two samples were chosen, one at 13-13.25 cm (clay) and one at 15-15.25 cm (coarser sand). Because no grading is visible on the core representing the Aare signal, just one sample at 15-15.25 cm was chosen. Finally, the test suggested an optimal sample amount of 200 mg. All the samples were then weighted again and measured with the Malvern Mastersizer, with an obscuration level between 10 and 20%.

3.7 Total Inorganic Carbon Analysis

3.7.1 Introduction to Carbon Content Analysis

Carbon content analysis is a common procedure on soil samples. Lake sediments accumulate three different forms of carbon, such as elemental, organic and inorganic carbon (Schumacher, 2002). Those three forms of carbon differ in their sources, with elemental carbon forming as a result of incomplete combustion of organic matter (e.g. charcoal, graphite), organic carbon forming after decomposition of animals and plants (e.g. humus, leaves) and inorganic carbon deriving from geologic sources and mostly present in the sediments as carbonate ($CacO_3$) and dolomite [$CaMg(CO_3)_2$] (Schumacher, 2002).

Because of the dependency of inorganic carbon from geology, total inorganic carbon (TIC) is used in this project in order to differentiate the different sub-catchments surrounding Lake Brienz. Specifically, it is expected to measure higher TIC concentration in cores presenting a Lütschine signal (more carbonate bedrock in its catchment) than the ones presenting an Aare signal (more crystalline bedrock in the catchment). For this purpose, a Carlo-Erba NA 1500 at the Geology Institute of the University of Bern was used (Fig. 3.5). This instrument allows the determination of total carbon and total nitrogen from organic and inorganic samples such as soil, plant tissues and fertilizers, for example (Stanford, n.d).

Fig. 3.5 Carlo-Erba NA 1500 at the Institute of Geology, University of Bern (D. Motta, 2016)

The apparatus follows the method of flash combustion, which oxidises the chosen sample and subsequently converts it into a combustion product (gases). Tin cups containing the sediment samples are put in a combustion tube at 1000°C, filled with helium (He) as carrier gas and temporally filled with O_2. The melted tin reacts with the oxygen, resulting in the oxidation of all the substances contained in the sample and to the formation of combustion products such as CO_2, SO_2, H_2O, N_2 and NO_x. These combustion products are then transported to the Thermal Conductivity Detector by helium as carrier gas. Here, nitrogen oxides and oxygen are reduced, water is absorbed and N2 and CO_2 are separated. In

the Thermal Conductivity Detector (TCD), the concentration of N and C is derived (the TCD produces an electric signal, which is proportional to the concentration of N and C) (Stanford, n.d; Radboud University, n.d). Similar methods, such as Dumas and Kjeldahl, are similar and can therefore be used as well. However, the Elemental Analyser and its flash combustion give fast, reliable and reproducible results, with no production of dangerous waste (Stanford, n.d).

3.7.2 Procedure

3.7.2.1 Total Carbon, Total Nitrogen and Total Sulphur

For this analysis, two different sampling procedures were performed. Firstly, sub-samples from the 2005 turbidite were taken at 2.5 mm intervals. All the samples were freezed and then freezed-dried. Because of the need of homogeneous and uniform composition of the sediment samples, a second step consisted in their grinding until a dust-sized homogenised sample was obtained. The last step consisted in weighting each samples using a micro-balance in order to have around 4 mg of material per sample. All the weighted samples were then inserted into tin cups, folded and subsequently measured (Fig 3.6).

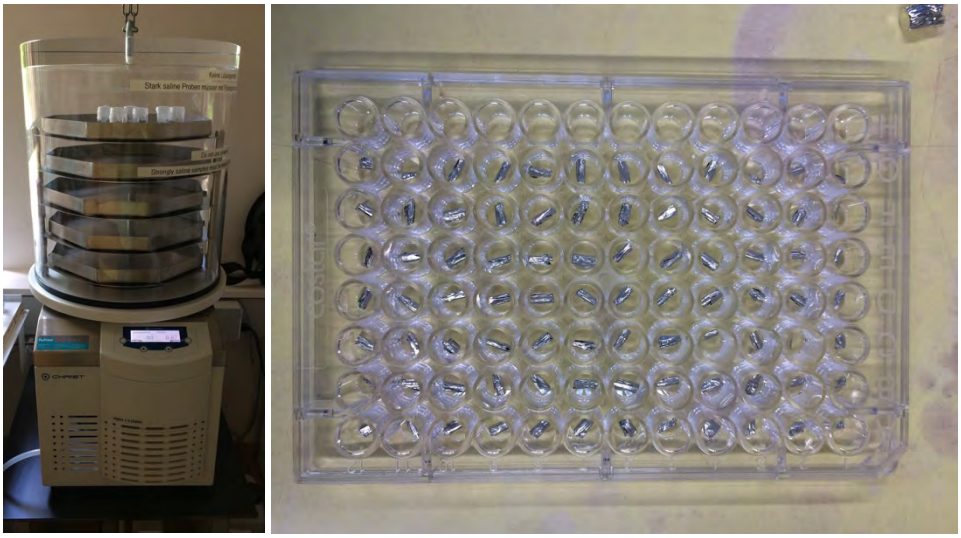

Fig. 3.6 Freeze-drier at the Institute of Geology at the University of Bern (left); Tin folded capsules containing sediment samples (right) (D. Motta, 2016)

In order to try determining the contribution of the different tributaries on the turbidite, samples containing the fine fraction transported from the four tributaries of interest were taken from the rivers (Aare, Lütschine and Glyssibach deltas and Trachtbach riverbed). This was with the aim of comparing the carbonate content of the different inflows with the signal measured in the turbidite. Because the samples contained a large range of grain sizes and not only the fine fraction, a sieving procedure was applied in order to separate pebbles (> 2mm diameter), coarse sand (> 600 µm), fine sad (63-600 µm) and silt (< 63 µm). Clay-size particles (< 2 µm) were not present in the samples. All the samples containing the different fractions were dried overnight in an oven at the Limnology laboratories of the University of Bern, at a temperature of 60°C. The choice of the oven for the drying procedure was based on two criteria: firstly, the procedure was less time-consuming than the freeze-drying process, which requires the samples to freeze first and then be dried. Secondly, since the aim was to measure inorganic carbon, a delicate procedure such as freeze-drying – which does not compromise the organic matter present in the samples – was not needed. Finally, in order to obtain the representative particle composition of the different inflows, the silt and fine sand fractions were combined and ground. From

all the samples, 4 mg of material was then inserted into the tin cups, folded and measured. The output data are expressed as concentration (%).

3.7.2.2 Total Organic Carbon

In a second step, Total Organic Carbon (TOC) was measured. For this procedure, 4 mg of ground samples were inserted into silver capsules, and phosphoric acid (H_3PO_4) was added in order to completely dissolve organic carbon. After the $CaCO_3$ was completely dissolved, the Ag capsules were then folded and inserted in tin capsules. The same procedure described above was then used to measure TOC on tin capsules. Also for TOC, the output data are expressed as concentration (%). In order to retrieve TIC concentration, the following calculation was applied:

$$TIC\ (\%) = TC\ (\%) - TOC\ (\%)$$

All the measurements for TC, TN, TS and TOC were executed by Julijana Krabnjevic at the Geology Institute of the University of Bern.

3.8 Hydrological and Precipitation Analysis

Aside from the different sedimentological and mineralogical analyses presented in the previous sections, an analysis of discharge and precipitation during the 2005 event was also carried out in order to retrieve the temporal succession of the event.

3.8.1 Precipitation Analysis

Precipitation analysis was carried out based on a RHiresD grid-data product from MeteoSchweiz, containing daily precipitation totals from the rain-gauge network of Switzerland from 1961 to present. This dataset, provided by the Geography Institute of the University of Bern, was used for time-series analysis of precipitation in the catchment.

In principle, a second dataset containing hourly precipitation would have been used in order to have a more detailed overview of the amount of precipitation fell in the catchment during the event. However, such data only existed for 2005 for the area surrounding Interlaken. Measurement in Brienz only started in 2009.

A detailed time-series analysis of daily precipitation data was performed for the RHiresD dataset using the hydroTSM package of RStudio. With this package, monthly, yearly and seasonal values of precipitation were extracted. A time series analysis of monthly data was performed, and the trend and seasonal component was defined and isolated. Monthly values were also used to calculate the distribution of rain for all the time period going from 1961 to 2011. Monthly time series and boxplot were then created in order to get an overview of precipitation distribution and variation throughout the years. Annual precipitation values were plotted mainly for visual purposes. A seasonal analysis was then performed on the dataset, extracting the mean values and mean distribution for winter (DJF), spring (MAM), summer (JJA) and autumn (SON) in order to visualize the time evolution of the seasonal precipitation values.

3.8.2 Hydrological Analysis

A hydrological analysis was performed in order to assess the temporal succession of the discharges and peak discharge during the event. For Aare and Lütschine river, two separated datasets were used. The first dataset contains daily discharge from 01-01-1974 to 20-11-2015, which was measured at the gauging-stations of Aare Brienzwiler and Lütschine Gsteig. A general analysis of daily, monthly and annual discharge was performed on this dataset. A second dataset from the same gauging stations contained 10-min discharge measurements, and was used for the analysis of temporal succession of Aare and Lütschine discharge. Both datasets were provided from MeteoSchweiz.

While Aare and Lütschine discharge is continuously measured from the two gauging stations, continuous observations for Trachtbach and Glyssibach discharge do not exist. For this reason, a discharge and precipitation model for the catchments of the latter torrents was provided from the Hydrology Group of the University of Bern (Ole Rössler). As a result, hourly precipitation and discharge data were retrieved for the two streams, and were used to determine the temporal succession of their peak discharges. Data are presented in the Annex (Tables A.1.1 and A.1.2).

A similar analysis as for precipitation data was performed on discharge data from Aare and Lütschine. Through the hydroTSM package, daily discharge data were aggregated into monthly, annual and seasonal data in order to have an overview of water-flow characteristics and variations throughout different time periods. Monthly distribution of discharge for the entire time period (01-01-1990 to 31-12-2015) was calculated, and annual, seasonal discharge time series were plotted for visual purposes. Boxplots of monthly and seasonal discharge were plotted in order to visualize the distribution variation in different seasons.

The dataset containing 10-min discharge measurements was plotted for 20-24th of August for both Aare and Lütschine, in order to retrieve the temporal succession of the two inflows during the event. The same plots were created for the hourly discharge of Trachtbach and Glyssibach. Following, hydrographs for the 20-24th of August time period were created with the aim of assessing the runoff response to the extreme precipitation event.

4 Results

4.1 Sediment Description

Figure 4.1 presents the sediment description for Cores LB15-14 (Fif. 4.1a) and LB15-18 (Fig. 4.1b), which are considered representative cores for Lütschine and Aare input, respectively. The choice of the two cores was determined by their lengths and therefore by their ability of representing the two catchment's sedimentary signals. Along the cores, five lithotypes (from I to V) were distinguished and differentiated between each other.

Regular Background Sedimentation (Lithotype I)

LITHOTYPE I defines fine-grained background sedimentation. The normal background sedimentation within the core is characterized by a succession of light bluish grey (HUE GLEY 2 7/10B) laminations of silty clastic material and dark bluish grey (HUE GLEY 2 4/10B) laminations of allochtonous detrital origin. Thickness of laminations is on a millimetre to sub-millimetre scale for both cores.

Event Layers (Lithotypes II-V)

Event layers differentiate from background sedimentation from colour, grain size and thickness of layers.

LITHOTYPE II defines deposits of 2 to 5 mm thick, which present a faint normal grading. Grain size is mainly represented by silt and fine sand. The source of these thin layers can be related to small flood deposits coming from the smaller, lateral torrents. Colours differ depending on the detrital layer, varying from greyish brown (HUE 2.5Y 4/2, especially LB15-14) to very dark greyish brown (HUE 2.5Y 3/2, especially LB15-18), to dark grey (HUE 2.5Y 4/1), to very dark-grey layers (HUE 2.5Y 3/1). This lithotype is interpreted to represent turbidite deposits reflecting small-to-medium flood events.

LITHOTYPE III represents thick graded deposits of more than 5 mm. While for LB15-14 the maximum thickness lies around 3-4 cm, LB15-18 counts a maximum thickness of 10 cm (related to the 1996 turbidite, Girardclos et al., 2007). These deposits are also characterized by a coarser grain size, from silt to medium sand. Such deposits present a much more visible grading, which can be either normally or inversely graded depending on the deposit. The sedimentological process behind these deposits is related to turbidity currents caused by either increased discharge of the main tributaries (major floods, **LITHOTYPE IIIA**) or by mass-movements within the lake (**LITHOTYPE IIIB**) (T. Mulder et al., 2001). For Lithotype IIIA, LB15-14 and LB15-18 present differences in colour. While most of the graded deposits for LB15-18 are characterized by a greyish brown- dark greyish brown colour (HUE 2.5Y 5/2-4/2), LB15-14 also contains very dark grey layers (HUE GLEY 1 3/N). Lithotype IIIB is mainly characteristic for the mass-movement induced turbidite of 1996 (Girardclos et al., 2007), which is characterized by a coarser base and an overlying fining-up sequence with a thick rather homogeneous central part capped by a thin clay layer. Such a sequence is composed by coarse grey sand at the bottom (HUE GLEY 1 5/N), which fines up into a light grey silt (HUE GLEY 1 7/N) and finally to a white clay top (HUE GLEY 1 8/N).

LITHOTYPE IV represents thick and ungraded deposits, which are characterized by medium to coarse very dark-grey sand (HUE GLEY 1 3/N). This lithotype is characteristic only for one layer within the LB15-14 and it is interpreted to be deposited by a Lütschine flood.

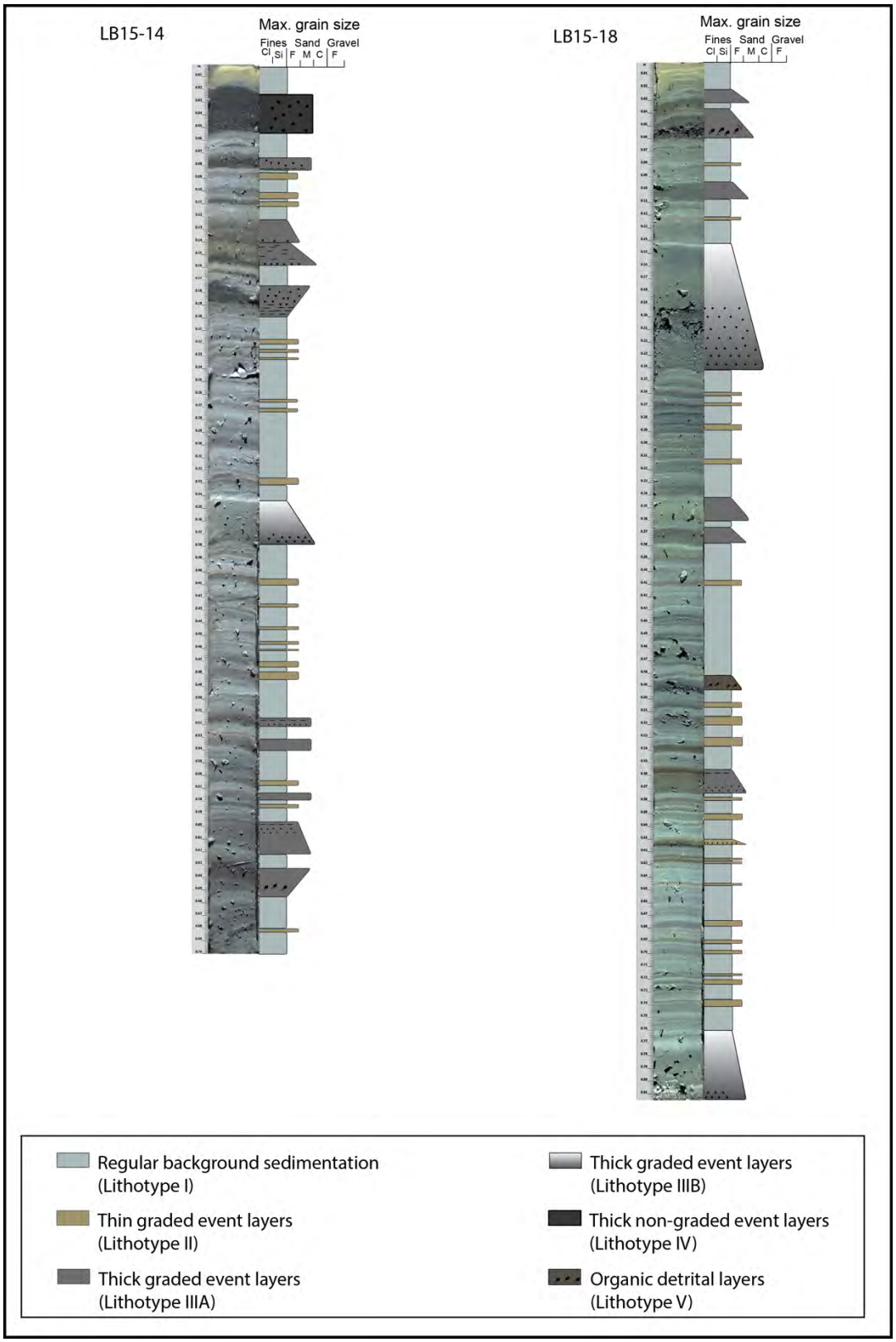

Fig. 4.1 Description of the representative cores for Lütschine (LB15-14, left) and Aare (LB15-18, right). Note that the difference in colour in figure 4.1 is only due to a different setting of the RGB camera, and not by a difference between the cores.

LITHOTYPE V is related to terrestrial organic detrital layers, which are composed of remains of leaves and other organic matter and therefore characterized by a very dark greyish brown colour (HUE 2.5Y 3/2) and a variable thickness (from 5 mm to 1 cm). Such layers, only found in LB15-18 and partly in LB15-19, are expected to be organic detrital layers. As the Aare and Lütschine have a long flow path, stemming from glacial outflows, it is highly likely that any organic material found in the sediments of the Lake originates from flood events and debris-flows surrounding the catchment. This issue will be addresses in the discussion section.

Especially for Lithotypes IIIA and IIIB, event layers can be characterized by erosive bases. While LB15-18 is characterized by a less disturbed laminated succession compared to LB15-14, erosive bases can be found at the bottom of 1996 turbidite (see also Girardclos et al., 2007), as well as of 2005 detrital layer.

4.2 Core Correlation and 2005 Flood Layer Identification

4.2.1 Core Correlation

A core correlation was retrieved using all the seventeen cores from the lake, with the aim of identifying the August 2005 flood event along the WE transect of the basin. Visual observation of colour and lithology was performed, as well as a comparison with core images from the same basin in the study of Girardclos et al. (2007) and Anselmetti et al. (2007), who previously conducted sedimentological studies on Lake Brienz. Such methodology allowed the author to identify, with a strong level of certainty, the 2005 layer in nine cores along the basin.

An attempt of identifying the 2005 layer was also performed on all cores showing clear layering through bulk density and magnetic susceptibility (MS) profiles (Fig. 4.2). Therefore, the cores located in the central area of the basin (LB15-15c, LB15-16, LB15-17) were also included in the analysis, in order to attempt to identify changes in profiles on the top layers and retrieve a signal from the 2005 event. For all the profiles, the MS profiles show only little variations throughout the cores, while Bulk Density mainly follows grain size changes. However, the profiles do not highlight all the visible event layers present in the cores. Concerning the central cores, which comprise major coring-induced disturbance, bulk density shows only an increase for LB15-17 at around 5 cm depth, while the other two central cores do not show a similar variation. Such profiles therefore were not suitable for the identification of the single 2005 layer.

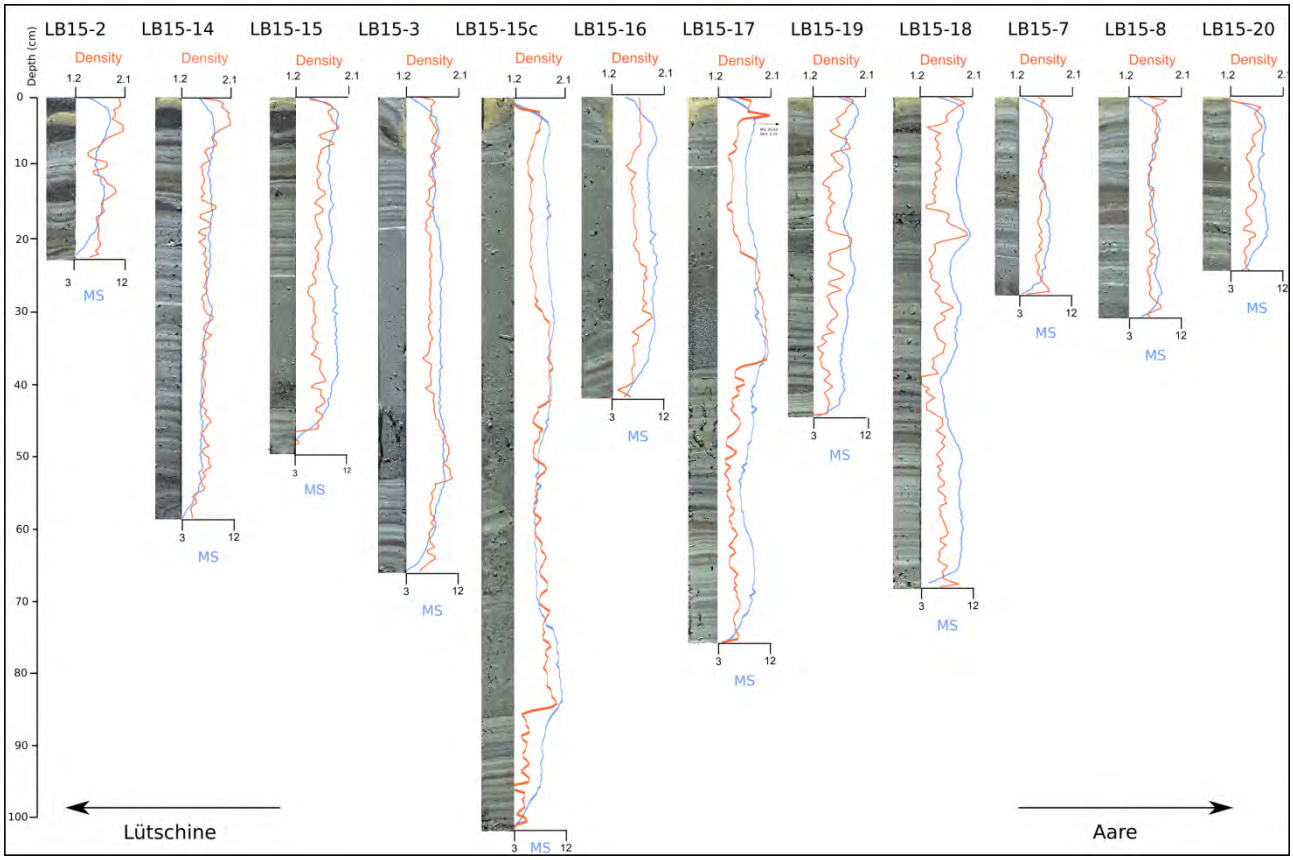

Fig. 4.2 Bulk density (g/cc) and Magnetic susceptibility (SI x 10^{-5}) profiles for the 12 cores presenting a visible layering

Figure 4.3 shows the retrieved core correlation along the basin. The cores are aligned following the WE transect, with the Lütschine inflow on the left and the Aare inflow on the right. As presented before, only nine cores out of seventeen show the 2005 layer: LB15-2, LB15-14, LB15-15, LB15-3, LB15-7, LB15-8, LB15-18, LB15-19 and LB15-20. In pink, the 2005 layer is shown, while in blue the 1996 delta collapse is highlighted.

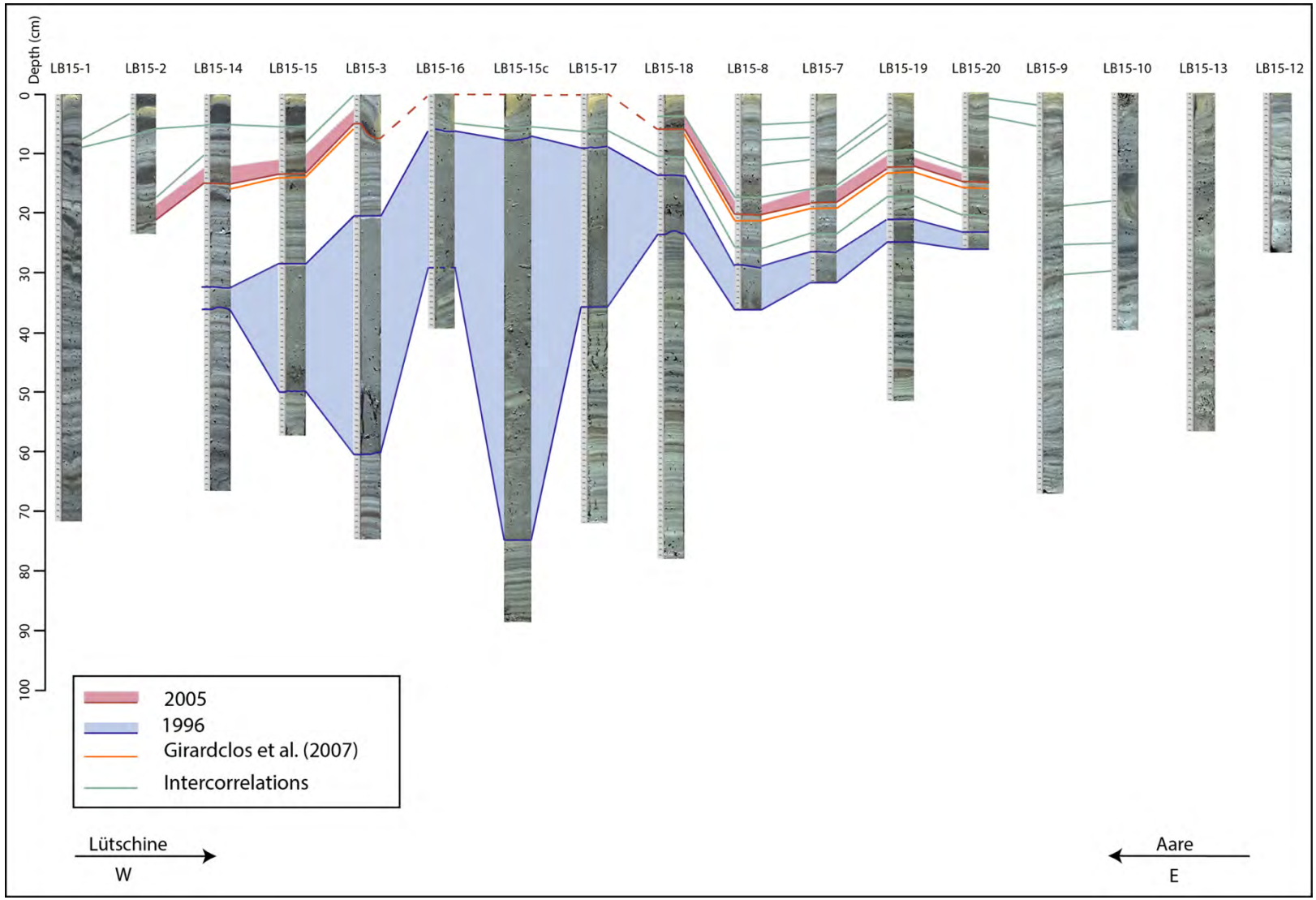

Fig. 4.3 Core correlation on Lake Brienz. Blue shading represents the mass-movement induced turbidite from 1996 (Girardclos et al, 2007). The red shading indicated the layer associated to the 2005 flood event. Note that a respective layer could not be recovered in the central part of the lake (see discussion section for possible explanations)

As it can be observed, cores LB15-1, LB15-16, LB15c, LB15-17, LB15-9, LB15-10, LB15-12 and LB15-13 did not show the 2005 layer. It is expected that the cores located closer to the inflows of both Aare and Lütschine present a dynamic depositional system (channels in front of delta, high potential of erosion and patchy sedimentation, thus causing disturbed layering), which does not allow a clear identification of the 2005 layer. In contrast, the cores located in the centre present a different problematic. When compared to the cores retrieved from the previous studies of Anselmetti et al. (2007) and Girardclos et al. (2007), LB15-15c, LB15-16 and LB15-17 present around 10 years of missing layers.

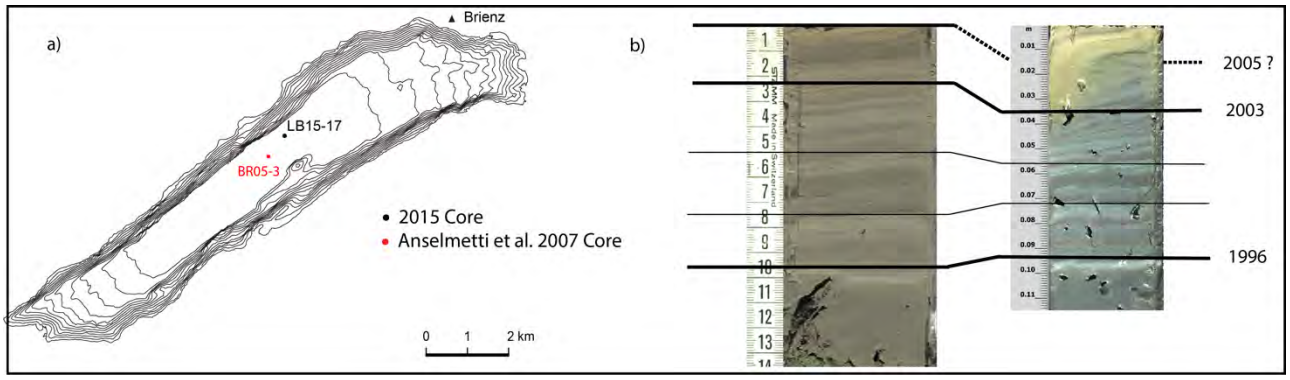

Fig. 4.4 Correlation between central cores from Anselmetti et al. (2007, Core BR05-3 taken in early 2005 prior to the event) and LB15-17

Figure 4.4 shows the correlation between the cores retrieved from Anselmetti et al. in 2005 (before the August flood event) and one of the central cores retrieved in 2015 for this project. Fig. 4.4 (a) illustrates the location of the two cores. In Figure 4.4 (b), the correlation between the two cores is presented, with BR05-3 core on the left and the 2015 core on the right. As it can be observed, the two successions show a very similar layering, both correlating the 1996 and 2003 layers. As it can be observed, the top core taken by Anselmetti et al. (left) ends with 2005 layer, however not including the flood-induced turbidite which will be deposited few months later. The core retrieved for this study, despite a time span of 11 years, does not show the flood-induced turbidite of August 2005 either, therefore missing around 10 years of sedimentation. As shown in Figure 4.2, the same pattern can be observed for the other two central cores LB15-15c and LB15-16. As a consequence, the cores from the actual depocentre in the central part of the lakes could for some reasons (see discussion section) do not contain the 2005 event layer, so that the presented data focuses on the zones towards both major deltas, where coring clearly recovered the targeted layer.

4.2.2 August 2005 Layer Identification

Despite the 2005 layer present in the nine cores is interpreted to be the consequence of the same event, sedimentological differences are related to different locations within the lake. Figure 4.5 shows, through three representative cores, such differences.

Fig. 4.5 (a) shows the 2005 layer of core LB15-14, which is representative for the cores closer to the Lütschine input and therefore located on the Western side of the lake. This particular pattern of the 2005 layer can be observed in cores LB15-2, LB15-3, LB15-14 and LB15-15. A coarser, darker base is overlaid by two visually different layers, which present slightly different colours. Figure 4.5 (b) is more representative for cores LB15-18 and LB15-19 and in general of the Aare signal, however from more a central location. Such turbidites present a different layering, with a layer composed of organic matter containing plant macrofossils and diatoms and an overlying detrital layer. Fig 4.5c shows LB15-8 2005

layer, which is representative for the cores closer to the Aare inflow, such as LB15-7 and LB15-20. These layers show a more homogeneous signal, with no overlying layer but only a single graded turbidite.

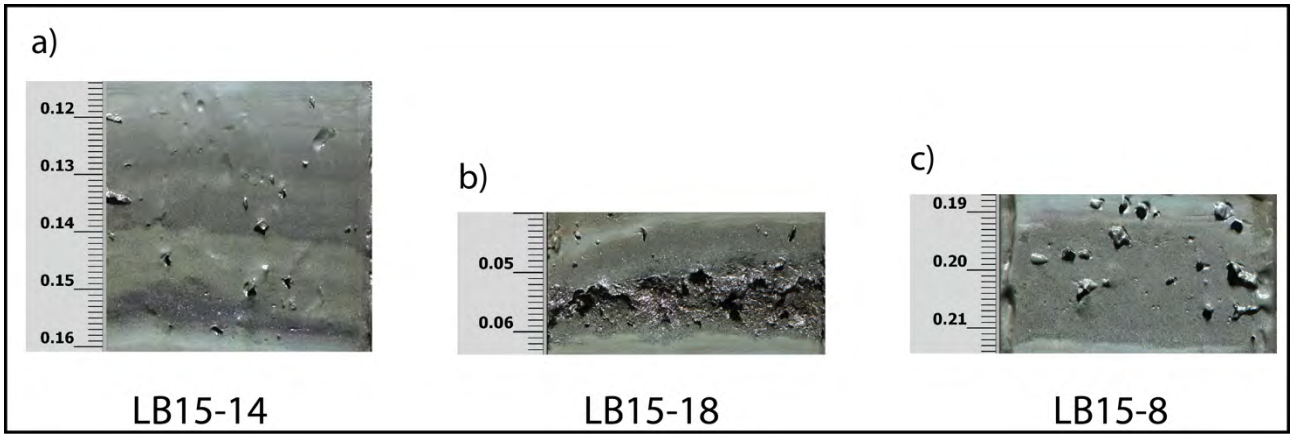

Fig. 4.5 Sedimentological differences in 2005 layer within cores

Finally, Figure 4.5 (c) shows LB15-8 2005 layer, and is representative for the cores closer to the Aare inflow,

In general, all the 2005 layers present a thickness varying from 1.5 cm thick for the cores closer to the Aare to 3.5 cm thick for the cores closer to Lütschine. As the 2005 layers from the central part of the lake could not be recovered, no thickness information is available for the theoretical depot centre.

4.3 Geochemical Signatures

4.3.1 Elemental Profiles

4.3.1.1 Long Cores

As presented in the methodology section, elemental profiles were plotted in order to first identify a proxy for turbidites in Lake Brienz. Secondly, a more detailed analysis was performed in order to establish and isolate elements indicative for Aare (and its rather crystalline catchment) and Lütschine (with a more sedimentary input) signal. In order to identify flood layers, zirconium (Zr) was chosen to be the most representative in the identification of turbidite along whole cores. This element is usually associated with heavy and high resistant minerals (Croudace et al., 2006; Kylander et al., 2011), and in the literature is often found to be related to both detrital input and changes in grain size (I.W. Croudace et al., 2006; Kylander et al., 2011; L. Schulte, Peña, et al., 2015).. Fig. 4.6 shows the three cores which have been fully analysed with ITRAX: LB15-14 (entirely), LB15-18 (from 14 cm to the end) and LB15-8 (0-31 cm). The relative Zr measurements are presented in the Annex (Tables A.2.1-A.2.3).

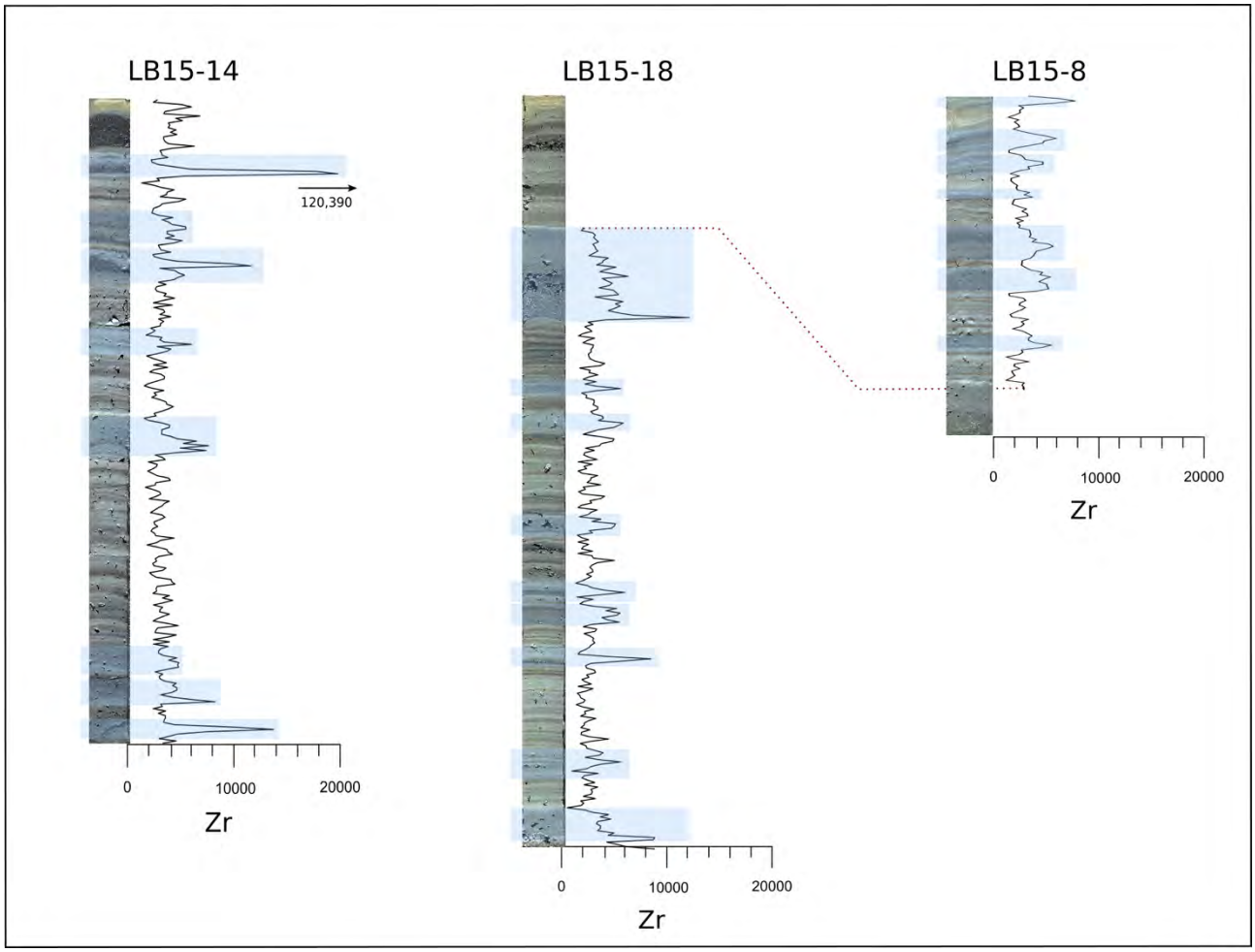

Fig. 4.6 Zirconium (Zr) profiles for Lütschine (LB15-14) and Aare (LB15-8, LB15-18) signal. Blue rectangles show flood layers along the cores and the related Zr profile changes. The red dotted line marks the correlation between the two composite sections (upper section: LB15-8; lower section: LB15-18)

As visible in Fig. 4.6, Zr profile accurately follows changes in grain size (blue rectangles). Increases in the elemental profile correspond in fact to what has been previously characterized as event layers. In particular, peaks in Zr are related to the coarser particles within the event layers. For this reason, Zr has been chosen as proxy for event layers and coarser grain size, which is in line with previous studies both on Lake Brienz (Schulte et al., 2015) as well as in other regions (examples can be found in Croudace et al., 2015).

4.3.1.2 2005-Layer Elemental Profiles

Focusing on the individual 2005 layers, elemental and elemental ratios profiles were plotted for cores LB15-14 (Lütschine), LB15-8 and LB15-15 (Aare). In the following Fig. 4.7 and Fig. 4.8, the elemental and ratios profiles for LB15-14 (Lütschine) are shown. The relative data are presented in the Annex (Tables A.2.4-A.2.12)

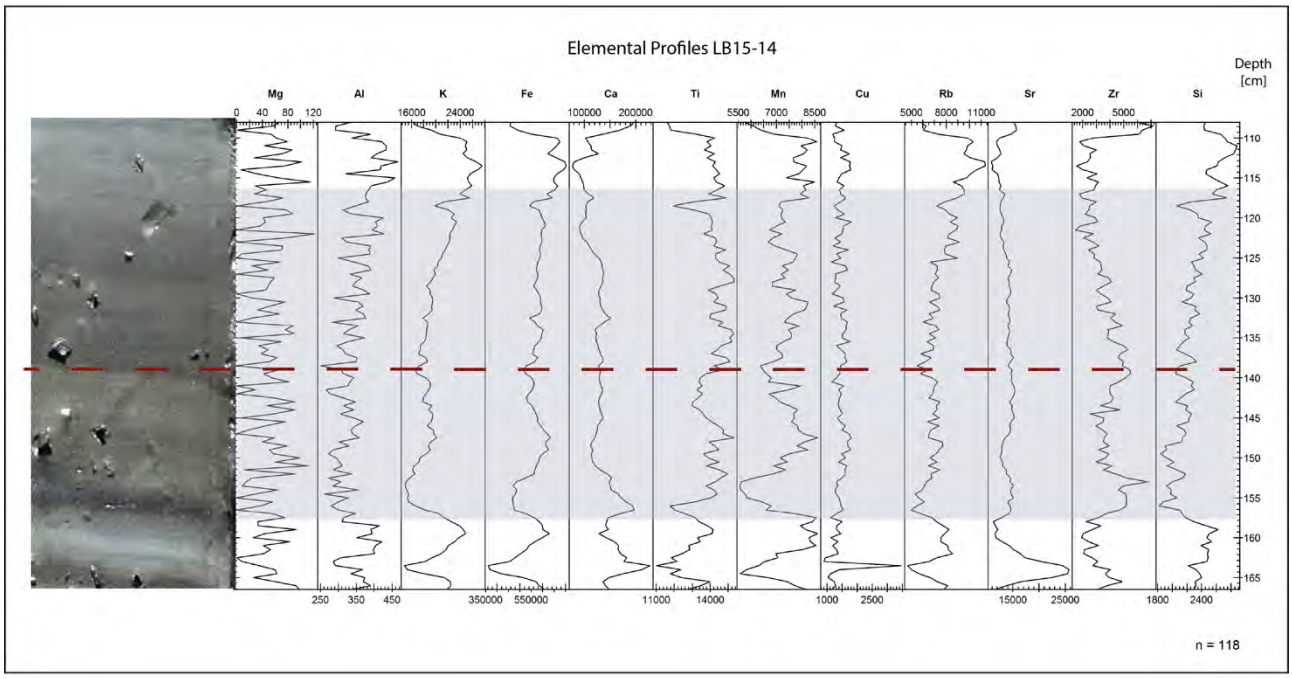

Fig. 4.7 Elemental profiles for the 2005 layer in LB15-14. In grey, the limits and location of the flood layer. The red dotted line highlights the visual difference within the layer

The 2005 layer, highlighted by the grey rectangle, is located between 117 and 159.75 mm. At 140 mm depth, a change in the profile can be seen for almost every element presented in Fig. 4.7, and corresponds to the visual difference in sedimentation within the 2005 layer (red dotted line). Such change in sedimentation at 140 mm shows a visible coarsening and darkening of the sediment, which could be indicative for another layering overlying the first one. From now on, the layer between 117-140 mm and 140-159.75 mm will be addressed as sub-layers A and B, respectively. The profiles of Mg, Al and Cu are too noisy and do not show a representative pattern. The most interesting elemental profiles are K, Ca, Ti, Rb and Zr, which present variations along the 2005 layer.

K, which is usually enriched in fine-grained fraction such as in clay, micas and feldspar (Croudace & Rothwell, 2015), shows an increase in counts through the sub-layer A. Ca, representative for carbonate input and enriched in allochtonous material (Croudace & Rothwell, 2015), is the second most present element (after Fe). Despite a more constant profile, it still shows higher counts in the sub-layer B. A peak of Ca is also found at around 132 mm depth. Ti also shows an interesting pattern: enriched in coarse silt and sand and usually associated to quartz (Kylander et al., 2011), it presents higher counts in the sub-layer A. Rb, enriched in clay minerals (Croudace & Rothwell, 2015), is characterized by a similar behaviour, with a clear increase throughout the entire sub-layer A, while in B the profile is more constant. Zr, usually related to coarser grain size (Cuven et al., 2010), follows the visual grading visible on the core image, with higher counts of Zr at the base of each sub-layer, both followed by a decrease. Finally, the Si profile is characterized by a constant upcore increase along the sub-layer B, which gets more pronounced along the sub-layer A.

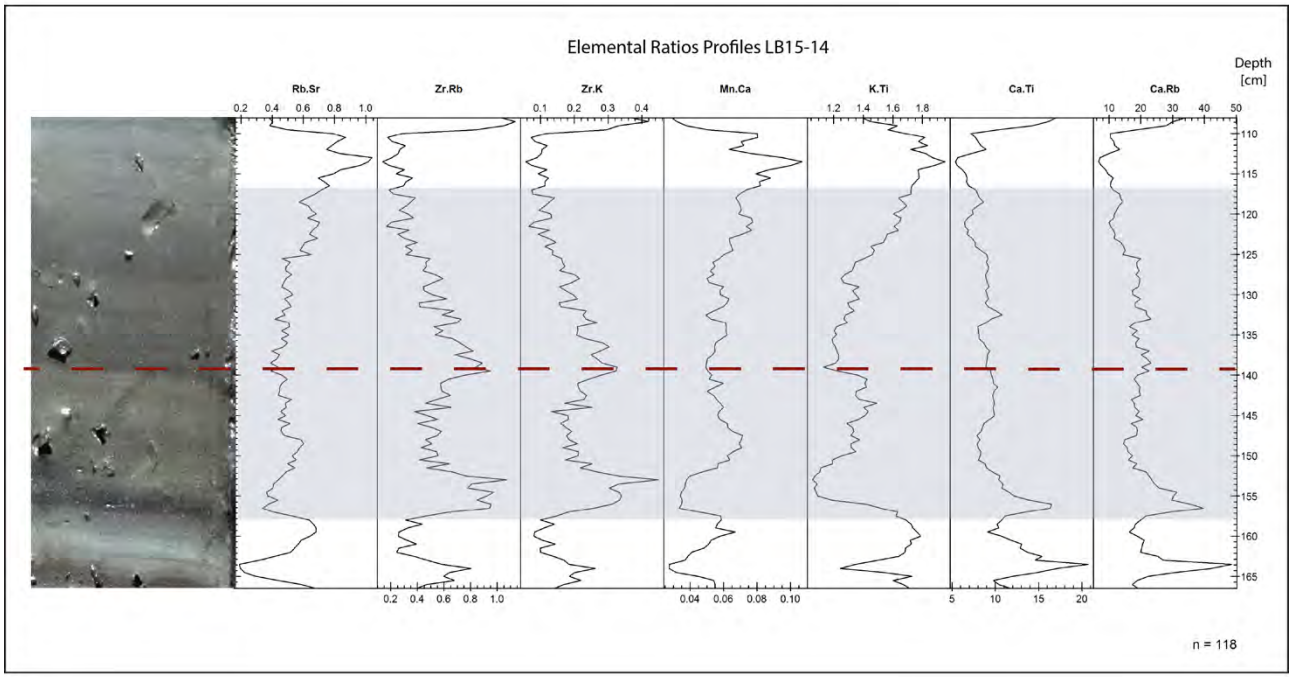

Fig. 4.8 Ratio profiles for the 2005 layer in LB15-14. In grey, the limits and location of the flood layer. The red dotted line highlights the visual difference within the layer

In Fig. 4.8, elemental ratios chosen for the analysis are shown: Zr/Rb and Zr/K nicely follow the pattern previously described for Zr, with increasing values related to the bottom of both sub-layers followed by a upcore decrease. Ca/Rb, chosen to be the representative ratios to identify Aare (Rb) and Lütschine (Ca) signals, shows higher ratio in the sub-layer B, with a subsequent upcore decrease in sub-layer A.

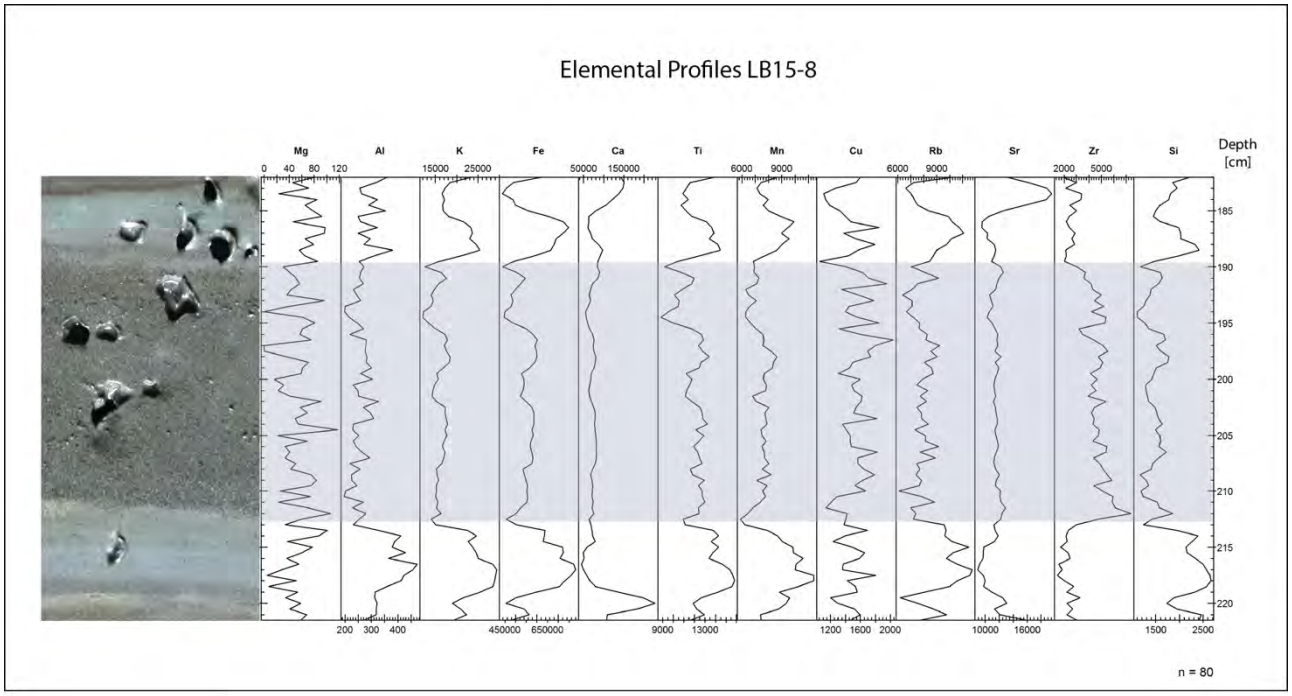

Fig. 4.9 Elemental profiles for the 2005 layer in LB15-8. In grey, the limits and location of the flood layer

Fig. 4.9 shows the elemental profiles of the core LB15-8, representative for Aare signal. The turbidite, which consists in the layer between 190 and 212.5 mm, shows a very different pattern than the previous core, with no changes within the layer shown in the visual image nor in the elemental profiles. All the elemental profiles are in fact stable and continuous, with little or no change throughout the turbidite. In this core, K does not increase through the layer, and Ca presents a much lower concentration than for the previous core. Rb is characterized, on the other hand, by higher concentrations. The Zr profile is shows a higher concentration at the bottom of the 2005 layer, followed by an upcore decrease.

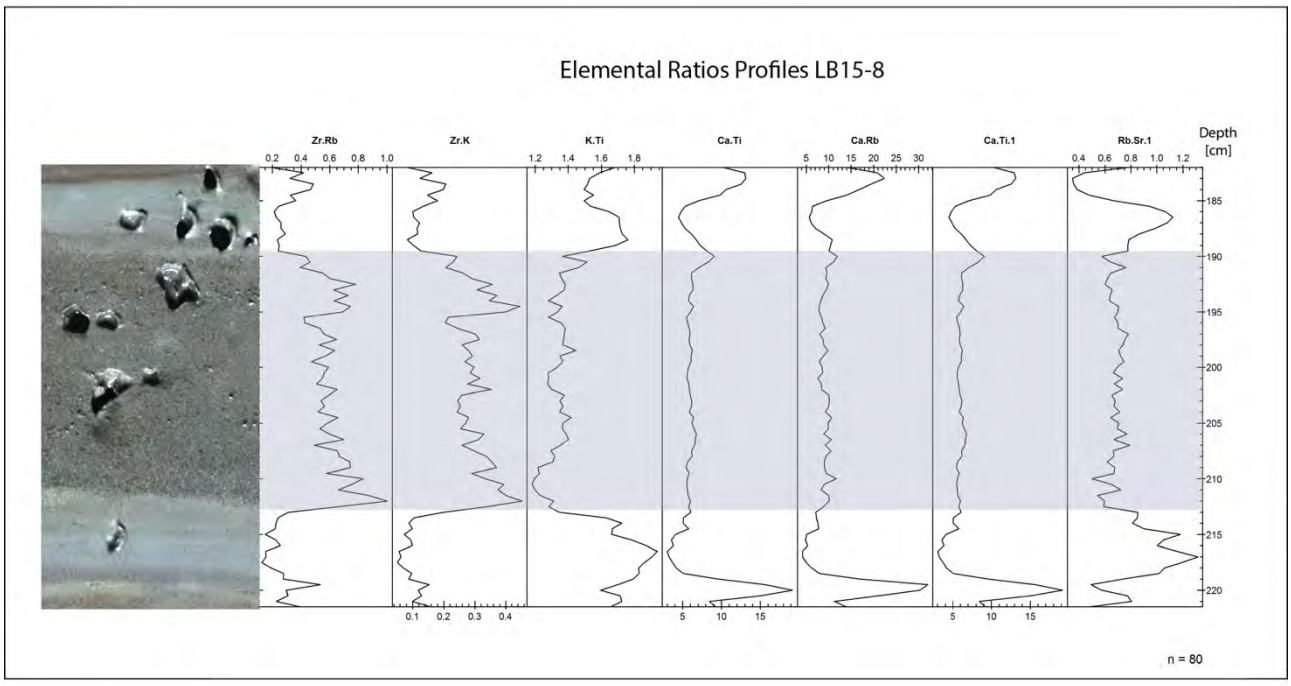

Fig. 4.10 Ratio profiles for the 2005 layer in LB15-8. In grey, the limits and location of the flood layer

Figure 4.10 shows the elemental ratios for LB15-8. No trend is visually detectable for Ca/Ti, Ca/Rb and Rb/Sr. However, Ca/Ti and Ca/Rb presents a lower ratios compared to LB15-14, which implies higher concentration of Ti and Rb in the turbidite than Ca. Zr/Rb and Zr/K show, instead, a much more variable profile, with higher ratios at the bottom followed by a slight decrease towards the top of the turbidite. At 195 mm, further increases in Zr/Rb and Zr/K ratios are visible, which may imply an increase in grain size at that depth.

Finally, Fig. 4.11 shows the elemental profiles for LB15-15. The turbidite lies between 114 an and 141 mm, with a visible change in sedimentation at around 120 mm. Also in this case, the layer between 114-120 mm will be addressed as sub-layer A and the layer between 120 and 141 mm as sub-layer B. Despite the large similarity to LB15-14, both for elemental and ratio profiles, the most interesting feature characterizing LB15-15 is related to the elements Ca and Rb. Ca counts are not only much lower than for LB15-14, but also present a strong decrease from sub-layer B to sub-layer A. The increase in Rb counts – already shown in LB15-14 – in sub-layer A is in fact much more pronounced than for the previous core. Because of its similarity with LB15-14, ratios profiles are not shown here, and can be found in the Annex (Fig. A.2.1).

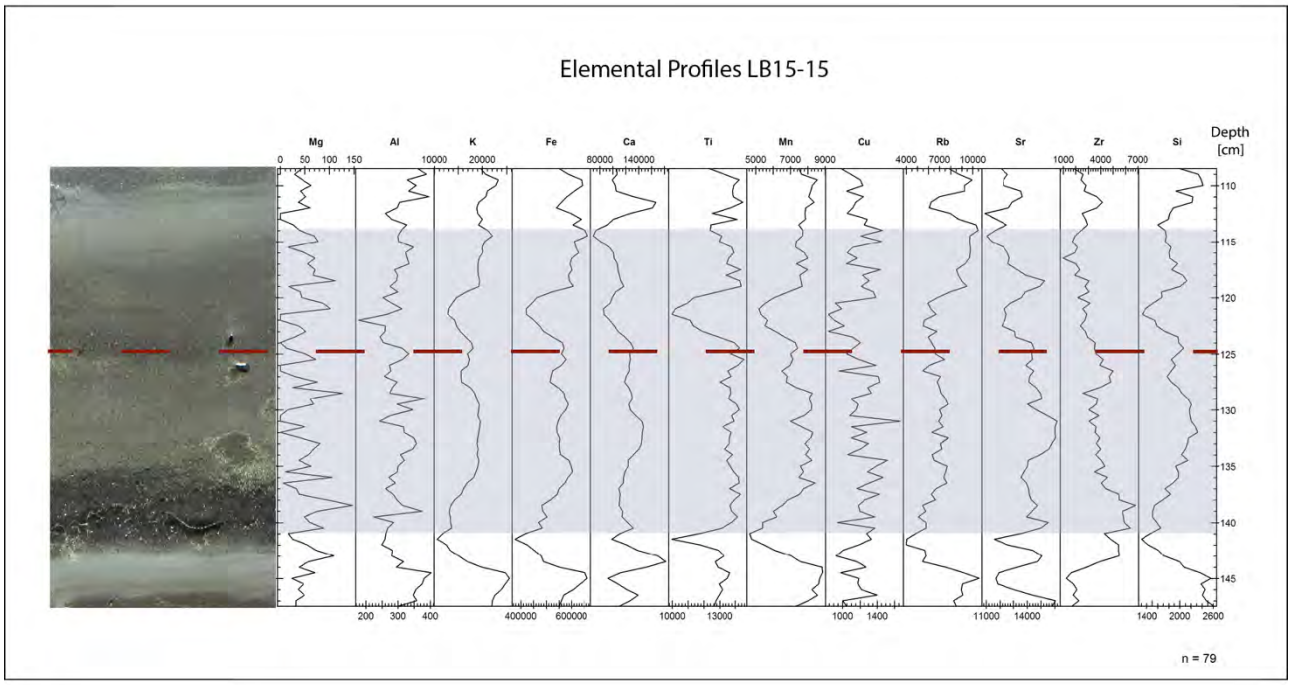

Fig. 4.11 Elemental profiles for the 2005 layer in LB15-14. In grey, the limits and location of the layer. The red dotted line highlights the visual difference within the flood layer

4.3.2 Elemental Correlation and Principal Component Analysis

The relationship between different elements was investigated through two types of statistical analysis, such as Spearman's correlation and Principal Component Analysis. This was done in order to retrieve the elemental fingerprints significant for the two catchment of Aare and Lütschine and therefore to identify the source of sediments in the different cores.

4.3.2.1 Correlation

In the following tables, the correlation between standardized variables (elemental profiles) is shown for LB15-14 and LB15-8. The lower section of the matrix presents the correlation, while the upper section (in italic) shows the level of significance. In bold, the strong positive significant correlations are shown.

Table 4.1 Spearman's correlation matrix for LB15-14. The lower left-hand corner shows the correlation coefficients, with highest correlations in bold, while the upper right-hand corner (italic) shows the levels of significance (P). A value of P < 0.05 is considered as significant

	Fe	Mg	Al	K	Ca	Ti	Mn	Cu	Rb	Sr	Zr	Si
Fe	1	*0.2654*	*0.0001*	*0*	*0*	*0.0029*	*0*	*0.007*	*0*	*0*	*0*	*0*
Mg	0.12	1		*0.8136*	*0.0365*	*0.7682*	*0.4317*	*0.8169*	*0.6404*	*0.0143*	*0.908*	*0.5322*
Al	0.41	0.18	1	*0*	*0.1059*	*0.1183*	*0.0052*	*0.6074*	*0.0002*	*0.0362*	*0*	*0*
K	**0.67**	0.03	0.55	1	*0.0017*	*0.7831*	*0*	*0.5494*	*0*	*0*	*0*	*0*
Ca	-0.63	-0.23	-0.18	-0.34	1	0.2417	*0.2461*	*0.0133*	*0*	*0*	*0*	*0.1527*
Ti	0.32	-0.03	0.17	-0.03	-0.13	1	*0.6425*	*0.0085*	*0.7947*	*0.6185*	*0.9989*	*0.2438*
Mn	**0.62**	0.09	0.3	**0.54**	-0.13	0.05	1	*0.1137*	*0.0029*	*0.0063*	*0*	*0.0113*
Cu	0.29	0.03	-0.06	-0.07	-0.27	0.29	0.17	1	*0.8368*	*0.3346*	*0.7794*	*0.2506*
Rb	**0.65**	0.05	0.4	**0.68**	-0.56	0.03	0.32	-0.02	1	0	*0*	*0*
Sr	-0.65	-0.27	-0.23	-0.5	**0.46**	-0.06	-0.3	-0.11	-0.53	1	*0*	*0.0103*
Zr	-0.69	-0.01	-0.42	-0.82	**0.46**	0	-0.5	0.03	-0.73	**0.56**	1	*0*
Si	0.45	-0.07	**0.63**	**0.79**	-0.16	0.13	0.28	-0.13	**0.62**	-0.28	-0.62	1

As it can be observed, the following elements correlate with each other:

- Fe, K, Mn, Rb present a strong, positive correlation between each other. They also present a positive but weaker correlation with Al and Si. Ti, Cu and Mg are weakly correlated. All those elements are negatively significantly correlated with Ca, Sr and Zr

- Ca, Sr, Zr correlate positively with each other and are negatively correlated with all the other elements

Table 4.2 Spearman's correlation matrix for LB15-8. The lower left-hand corner shows the correlation coefficients, with highest correlations in bold, while the upper right-hand corner (italic) shows the levels of significance (P). A value of P < 0.05 is considered as significant

	Fe	Mg	Al	K	Ca	Ti	Mn	Cu	Rb	Sr	Zr	Si
Fe	1	*0.8396*	*0.0156*	*0*	*0.0001*	*0*	*0*	*0.2772*	*0*	*0.0378*	*0.432*	*0*
Mg	0.03	1	*0.9832*	*0.712*	*0.7693*	*0.7105*	*0.7905*	*0.6703*	*0.5437*	*0.6437*	*0.7266*	*0.9601*
Al	0.38	0	1	*0.0083*	*0.0115*	*0.1441*	*0.0548*	*0.1236*	*0.0016*	*0.3049*	*0.5573*	*0.0048*
K	**0.88**	0.06	**0.41**	1	*0*	*0*	*0*	*0.2033*	*0*	*0.0022*	*0.872*	*0*
Ca	**0.56**	-0.05	0.39	**0.72**	1	*0.0004*	*0.0097*	*0.6997*	*0.0021*	*0*	*0.3659*	*0*
Ti	**0.91**	0.06	0.23	**0.84**	**0.53**	1	*0*	*0.2328*	*0.0019*	*0.0093*	*0.3869*	*0*
Mn	**0.72**	0.04	0.3	**0.65**	0.4	**0.69**	1	*0.6311*	*0.005*	*0.0595*	*0.418*	*0.0021*
Cu	0.17	0.07	0.24	0.2	0.06	0.19	0.08	1	*0.4617*	*0.3441*	*0.0531*	*0.2941*
Rb	**0.57**	-0.1	0.48	**0.62**	**0.47**	**0.47**	**0.43**	0.12	1	*0.0079*	*0.9914*	*0*
Sr	0.33	-0.07	0.16	**0.47**	**0.59**	**0.4**	0.3	0.15	**0.41**	1	*0.1676*	*0.0051*
Zr	0.13	0.06	-0.09	0.03	-0.14	0.14	0.13	0.3	0	-0.22	1	*0.4633*
Si	**0.73**	-0.01	**0.43**	**0.89**	**0.73**	**0.64**	**0.47**	0.17	**0.68**	**0.43**	-0.12	1

The correlation between standardized variables in LB15-7 shows the following results:

- Fe, K, Ca, Ti, Mn, Rb and Si present a strong, positive significant correlation with each other.

- Ca shows a positive significant correlation with Ti, Sr, Rb and Si, Ti. However, it does not show a positive significant correlation with Zr

- Sr and Zr do not show a significantly correlation between each other. However, Sr correlates with Si

As it can be observed, there is a visible difference in correlation between the two cores, with Ca correlating only with Sr and Zr for LB15-14, while in LB15-8 it correlates with elements such as Ti, Si and Fe, as well with Rb.

4.3.2.2 Principal Component Analysis

A PCA was applied to the two representative cores LB15-14 and LB15-8. LB15-15 was also chosen for this analysis: the core was retrieved near to the Lütschine core LB15-14 and presents a similar sub-layering structure. However, it is located more towards the centre of the lake, and was therefore chosen in order to try identifying contributions from both the Aare and Lütschine during the event.

Dataset 1, containing Fe, Mg, Al, K, Ca, Ti, Mn, Cu, Rb, Sr, Zr and Si was used for the analysis. The resulting PCs were 12, with eigenvalues > 1 for the first three PCs. The number of PC retained for further analysis was determined using the broken-stick method.

In order to interpret biplots, some characteristics must be retained:

- The angle between vectors and the axis (representing a PC) is indicative of the importance of the contribution from the variable to the axis dimension (PC)

- The angle between two vectors pointing away from the origin (0,0) indicates the strength of correlation between the two variables. A small angle, characterized by two vectors pointing in the same direction, is indicative for high correlation. An angle of about 180° indicates a negative correlation, while 90° angle corresponds to no correlation

- Points (here expressed as depth) which are close to each other indicate that such observations are similar

In the following biplots, vectors represent elements and the points are substituted with depths, in order to see at which depth a specific elemental signal is stronger.

Fig. 4.12 shows the piblot for the PCA of LB15-14, as well as the resulting loadings. PC1 accounts for 45% of the variance, while PC2 accounts for 13%. Following the broken stick method (Annex, Fig. A.2.2), only the first PC was retained as representative.

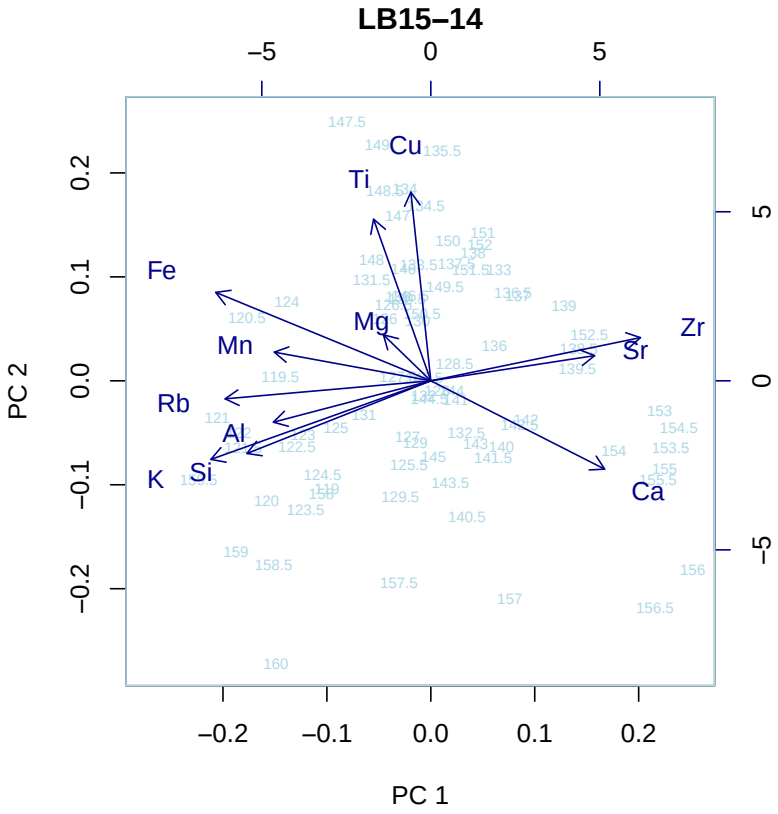

Fig. 4.12 Biplot of PC1 and PC2 showing elemental distribution along the 2005 layer of core LB15-14

As it can be observed in the biplot, Ca, Sr and Zr are characteristics for PC1, with Sr and Zr strongly correlating with each other and presenting an important contribution to PC1. The relationship between Ca and Sr, both enriched in carbonates, is clearly visible from the plot, and a strong relationship with grain size is presented by Zr. PC2, instead, is mostly explained by the elements Fe, Ti and Cu, which highly correlate with each other. Another visible strong correlation is characterized by Al, K, Si, and Rb, which is indicative of a similar composition. From the biplot, it can also be observed that Ca and Fe are negatively correlated, with an angle of 180° between each other. Table 4.3 shows the correlation between PC1 and the initial variables:

Table 4.3 Correlation between the initial standardized variables and PC1 for LB15-14. In bold, the highest positive correlations are highlighted.

	PC1
Fe	-0.87
Mg	-0.19
Al	-0.64
K	-0.89
Ca	**0.71**
Ti	-0.23
Mn	-0.63
Cu	-0.08
Rb	-0.84
Sr	**0.66**
Zr	**0.85**
Si	-0.75

Figure 4.12 shows the biplot for PC1 and PC2 for LB15-15. Using the broken stick method (Annex, Fig. A.2.3), the two first PCs were retained as both representatives. PC1 alone counts for 40% of the variance, while PC2 for 26%.

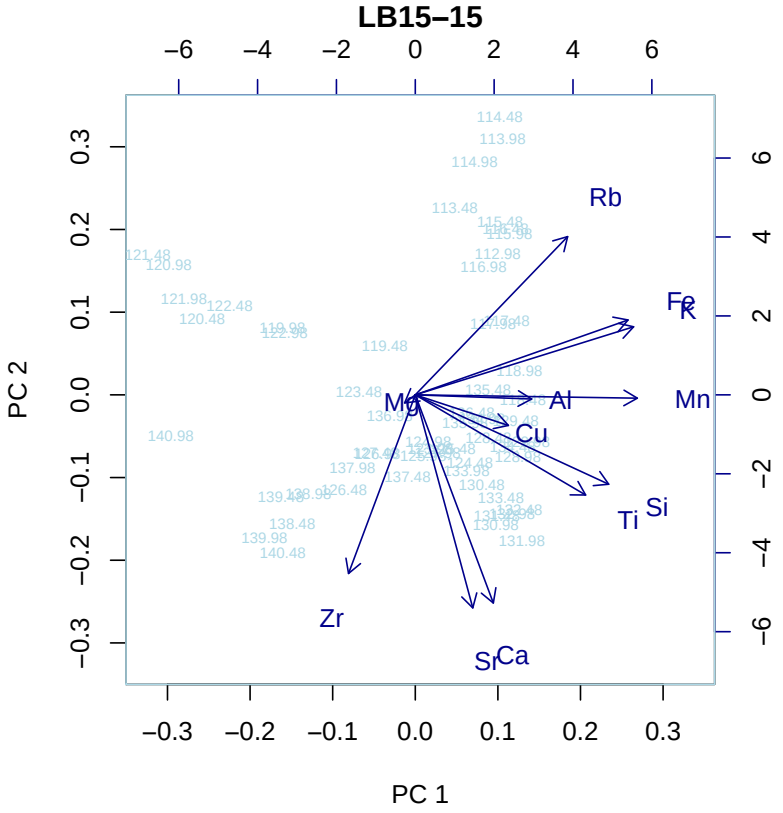

Fig. 4.12 Biplot of PC1 and PC2 showing elemental distribution along the 2005 layer of core LB15-15

PC1 contains high loadings of Fe, K, Ti , Mn and Si, and also Al. These elements are typically related to phyllosilicates. Second PC axis (PC2) is positively correlated to Rb, and negatively correlated to Zr.
As it can be observed from the biplot, Sr and Ca are very strictly correlated, following the relationship seen in the previous plots. Ti and Si, as well with Cu, correlate between each other, as well as Fe and K and Al and Mn. Sr and Ca are not correlated with Fe and K, as it can be observed from the 90° angles in the plot. Zr and Rb are negatively correlated, with an angle almost reaching 180°.

In Table 4.4 the correlation between variables and the two principal components is shown. As it can be observed, the pattern characteristic for LB15-15 is different from LB15-14, despite their closeness. PC1 presents strong correlation with Fe, K, Ti, Mn, Rb and Si, while PC2 presents a high correlation only with Rb.

Table 4.4 Correlation between the initial standardized variables and PC1 for LB15-15. In bold, the highest positive correlations are highlighted

	PC1	PC2
Fe	**0.9**	0.31
Mg	-0.04	-0.03
Al	0.49	-0.01
K	**0.92**	0.28
Ca	0.33	-0.88
Ti	**0.72**	-0.42
Mn	**0.94**	-0.01
Cu	0.39	-0.12
Rb	**0.64**	**0.66**
Sr	0.24	-0.9
Zr	-0.28	-0.75
Si	**0.81**	-0.37

Despite their spatial closeness between the two cores, the results for LB15-15 quite differ from the ones for LB15-14.

Because both of the cores present two different sub-layers (Fig. 4.13), a second PCA was run on both the sub-layers for each core. While the biplots can be found in the Annex (Figures A.2.4-A.2.7), Table 4.5 and Table 4.6 show the correlation between the scores for PC1 and PC2 and the initial standardized variables. Table 4.5 shows the results for LB15-14, while Table 4.6 shows the results for LB15-15.

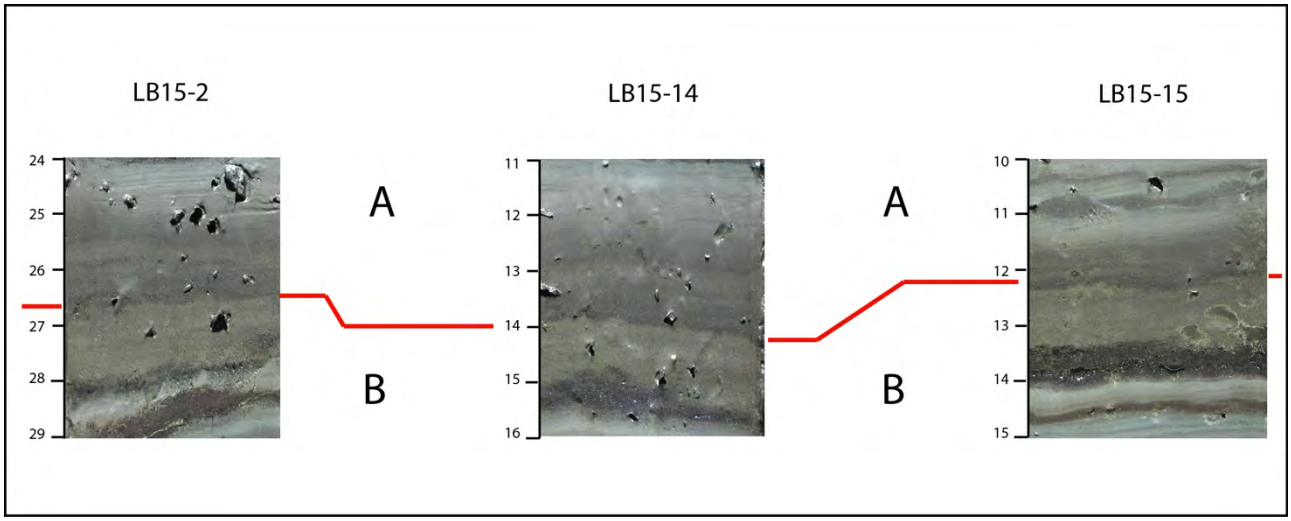

Fig. 4.13 Cores proximal to Lütschine inflows presenting two different sedimentary sequences overlaying each other. The top sequence (above red line) is indicated as sub-layer A, while the bottom sequence (under red line) is indicated as sub-layer B

Table 4.5 Correlation for sub-layer A (left) and sub-layer B (right) between the initial standardized variables and PC1 of LB15-14. In bold, the highest positive correlations are highlighted

LB14	*SUB LAYER A*		*SUB LAYER B*		
	PC1	PC2		PC1	PC2
Fe	-0.77	**0.48**	Fe	-0.97	0.05
Mg	-0.11	0.07	Mg	-0.27	0.32
Al	-0.5	0.36	Al	-0.26	-0.307
K	-0.96	-0.05	K	-0.82	-0.47
Ca	**0.82**	0.37	Ca	**0.88**	-0.06
Ti	0.36	**0.56**	Ti	-0.21	**0.43**
Mn	-0.09	**0.8**	Mn	-0.94	-0.16
Cu	0.04	0.26	Cu	-0.67	0.44
Rb	-0.9	-0.02	Rb	-0.72	-0.13
Sr	**0.85**	0.31	Sr	**0.47**	-0.83
Zr	**0.89**	-0.05	Zr	**0.8**	0.11
Si	-0.83	0.18	Si	-0.19	-0.86

Table 4.6 Correlation for sub-layer A (left) and sub-layer B (right) between the initial standardized variables and PC1 of LB15-15. In bold, the highest positive correlations are highlighted

LB15-15	*SUB LAYER A*		*SUB LAYER B*		
	PC1	PC2		PC1	PC2
Fe	-0.96	0.11	Fe	**0.84**	**0.46**
Mg	-0.27	0.146	Mg	-0.23	-0.07
Al	-0.6	0.51	Al	0.37	-0.42
K	-0.96	0.13	K	**0.97**	0.03
Ca	-0.46	-0.79	Ca	0.6	-0.6
Ti	-0.96	-0.15	Ti	0.36	**0.52**
Mn	-0.98	0.003	Mn	**0.88**	0.22
Cu	-0.64	-0.02	Cu	-0.02	**0.48**
Rb	-0.89	0.29	Rb	**0.8**	0.21
Sr	-0.38	-0.8	Sr	**0.42**	-0.77
Zr	**0.48**	-0.66	Zr	-0.81	-0.03
Si	-0.86	-0.38	Si	**0.95**	-0.13

As it can be observed from Tables 4.5 and 4.6, the correlation between layers highly differ between the two cores. In LB15-14, sub-layer A, PC1 accounts for 48% of the variance, and it is characterized by high correlation between Ca, Sr and Zr, with relatively high correlation for Ti. PC2, accounting for 14% of the variance, presents high positive correlation for Ti and Mn, and relatively high correlation for Fe, Al and Sr. Sub-layer B (bottom) presents a similar pattern, with high correlation in PC1 (44% variance) for Ca, Zr and Sr and in PC2 (19%) relatively high correlation with Cu, Ti and Mg. A difference between the composition of the two layers is visible, however not so clear.

Interestingly, LB15-15 does not follow the same pattern. For sub-layer A (top), PC1 explains 56% of the variance, while PC2 explains 19%. In PC1, the only positive correlation is with Zr, while the other elements present a negative correlation. PC2, however, presents positive correlations with Rb, Al, Mg and Fe, with negative strong correlation for Ca, Sr and Zr. In sub-layer B (bottom), PC1 accounts for 47% of the variance and PC2 for 16%. Strong positive correlation in PC1 are visible for Fe, K, Mn, Rb, Sr and Si, as well as with Ca and Sr. PC2, instead, presents high positive correlation with Cu, Ti, and Fe, and to a minor extent for Rb and Mn.

Finally, Fig. 4.14 shows the biplot of PC1 and PC2 for LB15-8. However, following the broken stick method (Annex, Fig. A.2.8), only PC1 can be retained as representative.

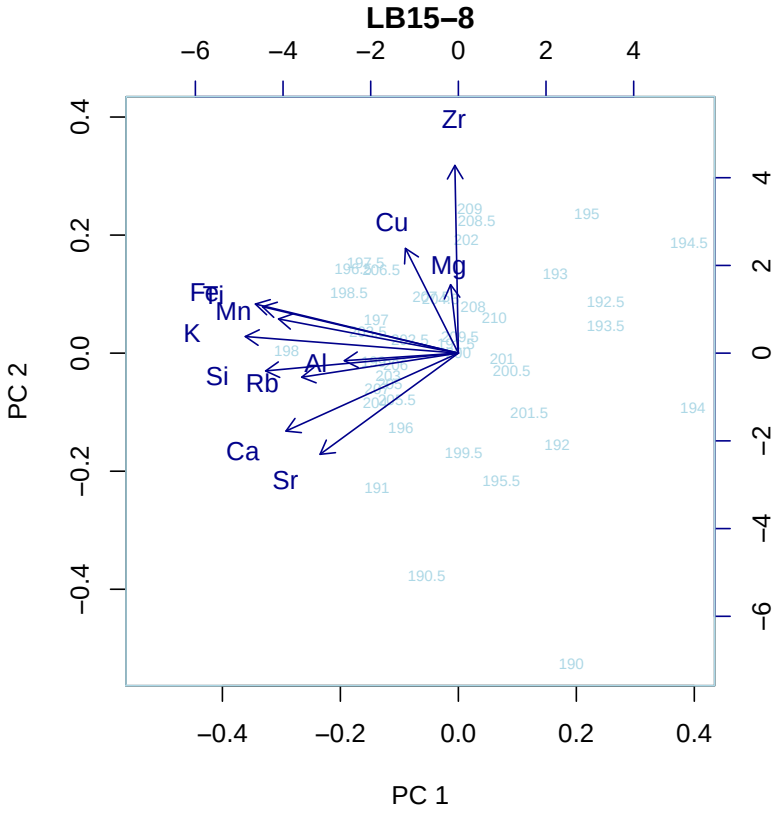

Fig. 4.14 Biplot of PC1 and PC2 showing elemental distribution along the 2005 layer of core LB15-8

PC1 accounts for 48% of the variance. As it can be observed from the plot, the elements characterizing PC1 are Fe, K, Ca, Ti, Mn and Si, with slight weaker loadings for Sr and Rb. However, those loadings are negative.

Table 4.7 Correlation between the initial standardized variables and PC1 for LB15-8

	PC1
Fe	-0.91
Mg	-0.03
Al	-0.51
K	-0.96
Ca	-0.77
Ti	-0.88
Mn	-0.81
Cu	-0.23
Rb	-0.7
Sr	-0.62
Zr	-0.01
Si	-0.86

As it can be observed from Table 4.7, the elements which correlate the most with PC1 are Fe, K, Ti, Mn, Al, Ca, Sr and Si. This pattern very much differs with that of LB15-14 or LB15-15.

4.4 Differences in Carbonate Content from Smear-slide Analysis

Smear-slide analysis was performed in order to retrieve a visual image of the differences in carbonate content and grain size between the various 2005 layers. A cross-polarized filter was applied to better visualize the characteristic mineral content of the sediment (Fig. 4.13 from a to j). The two layers containing large amounts of organic matter were also analysed without a cross-polarized filter in order to identify organic matter components (Fig. 4.15 k, l).

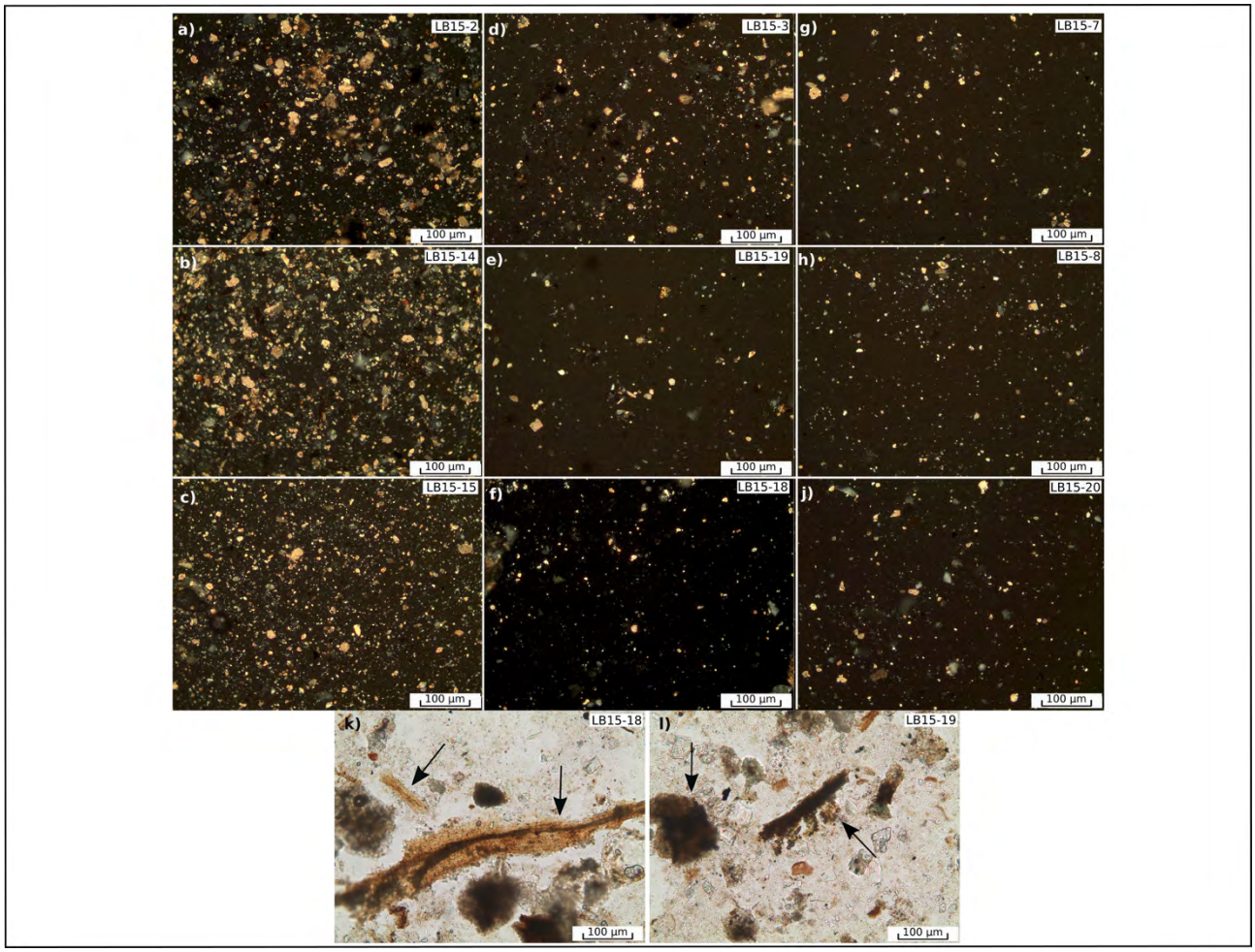

Fig. 4.15 Smear Slides for the 2005 layers in all cores (from a) to l)). Fig. 4.13 (a) to Fig. 4.13 (b) shows smear slides with a cross-polarized filter. Fig. 4.13 (k) and (l) show smear slides without a cross-polarized filter for the visualization of organic matter. Black arrows indicate plant macrofossils

As it can be observed from Fig. 4.15, the cores closer to Lütschine (a, b, c) are characterized by a much higher content in carbonates than the rest of the cores. The estimated percentage of carbonates for a, b and c is ~25-30%, with a mean grain size of ~20-30 µm. Fig. 4.15d represents core LB15-3, which still has a Lütschine signal but is located further away from the inflow: the percentage of carbonates is smaller (~20%) and mean grain size is ~20 µm. The cores closer to the Aare inflow (e to j) are characterized on the opposite by a lower content in carbonates varying around 10-20%. Mean grain size for such cores is on the order of 15-20 µm. LB15-18 (Fig. 4.15 k) and LB15-19 (Fig. 4.15 j) present the two non cross-polarized images. Both of the layers clearly show high detrital organic material and little carbonate content, with abundant plant macrofossils on the order of several hundreds of micrometres size causing a large organic matter content.

4.5 Grain Size

Grain-size analysis was performed on the 2005 layers in order to detect changes in sedimentation as well as differences between Aare and Lütschine signal. Grain size data in the 2005 layers of all the nine cores are presented in the Annex (Table A.2.13-A.2.14).

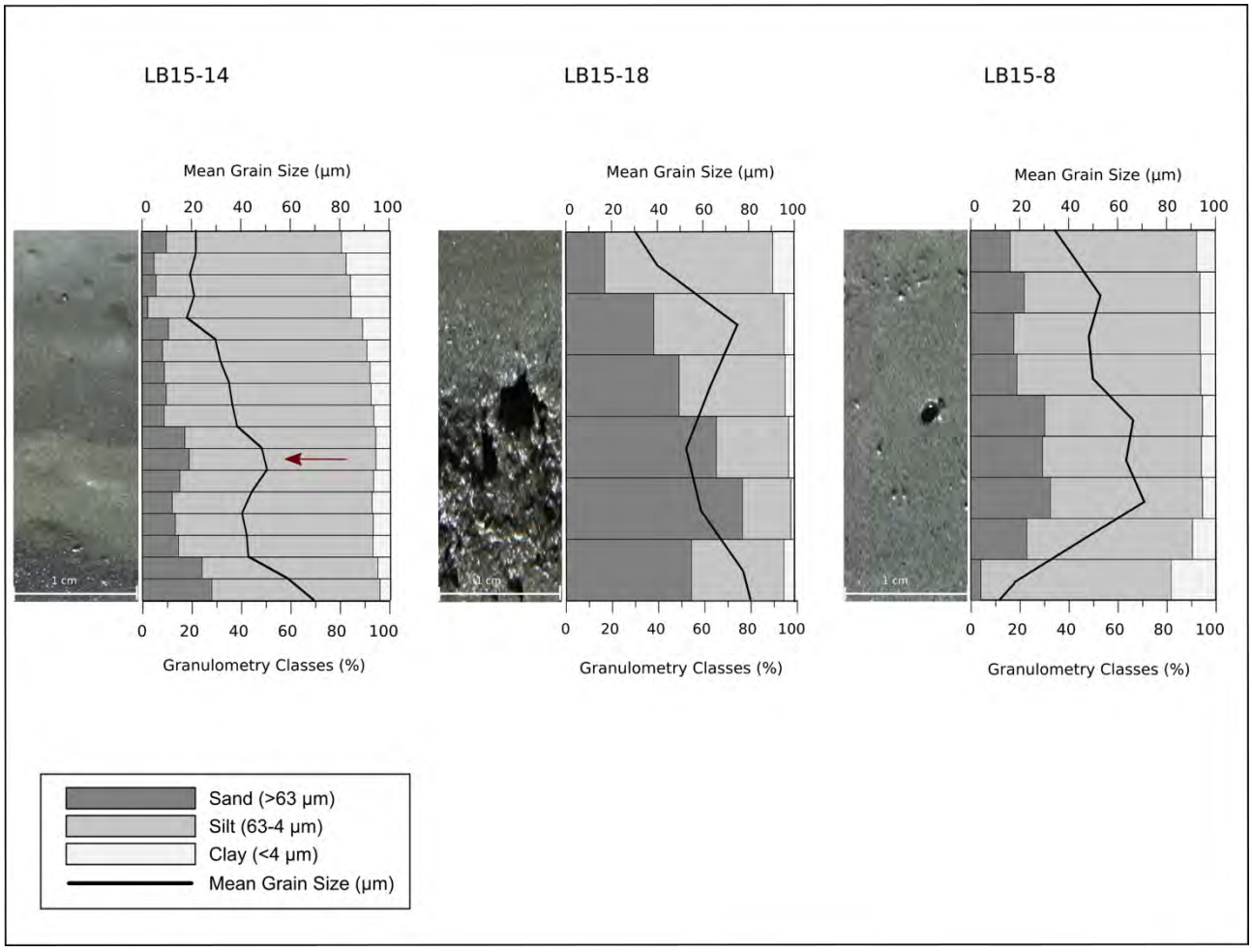

Fig. 4.16 Grain size profiles for Lütschine (LB15-14) and Aare (LB15-8) representative cores. LB15-18, also representative for Aare signal, has been chosen for grain size analysis because of the organic matter layer characteristic of the 2005 layer. Both granulometry classes (clay, silt, sand) percentages and mean grain size (microns) are presented. Each rectangle corresponds to 2.5 mm vertical core interval

Figure 4.16 shows grain-size measurements for the two most representative cores of the Lütschine (a) and Aare (b,c) signals. Fig. 4.16 (b) shows the core, which is characterized by an organic matter layer. In the figure, mean grain size has been plotted together with the different granulometry classes characterizing the lithological composition of the sediments. LB15-14 presents two separate fining-up sections, with an increase in sand at the base and in the middle of the flood layer (red arrow, corresponding to 140 mm depth). Both of the sub-layers (upper and lower) are followed by a fining-up sequence of silt-sized grains, which represent the major component of the flood layer. From 140 mm to the top of the layer, a more gradual grain-size change can be observed in respect to the lower section. This fining-up sequence starts with an increase in sand, followed by silt-sized grains and terminating with a light-grey clay top. The clay top is characteristic of fine-grained fallout deriving from the final decrease in discharge (Gilli et al., 2003).

LB15-8 presents a different pattern. Visually, the 2005 layer is more homogeneous than that of LB15-14. The section presents a fining-up gradual layering of grain size, however the differences from bottom to top are less remarkable as in LB15-14. However, the layer is characterized by generally coarser material compared to the Lütschine core, a difference, which is also shown by the mean grain size plot for both the 2005 layers.

Interestingly, LB15-18 shows a particular grain-size sequence. Sand-sized particles characterize the major component of the bottom part of the layer. Following, a fining-up sequence shows an increase in silt-sized particles towards the top, with a slight decrease in clay as well. However, the pattern followed by mean grain size is different, showing an upcore increase in grain size from the top of the organic matter layer.

4.4 TOC and TIC Content

In order to distinguish between the signals of the dominant-carbonate Lütschine and the dominant-crystalline Aare, a carbon content analysis was performed on the 2005 layer of all the cores. In addition, two representative flood layers from Aare (LB15-10) and Lütschine (LB15-1) were analysed, as well as four samples taken directly from the inflows of Aare, Lütschine, Trachtbach and Glyssibach. TOC and TIC values were retrieved, and from those values the percentage of organic matter (OM) and carbonate calculated (see Methods). From the analysis performed on single samples, the following results can be observed in Table 4.8.

Table 4.8. Organic matter and carbonate percentages derived from TOC and TIC measurement for the four tributaries

	Organic Matter (%)	**Carbonate (%)**
Aare		
• Exemplary turbidite	0.62 %	1.83%
• Inflow	0.65 %	2.34 %
Lütschine		
• Exemplary turbidite	0.94%	21.84%
• Inflow	0.96%	26.69%
Trachtbach	1.30 %	62.08 %
Glyssibach	0.83%	61.81%

As organic matter in the sampled fluvial sediment is barely a function of the catchment but rather of the depositional environment of the sediment and its preservation potential, we discuss here only the carbonate content. As it can be observed, values for carbonate content in Aare sediments are very low compared to the other inflows. The Lütschine sediments are characterized by high carbonate contents of over 20%. The highest values are present, however, in the samples taken from two mountain torrents, composed by more than 60% of carbonates.

In Fig. 4.17 the profiles of OM (blue) and calcite (red) for the 2005 layers in the cores are shown. Following the W-E transect of the lake (from right to left), a visible decrease in carbonate can be observed. Organic carbon follows a more stable pattern, with much more similar values along the entire transect, except for LB15-18 and LB15-19. The cores containing the highest percentages of calcite can be found in the first four cores from the left (West; Fig. 4.17 a to d), characterized by a strong Lütschine contribution. The percentage of carbonate in those cores is around 20-25% while the percentage of organic matter is around 2-3%. On the opposite, the lowest concentration of carbonate occurs in the cores containing a strong Aare signal (Fig. 4.17 e to i). Interestingly, LB15-18 and LB15-19 contain extremely high values of organic matter. If compared to the images, such peaks in organic matter (as well as carbonate, despite to a minor extent) correspond to the organic layers visible within the 2005 layer with a upcore decrease in both organic matter and carbonate overlying the organic layer. Data relative to all the layers can be found in the Annex (Table A.2.15).

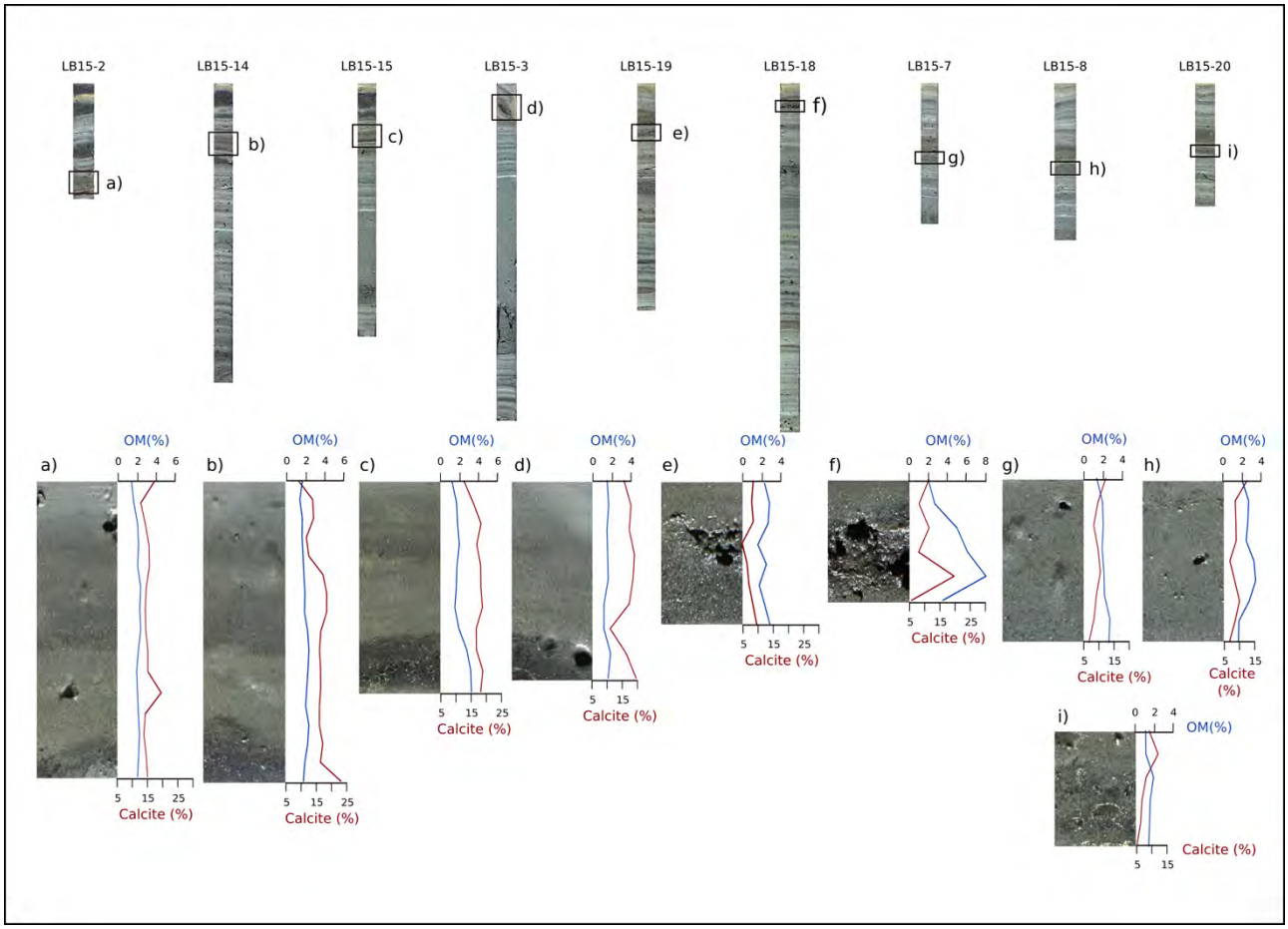

Fig. 4.17 Carbonate (red) and Organic matter (blue) profiles for the 2005 event layer

In general, the difference between Aare and Lütschine cores is remarkable, with twice the percentage of carbonate contained in the Lütschine-dominated layers. Concerning the Lütschine, the carbonate values retrieved along the 2005 layers are in line with the ones measured in fluvial sediments (Table 4.8). Carbonate values for Aare cores are higher than those of fluvial sediment (Table 4.8), and organic matter values are higher in all the cores compared to the fluvial sediments, reflecting the higher potential for organic matter preservation in lake sediments. Despite the sub-layering in the cores LB15-2, LB15-14, LB15-15 visible from the scans, no clear increasing or decreasing pattern can be observed in the distribution of carbonate and organic matter along the flood layer.

4.5 Event Succession

Concerning the temporal succession of discharge during the event, Fig. 4.18 shows the runoff evolution for all the four tributaries taken into consideration: Aare, Lütschine, Trachtbach and Glyssibach. Because Trachtbach and Glyssibach catchments present similar characteristics (mountain torrents, small catchments) runoff and precipitation have been modelled considering the same runoff coefficient for both rivers. For this reason, both the curves are very similar.

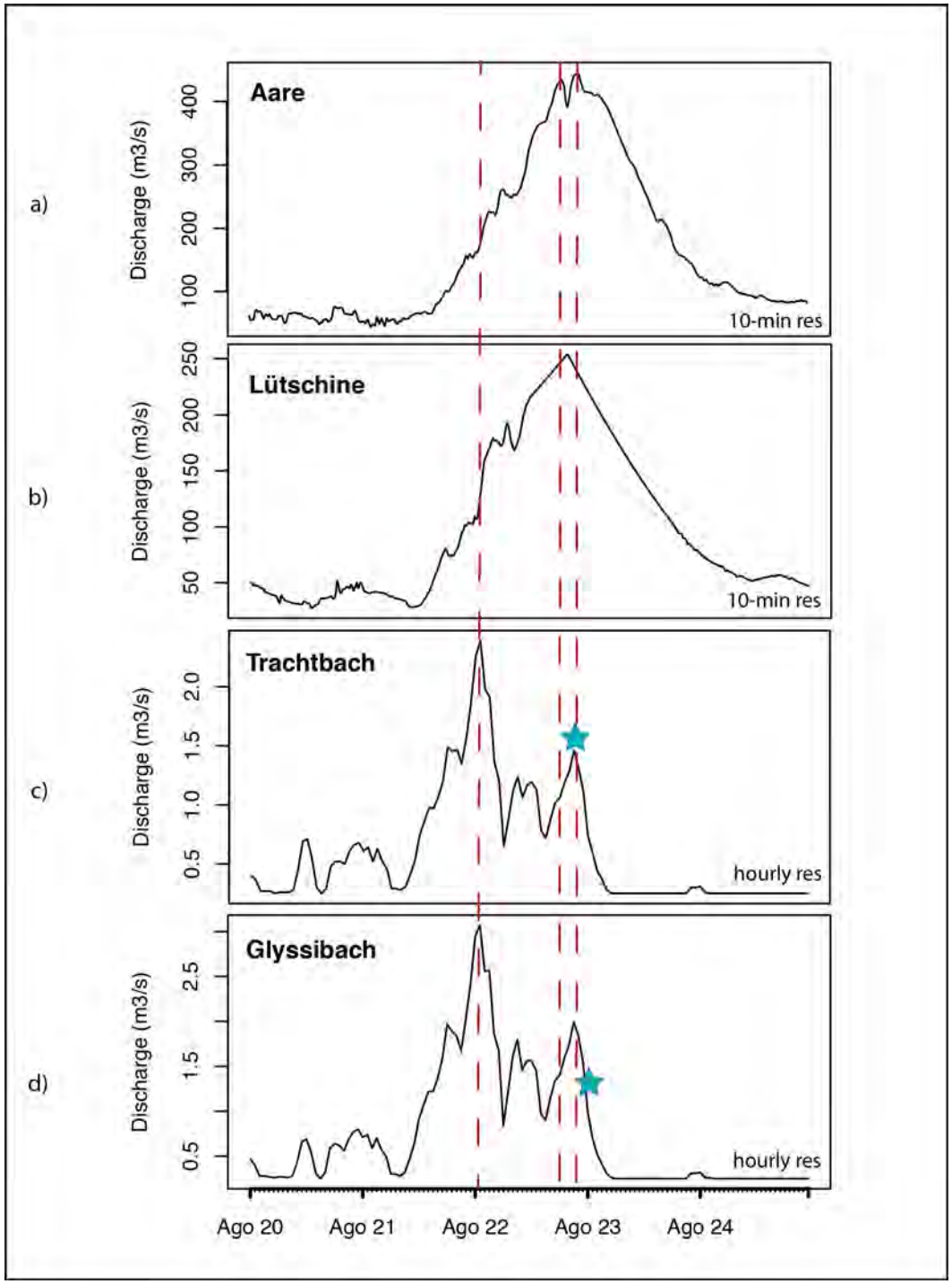

Fig. 4.18 Temporal discharge succession (in m^3/s) for Aare and Lütschine (a, b; 10-min time interval) and Trachtbach and Glyssibach (c, d; hourly time interval) during the 20-24th of August 2005. Red dotted lines highlight the major peak discharges, and blue stars indicates the two debris flows from Trachtbach and Glyssibach torrents

The plots present 10-min observations of Aare and Lütschine runoff (a, b) from the 20-24th August as well as hourly modelled data for Trachtbach and Glyssibach (c, d). The different time resolution is caused by the fact that modelling 10-min data for Trachtbach and Glyssibach would have resulted in a higher error uncertainty, while Aare and Lütschine 10-min data are accurate measurements.

The Aare runoff evolution (Fig. 4.16a) starts with increasing discharge on August 21st, at 01:00h. A strong increase in discharge followed the start, leading to an evolution from 65 m^3/s at 13:00h to 260 m^3/s at 06:30h of August, the 22nd. Following, a continuous increase in discharge occured, with two

different runoff peaks registered at around 19:00h and 23:00 on the 22nd. Discharges reached 434 m³/s and 444 m³/s, respectively, with the latter representing the highest peak discharge throughout the entire flood event. After these peaks, in fact, runoff sharply decreased, coming back to normal values by the end of August the 23rd.

Runoff evolution of Lütschine followed the one from the Aare, however it differs in some characteristics (Fig. 4.16 b). The initiation of the increasing discharge, for instance, was recorded at 11:00 h, several hours later than the initiation of Aare river. Lütschine was characterized by a single runoff peak of 254 m³/s, at 20:00 h on the 22nd. After this peak, a decrease in discharge was observed, and the flow came back to normality on 24th of August.

Concerning Trachtbach and Glyssibach runoffs (Fig. 4.16 c, d), both plots differ very slightly from each other concerning timing, while they differ in terms of discharge volume. Glyssibach, in fact, is characterized by a higher discharge than that of Trachtbach. For both rivers, the start of increasing runoff is modelled to have occured on the 21st, between 07:00-08:00h. After the initiation of higher discharge, a first peak was reached on the 22nd, at 01:00h. While Glyssibach's runoff reached 3.07 m³/s, Trachtbach's peak amounted to 2.39 m³/s. After these runoff peaks, both river's experienced a sharp and fast decrease in discharge, followed by a second peak on the 22nd at 12:00h, with 1.56 and 1.13 m³/s discharge for Glyssibach and Trachtbach, respectively. A final, third peak was registered later in the evening, at 21:00 pm, with 1.99 and 1.46 m³/s for Glyssibach and Trachtbach, respectively. As presented in Section 1.7.2.1, it was at this time that witnesses reported that in Trachtbach channel a low viscosity debris flow entered Brienz and overflew the channel (Müller, 2007). Following those peaks, a sharp decrease in discharge is observed in the plot, coming back to normal baseflow (0.25 m³/s) in the morning of 23rd of August, at 06:00 for both rivers. It was during this decrease in discharge, at 02:00 of the 23rd, that a very rapid debris flow was reported to come from the Glyssibach river and hit Brienz, leading to 2 casualties.

In order to summarize the temporal succession during the flood event Figure 4.19 presents a timeline with the different timings of initiation and peak runoff of each river.

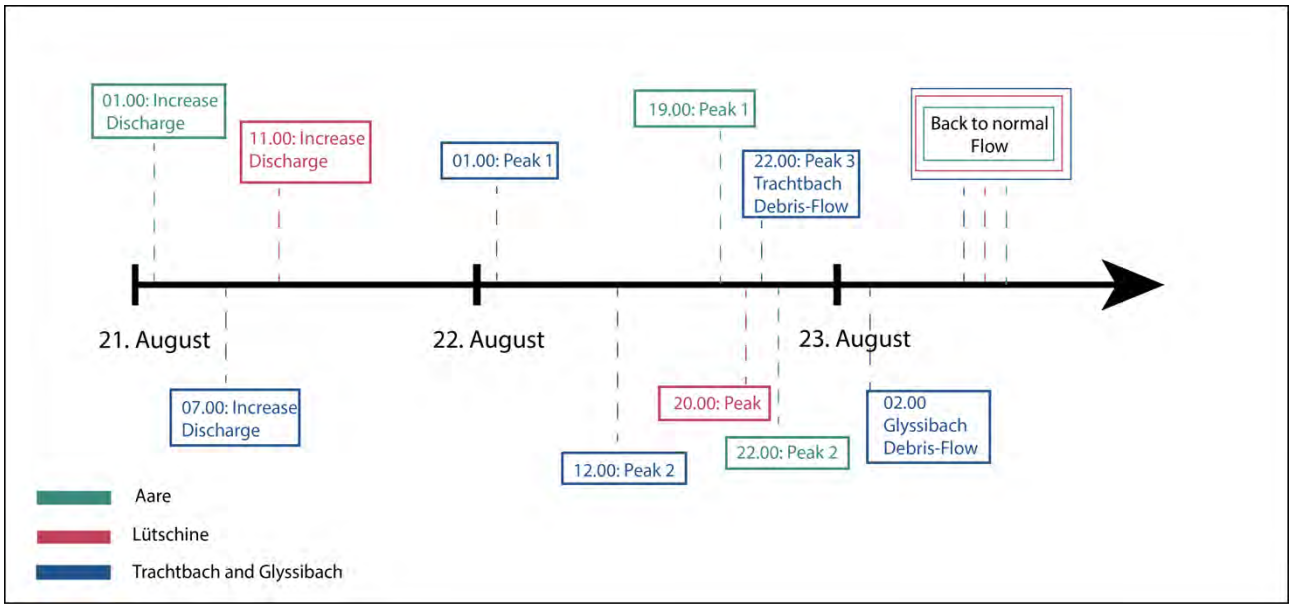

Fig. 4.19 Timeline of the 2005 August event from the 21st to the 23rd of August. Green characterizes Aare succession, while in red Lütschine discharge succession is presented. Because of their similar discharge pattern, Trachtbach and Glyssibach are both represented with the blue colour

5 Discussion

5.1 Flood Layers and Sedimentary Features in Lake Brienz

The analyses and observations performed on the numerous sediment cores from Lake Brienz allowed the differentiation and distinction between flood layers and background sedimentation within the entire sedimentary sequence of the lake. For lakes characterized by a steep watershed, a flat central basin and a few dominant inflows, transport of sediments during a flood event should provide allochtonous sedimentation, therefore leaving a visible signature in the sediment record (Schillereff et al., 2014). This has been shown by previous flood reconstructions located in different regions and under different conditions by Vasskog et al. (2011), Kämpf et al. (2012), Wilhelm et al. (2012) and Wirth et al., (2013). Dominated by clastic material, background sedimentation for Lake Brienz is characterized by an alternation of light and dark grey laminations on a millimetre and sub-millimetre scale. Such laminations are interbedded with event layers, which were visually distinguished based mainly on their thickness, by a visual difference in colour and finally by changes in grain size.

5.1.1 Identification of Flood Layers in the Sedimentary Record

Following the initial differentiation, flood layers were distinguished from mass-movement layers (such as the 1996 delta collapse presented in Girardclos et al., 2007) based on their depositional characteristics. In general, flood layers were identified based on the lack of a thick, homogenous central unit ('homogenite'), which is typical for mass-movement induced turbidites (Sturm & Matter, 1978), and their graded sedimentary structure (both normal and inverse), which usually mirrors waxing and waning phases of riverine discharge. A first distinction between turbidites from Aare, Lütschine and lateral torrents was based on the layer thickness. Thin (on a millimitre scale) graded event layers in the deep basin were interpreted to be the result of increased discharge from the lateral torrents, while thicker (centimetre to decimetre scale) layers were interpreted to be generated by Aare and Lütschine floods. A further distinction between Aare and Lütschine floods was based on colour, with turbidites from Lütschine characterized by a darker colour compared to Aare turbidites. Some of the Lütschine flood layers do not, however, present a visual grading. It is therefore expected that such detrital layers correspond to very rapid and short-lived discharges, while graded turbidites may be characteristics for more long-lasting events.

Not all the retrieved cores were suitable for the distinction of flood layers and the specific identification of the 2005 flood layer. The cores located in the basin plain were characterized by a clear sedimentary sequence, with a clear distinguishable succession of lamination and event layers. However, the cores located in proximity of the Aare and Lütschine deltas, as well as to the inflows of Trachtbach and Glyssibach, present a more disturbed layering, which impeded an intercorrelation between all the cores. As presented in the paper from Sturm and Matter (1978), Aare and Lütschine deltaic areas are characterized by dynamic channel, gullies and levees. For this reason, cores retrieved from deltaic areas may present a disturbed layering because of the disturbed topography. As presented from the British Society for Geomorphology (Frew, 2012), coring near the shores and on steep slopes should be avoided in order to not retrieve cores presenting disturbed layering because of sediment re-suspension. This could explain the disturbed cores retrieved in proximity of the Trachtbach and Glyssibach inflows.

5.1.2 Physical properties: Magnetic susceptibility and Bulk Density

Magnetic susceptibility and bulk density were measured for all the cores in order to identify flood layers based on their expected higher density and magnetic properties (Gilli et al., 2013). Magnetic susceptibility (MS), which reflects deposits rich in Fe-minerals, is usually higher for detrital input and coarser grain size (Chapron et al., 2005; Wolfe et al., 2006), while high bulk density should respond to coarser particles at the base of turbidites (Gilli et al., 2003; Gilli et al., 2013). Previous studies (i.e. Foster et al., 2003; Osleger et al., 2009; Gilli et al., 2013) showed that MS profiles are suited to highlight detrital input and therefore suitable for the identification of flood events. However, MS values (expressed as 10^{-5} SI) measured in Lake Brienz present relatively low values (ranging from 3 to 12 10^{-5} SI) and show only faint variations. An explanation for such behaviour could be related to the lithology and geology of the Lake Brienz catchment, which is mainly characterized by sedimentary and carbonate rocks (e.g. limestones, schists, marls) in the Lütschine catchment and by crystalline and intrusive rocks (e.g. granite, gneiss, quartz, diorite) in the Aare catchment. As reported from Dearing (1999) and Lascu (2009), carbonate and sedimentary rocks are characterized as diamagnetic, presenting weak or even negative magnetism. Crystalline and intrusive rocks are instead characterized as paramagnetic, and present a relatively low magnetism (Dearing, 1999; Lascu, 2009). This could be in line with the observations along the cores, for which cores proximal to the Aare present higher magnetic susceptibility values compared to the cores proximal to the Lütschine inflow.

Bulk density variations, instead, precisely follow changes in grain size, which is in line with what Gilli et al (2013) presented. Similar results have been described by Simonneau et al. (2013) in a study aiming at identifying flood layers in an Alpine lake presenting a similar geology to Lake Brienz. Therefore, bulk density profiles support the initial visual differentiation between background sedimentation and flood layers.

5.1.3 Elemental Proxy for Grain Size

Together with bulk density, zirconium (Zr) elemental profiles on long cores were used as main proxy for grain-size changes and therefore for the identification of turbidites along the cores. Zr is usually associated with heavy and high resistant minerals (Croudace et al., 2006; Kylander et al., 2011), and in the literature is found to be related to both detrital input and changes in grain size (Croudace et al., 2006; Kylander et al, 2011). Concerning grain size, this element is usually enriched in coarse silt and sand (Kylander et al., 2011), and therefore high values of Zr reflect coarser grains, which is the case for Lake Brienz cores. The same relationship was found to be true in a previous study on the Aare floodplain in the Brienz area by Schulte et al. (2015), which used Zr as a proxy for grain size as well as a tracer for sediment supply. As presented from Kylander et al. (2011), zirconium is often associated with quartz, which is found in the uppermost area of the Aare catchment in the crystalline rocks (e.g. amphibolite, granite). Quartz is also fund in sedimentary rocks in association with limestone, both present in Aare and Lütschine catchments (Johnsson, 1993; Schulte et al, 2009, 2015).

5.2 Identification of the August 2005 Flood Layer

The 2005-layer was first identified and isolated based on visual observations on the new cores and comparison with a core taken immediately prior to the event in a previous study from Anselmetti et al. (2007) (Core BR05-3). Layers corresponding to the 2005 flood event in the retrieved cores were identified and located also based on the thickness of the sediment. Theoretically, thickness of flood layers is largely dependent on the magnitude of the event, which determines the carrying capacity and

the duration of the discharge (Schillereff et al., 2014). Bøe et al. (2006) also linked thickness to an increase in grain size and a better sorting of the particles, which follows an increase in stream power that would be in line with the results for Lake Brienz. Grain-size analysis performed on the turbidite showed a poor sorting of particles indicating that the 2005 turbidite was a hyperconcentrated flow, as presented by Marren (2002). Hyperconcentrated flows are poorly sorted and characterized by coarse grain size (Webb et al., 1989). The identified 2005-layers are characterized by thicknesses varying between 1.5 cm (for cores proximal to Aare) and 3.5 cm (for cores proximal to Lütschine). Despite single cores being characterized by event layers of even higher thicknesses, the 2005 layer is the only detrital event presenting similar thickness along the entire transect of the lake. Thicker events are only characteristics for the area in proximity of one of the major tributaries (Aare or Lütschine). The only consistently thicker event layer in the sediment record is the 1996 megaturbidite layer, which is visible in almost all the cores retrieved. However, this event layer was triggered by a sudden collapse of the Aare delta, and not by a flood event (Girardclos et al., 2007).

In some studies, layer thickness (and therefore the amount of transported sediments) has been related to the amplitude of the flood event (Lamoureux, 2000; Lamb et al., 2010; Schiefer et al., 2011). Based on this relationship, a rough estimate of the amount of material transported could be derived from the similar layer thickness along the different cores, as will be discussed later on. However, it is important to also consider the availability of sediments within the catchment: flood events with the same magnitude may lead to different sediment thicknesses due to more or less availability of sediments (Schillereff et al., 2014). This could be an explanation of why, for instance, other turbidites present in the core are thicker when compared to the 2005 flood event, despite the latter represent the highest magnitude and discharge of the last 80 years (Bezzola & Hegg, 2007).

The difference in thickness between the Aare and Lütschine cores could also be explained by the role played by the hydropower basins upstream from the Aare catchment. As shown by Anselmetti et al. (2007) and Finger (2006), the upstream reservoirs retain a large volume of suspended sediments, which are trapped in the basin. Moreover, the upstream dams contributed to a reduction of the Aare discharge during the flood event in 2005 by almost 20% (Bezzola & Hegg, 2007) . This may be a reason why 2005 layers in Aare cores present thinner sections compared to ones of Lütschine.

5.3 Identification and Differentiation of the Catchments Fingerprints and Riverine Contribution

5.3.1 Grain Size

Grain-size analysis was performed on the 2005 layer with the aim of identifying the influences of Aare and Lütschine rivers along the cores. Another aim was to determine whether the hypothesized 2005 layers correspond to a turbidite, following the relationship between variations in grain size and depositional processes presented by the studies of Vasskog et al. (2011) and Czymzik et al. (2013), in which they related graded layers as being a consequence of hyperpycnal flows deriving from flood events. As reported by Schillereff et al. (2014), lake sediments characterized by a major clastic composition should mirror an increase in river discharge through an upcore increase in grain size. Positive correlations between coarser grain size and higher discharge (related to flood events) have been found, for instance, in the studies from Campbell (1998) and Lenzi & Marchi (2000). Since sedimentation in Brienz is mainly controlled by Aare and Lütschine inflows (Sturm & Matter, 1978), the 2005 layers were interpreted to be related to an increase in discharge from the two main tributaries.

The results from particle-size analysis showed, in general, a major composition in coarse to fine silt, which follows previous results from Sturm (1976) and Sturm & Matter (1978). Moreover, a normal, fining-up sequence from coarser to finer grains (coarse silt-sand to fine silt) was characteristic for all the layers along the WE transect. Such normal grading is interpreted to be reflecting the evolution of discharge under the flood event, with coarser grains at the base mirroring peak discharge and a fining-up sequence following decrease in discharge power. Peak discharge for large flood events often results in a hyperpycnal plume travelling as underflow, depositing coarsest particles at the base of the turbidite. The decrease in discharge following the peak runoff is usually characterized by a lower carrying capacity (lower sediment load) and therefore by less and smaller suspended particles. Such water mass may therefore enter the lake as inter- or overflow, depending on the thermal stratification of the lake, and deposit the finer particles above the initial coarse base. Larger grain size can therefore also be related to a rapid current velocity of the river. Such behaviour has been observed in other studies, for instance from Arnaud et al. (2002), Cockburn & Lamoureux, (2008), Giguet-Covex et al. (2012) and Simonneau et al. (2013).

The 2005 layers do not present, however, the same depositional mechanism for all the cores. The cores located proximal to the Aare inflow are characterized by a visually more homogeneous layer, also presenting smaller variations in grain size. However, despite not being visually detectable, grain-size analysis showed a fining up sequence characterized by a higher input of sand rather than silt or clay. The cores presenting this type of deposition are LB15-7, LB15-8, LB15-20, and have been interpreted as containing an Aare signal. LB15-18 and LB15-19 presented an interesting result. The two 2005-layers are characterized by organic material (as described in section 4.4) over- and underlain by what it was interpreted to be the turbidic flow coming Aare. The results of grain-size analysis showed that the organic matter layer is largely composed by sand-sized particles (up to 80%), which decreases at the contact with the overlying turbidite. While the percentage of sand-sized particles decreases, mean grain size increases up to 80 microns, which is consistent with what is found in the Aare turbidite of the representative core LB15-8. Therefore, the layers over- and underlying the organic matter section present in LB15-18 and LB15-19 were interpreted to be part of the Aare turbidite. The organic detrital layer will be discussed in section 5.3.3.

The cores proximal to Lütschine inflow (LB15-2, LB15-14, LB15-15, LB15-3) present a different depositional sequence. The 2005 layers for those cores are characterized by two visually overlying fining-up sequences of much finer particles compared to Aare cores. First, coarser grain size is characteristic for the base of the layer. Such a coarser and darker layer is then overlain by a decrease in grain size, which is in line with the expected waning behaviour of a flood-derived discharge. However, in the middle of the layer a coarsening of particles is visible, followed by another fining-up sequence. A first hypothesis suggested that this sub-layering was due to an superposition of turbiditic flows, with the basal sub-layer (B) corresponding to Lütschine discharge and the upper sub-layer (A) corresponding to Aare discharge. Previous studies on the lake by Sturm and Matter (1978) showed in fact that Aare turbidites are likely to travel along the lake towards the Lütschine inflow, while the opposite has not yet been observed. As it will be presented in the next few sections, however, this hypothesis is no longer supported.

5.3.2 Geochemical Signature

A geochemical analysis was performed through XRF analysis on the 2005-layers, as well as on chosen representative long cores. The aim was to identify representative elements characteristic for Aare and Lütschine signatures, which in turn are determined by their catchments' geology. The final scope of this

analysis was to discern the source of each 2005 layer and sub-layers within the set of cores, between Aare and Lütschine input and therefore determine the extent of the turbidic plumes of the tributaries during the event.

While on long cores Zr was mostly used (Fig. 4.6), on 2005-layers the ratios Zr/Rb were used as proxy for grain size, perfectly following the sedimentological grading present in the cores. Despite Zr/K was first used as hypothetical proxy for grain size, Zr/Rb represented a more sensitive signal, following the different grain size signatures much more precisely. This combination of elements as proxy for grain size was also used in previous studies from Norway (Vasskog et al., 2011) as well as in the Aare floodplain (Schulte et al., 2015). Because Rb, a heavy mineral resistant to weathering (Vasskog et al., 2011), is usually associated with clay fraction and Zr in coarse silt and sand, higher values of Zr/Rb correspond to coarser particles, which is in line with the findings from the two previously mentioned papers from Vasskog et al. (2011) and Schulte et al. (2015). Rb profiles also showed a decrease in signal for the 2005-layer: a similar pattern was also recorded in the study from Vasskog et al (2011) at Lake Oldevatnet, Norway. The lake, mainly composed by siliciclastic material transported through glacial outwash, presented in fact higher concentrations of Rb in background sedimentation and lower values within the different event layers. Rb associated with Sr (Rb/Sr) was in fact used to detect darker event deposits (largely composed by chemically-weathered material) from the Rb-rich, light-coloured background sedimentation. The same pattern was observed in Lake Brienz, looking at elemental profiles. While the association of Ca/Ti was presented by Schulte et al (2015) as representative for grain-size changes, the signal was not as strong as it was with the Zr/Rb couplet.

Concerning the individual elemental profiles, K, Ca, Ti, Rb and Zr present the most interesting profiles with the strongest signals. Such strong signals can be explained for Ti, Rb, K and Zr with their high resistance to weathering and conservative nature during transport (Kylander et al., 2011; Rothwell & Croudace, 2015; Vasskog et al., 2011). Ca is present in the lake in both as allochtonous and autochtonous origin (Sturm, 1976). However, since Ca is usually enriched in allochtonous material (Rothwell & Croudace, 2015), a strong signal was characteristic for the 2005-layer along the entire set of cores. The cores proximal to Lütschine, however, present a much higher content in Ca compared to the cores proximal to Aare. Such pattern is consistent with the lithology of the Lütschine catchment, mainly composed by sedimentary and carbonate rocks (Schulte et al., 2009).

The relationship between elements was explored through Spearman's Correlation and Principal Component Analysis (PCA), with the aim of identifying groups and associations of elements, which could be related to the lithological composition of the Aare and Lütschine catchment. The core proximal to Lütschine (LB15-14) presents a strong, positive correlation between Ca, Sr and Zr. Sr, associated with both carbonate and siliciclastic rocks (Kylander et al., 2011; Schulte et al., 2015,) is interpreted here as both a carbonate and grain-size signal. Sr can be easily mobilized through weathering (Salminen et al., 2005) and was also found to correlate with Zr in association with sand fraction (Schulte et al. (2015). Such results can be confirmed from the PCA of LB145-14 (Lütschine core), in which the biplot shown in Fig. 4.12 clearly shows a strong relationship between Sr and Zr. Therefore, the correlation between Ca, Sr and Zr is here interpreted to be both a signal of the lithological composition of Lütschine catchment as well as for variations in grain size. Another strong and positive correlation, which was found in the Lütschine cores, was that between Fe, K, Mn and Rb and to a minor extent with Al and Si. Si, Al and Fe were previously interpreted as being related to an aluminosilicate and limestone composition of the bedrock of Lütschine catchment (Schulte et al. (2009). Fe, Ti and K were interpreted in the same study as phyllosilicate minerals indicative for the crystalline rocks (such as biotite and chlorite) coming from the uppermost part of the catchment, whereas phyllosilicates were found to be related to grain size, and

most specifically with silt-sized grains, while coarser grain size were associated with limestones. Rubidium (Rb) is usually related to mica and clay minerals, and it has been shown to be a valuable proxy for both detrital input and grain size at Lake Les Echets, France (Kylander et al., 2011). Because Rb is a substitute for K and often found in granitic and metamorphic rocks (Salminen et al., 2005), it was expected for this project to be representative for Aare signal. Such correlations were interpreted to reflect the two main sedimentary sources of the Lütschine catchment, such as carbonate (Ca) and siliciclastic (phyllosilicates and aluminosilicates), which is in line with the results from Schulte et al. (2009).

Elemental composition of the core proximal to Aare (LB15-8) presented a different signal, with strong positive correlation between Fe, K, Ca, Ti, Mn, Rb and Si. Ca also presented a weak correlation with Sr, however, no correlation with Zr was found. Such results were in line with a previous study on the Aare floodplain (Schulte et al. (2015), relating Fe, Ti, Rb, K, Al and Mn to phyllosilicate group deriving from the metamorphic rocks characteristics for the Aare catchment. This study also presented a relationship between such phyllosilicate group with silt-sized grains, as for the Lütschine core. Finally, the 2005-turbidite of LB15-15 presents a high composition in phyllosilicates, which, however, could be related to both Aare and Lütschine catchments.

In general, geochemical analysis highlighted the lithological composition of the two catchments, with Lütschine mainly controlled by carbonate and siliciclastic sediments, and Aare mainly characterized by elements from the siliciclastic group. For both LB15-14 and LB15-8, the geochemical analysis provided insights on two main controlling factors, such as lithology (and therefore provenance of the sediments) and grain-size signal. In fact, a strong relation between the geochemical composition of the sediments and grain size was present for both Aare (LB15-8) and Lütschine (LB15-14) cores. Such relation can be explained by the susceptibility of different elements and their associated minerals to erosion and weathering processes, and can be reflected in the sediments, as presented by Bloemsma et al. (2012). Other studies relating geochemistry to grain-size are, for instance, those of Cuven et al., (2010), Kylander et al. (2011) and Moreno et al. (2011).

This double-relationship may explain the large variability of LB15-15, the core which was hypothesized to have recorded a double signal from both Lütschine (sub-layer B, at the base of the 2005 layer) and Aare (sub-layer A, overlying B). Such hypothesis was supported by the elemental profile, showing a decrease in Ca and an increase in Rb in the overlying sub-layer A. However, as a strong relationship between grain size and geochemistry of the catchment was found, the increase in Rb is expected to be related not to an Aare plume but more to an increase in fine-sized material, as the grading characteristic of flood layers suggests. This statement is supported by PCA performed on the two sub-divided layers, which did not show a significant change in composition. A possible explanation for the lack of significant results could be related to the used small dataset, contrasting with the main usage of a PCA, which is a reduction of dataset. Moreover, despite the Aare and Lütschine catchment are characterized by different compositions, with a major crystalline composition for Aare and a major sedimentary and carbonate composition for Lütschine, they both show a common phyllosilicate signal - as highlighted by the PCA – which could lead to misinterpretation and difficulty in differencing the geochemical signatures of the two catchments. Following the results and interpretation, the main element chosen to distinguish Aare and Lütschine input with a large degree of certainty is Calcium.

5.3.3 Carbonate Content

Because of the major importance of carbonate within the lake and for the Lütschine catchment composition, smear slides and carbon content analysis were performed on the 2005-layers. The aim was to differentiate between the Aare and Lütschine input based on their mineralogical composition and detrital (inorganic) carbon content. Lakes dominated by detrital clastic material such as Brienz are expected to contain primarily siliciclastics and reworked carbonates (Einsele, 2000). Detrital carbonate generates from weathering and inwash of carbonate rocks in the catchment and it is transported in the lake via streams and rivers (Smol et al., 2004). Because of the lithological composition of its catchment, Lütschine contribution of detrital carbonate was therefore expected to be reflected in the sediments, leading to an increase in inorganic carbon in the 2005-layers characterized by its signal.

In general, both analyses showed a higher carbonate content for Lütschine compared to Aare cores, which follows the results previously presented by Sturm (1976). Smear-slide analysis (Fig. 4.13) exhibits a much higher content in inorganic carbon in the cores proximal to the Lütschine inflow. Fig. 4.15 showing the distribution of organic and inorganic carbon content within the 2005-layers confirmed what previously observed through smear slide analysis. Lütschine cores (LB15-2, LB15-14, LB15-15 and LB15-3, following the WE transect) are characterized by a higher content in inorganic carbon, expressed as percentage of carbonate (including calcite, aragonite and dolomite). While the samples analysed from the Lütschine cores contain in average 26% of carbonate, Aare cores (LB15-20, LB15-8, LB15-7, LB15-18 and LB15-19) contain only 2.3%. Previous studies already indicated that carbonate concentration in the cores influenced by Lütschine contribution was at the time 3 times higher than what was found in cores related to Aare input (33 and 10% for Lütschine and Aare, respectively (Matter & Sturm, 1982). Such results are in line with the large difference measured in this study (Fig. 4.15).

Concerning the Lütschine cores, however, the initial hypothesis of the presence of two overlaying sub-layers (Section 4.3.2.2) contrasts with the carbonate content results. Initially, it was hypothesized that carbonate content would have supported the double-layering from Lütschine (bottom) and Aare (top) by showing differences in carbonate profiles for the two sub-layers. However, no clear pattern could be detected: there is no substantial increase or decrease in carbonate content along the layers. For this reason, the initial hypothesis can no longer be supported. A possible explanation for such depositional pattern may be that such sedimentary succession for Lütschine 2005 layers reflect the shape of the hydrograph. As shown in Fig. 4.16, before the peak discharge in the late night of August 22nd, a very rapid increase in runoff was recorded in the early hours of August 21st. It may be that such sharp increase in discharge was able to deliver sufficient sediment to generate an underflow (hyperpycnal flow) and depositing the first, coarse base. Based on this evidence, it is likely that sediment deposition followed two pulses resulting from the dual peaks (Fig. 4.16). As presented in section 1.7.2, large parts of the mobilized sediments during the 2005 event from the Lütschine catchment accumulated in the floodplain, and only in minor part entered the lake. It may therefore be that peak discharge does not mirror the highest sediment load during the event.

For the two lateral torrents, the very high concentration in carbonate for Trachtbach and Glyssibach shown in Table 4.6 (around 60% for both) is also in line with the previously mentioned study of Sturm (1976), in which it is presented that the lateral streams surrounding Brienz presented very high carbonate contents (up to 80%). The same study also showed that while the carbonate input from most of the lateral torrents is not detectable in the sediment record, high carbonate concentration in the stream torrents close to the village Brienz is recorded in in the sediment proximal to the shores (Sturm, 1976). Such strong differences in carbonate content between Aare and the two lateral torrents are used

in this study in order to identify the material transported from Trachtbach and Glyssibach torrents during the event. Interestingly, in LB15-18 and LB15-19 2005, layers with a different sedimentary structure compared to other Aare and Lütschine cores occur. Both sections were in fact characterized by a layer with remains of plant macrofossil and pollens, as shown by smear-slide analysis (Fig. 4.13) 'sandwiched' in layers presenting similar characteristics of Aare signal in terms of colour, grain size and carbonate content. These high-carbonate layers also contained much higher organic matter when compared to the observed values of Lütschine and Aare sediments (up to 20% of organic in LB15-18). These lithological signature, only occurring in those two eastern cores, is interpreted as being representative for detrital layers coming from the Trachtbach and Glyssibach debris flows. As Kämpf et al. (2012) presented in their study, detrital layers characterized by sand-sized particles and organic plant macrofossils may be indicative for "*short-range transport of littoral sediments from the steep lateral slopes, probably driven by local debris flows".* As presented in the previous sections, plant macrofossils have been found only in those two layers, and therefore the concluding hypothesis states that the two event layers are the result of the high-energy debris-flows of Glyssibach, and maybe of Trachtbach as well. As presented by Müller & Loew (2009), it was reported by eye witnesses that the debris flows of Trachtbach and Glyssibach were "high viscosity" masses caused by the liquefaction of precedent landslides in the catchments. Such masses can be defined as (hyper-)concentrated density flows (Mulder & Alexander (2001),. Subaerial concentrated density flows can occur during flash floods in mountainous catchments characterized by highly erosive areas, and are usually related to convective rainstorms (McArdell et al., 2007). When such density flows enter a lake their deposit is characterized by little or no grading, "*because suspension fall-out is relatively unimportant*" (Mulder & Alexander, 2001). Moreover, they can be strongly erosional. This is supported by the study from Müller & Loew (2009), in which it is presented that Trachtbach and Glyssibach debris-flows caused strong channel erosion in the range of 4-6 m deep. This erosive character is maintained even underwater (basal erosion) and allows the flow to continue moving for long-distances (Mulder & Alexander, 2001). This issue will be discussed in more details in the following section.

In general, despite Lütschine contains a high carbonate content compared to Aare, the difference with the two lateral torrents (characterized by a very high carbonate content) is very large. Such difference may be due to the fact that both Aare and Lütschine rivers originate from glaciers in the upper area of both catchments, and travel downstream for several kilometres before reaching the lake. Throughout the long path, carbonate particles contained in the water-mass may be more susceptible to dissolve and thus not reach the lake. Trachtbach and Glyssibach catchments' lithology is instead mainly characterized by carbonate and sedimentary rocks such as limestones and partly marls (Swisstopo). Because the upper reaches above the two catchments are marked by strong erosion (Müller, 2007), weathered carbonate can be easily transported downlospe and into the watershed network of the area. However, the travel path of the lateral torrents from the source to the lake is much shorted and rapid compared to the Aare and Lütschine path, leading to a more direct transport of the weathered carbonate in the lake, without deposition or dissolution. Finally, the area surrounding the two mountain torrents is forested, which could imply a higher input of organic matter in the watershed, also matching the lithological signature.

5.4 Missing Layers

Three cores retrieved from the centre of the lake do not include a clear 2005 event layer, moreover, their layering is disturbed and several attempts at these central locations did not result in successful recovery of undisturbed long cores.

A first explanation for this absence could rely on erosive processes, as previously mentioned for LB15-18 and LB15-19. Firstly, it can be hypothesized that the rapid debris flows of Trachtbach and Glyssibach triggered in August 2005 presented a highly erosive power and lead to a massive erosion of the sediments when entered the lake. High-magnitude floods, which lead to hyperpycnal flows may cause basal erosion due to the high density, speed and volume of the turbidity flow (Mulder et al. (2003). A similar hypothesis was formulated by Czymzik et al. (2013), who explained missing layers along the cores as caused by erosive processes during flood events. Others studies presenting basal erosion due to hyperpycnal flows, for example, are those of Simonneau et al. (2013) at Lake Ledro (IT) and of Thorndycraft et al. (1998) at Petit Lac d'Annecy (FR). However, the presented explanation is more a speculative hypothesis rather than a conclusive statement. Missing layers have been detected in other studies aiming at reconstructing palaeofloods in lakes, such as in Lamoureux (2000), Gilli et al. (2003), Czymzik et al. (2010) and Schiefer et al. (2011). Nonetheless, for most of the studies explanations for missing layers (which can be not deposited, not detected or not preserved) are rarely conclusive and often remain unproved.

However, erosive processes do not explain the disturbed layering that is characteristic for all central cores. Alternatively, the difficulties in recovering the cores in several attempts (not a challenge in pre-2005 campaigns in the deep Lake Brienz basin from the study of Anselmetti et al., (2007) might indicate the presence of a very coarse layer that is prone to slip out of the liner upon ascending while coring. The disturbed layering with partly vertical layering, the presence of the oxidized lake floor, and general disturbed layering might point towards chaotic and coarse lithologies that are not preserved through the non-piston type of coring. This lack of sediment information would represent a major drawback to fully understand the signatures and layers of the 2005 event in Lake Brienz and further analysis will be required to fully pinpoint the sedimentation processes in the middle of the lake (see Outlook).

5.5 Event Succession

The 2005 flood event was characterized by a succession of processes occurred in different parts of Lake Brienz catchment. From the 20th of August, high precipitation was recorded in the catchment, with a peak in rainfall during the 22nd of August reaching up to 98 mm of rain. In total, between the 20th and the 22nd of August, Brienz experienced 207 mm of precipitation. During the 21st of August, the inflows were characterized by a strong increase in discharge, which for all inflows was registered in the morning. However, peak discharges differ between the ones of Aare and Lütschine and the ones of Trachtbach and Glyssibach.

While the two major inflows (Aare, Lütschine) were characterized by a major peak discharge in the evening of the 22nd of August, the two torrents present a different discharge evolution with three separate peaks. However, the major peak in discharge (at 01.00h of 22nd of August, Fig. 4.18) does not correspond with the debris flow events, which hit Brienz and Schwanden b. Brienz in the night between the 22nd and 23rd of August and which likely brought the maximum of particle load. As presented in the reports about Trachtbach and Glyssibach events Zimmermann (2006 a, b), the third peak at 21-22 pm corresponds to the observation of the viscous debris flow along the Trachtbach channel in Brienz. However, it does not correspond to the destructive debris flow of Glyssibach, which hit Schwanden b. Brienz between 02.15-02.30 of the 23rd of August, despite the landslide is thought to have been initiated right before midnight. Such delay in timing between the landslide and the actual destructive debris flow may be explained the high sediment transport observed from 22pm onwards in the channel: as reported from eye witnesses, the increased sediment load accumulated on bridges and protective dams along the channel, as well as along the channel itself. Moreover, the lake was characterized by a higher water level,

which contributed to blocking the sediments along the channel from the bottom (Zimmermann, 2006b). When the landslide initiated, the moving mass transformed in a debris flow and travelled over the previously transported and blocked mass along the channel, outflowing the channel and destroying the village.

The modelled peak discharges (on the basis of precipitation time series) for Trachtbach and Glyssibach do not correspond to the estimated discharge as reported from Zimmermann (2006 a, b), both in timing and volume. Modelled discharges are characterized by a peak in the evening of the 21nd and they range from 2.5 m^3/s for Trachtbach to 3 m^3/s for Glyssibach, while in the night of the 22nd discharges reach a maximum of 1.5 m^3/s (T) and 2m^3/s (G). However, the report on the Trachtbach and Glyssibach events stated that the discharge peaks from the two torrents were recorded on the night of the 22nd of August, and not on the 21st as presented from the model (Fig. 4.18). Moreover, in the report, peak discharges of Trachtbach and Glyssibach were estimated to range from 120 to 160 m^3/s, respectively (Zimmermann, 2006), which is not in accordance with what showed in Fig. 4.18 (1.5 m^3/s for Trachtbach and 2 m^3/s for Glyssibach). A possible explanation for such a lag could be the difficulty of modelling such small and mountainous catchments with a wide range of parameters, such as rheological properties of the area, elevation, slope angle, etc. (Arattano & Franzi, 2004; Hall et al., 2014). Firstly, the heterogeneity of the terrain is problematic for discharge modelling. Secondly, under a high and intense precipitation event, mountain streams can rapidly transform into torrential rivers, which far exceed the expected discharge, especially if soils were already saturated from previous precipitation (Zillgens et al., 2005), as it is the case for the 2005 flood event. Moreover, the involved geomorphic processes characterizing the events, such as landslide and debris flows, are not taken into account in the model: modelled discharge for Trachtbach and Glyssibach is only based on precipitation and runoff coefficient for small and reactive mountain catchments (0.7). This could also be an explanation why a first major peak is observed not on the night of the 22nd, as for Aare and Lütschine, but on the night of the 21st, following the increase in precipitation observed in the area. Zillgens et al. (2005) reported spatio-temporal patterns of runoff generation in Alpine regions indicating that catchment's response to a precipitation event is very fast (hours). They discern between two types of runoff response depending on the type of rainfall. Short, intense precipitation events during a dry period can in fact cause a rapid runoff response characterized by a single direct peak (Fig. 5.1A, unimodal), while long-lasting precipitation events can cause a bimodal peak discharge, with an initial, direct peak response followed by a delayed peak in discharge (Fig. 5.1B, bimodal). The delayed peak, which is also function of the initial precipitation volume, can be characterized by an event (e.g. flood, debris flow) caused by additional rain following the initial precipitation volume.

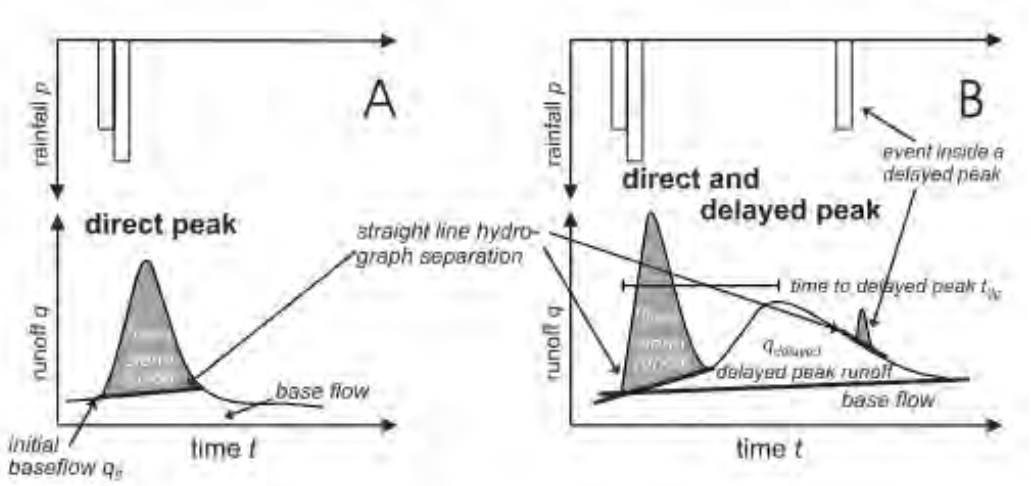

Fig. 5.1 Representation of hydrographs for unimodal (A) and bimodal (B) peak discharge, as presented by Zillgens et al. (2005)

Onda et al. (2001) also observed such bimodal behaviour with a delayed peak on one of the studied mountain torrents in Japan. They concluded that delayed peaks generally occur in watersheds which are characterized by a thick colluvium: the delayed peak is therefore related to the time water needs to flow into the bedrock cavities. In general, the modelled discharge of the two mountain torrents thus relates well to these previous studies as they follow the bimodal peak discharge shown in Fig. 5.1. Such bimodal distribution is characterized by an initial rapid response to rainfall followed by one (or even two) major peak runoff, and it is in line with the observations for the two mountain torrents.

In general, Trachtbach and Glyssibach were characterized by a rapid response to precipitation, with a second, major peak discharge starting and terminating rapidly. On the contrary, Aare and Lütschine discharge was much less abrupt, and once the peak was reached, the decrease towards a normal-state runoff took much longer than for the two mountain torrents.

5.6 Flow Paths and Sediment Volumes

To summarize, Fig. 5.2 presents the contribution of the different inflows to the sedientary records of the August 2005 flood event (Fig. 5.2a), as well as the geographical extent of their contribution (Fig. 5.2b). In general, the cores recording a Lütschine signal (based on colour, grain size, geochemical and carbonate-content analysis) comprise LB15-2, LB15-14, LB15-15 and LB15-3 and have been highlighted in red. On the other hand, the cores recording the Aare signal are represented by LB15-20, LB15-7, LB15-8 as well as LB15-18 and LB15-19. LB15-19 and LB15-18 also partly recorded the incoming flow from Glyssibach and Trachtbach - in green - that was deposited above and below an Aare layer (for LB15-19) and below (for LB15-18). It is expected that the bottom Aare layer shown for LB15-19 was also present in LB15-18 but has been eroded by the turbidity flow. Because of their very similar catchment (and therefore very similar signal), it was not possible to distinguish whether the organic detrital layer was deposited from one or both creeks. For this reason, the expected flow was presented in Fig. 5.2b as a result of both Trachtbach and Glyssibach torrents. Despite this, it can be hypothesized that the Aare turbidite extended towards the central and deepest basin (Anselmetti et al., 2007), however, the missing cores/layers in the depocentre do not allow further investigations. For this reason, Fig. 5.2 strictly relates to the signal observed in the 9 cores presenting the 2005 layer.

The exact volume of sediment transported and deposited during the event is not yet known. A few studies on single inflows related to the event have proposed estimations based on observations, however, no final statements or exact volumes transported have been found in the literature. For the Aare river, Bezzola & Hegg (2007) estimated that the total transported material during the event was ~350'000 m^3. However, an estimation on the amount of material, which actually reached the lake, has not been reported. For the Lütschine river, a report from the Tiefbauamt des Kantons Bern (2007) analysed the transported load during the event, indicating that in the area of Bönigen (Lütschine-Gsteig) 25'000 m^3 of material was deposited, while erosion in the area amounts to 20'000 m^3. According this publication, an estimated volume of 20'000 m^3 of material was transported in the lake.

The studies on Trachtbach and Glyssibach focused on the debris-flow events (Zimmermann, 2006a, 2006b). The studies do not provide information on the material transported into the lake, and mainly focus on the amount of detached material in the area above the villages of Brienz and Schwanden bei Brienz. For Trachtbach, the estimated initially mobilized material is estimated to be ~60'000 m^3, of which 10'000 m^3 are expected to have entered the lake under present conditions (Zimmermann, 2006a; Müller, 2007). Studies on the Glyssibach event assessed an initial mobilized volume of about 80'000 m^3, of which 50'000 m^3 was transported in the channel and developed into a 70'000 m^3 debris flow reaching the village of Schwanden bei Brienz (Zimmermann, 2006b; Müller, 2007). However, no further estimations on the amount of material transported in the lake could be found.
In general, it was not possible to retrieve an estimation of the sediment load transported in the lake during the event from the literature. All the reports mainly focus on damage and on future perspectives concerning mitigation and adaptation strategies of expected events in the future. The estimations for Trachbach and Glyssibach, moreover, only focus on the debris flows of the 22-23rd of August, and not on the entire length of the event, therefore likely underestimating the mobilized material. For this reason, an empirical estimation of the volume of deposited sediments has been calculated for this project, based on the mean sediment thickness of the 2005 layer and a simplified basin morphology of Lake Brienz. Table 5.1 shows the thickness values used for the calculation of mean thickness, while Table 5.2 shows the values used for the calculation of total deposited volume.

Table 5.1 Thickness and total mean thickness of the 9 cores presenting the 2005 layer

Core	**Thickness [cm]**
LB15-2	3.7
LB15-14	3.6
LB15-15	2.7
LB15-3	2.5
LB15-18	2.6
LB15-19	1.9
LB15-8	2.1
LB15-7	2
LB15-20	1.4
Total	**2.5 cm (0.025 m)**

Table 5.2 Calculation of total deposited volume during the 2005 event in Lake Brienz

Mean thickness	0.025 m
Basin length	14'000 m
Basin width	3'000 m
Total	0.025 x 14'000 x 3'000 = **1'050'000 m^3**

The mean thickness was calculated based on the thickness of each visible 2005 layer, while basin length and width was retrieved from the literature (Sturm & Matter, 1978). As shown in Table 5.2, the estimated volume of sediment deposited on the lake basin during the 2005 event is ~1 Mio m^3. However, the calculation is only based on the amount of sediments observed from the 9 cores showing the 2005 layer and must therefore be taken as a rough estimation rather than a conclusive statement. The calculation is based on two main assumptions:

- Thickness in the depocentre (missing layers) is similar to the one calculated based on the 9 cores. As shown from Anselmetti et al. (2007), however, the central basin (missing layers) is characterized by higher deposition in respect to the other areas of the lake

- The calculation is based on a largely simplified basin morphology, defined only by the length of the lake (14 km) and the maximum width of 3 km as reported from Sturm & Matter (1978). Therefore, the basin area calculated in Table 5.2 (14 x 3 km) is only a rough estimate and does not take into account slope gradients or morphological features of the basin

Following these assumptions, the real volume of deposited material may be larger than what was estimated here depending on real basin morphology and accumulation of sediments in the depocentre. Therefore, the result as proposed in Table 5.2 needs to be considered biased. However, this estimation may give an idea on the intense transport of material during the 2005 flood event, which lead to ~ 1 Mio m^3 of material deposition in the lake basin.

A further estimation of the volume of sediments transported by the individual inflows was calculated based on the theoretical area and thickness presented in Fig. 5.2. The basin area taken into consideration was retrieved based on the distribution of sediment cores presenting a specific riverine signal, and calculated on Swisstopo. Mean sediment thickness for each individual inflow was estimated based on the values presented in Table 5.1. For Trachtbach and Glyssibach signal, LB15-18 presents 1 cm of detrital organic material, while LB15-19 0.5 cm. Mean thickness for the two lateral torrents is therefore considered to be 0.75 cm.

Table 5.3 Transported sediment volume calculation for individual inflows

Inflow	Area [km^2]	Mean Thickness (cm)	**Tot Volume [m^3]**
Aare	8	2	160'000
Lütschine	5.5	3.12	171'600
Trachtbach & Glyssibach	2.3	0.75	17'250

As shown in Table 5.3, the estimated volume of sediments transported from the Aare river is about 160'000 m^3, while for Trachtbach is around 170'000 m^3. Trachtbach and Glyssibach sediment volume contribution as estimated to be around 17'000 m^3. For the two lateral torrents, it was not possible to discern between individual contributions and therefore the value is representative for both of them

together. Because the area taken into account for the calculation was only based on the location of cores presenting individual signals from the inflows, it is likely that the deposited sediments extend over a much broader area, therefore the real volume for each river contribution may be higher than the value presented in Table 5.3. This could explain the large difference between the total mass volume calculated in Table 5.2 and the individual contributions presented in Table 5.3 which, if summed, would lead to a total sediment volume of around 350'000 m^3, a much lower volume compared to the first total estimated. Moreover, the depocentre of the lake was not considered in the calculations because of the missing layers, therefore the calculation of individual contributions only shows a very minimal volume.

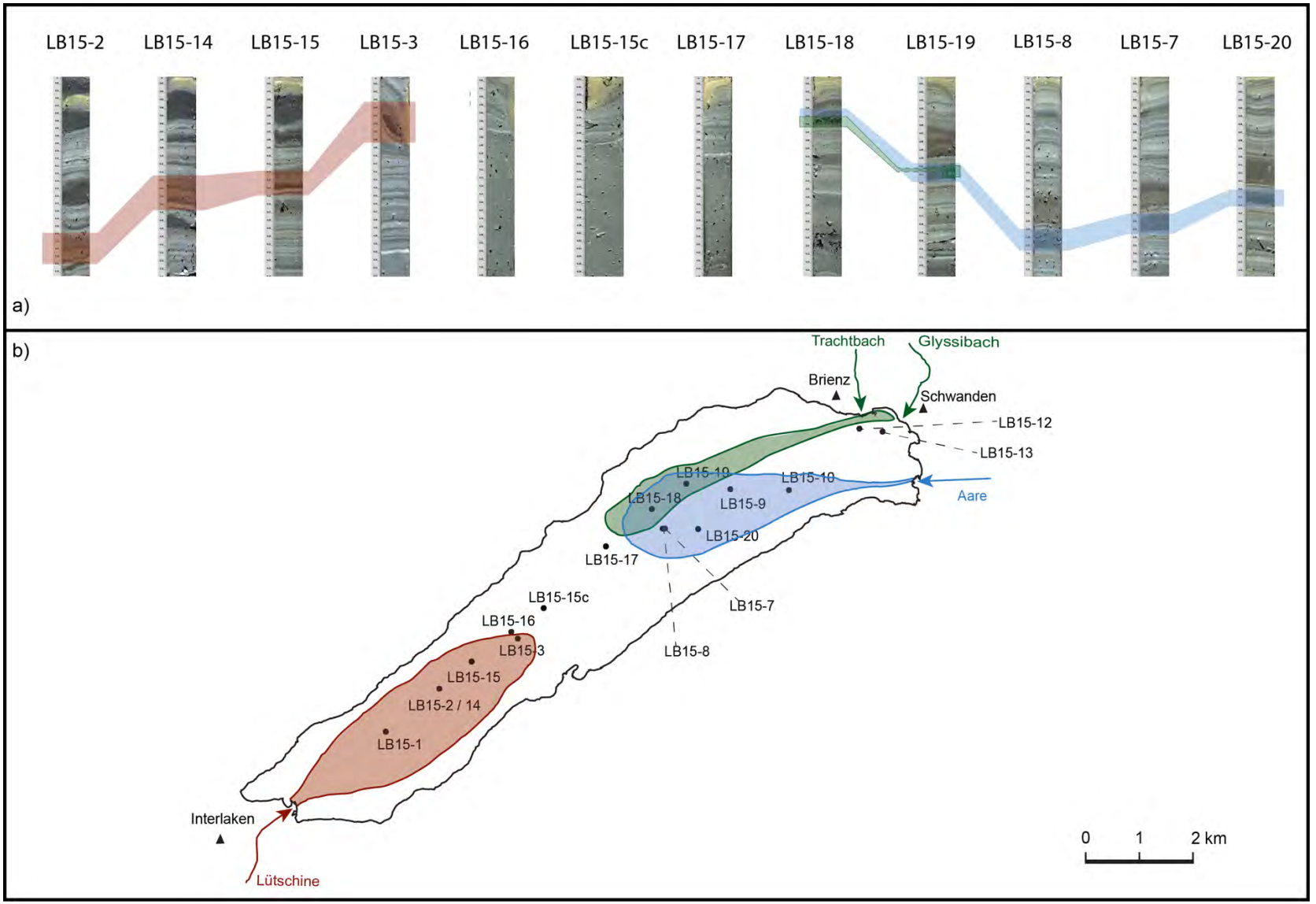

Fig. 5.2 Sketch representing the contribution (a) and extent (b) of the different inflows during the August 2005 flood event. Cores and extension of Lütschine signal is shown in red, Aare in blue and Trachtbach and Glyssibach in green

6 Conclusions and Outlook

6.1 Conclusions

Based on a number of sedimentological, physical and geochemical analysis, the sediment cores of Lake Brienz allowed to analyse and reconstruct the depositional processes in context of the August 2005 flood event. As a conclusion, the initial research questions will be addressed.

6.1.1 Distinction of Individual Flood Layers in the Sediment Record

Can we distinguish the individual flood layers from the respective inflows?

A visual observation, combined with an analysis of the physical properties of the sediments, grain size and elemental profiles allowed the distinction of numerous flood layers within the sediment record. In the clastic sediments of Lake Brienz, event layers deriving from allochtonous input of material are characterized by thicker, darker and coarser laminations, and can therefore be distinguished from the background normal sedimentation. Thick (centimetre to decimetre) dark layers represent both flood-related and one mass-movement induced detrital layer, which are distinguished based on their sedimentary structure. The only mass-movement induced turbidite layer derives from the Aare delta collapse in 1996 producing an up to 50 cm thickness in the cores retrieved for this study (90 cm in the study of Girardclos et al., 2007). Flood-triggered event layers are instead characterized by a few (up to 3-4 cm) thickness, and can visually be assigned to Lütschine or Aare based on the darker and lighter colour, respectively. The sedimentary record of Lake Brienz contains also thin (on a millimetre to a centimetre scale) event layers, darker and coarser than the background sedimentation. Such layers are interpreted to be deriving from an increase in discharge of lateral torrents around Lake Brienz.

6.1.2 Distinction of the August 2005 Flood Event in the Sediment Record

Can we distinguish the 2005 event layer in the sediment record?

The August 2005 flood event was identified in the sediment cores based on visual observation of thickness, sedimentological features and a correlations and comparisons with previous cores retrieved on the lake. Further grain-size analysis showed that all the event layers present the characteristics of a turbidite, with a coarser base followed by a fining-up sequence of particles size. Such layers have been interpreted to be the result of a massive flood event, mirroring waxing and waning of discharge. However, the 2005 turbidite was not identified in all the retrieved cores. While the cores in proximity of the shores and of the Aare and Lütschine delta present a disturbed sedimentary sequence, three cores retrieved from the centre of the lake do not contain the 2005 turbidite. Those missing layers can be interpreted in two different ways. First, such missing layers can be hypothesized to be the result of a massive basal erosion caused by the two debris flows initiated in the Trachtbach and Glyssibach catchments, which partly destroyed Brienz and Schwanden b. Brienz during the event. Alternatively, a very coarse and thick 2005 flood layer in the central depocentre could inhibit successful core recovery, as coarse irregular material might easily slip out of the core tube upon ascending through the water column.

6.1.3 Catchment Fingerprints and Extent of the Riverine Contributions

Can we distinguish the extent of the contribution of the different catchments during the 2005 event as recorded in the sediments of Lake Brienz?

The different catchment's fingerprints have been highlighted through a visual difference in colour, as well as geochemical, grain-size and carbon-content analysis. The Aare turbidite is characterized by lighter, coarser material composed by phyllosilicates and only very low carbonate content deriving from the metamorphic and crystalline rocks composing the majority of the catchment. The Lütschine can be identified based on a darker colour, finer particles (except for some recent event layers presenting very dark and coarser grains) and a carbonate (high) and siliciclastic (low) signal deriving from the lithological composition of the catchment (mainly sedimentary and carbonate rocks).
The 2005 layers of the two lateral torrents were identified in two cores based on the very high contribution of carbonate, which is higher than for both the two major inflows. The catchment lithology of Trachtbach and Glyssibach is almost purely composed by sedimentary rocks such as limestones and marls. The erosive processes characteristics for the upper area of the catchments contribute to the weathering and transport of detrital carbonates in the stream network. During the event, the the two debris flows transported large amount of material in the lake, therefore leaving a clear signal through their high content in carbonate. Moreover, detrital organic material was also a major component of these detrital layers: the debris flows, initiated in a forested area, transported downhill large amount of organic material (e.g. woods, leaves) which became deposited in the layer.

6.1.4 Sediment Transport During the Event

How much sediment was transported to the lake from the different catchments?

Because the cores located in the depocentre were missing the August 2005 event layer, an accurate calculation of the amount of sediment transported from the different tributaries was not possible. An empirical estimation accounts for 1 Mio m^3 of material deposited in the lake. However, the calculation is based on a simplified morphology of the basin and a mean thickness observed along the retrieved cores. From a simplified calculation, it was estimated that Aare contribution is of 160'000 m^3, that of Lütschine 171'6000 m^3 and that of Trachtbach and Glyssibach 17'250 m^3. However, this is rather a minimum volume calculation, and the transported volume from individual inflows is expected to be higher. Moreover, the depocentre of the lake provides no data for this calculation, bur represents the area that usually records the highest amount of sediments during an event, therefore the deposited volume is expected to be larger.

6.1.5 Temporal Succession of the August 2005 Flood Event

What was the temporal succession of extreme runoffs and can that be reconstructed using the set of sediment cores?

The temporal succession of the 2005 flood event in Brienz was reconstructed based on discharge measurements and the event layers in the cores. We propose the following succession:

1. Aare discharge started to increase in the early morning of 21st of August (01.00h).
2. Trachtbach and Glyssibach rapidly responded to precipitation and their discharge started increasing in the morning of the 21st of August (07.00h).

3. Lütschine river recorded an increase in discharge around 11.00 of 21st of August.
4. In the early morning of the 22nd of August (00.00-01.00h) Trachtbach and Glyssibach recorded a first peak in discharge. The modelled peak, however, did not correspond to the highest discharge from the catchments. At the same time, a very rapid increase in Lütschine is expected to have lead to a hyperpycnal flow, which caused the first dark and coarse basal layer in the Lütschine cores.
5. In the evening of the 22nd of August (19.00h and 22.00h) the Aare registered two similar peak discharges. The hyperpycnal Aare flow probably entered the lake at this time.
6. Lütschine peaked in discharge three hours after Aare (20.00h of 22nd of August). It is expected that such discharge contained lower amount of suspended particles, and was recorded in the sedimentary record as an overlying layer on top of the previously deposited one with a similar fining-up sequence.
7. Around 22.00h-23.00h of the 22nd of August, a debris flow from Trachtbach hit Brienz. Around 02.15h of the 23rd of August, another debris flow from Glyssibach hit and partly destroyed the village of Schwanden b. Brienz. The debris flows from the two mountain torrents entered the lake and are expected to have travelled towards the centre, possibly eroding the first deposited Aare sediments. A very rapid decrease in discharge followed the debris flows, and the flows came back to normality in the early hours of the 23rd of August.
8. After the debris flows, Aare and Lütschine recorded a still high -but decreasing- discharge until mid- 23rd of August. The continuous discharge from Aare lead to another sediment layer which overlaid the debris flow layer previously deposited.

6.2 Outlook

The results presented in this thesis provided an insight on the extreme flood event of August 2005 in Switzerland from the sediments of Lake Brienz. The lake proved to be a reliable archive recording the succession of the events and the contribution of the different catchments. The destructive power of the event is highlighted by the very large amount of material transported into the lake, as well as through the erosive character of the two debris flows. However, to fully understand the processes behind the 2005 flood, multibeam bathymetric measurements should be performed in the lake in order to retrieve a precise bathymetric map and morphological profiles of the basin. Such analyses would allow to understand netter the subaquatic flow paths of the various inflows. Moreover, a new reflection seismic survey imaging the lateral distribution and thickness of the 2005 flood layer (if thickness is above seismic resolution of 10 cm in the centre, where data yet is missing) would explain the missing layers in the depocentre, as well as would provide more information on the volume of sediments transported in the lake.

Flood events such the August 2005 flood in Lake Brienz highlight the importance of better understanding triggers and processes behind natural hazards in mountainous area, especially under a changing climate. Changes in climatic patterns such as changes in air temperature and precipitation, as well as the increase in extreme meteorological events expected for the future (as predicted from the IPCC report) would lead to substantial changes in the hydrological cycle as it is, in this example, discharge and related flood events. Because climate change is happening, it is therefore extremely important to being able to understand not only streamflow trends per se, but also integrate their behaviour in a much broader perspective, taking into consideration all the different actors and processes influencing discharge in the Alpine area. As introduced at the beginning of this project, the role the Swiss Alps have on transport and distribution of water, as well as for human settlements, is of extreme importance for both the Swiss population and the surrounding regions. Following, changes in

the hydrological cycle and in the magnitude and frequency of flood events may lead to a substantial increase in danger for the natural habitat and for anthropogenic activities. Therefore, more detailed and comprehensive studies on Alpine regions and their relationship with changes in climate should be performed in order to better understand the complexity of the sub-Alpine and Alpine areas and the relative relationship with shifts in natural climate. Another factor which should be addresses in further studies is the influence between global large scale circulation and processes such as the North Atlantic Oscillation (NAO) and the hydrological regime of the Alps. The alpine area is in fact located in a transition region between different climatic zones, and it is influenced by the Mediterranean, Atlantic regime and continental regime (NAO). It is therefore important to understand the effect that changes in these different climatological regimes will have on the future hydrology of the Alps.

To conclude, the present study provides valuable information how extreme flood events during the Holocene get recorded in the lake sediment record. The 2005 flood is the result of an extreme precipitation event, which has not been proved to be caused by a change in the climate system, but it was rather the result of natural climate variability in a mountainous region such as Switzerland. Calibrating the lacustrine flood layer with the observed and measured processes of the event allows a more comprehensive understanding of Holocene natural climate variability using the longer Lake Brienz sedimentary record. The extreme event discussed in this thesis can be used as a textbook case to interpret climatic conditions of other similar events that were created by heavy precipitation. Moreover, the 2005 event can be used as an example for the potential modelling of future extreme events, a phenomenon which is projected to increase towards the end of the century.

References

Adams, E. W., Schlager, W., & Anselmetti, F. S., 2001. "Morphology and curvature of delta slopes in Swiss lakes: Lessons for the interpretation of clinoforms in seismic data." *Sedimentology* 48(3): 661–679.

Amann, B., Szidat, S., and Grosjean, M., 2015. "A millennial-long record of warm season precipitation and flood frequency for the North-western Alps inferred from varved lake sediments: implications for the future." *Quaternary Science Reviews* 115: 89–100.

Anselmetti, F. S., Bühler, R., Finger, D., Girardclos, S., Lancini, A., Rellstab, C., and Sturm, M., 2007. "Effects of Alpine hydropower dams on particle transport and lacustrine sedimentation." *Aquatic Sciences* 69(2): 179–198.

Arattano, M., and Franzi, L., 2004. "Analysis of different water-sediment flow processes in a mountain torrent." *Natural Hazards and Earth System Sciences* 4: 783–791.

Arnaud, F., Lignier, V., Revel, M., Desmet, M., Beck, C., Pourchet, M., Charlet, F., Trentesaux, A., and Tribovillard, N., 2002."Flood and earthquake disturbance of 210Pb geochronology (Lake Anterne, NW Alps)". *Terra Nova* 14(4): 225–232.

Barredo, J. I., 2007. "Major flood disasters in Europe: 1950-2005." *Natural Hazards* 42(1): 125–148.

Bauselinck, L., Govers, G., Poesen, J., Degraer, G., & Froyen, L., 1998. "Grain-size analysis by laser diffractometry: comparison with the sieve-pipette method." *Catena* 32: 193–208.

Beniston, M., 2006. "August 2005 intense rainfall event in Switzerland: Not necessarily an analog for strong convective events in a greenhouse climate." *Geophysical Research Letters* 33(5): 1–5.

Beniston, M., 2010. "Impacts of climatic change on water and associated economic activities in the Swiss Alps." *Journal of Hydrology* 412: 291–296.

Bezzola, G. R., & Hegg, C., 2007."Ereignisanalyse Hochwasser 2005, Teil 1 - Prozesse, Schäden und erste Einordnung." *Umwelt BAFU, Eidgenössiche Forschungsanstalt WLS. Umwelt-Wissen* 0707: 1-215

Birsan, M. V., Molnar, P., Burlando, P., and Pfaundler, M., 2005. "Streamflow trends in Switzerland." *Journal of Hydrology* 314(1-4): 312–329.

Bloemsma, M. R., Zabel, M., Stuut, J. B. W., Tjallingii, R., Collins, J. A., and Weltje, G. J., 2012. "Modelling the joint variability of grain size and chemical composition in sediments." *Sedimentary Geology* 280: 135–148.

Bøe, A.-G., Dahl, S. O., Lie, Ø., and Nesje, A., 2006. "Holocene river floods in the upper Glomma catchment , Southern Norway : a high-resolution multiproxy record from lacustrine sediments." *The Holocene* 3: 445–455.

Campbell, C., 1998. "Late Holocene lake sedimentology and climate change in Southern Alberta, Canada." *Quaternary Research* 49(1): 96–101.

CH2011, 2011. "Swiss Climate Change Scenarios CH2011." *Published by C2SM, MeteoSwiss, ETH, NCCR Climate, and OcCC, Zürich, Switzerland.*

CH2014-Impacts, 2014. "Toward quantitative scenarios of climate change impacts in Switzerland."

Published by OCCR, FOEN, MeteoSwiss, C2SM, Agroscope, and ProClim, *Bern, Switzerland.*

Chapron, E., Arnaud, F., Noël, H., Revel, M., Desmet, M., and Perdereau, L., 2005. "Rhone River flood deposits in Lake Le Bourget: a proxy for Holocene environmental changes in the NW Alps, France." *Boreas* 34(4): 404–416.

Cockburn, J. M. H., and Lamoureux, S. F., 2008. "Inflow and lake controls on short-term mass accumulation and sedimentary particle size in a High Arctic lake: Implications for interpreting varved lacustrine sedimentary records." *Journal of Paleolimnology* 40(3): 923–942.

Cohen, A. S., 2003. *Paleolimnology: The History and Evolution of Lake Systems.* Oxford University Press, New York, 528 pp..

Croudace, I. W., Rindby, A., and Rothwell, R. G., 2006. "ITRAX: description and evaluation of a new multi-function X-ray core scanner." *Geological Society* 267: 51-63.

Croudace, I. W., and Rothwell, R. G., 2015. *Micro-XRF Studies of Sediment Cores: Applications of a non-destructive tool for the environmental sciences.* Developments in Paleoenvironmental Research 17. Springer, Dordrecht, 649 pp.

Cuven, S., Francus, P., and Lamoureux, S. F., 2010. "Estimation of grain size variability with micro X-ray fluorescence in laminated lacustrine sediments, Cape Bounty, Canadian High Arctic." *Journal of Paleolimnology* 44(3): 803–817.

Czymzik, M., Dulski, P., Plessen, B., Von Grafenstein, U., Naumann, R., and Brauer, A., 2010. "A 450 year record of spring-summer flood layers in annually laminated sediments from Lake Ammersee (southern Germany)." *Water Resources Research* 46(11): 1-16

Czymzik, M., Brauer, A., Dulski, P., Plessen, B., Naumann, R., von Grafenstein, U., and Scheffler, R., 2013. "Orbital and solar forcing of shifts in Mid- to Late Holocene flood intensity from varved sediments of pre-alpine Lake Ammersee (southern Germany)." *Quaternary Science Reviews* 61: 96–110.

Dearing, J. A., 1999. *Environmental Magnetic Susceptibility.* 2nd Edition, Chi Publishing, Kenilworth, 52 pp.

Di Stefano, C., Ferro, V., and Mirabile, S. (2010). "Comparison between grain-size analyses using laser diffraction and sedimentation methods." *Biosystems Engineering* 106(2): 205–215.

Finger, D. C., 2006. "Effects of hydropower operation and oligotrophication on internal processes in Lake Brienz." *Diploma Thesis, Swiss Federal Institute of Technology (ETHZ).*

Foster, G. C., Dearing, J. A., Jones, R. T., Crook, D. S., Siddle, D. J., Harvey, A. M., James, P. A., Appleby, P. G., Thompson, R., Nicholson, J., and Loizeau, J. L., 2003. "Meteorological and land use controls on past and present hydro-geomorphic processes in the pre-alpine environment: An integrated lake-catchment study at the Petit Lac d'Annecy, France." *Hydrological Processes* 17(16): 3287–3305.

Frei, C., Davies, H. C., Gurtz, J., and Schär, C., 2000. "Climate dynamics and extreme precipitation and flood events in Central Europe." *Integrated Assessment* 1: 281–299.

Frew, C., 2012. Section 4.1.1: Coring Methods. In: Cook, S.J., Clarke, L.E. and Nield, J.M (Eds.). *Geomorphological Techiniques*. British Society for Geomorphology, London, UK.

Froidevaux, P., and Martius, O., 2016. "Exceptional integrated vapour transport towards orography : an important precursor to severe floods in Switzerland." *Quarterly Journal of the Royal Meteorological Society*.

Giguet-Covex, C., Arnaud, F., Enters, D., Poulenard, J., Millet, L., Francus, P., David, F., Rey, P-J., Wilhelm, B., and Delannoy, J. J., 2012. "Frequency and intensity of high-altitude floods over the last 3.5ka in northwestern French Alps (Lake Anterne)." *Quaternary Research* 77(1): 12–22.

Gilli, A., Anselmetti, F. S., Ariztegui, D., and McKenzie, J. A., 2003. "A 600-year sedimentary record of flood events from two sub-alpine lakes (Schwendiseen, Northeastern Switzerland)." *Eclogae Geologicae Helvetiae* 96: 49–58.

Gilli, A., Anselmetti, F. S., Glur, L., and Wirth, S. B., 2013. "Lake Sediments as archives of recurrence rates and intensities of past flood events." *Advances in Global Change Research* 47: 225–242.

Girardclos, S., Schmidt, O. T., Sturm, M., Ariztegui, D., Pugin, A., and Anselmetti, F. S., 2007. "The 1996 AD delta collapse and large turbidite in Lake Brienz." *Marine Geology* 241(1-4): 137–154.

Hall, J., Arheimer, B., Borga, M., Brázdil, R., Claps, P., Kiss, A., Kjeldsen, T.R., Kriauciuniemé, J., Kundzewicz, Z.W., Lang, M., Llasat, M.C., Macdonald, N., McIntyre, N., Mediero, L., Merz, B., Merz, R., Molnar, P., Montanari, A., Neuhold, C., Parajka, J., Perdigao, R.A.P., Placovà, L., Rogger, M., Salinas, J.L., Sauquet, E., Schär, C., Szolgay, J., Viglione, A., and Blöschl, G., 2014. "Understanding flood regime changes in Europe: A state-of-the-art assessment." *Hydrology and Earth System Sciences* 18(7): 2735–2772.

Hänni, R., and Pfiffner, O. A., 2001. "Evolution and internal structure of the Helvetic nappes in the Bernese Oberland." *Eclogae Geologicae Helvetiae* 94(2): 161–171.

Hilker, N., Badoux, A., and Hegg, C., 2009. "The swiss flood and landslide damage database 1972-2007." *Natural Hazards and Earth System Science* 9: 913–925.

IPCC, 2012. *Managing the risks of extreme events and disasters to advance climate change adaptation.* A special report of Working Groups I and II of the Intergovernmental Panel on Climate Change [Field, C.B., Barros, V., Stocker, T.F., Dokken, D.J., Ebi, K.L., Mastrandrea, M.D., Mach, K.J., Plattner, G-J., Allen, S.K., Tignor, M., and Midgley, P.M. (eds.)]. Cambridge University Press, Cambridge, UK, and New York, NY, USA, 582 pp.

IPCC, 2013. *Climate change 2013: The physical science basis*. Contribution of Working Group I to the Fifth Assessment Report of the Intergovernmental Panel on Climate Change [Stocker, T.F., Qin, D., Plattner, G-K., Tignor, M., Allen, S.K., Boschung, J., Nauels, A., Xia, Y., Bex, V., and Midgley, P.M (eds.)]. Cambridge University Press, Cambridge, United Kingdom and New York, NY, USA, 1535 pp.

Jaeggi, M., 2007. "The floods of August 22-23, 2005, in Switzerland: some facts and challenges." *Developments in Earth Surface Processes* 11(07): 587–603.

Jansen, J. H. F., Van Der Gaast, S. J., Koster, B., and Vaars, A. J., 1998. "CORTEX, a shipboard XRF-scanner for element analyses in split sediment cores." *Marine Geology* 151(1-4): 143–153.

Kämpf, L., Brauer, A., Dulski, P., Lami, A., Marchetto, A., Gerli, S., Ambrosetti, W. and Guilizzoni, P., 2012. "Detrital layers marking flood events in recent sediments of Lago Maggiore (N. Italy) and their

comparison with instrumental data." *Freshwater Biology* 57(10): 2076–2090.

Köplin, N. (2012). "Hydrological impacts of climate change in Switzerland during the 21st century." *Master Thesis*, *University of Bern.*

Köplin, N., Schädler, B., Viviroli, D., and Weingartner, R., 2014. "Seasonality and magnitude of floods in Switzerland under future climate change." *Hydrological Processes* 28(4): 2567–2578.

Kundzewicz, Z. W., Kanae, S., Seneviratne, S. I., Handmer, J., Nicholls, N., Peduzzi, P., Mechler, R., Bouwer, L.M., Arnell, N., Mach, K., Muir-Wood, R., Brakenridge, G.R.,Kron, W., Benito, G., Honda, Y., Takahashi, K., and Sherstyukov, B., 2014. "Flood risk and climate change: global and regional perspectives." *Hydrological Sciences Journal* 59(1): 1–28.

Kylander, M. E., Ampel, L., Wohlfarth, B., and Veres, D., 2011. "High-resolution X-ray fluorescence core scanning analysis of Les Echets (France) sedimentary sequence: New insights from chemical proxies." *Journal of Quaternary Science* 26(1): 109–117.

Lamb, M. P., McElroy, B., Kopriva, B., Shaw, J., and Mohrig, D., 2010. "Linking river-flood dynamics to hyperpycnal-plume deposits: Experiments, theory, and geological implications." *Bulletin of the Geological Society of America* 122(9-10): 1389–1400.

Lamoureux, S., 2000. "Five centuries of interannual sediment yield and rainfall-induced erosion in the Canadian High Arctic recorded in lacustrine varves." *Water Resources Research* 36(1): 309–318.

Lascu, I., 2009. "Magnetic susceptibility logging for cores." *Limnological Research Center Core Facility, SOP Series.*

Lenzi, M. A., and Marchi, L., 2000. "Suspended sediment load during floods in a small stream of the Dolomites (northeastern Italy)." *Catena* 39(4): 267–282.

Liechti, P., 1994. "Der Zustand der Seen in der Schweiz." *BUWAL*, *Schriftenreihe Umwelt*, 159 pp.

Marren, P. M., 2002. "Criteria for distinguishing high magnitude flood events in the proglacial fluvial sedimentary record." *The Extremes of Extremes: Extraordinary Floods* 271: 237–241.

Matter, A., and Sturm, M., 1982. "Sedimentologische Untersuchungen in den grossen Berner Seen : Brienzer- , Thuner- und Bielersee." *Mitteilungen der Naturforschenden Gesellschaft in Bern* 39: 59-73.

McArdell, B. W., Bartelt, P., and Kowalski, J., 2007. "Field observations of basal forces and fluid pore pressure in a debris flow." *Geophysical Research Letters* 34(7): 2–5.

Messerli, B., Viviroli, D., and Weingartner, R., 2004. "Mountains Vulnerable of the World : Water Towers for the 21st Century." *AMBIO Special Report* 13(13): 29–34.

Messmer, M., Gómez-Navarro, J. J., and Raible, C. C., 2015. "Climatology of Vb cyclones, physical mechanisms and their impact on extreme precipitation over Central Europe." *Earth System Dynamics* 6(2): 541–553.

Moreno, A., Lopez-Merino, L., Leira, M., Marco-Barba, J., Gonzalez-Sampériz, P., Valero-Garcés, B. L., Lopez-Saez, J.A., Santos, L., Mata, P., and Ito, E., 2011. "Revealing the last 13,500 years of environmental history from the multiproxy record of a mountain lake (Lago Enol, northern Iberian

Peninsula)." *Journal of Paleolimnology* 46(3): 327–349.

Moreno, A., Valero-Garcés, B. L., Gonzàlez-Sampériz, P., and Rico, M., 2008. "Flood response to rainfall variability during the last 2000 years inferred from the Taravilla Lake record (Central Iberian Range, Spain)." *Journal of Paleolimnology* 40(3): 943–961.

Mountain Agenda, 1998. "Mountains of the World: Water Towers for the 21 st Century Case." *Mountain Agenda, Bern.*

Mulder, T., and Alexander, J., 2001. "The physical character of subaqueous sedimentary density flows and their deposits." *Sedimentology* 48(2), 269–299.

Mulder, T., Migeon, S., Savoye, B., and Faugères, J. C., 2001. "Inversely graded turbidite sequences in the deep Mediterranean: A record of deposits from flood-generated turbidity currents?" *Geo-Marine Letters* 21(2): 86–93.

Mulder, T., Syvitski, J. P. M., Migeon, S., Faugères, J. C., and Savoye, B., 2003. "Marine hyperpycnal flows: Initiation, behaviorand related deposits. A review." *Marine and Petroleum Geology* 20(6-8): 861–882.

Müller, R., 2007. "The destructive debris slides - Debris flows of Brienz, August 2005." *Diploma Thesis, Swiss Federal Institute of Technology (ETHZ).*

Müller, R., and Loew, S., 2009. "Predisposition and cause of the catastrophic landslides of August 2005 in brienz (Switzerland)." *Swiss Journal of Geosciences* 102(2), 331–344.

Nydegger, P., 1967. "Untersuchungen über Feinststofftransport in Flüssen und Seen , über Entstehung von Trübungshorizonten und zuflußbedingten Strömungen im Brienzersee und einigen Vergleichsseen" *Beiträge zur Geologie der Schweiz - Hydrologie* 16: 1-90.

Onda, Y., Komatsu, Y., Tsujimura, M., and Fujihara, J. I., 2001. "The role of subsurface runoff through bedrock on storm flow generation." *Hydrological Processes* 15(10): 1693–1706.

Osleger, D. A., Heyvaert, A. C., Stoner, J. S., and Verosub, K. L., 2009. "Lacustrine turbidites as indicators of Holocene storminess and climate: Lake Tahoe, California and Nevada." *Journal of Paleolimnology* 42(1): 103–122.

Ozer, M., and Orhan, M., 2015. "Determination of an Appropriate Method for Dispersion of Soil Samples in Laser Diffraction Particle Size Analyses." *International Journal of Computational and Experimental Science and Engineering* 1(1): 19–25.

Pfiffner, O. A., 2011. "Structural Map of the Helvetic Zone of the Swiss Alps, including Vorarlberg (Austria) and Haute Savoie (France), 1:100 000." *Geological Special Map 128 (Explanatory notes).*

Pfister, C., 2009. "Die „ Katastrophenlücke " des 20 . Jahrhunderts und der Verlust traditionalen Risikobewusstseins." *Gaia Ecological Perspectives For Science And Society* 3: 239 – 246.

Richter, T. O., Van der Gaast, S., Koster, B., Vaars, A., Gieles, R., Stigter, H., de Haas, H., and van Weering, T., 2006. "The Avaatech XRF Core scanner: Technical description and applications to NE Atlantic sediments." *Geological Society, London, Special Publications* 267(1): 39-50.

Rickenmann, D., and Koschni, A.,2010. "Sediment loads due to fluvial transport and debris flows during

the 2005 flood events in Switzerland." *Hydrological Processes* 24(8): 993–1007.

Rollinson, H.R., 1993. *Using geochemical data: evaluation, presentation, interpretation.* 2nd Edition, Routledge, New York, USA, 344 pp.

Rothwell, R. G., 1989. *Minerals and mineraloids in marine sediments: An optical identification guide.* Elsevier Applied Science, London, UK, 279 pp.

Rothwell, R. G., and Rack, R., 2006. "New techniques in sediment core analysis : an introduction."*Geological Society, London, Special Publications* 267: 1–29.

Ryzak, M., and Bieganowski, A., 2011. "Methodological aspects of determining soil particle-size distribution using the laser diffraction method." *Journal of Plant Nutrition and Soil Science* 174: 624-633.

Schiefer, E., Gilbert, R., and Hassan, M. A., 2011. "A lake sediment-based proxy of floods in the Rocky Mountain Front Ranges, Canada." *Journal of Paleolimnology* 45(2): 137–149.

Schillereff, D. N., Chiverrell, R. C., Macdonald, N., and Hooke, J. M., 2014. "Flood stratigraphies in lake sediments: A review." *Earth-Science Reviews* 135: 17–37.

Schmocker-Fackel, P., and Naef, F., 2010. "More frequent flooding? Changes in flood frequency in Switzerland since 1850." *Journal of Hydrology* 381(1-2): 1–8.

Schnurrenberger, D., Schnurrenberger, D., Russell, J., Russell, J., Kelts, K., and Kelts, K., 2003. "Classication of lacustrine sediments based on sedimentary components." *Journal of Paleolimnology* 29:141–154.

Schulte, L., Veit, H., Burjachs, F., and Julià, R., 2009. "Lütschine fan delta response to climate variability and land use in the Bernese Alps during the last 2400 years." *Geomorphology* 108(1-2): 107–121.

Schulte, L., Peña, J. C., Carvalho, F., Schmidt, T., Julià, R., Llorca, J., and Veit, H., 2015. "A 2600-year history of floods in the Bernese Alps, Switzerland: Frequencies, mechanisms and climate forcing." *Hydrology and Earth System Sciences* 19(7): 3047–3072.

Schultheiss, P. J., and Weaver, P. P. E., 1992. "Multi-sensor Core Logging For Science And Industry." *OCEANS 92 Mastering the Oceans Through Technology*, 608–613.

Schumacher, B. A., 2002. Methods for the Determination of Total Organic Carbon in Soils and Sediments. *United States Environmental Protection Agency*

Simonneau, A., Chapron, E., Vanniere, B., Wirth, S. B., Gilli, A., Di Giovanni, C., Anselmetti, F.S., Desmet, M., and Magny, M., 2013. "Mass-movement and flood-induced deposits in Lake Ledro, southern Alps, Italy: Implications for Holocene palaeohydrology and natural hazards." *Climate of the Past* 9(2): 825–840.

Sperazza, M., Moore, J. N., and Hendrix, M. S., 2004. "High-Resolution Particle Size Analysis of Naturally Occurring Very Fine-Grained Sediment Through Laser Diffractometry." *Journal of Sedimentary Research* 74(5):736-743.

Støren, E. N., 2011. "Identifying flood deposits in lake sediments." *Diploma Thesis, University of Bergen.*

Stucki, P., Rickli, R., Brönnimann, S., Martius, O., Wanner, H., Grebner, D., and Luterbacher, J., 2012.

"Weather patterns and hydro-climatological precursors of extreme floods in Switzerland since 1868." *Meteorologische Zeitschrift* 21(6): 531–550.

Sturm, M., 1976. "Die Oberflächensedimente des Brienzersees." *Eclogae Geologicae Helvetiae* 69(1): 111- 123.

Sturm, M. and Matter, A., 1978. "Turbidites and varves in Lake Brienz (Switzerland): deposition of clastic detritus by density currents." *Special Publications International Association of Sedimentologists* 2: 147-168.

Thevenon, F., Wirth, S. B., Fujak, M., Poté, J., and Girardclos, S., 2013. "Human impact on the transport of terrigenous and anthropogenic elements to peri-alpine lakes (Switzerland) over the last decades." *Aquatic Sciences* 75(3): 413–424.

Thompson, R., Battarbee, R. W., O'Sullivan, P. E., and Oldfield, F., 1975. "Magnetic susceptibility of lake sediments. *Limnology and Oceanography* 20(5): 687–698.

Thorndycraft, V., Hu, Y., Oldfield, F., Crooks, P. R. J., and Appleby, P. G., 1998. "Individual flood events detected in the recent sediments of the Petit Lac d'Annecy, eastern France." *Holocene* 8(6): 741–746.

Tiefbauamt des Kantons Bern, 2007. "Lokale Lösungsorientierte Ereignisanalyse - Lütschine." - *unpublished report*

Vasskog, K., Nesje, A., Storen, E. N., Waldmann, N., Chapron, E., and Ariztegui, D., 2011. "A Holocene record of snow-avalanche and flood activity reconstructed from a lacustrine sedimentary sequence in Oldevatnet, western Norway." *The Holocene* 21: 597–614.

Viviroli, D., Wehren, B., Weingartner, R., and Scha, B., 2010. "General characteristics of alpine waters." In: *Alpine Waters*, 6. Spring, Berlin Heidelber, 17-59.

Viviroli, D., and Weingartner, R., 2004. "The hydrological significance of mountains: from regional to global scale." *Hydrology and Earth System Sciences* 8(6): 1017–1030.

Wanner, H., Rickli, R., and Salvisberg, E., 1997. "Global climate change and variability and its influence on alpine climate—concepts and observations." *Theoretical and Applied Climatology* 243: 221–243.

Webb, R. H., Pringle, P. T., and Rink, G. R., 1989. "Debris Flows from Tributaries of the Colorado River, Grand Canyon National Park, Arizona." *U.S. Geological Survey Professional Paper*, *Vol. 1492*.

Weingartner, R., Barbena, M., and Spreafico, M., 2003. "Floods in mountain areas - An overview based on examples from Switzerland." *Journal of Hydrology* 282(1-4): 10–24.

Wilhelm, B., Arnaud, F., Enters, D., Allignol, F., Legaz, A., Magand, O., Revillon, S., Giguet-Covex, C., and Malet, E., 2012. "Does global warming favour the occurrence of extreme floods in European Alps? First evidences from a NW Alps proglacial lake sediment record." *Climatic Change* 113(3-4): 563–581.

Wirth, S. B., Girardclos, S., Rellstab, C., and Anselmetti, F. S., 2011. "The sedimentary response to a pioneer geo-engineering project: Tracking the Kander River deviation in the sediments of Lake Thun (Switzerland)." *Sedimentology* 58(7): 1737–1761.

Wirth, S. B., Glur, L., Gilli, A., and Anselmetti, F. S., 2013. "Holocene flood frequency across the Central Alps – solar forcing and evidence for variations in North Atlantic atmospheric circulation." *Quaternary Science Reviews* 80: 112–128.

Wolfe, B., Hall, I. R., Last, W. M., Edwards, T., English, M. C., Karst-Riddoch, T., Paterson, A., and Palmini, R., 2006. "Reconstruction of multi-century flood histories from oxbow lake sediments, Peace-Athabasca Delta, Canada." *Hydrological Processes* 20: 4131–4153.

Wüest, A., Zeh, M., and Ackerman, J. D., 2007. "Lake Brienz Project: An interdisciplinary catchment-to-lake study." *Aquatic Sciences* 69(2): 173–178.

Zillgens, B., Merz, B., Kirnbauer, R., and Tilch, N., 2005. "Analysis of the runoff response of an Alpine catchment at different scales." *Hydrology and Earth System Sciences Discussions* 2(5): 1923–1960.

Zimmermann, M., 2006. "Lokale lösungsorientierte Ereignisanalyse - Trachtbach." *Unpublished report*

Zimmermann, M., (2006a). "Lokale lösungsorientierte Ereignisanalyse - Glyssibach." *Unpublished report*

Zimmermann, M., (2006b). "Lokale lösungsorientierte Ereignisanalyse - Trachtbach." *Unpublished report*

Online Resources

Cox Analytical Systems, 1999. “Itrax drillcore scanner. ” Available at: http://www.coxsys.se/our-scanners/the-itrax-drillcore-scanner/ [Accessed on 25.07.2016]

Escubed Ltd. “Particle size analysis by laser diffraction.” Available at: http://www.escubed.co.uk/sites/default/files/particle_size_analysis_(an003)_laser_diffraction.pdf. [Accessed on 19.07.2016]

Swisstopo. “Maps of Switzerland. ” Available at: https://map.geo.admin.ch/ [Accessed on 19.07.2016]

Geotek. “MSCL-S.” Available at: http://www.geotek.co.uk/products/mscl-s [Accessed on 09.07.2016]

Geotek. “Geoscan IV linescan imaging.” Available at: http://www.geotek.co.uk/products/geoscan [Accessed on 10.07.2016]

Geotek. “Gamma Density.” Available at: http://www.geotek.co.uk/products/gammadensity [Accessed on 14.07.2016]

Myrbo, A., 2007. "Smear slide identifications: the practical basics". Available at: http://lrc.geo.umn.edu/laccore/assets/pdf/sops/smearslides.pdf [Accessed on 20.04.2016]

Protection forest, Loat BWG, 2005. “Debris flow Brienz.” Available at: http://www.planat.ch/en/images-details/datum/2011/06/22/murgaenge-brienz-2005/ [Accessed on 22.06.2016]

Radboud University. “CN elemental analyzer.” Available at: http://www.ru.nl/science/gi/facilities/elemental-analysis/cn-elemental/ [Accessed on

27.06.2016]

Stanford University. “Carlo Erba CN elemental analyzer.” Available at: http:// em1.stanford.edu/Schedule/CNS/Index.htm. [Accessed on 14.06.2016]

Swiss Statistics. “Permanent and non permanent resident population by institutional units, sex, citizenship and age.” Available at: https://www.pxweb.bfs.admin.ch/Selection.aspx? px_-language=en&px_db=px-x-0102010000_101&px_tableid=px-x-0102010000_101\px-x-0102010000_101.px&px_type=PX [Accessed on 28.06.2016]

The National Severe Storms Laboratory. "Severe Weather 101: Thunderstorm types". Available at: http://www.nssl.noaa.gov/education/svrwx101/thunderstorms/types/ [Accessed on 25.07.2016]

WW2010. "Convection – Atmospheric motions in the vertical direction". Available at: http://ww2010.atmos.uiuc.edu/(Gl)/guides/mtr/hyd/cond/conv.rxml [Accessed on 30.07.2016]

Visual Material

Hunziker, S., 2014, "150 Jahre gegen Hochwasser", *Berner Zeitung.* Available at: http://www.bernerzeitung.ch/region/thun/150-Jahre-gegen-Hochwasser/story/18870954 [Accessed on 20.08.2016]

Hegg, C., 2013. "The ocean, atmosphere, climate and weather". Available at: http://slides.com/tofergregg/the-ocean-atmosphere-climate-and-weather#/ [Accessed on 15.08.2016]

Regez, S., 2005. "Ein Bild der Trauer und Werwüstung in Brienz". Available at: http://www.jungfrauzeitung.ch/artikel/57931/ [Accessed on 16.08.2016]

MySwitzerland. “Jahrhundert Hochwasser: Oey Diemtigen". Available at: http://www.myswitzerland.com/de-ch/jahrhundert-hochwasser.html [Accessed on 30.08.2016]

MySwitzerland. “Grand Tour of Switzerland". Available at: MySwitzerland. Jahrhundert Hochwasser: Oey Diemtigen". Available at: http://www.myswitzerland.com/de-ch/jahrhundert-hochwasser.html [Accessed on 30.08.2016] [Accessed on 29.08.2016]

Müller, A., 2007. "Hochwasser 5. August 2005". Available at: http://www.panoramio.com/photo/5022111 [Accessed on 22.08.2016]

Schweizer Luftwaffe, 2005. “Klosters – Autoverlad Selfranga.” Available at: http://luftbilder-der-schweiz.ch/images/e/e1/Klosters%2C_August_05_1_20056749.jpg [Accessed on 23.08.2016]

SRF, 2014. "Sarnen mit Stollen vor Hochwasser schnützen". Available at: http://www.srf.ch/news/schweiz/abstimmungen/abstimmungen/abstimmungen-ow/sarnen-mit-stollen-vor-hochwasser-schuetzen [Accessed on 17.08.2016]

Appendix

Annex 1: Methods

Table A.1.1 Magnetic Susceptibility (SI x 10-5) and Bulk Density (g/cc) for LB15-2, LB15-14, LB15-15, LB15-3 and LB15-15c. From 0 to 40 cm depth

	LB15-2		LB15-14		LB15-15		LB15-3		LB15-15c	
Depth	Density	MS	Density	MS	Density	MS	Density	MS	Density	MS
0	1.987	5.349	1.491	5.878	1.441	5.143	1.421	3.619	1.014	1.454
0.5	2.003	6.678	1.836	6.417	1.723	6.869	1.662	4.325	0.650	2.440
1	2.020	7.480	1.908	6.700	1.802	8.219	1.697	5.161	0.495	3.394
1.5	2.007	8.382	1.876	7.179	1.838	9.274	1.633	5.900	1.295	5.099
2	1.899	9.040	1.937	7.405	1.750	9.901	1.634	6.530	1.690	6.695
2.5	1.922	9.173	2.001	8.121	1.774	10.377	1.642	7.290	1.700	7.929
3	1.928	9.313	1.974	8.172	1.815	10.528	1.635	7.139	1.727	8.819
3.5	1.871	9.370	2.010	8.316	1.815	10.307	1.605	8.211	1.710	9.663
4	1.972	9.375	2.022	8.309	1.866	10.241	1.639	8.002	1.680	9.767
4.5	2.055	9.190	2.019	8.385	1.931	10.170	1.670	8.204	1.696	9.961
5	2.066	8.935	1.923	8.570	1.924	10.246	1.694	8.382	1.615	9.942
5.5	2.057	8.694	1.819	8.539	1.730	10.131	1.736	8.593	1.598	9.649
6	1.947	8.685	1.764	8.468	1.610	9.680	1.713	8.547	1.585	9.531
6.5	1.810	8.431	1.710	8.414	1.639	9.611	1.672	8.360	1.571	9.370
7	1.732	8.049	1.750	8.179	1.804	9.375	1.654	8.248	1.537	9.295
7.5	1.696	7.845	1.798	8.418	1.848	9.009	1.642	8.060	1.504	9.041
8	1.635	7.556	1.775	8.480	1.710	9.000	1.707	8.076	1.504	8.874
8.5	1.527	7.171	1.633	8.290	1.635	8.901	1.781	7.881	1.477	8.861
9	1.446	6.860	1.588	8.242	1.637	8.957	1.723	7.691	1.450	8.620
9.5	1.452	6.979	1.621	7.846	1.598	8.953	1.654	7.864	1.465	8.734
10	1.549	6.770	1.644	8.163	1.598	8.914	1.624	7.762	1.468	8.721
10.5	1.768	7.008	1.661	7.745	1.593	8.844	1.683	7.488	1.458	8.790
11	1.792	6.635	1.578	7.854	1.577	8.547	1.709	7.672	1.496	9.111
11.5	1.736	7.070	1.526	7.603	1.566	9.045	1.667	8.076	1.552	9.154
12	1.537	7.178	1.549	7.645	1.593	9.010	1.651	7.551	1.517	9.277
12.5	1.554	7.351	1.548	7.406	1.631	9.071	1.607	7.547	1.507	9.207
13	1.711	7.773	1.560	7.466	1.615	8.822	1.596	7.611	1.527	9.338
13.5	1.754	7.702	1.588	7.846	1.565	8.866	1.652	7.728	1.538	9.404
14	1.780	7.746	1.578	7.708	1.572	8.888	1.662	7.990	1.518	9.272
14.5	1.884	8.328	1.560	7.969	1.589	9.001	1.710	7.912	1.508	9.531
15	1.932	8.215	1.528	7.846	1.595	9.184	1.653	7.912	1.497	9.908
15.5	1.934	8.336	1.558	7.865	1.698	9.154	1.592	8.079	1.482	9.408
16	1.864	8.345	1.585	7.973	1.706	9.408	1.608	7.888	1.531	9.780
16.5	1.776	8.107	1.535	8.167	1.629	9.216	1.600	7.877	1.556	10.096
17	1.693	8.111	1.539	7.920	1.567	9.150	1.593	7.757	1.560	9.422
17.5	1.684	8.067	1.640	8.040	1.524	9.268	1.550	7.503	1.526	9.568
18	1.706	7.880	1.777	8.063	1.615	9.639	1.586	7.686	1.510	9.455
18.5	1.736	7.932	1.773	8.116	1.673	9.597	1.682	7.698	1.515	9.606
19	1.684	7.746	1.650	8.207	1.657	9.154	1.630	7.549	1.521	9.649
19.5	1.595	7.457	1.515	8.144	1.542	8.975	1.609	7.616	1.544	9.582
20	1.598	7.237	1.510	8.008	1.534	8.909	1.630	7.825	1.515	9.411
20.5	1.629	7.121	1.614	7.904	1.547	8.896	1.566	7.764	1.512	9.265
21	1.637	7.084	1.696	7.841	1.571	9.089	1.542	8.083	1.513	9.402
21.5	1.643	6.906	1.678	7.799	1.572	9.023	1.563	8.160	1.542	9.525
22	1.631	6.601	1.523	7.931	1.619	9.456	1.534	8.543	1.549	9.487
22.5	1.626	5.890	1.487	7.668	1.618	9.220	1.563	8.655	1.527	9.535
23	1.617	5.682	1.601	7.494	1.653	9.320	1.622	8.667	1.499	9.601
23.5	1.651	5.313	1.586	7.505	1.642	9.465	1.624	8.680	1.505	9.715
24	1.673	5.019	1.496	7.691	1.596	9.408	1.624	8.814	1.543	9.720
24.5	1.630	4.705	1.543	7.883	1.576	9.503	1.619	8.926	1.555	9.772
25	1.580	4.060	1.603	7.766	1.531	9.193	1.605	8.818	1.560	9.947
25.5	1.629	3.529	1.602	7.630	1.568	9.145	1.607	8.872	1.568	9.762
26	1.476	2.948	1.565	7.879	1.598	9.066	1.637	8.942	1.605	9.895
26.5			1.608	7.805	1.570	8.839	1.650	8.827	1.627	10.018
27			1.620	7.810	1.594	9.066	1.612	8.939	1.611	10.207
27.5			1.578	7.676	1.559	8.822	1.618	9.077	1.608	10.340
28			1.597	7.927	1.534	8.875	1.608	9.188	1.597	10.268
28.5			1.654	7.601	1.554	8.721	1.611	9.259	1.650	10.254
29			1.606	7.611	1.501	8.839	1.629	9.125	1.608	10.423
29.5			1.607	7.544	1.492	9.027	1.617	9.192	1.663	10.545
30			1.625	7.356	1.520	9.220	1.612	9.072	1.746	10.806
30.5			1.615	7.249	1.549	9.361	1.643	8.823	1.763	10.611
31			1.594	7.235	1.539	9.554	1.623	8.756	1.795	10.897
31.5			1.574	7.173	1.437	9.710	1.640	8.760	1.875	10.856
32			1.623	7.227	1.424	10.413	1.607	9.059	1.893	10.646
32.5			1.620	7.096	1.409	9.871	1.621	8.859	1.879	10.712
33			1.553	7.405	1.432	9.895	1.618	8.801	1.855	10.574
33.5			1.536	7.472	1.492	9.890	1.598	8.863	1.882	10.387
34			1.572	7.529	1.509	9.998	1.612	8.988	1.888	10.289
34.5			1.581	7.912	1.524	9.871	1.627	8.930	1.895	9.959
35			1.566	8.160	1.511	10.136	1.608	8.806	1.904	9.795
35.5			1.602	8.097	1.506	9.922	1.637	8.908	1.906	9.918
36			1.628	8.111	1.514	9.431	1.649	8.899	1.889	9.800
36.5			1.741	7.743	1.555	10.300	1.594	8.961	1.845	9.927
37			1.711	7.799	1.532	9.861	1.588	8.780	1.891	9.790
37.5			1.622	7.678	1.546	9.861	1.625	8.894	1.933	9.880
38			1.584	7.352	1.513	10.096	1.584	8.899	1.949	9.956
38.5			1.568	7.173	1.477	9.984	1.590	8.824	1.878	9.880
39			1.598	7.036	1.498	10.238	1.612	8.642	1.880	10.028
39.5			1.702	6.932	1.503	10.172	1.623	8.837	1.871	10.279
40			1.653	6.810	1.491	9.951	1.654	8.805	1.884	10.232

Table A.1.2 Magnetic Susceptibility (SI x 10^{-5}) and Bulk Density (g/cc) for LB15-2, LB15-14, LB15-15, LB15-3 and LB15-15c. From 40.5 to 79 cm depth

		LB15-14		LB15-15		LB15-3		LB15-15c	
Depth		Density	MS	Density	MS	Density	MS	Density	MS
40.5		1.5817	6.7459	1.5263	10.2534	1.6497	8.863	1.8968	10.2992
41		1.5559	6.7359	1.5905	10.0178	1.6058	8.7429	1.8998	10.1187
41.5		1.578	6.547	1.5445	9.9175	1.6157	8.7429	1.8955	10.2623
42		1.5947	6.6241	1.548	10.2899	1.6044	8.8848	1.8649	10.2472
42.5		1.6156	6.5021	1.5217	10.2184	1.5946	8.8805	1.8861	10.1336
43		1.6003	6.4252	1.4666	10.2648	1.5703	8.9556	1.7915	10.0769
43.5		1.5225	6.7359	1.5767	10.4067	1.4916	8.8936	1.6555	9.8292
44		1.6021	6.7592	1.6395	10.3156	1.5417	8.8394	1.6636	9.8197
44.5		1.6088	6.6469	1.6256	10.4326	1.6306	8.8251	1.6137	9.605
45		1.5779	6.6437	1.616	10.1736	1.6368	9.1666	1.5735	9.7961
45.5		1.5765	6.6502	1.6099	10.529	1.6298	8.7069	1.557	9.2277
46		1.534	6.7725	1.6311	10.2199	1.6174	8.8251	1.6273	9.5477
46.5		1.544	6.5181	1.6726	10.4728	1.6157	8.799	1.7517	9.1519
47		1.5893	6.2833	1.6953	10.1637	1.6326	8.647	1.6832	8.824
47.5		1.5941	6.407	1.7138	10.0326	1.6347	8.6567	1.695	8.6334
48		1.5977	6.407	1.5236	9.6016	1.6292	8.7817	1.6594	8.4803
48.5		1.565	6.3219	1.4638	9.4006	1.5393	8.8264	1.5816	8.155
49		1.5771	6.3219	1.6412	9.279	1.601	8.7601	1.5842	7.9653
49.5		1.5532	6.3882	1.6333	9.3581	1.6797	8.8004	1.5562	7.8173
50		1.5631	6.3851	1.6354	9.1752	1.6771	8.6311	1.5804	7.6754
50.5		1.5933	6.2529	1.6867	9.1886	1.6694	8.8805	1.5661	7.6754
51		1.5393	6.0546	1.7001	8.6954	1.6761	8.4885	1.6511	7.8038
51.5		1.5394	6.2404	1.6617	8.8218	1.6851	8.9256	1.7679	7.653
52		1.6223	6.1868	1.556	8.8919	1.6827	8.7215	1.8237	7.8566
52.5		1.5904	6.1028	1.5491	8.4513	1.6915	8.7129	1.7881	7.8
53		1.6089	6.4167	1.6425	8.128	1.7021	8.8986	1.6962	7.2235
53.5		1.6711	6.2252	1.6656	7.8879	1.7074	8.961	1.6412	7.4741
54		1.6979	6.5987	1.614	7.7377	1.7745	9.2187	1.6406	7.3423
54.5		1.632	6.4668	1.5599	7.2769	1.7664	9.2668	1.6187	8.2823
55		1.6147	6.4668	1.5996	6.7837	1.7836	9.4344	1.6069	7.5453
55.5		1.567	6.4637	1.5737	6.1985	1.8125	9.439	1.6388	7.6113
56		1.5224	6.2758	1.1939	5.531	1.8425	9.2537	1.607	7.3697
56.5		1.5772	6.401	0.8927	4.5671	1.877	9.634	1.628	7.6151
57		1.5808	6.21	1.0516	4.0018	1.872	9.1916	1.5738	7.1775
57.5		1.6065	6.2758	1.2469	3.588	1.8816	9.439	1.5735	7.181
58		1.6633	6.2131	1.2528	2.8708	1.9168	9.2582	1.564	6.8069
58.5		1.5578	6.0909	1.1014	2.7736	1.9311	9.3107	1.6128	6.9991
59		1.5448	6.4104	0.7288	2.3748	1.933	9.4344	1.72	7.1149
59.5		1.5903	6.0315	0.6266	1.8137	1.9364	9.2396	1.6708	6.9228
60		1.6602	6.3416	0.9225	1.2394	1.9016	9.2532	1.6161	7.1845
60.5		1.6596	6.21	0.9928	0.7728	1.9072	9.4868	1.5976	7.0756
61		1.6616	6.4668			1.8352	9.3107	1.5939	7.2553
61.5		1.6946	6.5826			1.8891	9.3244	1.6239	7.1358
62		1.6109	6.4637			1.9511	9.2623	1.6834	7.0696
62.5		1.5578	5.8408			1.9554	9.4622	1.7362	6.9466
63		1.5999	6.1567			1.9575	9.4622	1.7074	7.2021
63.5		1.5599	6.1537			1.997	9.5909	1.7192	7.3783
64		1.5215	6.3261			1.891	9.5909	1.7889	7.1986
64.5		1.5472	5.8934			1.702	9.4668	1.8213	7.2553
65		1.5903	5.8793			1.7082	9.3519	1.7751	7.3747
65.5		1.5502	5.8427			1.6839	8.9742	1.7531	7.1149
66		1.4278	5.4834			1.6368	8.9875	1.7067	7.1681
66.5		1.3831	5.3138			1.658	8.7257	1.6871	7.4191
67		1.4432	4.8966			1.6564	8.5888	1.7133	7.2965
67.5		1.4489	4.8788			1.6305	8.543	1.7777	7.2965
68		1.3816	4.4852			1.6134	8.1643	1.8427	7.4814
68.5		1.3519	3.9473			1.6158	7.9746	1.8399	7.3374
69		1.3846	3.1782			1.6324	8.0202	1.8373	7.3902
69.5		1.4613	2.5917			1.625	7.9707	1.7372	7.3316
70		1.1684	1.7003			1.6959	7.6629	1.6973	7.3338
70.5						1.6691	7.7796	1.6872	7.6437
71						1.6327	8.087	1.6864	7.8221
71.5						1.6877	8.0162	1.7787	7.8353
72						1.6471	7.9106	1.8833	8.132
72.5						1.6019	7.7643	1.8602	8.4419
73						1.5981	7.538	1.8134	8.9439
73.5						1.6159	6.9778	1.7796	9.1931
74						1.6117	6.7401	1.7555	9.2404
74.5						1.6522	6.657	1.7561	10.6101
75						1.687	6.5114	1.7899	10.803
75.5						1.5717	6.2726	1.7489	10.9961
76						1.5799	6.018	1.7653	11.2347
76.5						1.7006	5.7773	1.8718	11.4994
77						1.6986	5.4012	1.9054	11.328
77.5						1.6065	5.1328	1.8127	11.328
78						1.5525	4.6345	1.7992	11.7101
78.5						1.4797	3.643	1.8509	11.6893
79						1.4501	3.0283	1.8304	11.6893

Table A.1.3 Magnetic Susceptibility (SI x 10-5) and Bulk Density (g/cc) for LB15-2, LB15-14, LB15-15, LB15-3 and LB15-15c. From 79.5 to 102.5 cm depth.

		LB15-15c	
Depth		Density	MS
79.5		1.801	11.306
80		1.767	11.807
80.5		1.825	11.918
81		1.844	11.795
81.5		1.842	12.013
82		1.846	12.119
82.5		1.829	12.086
83		1.912	12.173
83.5		1.928	12.442
84		1.930	12.253
84.5		1.997	12.449
85		2.024	11.896
85.5		1.922	11.641
86		1.526	11.082
86.5		1.336	10.509
87		1.393	10.008
87.5		1.427	9.639
88		1.422	9.388
88.5		1.481	9.133
89		1.486	9.049
89.5		1.333	8.931
90		1.355	8.742
90.5		1.442	8.493
91		1.426	8.423
91.5		1.411	8.352
92		1.360	8.615
92.5		1.365	8.668
93		1.443	8.350
93.5		1.486	8.095
94		1.388	8.336
94.5		1.325	8.442
95		1.416	8.198
95.5		1.491	8.402
96		1.473	8.111
96.5		1.115	8.149
97		1.150	7.559
97.5		1.396	7.448
98		1.397	6.893
98.5		1.346	6.236
99		1.387	5.850
99.5		1.399	5.607
100		1.305	5.121
100.5		1.237	4.895
101		1.404	4.414
101.5		1.447	3.967
102		1.221	3.264
102.5		0.827	2.481

Table A.1.4 Magnetic Susceptibility (SI x 10^{-5}) and Bulk Density (g/cc) for LB15-16, LB15-17, LB15-18, LB15-19 and LB15-8. From 0 to 40 cm depth

	LB15-16		LB15-17		LB15-18		LB15-19		LB15-8	
Depth	Density	MS	Density	MS	Density	MS	Density	MS	Density	MS
0	1.6	4.9654	1.5857	4.6593	1.6883	5.6773	1.7573	7.597	1.5448	4.3256
0.5	1.6204	6.3453	1.8342	6.3048	1.8575	7.2486	1.8905	8.878	1.8235	4.9613
1	1.6242	7.7137	1.8071	7.5796	1.9329	8.602	1.8703	9.9598	1.7652	5.6228
1.5	1.6167	8.4911	1.7785	8.5446	1.819	9.5687	1.8126	10.4049	1.6265	6.7025
2	1.6259	9.1512	1.771	9.2318	1.7538	9.8754	1.7673	10.654	1.5788	7.3113
2.5	1.6429	9.4638	2.2532	20.626	1.6855	9.9321	1.7538	10.8109	1.6041	7.5046
3	1.6399	9.5635	1.675	9.845	1.6285	9.8657	1.6765	10.621	1.6653	7.7113
3.5	1.6186	9.8187	1.5982	10.1543	1.6219	9.6958	1.6094	10.1376	1.6581	7.9731
4	1.6194	10.0227	1.5654	9.7329	1.6412	9.3699	1.6264	10.2642	1.664	8.2701
4.5	1.6364	9.9515	1.5726	9.9204	1.5385	8.9223	1.6652	9.954	1.6488	7.8989
5	1.6307	9.8947	1.5913	9.55	1.3113	9.2246	1.607	9.7985	1.6688	7.9575
5.5	1.5654	9.3975	1.5709	9.3718	1.3888	8.738	1.5015	9.1976	1.6385	8.155
6	1.5182	9.226	1.5496	9.3061	1.529	8.9136	1.5516	9.0799	1.618	7.7643
6.5	1.5045	8.7282	1.4964	8.9965	1.4547	8.9877	1.646	8.5201	1.665	7.6599
7	1.4859	8.6448	1.5537	8.7612	1.4332	9.1288	1.778	8.7646	1.6818	7.5439
7.5	1.4668	8.587	1.5226	8.6827	1.481	9.199	1.78	8.7039	1.6617	7.4181
8	1.3973	8.6438	1.3993	8.446	1.4844	9.502	1.8243	8.5201	1.5807	7.3467
8.5	1.4495	8.5468	1.3938	8.2581	1.4514	9.5822	1.8394	7.7734	1.5815	7.2933
9	1.5547	8.4845	1.4615	8.332	1.5043	9.7148	1.6013	8.0178	1.5894	7.0369
9.5	1.5271	8.5415	1.4638	8.1479	1.5214	9.5206	1.5118	8.7209	1.6353	6.967
10	1.4739	8.5468	1.475	8.2057	1.5354	9.6485	1.5664	9.0405	1.6398	6.7838
10.5	1.4653	8.8602	1.4725	8.3978	1.4836	9.3452	1.5853	9.2201	1.6285	6.8436
11	1.5042	8.5343	1.4808	8.4501	1.4439	9.3498	1.6432	9.2291	1.5563	6.5304
11.5	1.4738	8.8823	1.4904	8.3279	1.5162	9.1736	1.7173	9.3471	1.5236	6.4006
12	1.4926	8.6974	1.4602	8.2756	1.5291	9.1641	1.6765	9.4176	1.574	6.4734
12.5	1.5176	8.6406	1.4643	8.4637	1.4373	9.0501	1.5366	9.2947	1.565	6.4671
13	1.5279	8.9529	1.4602	8.6339	1.4342	9.0057	1.5157	9.1065	1.5176	6.3436
13.5	1.5492	8.7551	1.4514	8.4296	1.4665	8.6745	1.4433	9.4222	1.5184	6.3405
14	1.5095	8.7551	1.4508	8.5525	1.4353	8.7539	1.3892	9.5068	1.5286	6.1507
14.5	1.5218	9.076	1.4612	8.4307	1.4172	8.7315	1.3856	9.6958	1.5346	6.0332
15	1.5173	9.1199	1.3638	8.6785	1.4543	8.8024	1.4909	9.6864	1.5282	6.0997
15.5	1.5185	8.9485	1.383	8.7569	1.3986	8.7401	1.4689	9.4358	1.5312	7.1034
16	1.5187	9.0494	1.4773	8.7356	1.387	8.798	1.5231	9.7382	1.6135	6.657
16.5	1.5415	9.1333	1.4832	8.8522	1.4418	8.9925	1.4688	9.5776	1.6008	6.325
17	1.5703	9.0627	1.4677	8.8616	1.4105	9.1871	1.4938	9.4268	1.5988	6.6407
17.5	1.5599	9.8657	1.4771	8.853	1.4465	9.3244	1.5754	9.2562	1.566	6.8336
18	1.5658	9.436	1.5077	9.1707	1.2851	9.3727	1.514	9.2426	1.5237	6.8965
18.5	1.5306	8.865	1.485	9.3809	1.2917	9.3773	1.4983	8.9311	1.5424	6.6976
19	1.5115	9.4974	1.5136	9.7519	1.5707	9.4251	1.516	8.7997	1.5463	6.9568
19.5	1.5521	9.4834	1.5726	9.7567	1.6654	9.6721	1.4671	8.6719	1.5487	7.1463
20	1.6012	9.5776	1.5946	9.9253	1.6625	9.6532	1.4507	8.4832	1.5466	7.2091
20.5	1.6096	10.0374	1.6306	9.9027	1.6279	9.8718	1.439	8.2218	1.5627	7.3287
21	1.6128	9.9433	1.6258	10.3206	1.6721	10.0325	1.4346	8.2999	1.5553	7.5823
21.5	1.6249	10.1902	1.6195	10.3922	1.7756	10.2172	1.4794	8.4666	1.574	7.1498
22	1.7211	9.6769	1.7364	10.5753	1.8823	10.6323	1.4676	8.5849	1.587	7.1138
22.5	1.7315	9.81	1.8807	10.295	1.9649	10.9552	1.5891	9.0317	1.5301	7.3647
23	1.6872	9.81	1.9427	10.356	1.9733	11.0769	1.8066	9.0229	1.4717	7.1182
23.5	1.7391	10.0769	1.9512	10.1723	1.7835	10.8984	1.8613	9.2902	1.482	7.3148
24	1.6827	9.8292	1.9606	10.2022	1.5406	10.6574	1.8635	9.3562	1.5668	7.6862
24.5	1.6802	9.5815	1.9974	10.0595	1.4225	10.1653	1.8377	9.4557	1.6059	7.6196
25	1.6849	9.4575	2.0024	10.1773	1.4331	9.6057	1.7877	9.3379	1.62	7.8767
25.5	1.6948	9.6387	1.9756	10.1922	1.4403	9.2351	1.6015	9.5216	1.588	7.81
26	1.6764	9.4575	1.944	10.3	1.4191	8.6122	1.4817	9.4222	1.537	7.9339
26.5	1.6681	9.2051	1.9595	10.6724	1.3698	8.3556	1.5114	9.4649	1.5341	8.0672
27	1.7305	9.3954	1.9706	9.8561	1.3257	8.0514	1.5096	9.5495	1.6424	7.9356
27.5	1.6719	9.4622	2.0256	10.0595	1.3652	7.7833	1.4666	9.9224	1.5811	7.555
28	1.6606	9.4003	2.0474	10.2634	1.3918	7.7909	1.4882	10.0595	1.547	7.7396
28.5	1.7988	9.5721	2.0778	10.305	1.3775	7.7434	1.5679	10.2634	1.5808	7.4994
29	1.8234	9.634	2.0641	10.1062	1.3376	7.6862	1.69	10.0644	1.5188	7.5476
29.5	1.7383	9.6864	2.0474	10.1872	1.3708	7.5624	1.7425	10.0644	1.4962	7.4109
30	1.6849	9.7387	2.0738	10.8215	1.3584	7.7719	1.6821	9.8283	1.5068	7.0939
30.5	1.5711	9.6722	2.0759	10.0742	1.4008	7.8922	1.5031	9.814	1.5419	7.3539
31	1.5031	9.6532	2.1215	10.8004	1.4872	7.8523	1.4691	9.885	1.5398	7.5123
31.5	1.5913	9.2652	2.0995	10.9785	1.5156	8.1013	1.6153	9.502	1.5457	7.8763
32	1.5932	9.1855	2.0988	11.4235	1.4549	8.0478	1.6858	9.3883	1.533	7.9987
32.5	1.5769	9.0009	2.1356	11.4179	1.4343	8.3132	1.5258	9.0324	1.5657	8.2248
33	1.4995	8.8213	2.1304	11.5387	1.499	8.6131	1.4461	8.7368	1.5471	8.3351
33.5	1.5097	8.9311	2.1172	12.0266	1.5228	8.8848	1.4807	8.7315	1.5346	8.4629
34	1.52	8.6931	2.1477	11.8382	1.534	8.9608	1.4903	8.7187	1.5537	7.878
34.5	1.5243	8.7551	2.1492	12.2115	1.6704	9.4072	1.5097	8.8559	1.6132	7.7983
35	1.531	8.6017	2.1565	12.0772	1.7327	9.5322	1.5496	8.9259	1.6549	7.7206
35.5	1.532	8.1478	2.1617	12.0772	1.6345	9.4652	1.5976	8.9925	1.7237	7.3212
36	1.4896	7.7375	2.1451	12.0713	1.5316	9.5087	1.6295	8.9128	1.7295	6.9874
36.5	1.4834	7.5772	2.1334	11.5501	1.5967	9.4416	1.5985	9.0318	1.6214	6.4991
37	1.5005	7.0128	1.9599	11.695	1.5932	8.9292	1.522	8.8024	1.4967	5.8898
37.5	1.5103	6.651	1.6539	10.8752	1.5142	8.8143	1.4969	8.8637	1.5421	4.926
38	1.4981	6.2453	1.5381	10.8294	1.4409	8.8674	1.4431	8.6745	1.1303	3.9227
38.5	1.4122	5.8713	1.5198	10.6205	1.4208	8.4885	1.4674	8.6618		
39	1.25	5.5203	1.5207	10.4479	1.4393	8.9292	1.5583	8.529		
39.5	1.3757	5.2556	1.688	10.3106	1.467	8.543	1.3915	8.2782		
40	1.4644	4.6112	1.7022	10.2034	1.4681	8.6631	1.3583	8.2133		

Table A.1.5 Magnetic Susceptibility (SI x 10^{-5}) and Bulk Density (g/cc) for LB15-16, LB15-17, LB15-18, LB15-19 and LB15-8. From 40.5 to 81.15 cm depth

		LB15-17		LB15-18		LB15-19		
Depth		Density	MS	Density	MS	Density	MS	
40.5		1.5346	9.6251	1.5192	8.4677	1.4399	8.3242	
41		1.6045	9.3809	1.6093	8.7788	1.3864	7.9226	
41.5		1.5907	9.7662	1.5994	8.8283	1.294	8.1152	
42		1.4668	9.2721	1.5761	8.8326	1.3189	7.9925	
42.5		1.4576	9.4696	1.5697	8.5709	1.385	7.9925	
43		1.5013	9.4113	1.4819	8.3312	1.3562	7.6642	
43.5		1.439	10.4169	1.3892	8.195	1.3228	7.9925	
44		1.4901	9.4682	1.4131	7.9377	1.3538	7.6717	
44.5		1.5699	9.7387	1.413	7.7853	1.3469	7.8566	
45		1.6198	9.7908	1.3839	7.4679	1.3876	7.9636	
45.5		1.626	9.885	1.4504	7.2492	1.4784	7.9071	
46		1.5907	9.6911	1.4837	7.1148	1.4991	8.3401	
46.5		1.5477	9.5729	1.1529	6.6033	1.4451	8.0413	
47		1.4659	9.3791	0.5785	6.208	1.4011	8.3524	
47.5		1.3686	9.3791	0.7068	6.0273	1.473	8.3927	
48		1.359	9.2426	1.2369	6.1027	1.5412	8.2355	
48.5		1.3531	8.6762	1.3358	6.2354	1.4829	8.5565	
49		1.4685	8.7423	1.2739	6.4132	1.4026	8.0849	
49.5		1.5544	8.6153	1.3428	6.3592	1.4311	7.8747	
50		1.4678	8.6771	1.4251	6.6098	1.4578	7.5699	
50.5		1.3342	8.3442	1.347	6.6538	1.4796	7.6275	
51		1.3338	8.4749	1.283	6.5432	1.4953	7.5251	
51.5		1.4364	7.5965	1.293	6.7206	1.4554	6.6907	
52		1.3689	8.0914	1.2954	6.7367	1.4615	5.8816	
52.5		1.3201	7.4705	1.3906	6.857	1.4453	5.0704	
53		1.3778	7.5269	1.4719	6.9807	0.9602	3.7118	
53.5		1.4113	6.9718	1.5593	6.8772			
54		1.3822	7.3938	1.5573	7.3124			
54.5		1.4369	7.1989	1.5658	7.2945			
55		1.362	7.1425	1.5212	7.3088			
55.5		1.3716	7.2646	1.4597	7.4957			
56		1.4126	7.4248	1.5325	7.751			
56.5		1.4552	7.4378	1.612	7.9455			
57		1.443	7.4378	1.5679	8.2563			
57.5		1.5094	7.4197	1.5422	8.497			
58		1.4856	7.8534	1.5986	8.6735			
58.5		1.4078	7.7955	1.5504	9.1205			
59		1.4099	7.9342	1.4965	9.2441			
59.5		1.462	7.9959	1.4617	9.4868			
60		1.4589	8.2313	1.5078	9.6198			
60.5		1.5392	8.5525	1.5366	9.6151			
61		1.5665	8.9315	1.5691	9.8004			
61.5		1.5091	9.0875	1.4744	9.5346			
62		1.4733	9.4667	1.5343	9.473			
62.5		1.3984	9.5272	1.4877	9.2743			
63		1.4971	9.7736	1.4836	9.199			
63.5		1.5304	9.7641	1.5295	9.2035			
64		1.4331	9.7367	1.5889	9.3745			
64.5		1.4188	9.8627	1.5829	9.5682			
65		1.4047	9.8129	1.4931	9.3791			
65.5		1.4307	9.9592	1.4839	9.3269			
66		1.508	10.0153	1.5623	9.2698			
66.5		1.5749	9.9592	1.6071	9.1327			
67		1.5217	9.8979	1.5967	9.2215			
67.5		1.5068	9.9446	1.6275	9.2879			
68		1.5521	9.6955	1.5248	9.3449			
68.5		1.5025	9.5687	1.5011	9.2652			
69		1.563	10.1841	1.5311	9.3312			
69.5		1.5473	9.0888	1.5183	9.6532			
70		1.585	9.5495	1.5516	9.5346			
70.5		1.6209	9.3413	1.5752	9.7812			
71		1.6124	9.0053	1.5964	9.5299			
71.5		1.5873	8.9259	1.6177	9.6438			
72		1.5209	8.4418	1.6301	9.8477			
72.5		1.4955	7.569	1.6575	9.9189			
73		1.4891	7.5279	1.6194	9.6579			
73.5		1.5286	7.2448	1.5227	9.7244			
74		1.5175	6.8005	1.5264	9.5253			
74.5		1.5486	6.3738	1.6184	9.6674			
75		1.5976	6.0032	1.5609	9.5916			
75.5		1.575	5.2614	1.5064	9.6391			
76		1.2659	4.1428	1.5069	9.6014			
76.5				1.5111	9.4222			
77				1.4827	9.4881			
77.5				1.5372	9.3608			
78				1.6435	9.2205			
78.5				1.6026	9.2361			
79				1.5565	9.0147			
79.5				1.5719	8.5851			
80				1.5631	7.3693			
80.5				1.6656	6.4016			
81				1.833	5.3149			
81.5				1.5171	4.0713			

Table A.1.6 Magnetic Susceptibility (SI x 10^{-5}) and Bulk Density (g/cc) for LB15-7 and LB15-8. From 0 to 40 cm depth

	LB15-7		LB15-20	
Depth	Density	MS	Density	MS
0	1.5314	3.4873	1.034	2.1301
0.5	1.6353	4.5013	1.1811	3.3492
1	1.5714	5.7302	1.5275	5.1824
1.5	1.5876	6.5959	1.6947	6.2588
2	1.6259	7.3535	1.6425	7.2235
2.5	1.6339	7.9265	1.5932	7.7772
3	1.668	8.171	1.6275	8.3158
3.5	1.6756	8.7273	1.6457	8.5159
4	1.6699	8.683	1.6725	8.5859
4.5	1.6871	8.6703	1.7187	8.7603
5	1.6773	8.4304	1.7007	8.7039
5.5	1.6503	8.3067	1.627	8.5723
6	1.6901	8.171	1.5665	8.2999
6.5	1.7129	7.8062	1.5523	8.3564
7	1.7003	7.6749	1.5704	8.312
7.5	1.6678	7.3539	1.6049	8.1758
8	1.634	7.5476	1.5415	8.254
8.5	1.6036	7.2374	1.5325	8.1192
9	1.6187	7.2233	1.4748	8.6059
9.5	1.6609	7.0472	1.4574	7.9831
10	1.6638	6.9304	1.4852	7.7302
10.5	1.5736	6.8066	1.5246	7.6039
11	1.5585	6.9168	1.5502	7.5965
11.5	1.5725	6.8503	1.5372	7.7848
12	1.5343	6.9799	1.5571	7.7151
12.5	1.5356	6.9067	1.5858	7.578
13	1.5513	6.8503	1.5536	7.7696
13.5	1.5668	6.9073	1.502	8.0138
14	1.598	7.2138	1.5017	8.0914
14.5	1.6431	7.2767	1.5254	8.0178
15	1.6624	7.2933	1.6086	8.5118
15.5	1.5946	7.5402	1.631	8.6339
16	1.5732	7.6637	1.6186	8.5775
16.5	1.552	7.5897	1.5969	8.4869
17	1.5537	8.0396	1.5534	8.443
17.5	1.5764	8.1219	1.4703	8.7654
18	1.5838	8.3108	1.4467	8.756
18.5	1.5746	8.1243	1.463	8.8218
19	1.5776	8.3271	1.5039	8.9439
19.5	1.5669	8.087	1.5463	8.8876
20	1.5524	8.2071	1.5468	9.0799
20.5	1.522	7.5773	1.4326	9.1976
21	1.518	7.8961	1.4114	9.1541
21.5	1.5412	8.1029	1.5944	8.8347
22	1.5631	8.2273	1.6103	9.0494
22.5	1.5889	8.083	1.5042	8.5034
23	1.5399	8.3312	1.525	8.2677
23.5	1.5785	8.1323	1.4936	7.9334
24	1.5974	8.3271	1.4384	7.3603
24.5	1.5668	8.0162	1.4172	6.7976
25	1.5372	7.9261	1.4489	6.5443
25.5	1.5856	7.9356	1.4636	6.3557
26	1.5308	7.6449	1.4289	6.0654
26.5	1.474	7.5365	1.451	5.909
27	1.4953	7.3819	1.4635	5.5406
27.5	1.4947	7.2747	1.5099	4.8481
28	1.5323	7.318		
28.5	1.5467	7.5614		
29	1.5175	6.8656		
29.5	1.5151	6.9832		
30	1.5659	6.9322		
30.5	1.5705	6.8654		
31	1.6014	6.5891		
31.5	1.6524	5.4112		
32	1.6969	5.274		
32.5	1.7168	4.448		
33	1.3293	3.4588		
33.5				
34				
34.5				
35				
35.5				
36				
36.5				
37				
37.5				
38				
38.5				
39				
39.5				
40				

Table A.1.1 Glyssibach discharge (m^3/s) at hourly resolution as modelled by Ole Rossler

Date	Time	Discharge
20.08.05	00:00	0.47
20.08.05	01:00	0.4
20.08.05	02:00	0.28
20.08.05	03:00	0.28
20.08.05	04:00	0.27
20.08.05	05:00	0.26
20.08.05	06:00	0.27
20.08.05	07:00	0.27
20.08.05	08:00	0.26
20.08.05	09:00	0.28
20.08.05	10:00	0.43
20.08.05	11:00	0.66
20.08.05	12:00	0.69
20.08.05	13:00	0.54
20.08.05	14:00	0.31
20.08.05	15:00	0.25
20.08.05	16:00	0.32
20.08.05	17:00	0.59
20.08.05	18:00	0.64
20.08.05	19:00	0.62
20.08.05	20:00	0.56
20.08.05	21:00	0.69
20.08.05	22:00	0.77
20.08.05	23:00	0.8
21.08.05	00:00	0.71
21.08.05	01:00	0.74
21.08.05	02:00	0.59
21.08.05	03:00	0.7
21.08.05	04:00	0.57
21.08.05	05:00	0.5
21.08.05	06:00	0.3
21.08.05	07:00	0.3
21.08.05	08:00	0.28
21.08.05	09:00	0.32
21.08.05	10:00	0.47
21.08.05	11:00	0.64
21.08.05	12:00	0.92
21.08.05	13:00	1.07
21.08.05	14:00	1.22
21.08.05	15:00	1.22
21.08.05	16:00	1.37
21.08.05	17:00	1.59
21.08.05	18:00	1.97
21.08.05	19:00	1.89
21.08.05	20:00	1.84
21.08.05	21:00	1.67
21.08.05	22:00	2.03
21.08.05	23:00	2.42
22.08.05	00:00	2.95
22.08.05	01:00	3.07
22.08.05	02:00	2.56
22.08.05	03:00	2.57
22.08.05	04:00	1.86
22.08.05	05:00	1.68
22.08.05	06:00	0.84
22.08.05	07:00	1.22
22.08.05	08:00	1.61
22.08.05	09:00	1.8
22.08.05	10:00	1.46
22.08.05	11:00	1.56
22.08.05	12:00	1.56
22.08.05	13:00	1.45
22.08.05	14:00	0.97
22.08.05	15:00	0.9
22.08.05	16:00	1.15
22.08.05	17:00	1.34
22.08.05	18:00	1.4
22.08.05	19:00	1.59
22.08.05	20:00	1.74
22.08.05	21:00	1.99
22.08.05	22:00	1.84
22.08.05	23:00	1.54
23.08.05	00:00	0.99
23.08.05	01:00	0.7
23.08.05	02:00	0.52
23.08.05	03:00	0.41
23.08.05	04:00	0.31
23.08.05	05:00	0.26
23.08.05	06:00	0.25
23.08.05	07:00	0.25
23.08.05	08:00	0.25
23.08.05	09:00	0.25
23.08.05	10:00	0.25
23.08.05	11:00	0.25
23.08.05	12:00	0.25
23.08.05	13:00	0.25
23.08.05	14:00	0.25
23.08.05	15:00	0.25
23.08.05	16:00	0.25
23.08.05	17:00	0.25
23.08.05	18:00	0.25
23.08.05	19:00	0.25
23.08.05	20:00	0.25
23.08.05	21:00	0.25
23.08.05	22:00	0.31
23.08.05	23:00	0.31
24.08.05	00:00	0.32
24.08.05	01:00	0.26
24.08.05	02:00	0.26
24.08.05	03:00	0.25
24.08.05	04:00	0.25
24.08.05	05:00	0.25
24.08.05	06:00	0.25
24.08.05	07:00	0.25
24.08.05	08:00	0.25
24.08.05	09:00	0.25
24.08.05	10:00	0.25
24.08.05	11:00	0.25
24.08.05	12:00	0.25
24.08.05	13:00	0.25
24.08.05	14:00	0.25
24.08.05	15:00	0.25
24.08.05	16:00	0.25
24.08.05	17:00	0.25
24.08.05	18:00	0.25
24.08.05	19:00	0.25
24.08.05	20:00	0.25
24.08.05	21:00	0.25
24.08.05	22:00	0.25
24.08.05	23:00	0.25

Table A.1.2 Trachtbach discharge (m^3/s) at hourly resolution as modelled by Ole Rossler

Date	Time	Discharge
20.08.05	00:00	0.4
20.08.05	01:00	0.36
20.08.05	02:00	0.27
20.08.05	03:00	0.27
20.08.05	04:00	0.27
20.08.05	05:00	0.25
20.08.05	06:00	0.26
20.08.05	07:00	0.26
20.08.05	08:00	0.26
20.08.05	09:00	0.28
20.08.05	10:00	0.45
20.08.05	11:00	0.69
20.08.05	12:00	0.71
20.08.05	13:00	0.54
20.08.05	14:00	0.3
20.08.05	15:00	0.25
20.08.05	16:00	0.29
20.08.05	17:00	0.48
20.08.05	18:00	0.52
20.08.05	19:00	0.52
20.08.05	20:00	0.5
20.08.05	21:00	0.61
20.08.05	22:00	0.66
20.08.05	23:00	0.68
21.08.05	00:00	0.61
21.08.05	01:00	0.64
21.08.05	02:00	0.52
21.08.05	03:00	0.63
21.08.05	04:00	0.52
21.08.05	05:00	0.46
21.08.05	06:00	0.29
21.08.05	07:00	0.29
21.08.05	08:00	0.28
21.08.05	09:00	0.31
21.08.05	10:00	0.41
21.08.05	11:00	0.53
21.08.05	12:00	0.74
21.08.05	13:00	0.86
21.08.05	14:00	0.97
21.08.05	15:00	0.97
21.08.05	16:00	1.07
21.08.05	17:00	1.2
21.08.05	18:00	1.49
21.08.05	19:00	1.45
21.08.05	20:00	1.47
21.08.05	21:00	1.35
21.08.05	22:00	1.57
21.08.05	23:00	1.87
22.08.05	00:00	2.26
22.08.05	01:00	2.39
22.08.05	02:00	1.98
22.08.05	03:00	1.91
22.08.05	04:00	1.36
22.08.05	05:00	1.2
22.08.05	06:00	0.65
22.08.05	07:00	0.88
22.08.05	08:00	1.12
22.08.05	09:00	1.24
22.08.05	10:00	1.06
22.08.05	11:00	1.17
22.08.05	12:00	1.19
22.08.05	13:00	1.13
22.08.05	14:00	0.78
22.08.05	15:00	0.72
22.08.05	16:00	0.88
22.08.05	17:00	1.02
22.08.05	18:00	1.06
22.08.05	19:00	1.19
22.08.05	20:00	1.28
22.08.05	21:00	1.46
22.08.05	22:00	1.31
22.08.05	23:00	1.12
23.08.05	00:00	0.74
23.08.05	01:00	0.59
23.08.05	02:00	0.44
23.08.05	03:00	0.37
23.08.05	04:00	0.28
23.08.05	05:00	0.25
23.08.05	06:00	0.25
23.08.05	07:00	0.25
23.08.05	08:00	0.25
23.08.05	09:00	0.25
23.08.05	10:00	0.25
23.08.05	11:00	0.25
23.08.05	12:00	0.25
23.08.05	13:00	0.25
23.08.05	14:00	0.25
23.08.05	15:00	0.25
23.08.05	16:00	0.25
23.08.05	17:00	0.25
23.08.05	18:00	0.25
23.08.05	19:00	0.25
23.08.05	20:00	0.25
23.08.05	21:00	0.25
23.08.05	22:00	0.3
23.08.05	23:00	0.3
24.08.05	00:00	0.31
24.08.05	01:00	0.26
24.08.05	02:00	0.25
24.08.05	03:00	0.25
24.08.05	04:00	0.25
24.08.05	05:00	0.25
24.08.05	06:00	0.25
24.08.05	07:00	0.25
24.08.05	08:00	0.25
24.08.05	09:00	0.25
24.08.05	10:00	0.25
24.08.05	11:00	0.25
24.08.05	12:00	0.25
24.08.05	13:00	0.25
24.08.05	14:00	0.25
24.08.05	15:00	0.25
24.08.05	16:00	0.25
24.08.05	17:00	0.25
24.08.05	18:00	0.25
24.08.05	19:00	0.25
24.08.05	20:00	0.25
24.08.05	21:00	0.25
24.08.05	22:00	0.25
24.08.05	23:00	0.25

Annex 2: Results

Table A.2.1 Zirconium (Zr) profile for LB15-14

LB15-14	
Depth	Zr
19.33	2699
21.83	2329
24.33	5058
26.83	5969
29.33	4656
31.83	3443
34.33	3324
36.83	6796
39.33	4487
41.83	5103
44.33	3765
46.83	3907
49.33	3736
51.83	4495
54.33	3965
56.83	4578
59.33	3317
61.83	3317
64.33	3436
66.83	3779
69.33	6237
71.83	4018
74.33	2969
76.83	3102
79.33	3156
81.83	3745
84.33	2129
86.83	2212
89.33	2794
91.83	4338
94.33	5895
96.83	18000
99.33	20000
101.83	5325
104.33	2679
106.83	2915
109.33	1201
111.83	2339
114.33	3101
116.83	4324
119.33	3646
121.83	3595
124.33	2982
126.83	5439
129.33	4781
131.83	3203
134.33	2934
136.83	2345
139.33	2270
141.83	2192
144.33	2784
146.83	4215
149.33	3181
151.83	3800
154.33	4115
156.83	5412
159.33	5452
161.83	3646
164.33	3648
166.83	4340
169.33	3493
171.83	5067
174.33	4317
176.83	2805
179.33	2928
181.83	3047
184.33	3997
186.83	2279
189.33	2434
191.83	3232
194.33	4686
196.83	9653

LB15-14	
Depth	Zr
199.33	11673
201.83	2950
204.33	4389
206.83	4720
209.33	5323
211.83	4665
214.33	4268
216.83	2798
219.33	3557
221.83	2653
224.33	2518
226.83	2691
229.33	3563
231.83	3338
234.33	4357
236.83	3208
239.33	2333
241.83	4135
244.33	2368
246.83	3287
249.33	3427
251.83	2957
254.33	3984
256.83	2839
259.33	3313
261.83	3004
264.33	2986
266.83	2065
269.33	2501
271.83	2176
274.33	1630
276.83	3158
279.33	2950
281.83	3345
284.33	6005
286.83	2692
289.33	3996
291.83	3642
294.33	2752
296.83	1694
299.33	2216
301.83	2927
304.33	3572
306.83	2353
309.33	3705
311.83	2399
314.33	1985
316.83	3063
319.33	3400
321.83	3351
324.33	2612
326.83	1885
329.33	1455
331.83	2197
334.33	3330
336.83	2397
339.33	2631
341.83	2185
344.33	2947
346.83	3550
349.33	3609
351.83	4249
354.33	3780
356.83	3130
359.33	2389
361.83	2598
364.33	1444
366.83	1880
369.33	3096
371.83	3891
374.33	3851
376.83	3132

LB15-14	
Depth	Zr
379.33	3133
381.83	3123
384.33	4048
386.83	4608
389.33	6478
391.83	5184
394.33	7636
396.83	4902
399.33	7398
401.83	4478
404.33	2499
406.83	3200
409.33	3463
411.83	1850
414.33	2709
416.83	2630
419.33	2281
421.83	1787
424.33	2251
426.83	2705
429.33	3794
431.83	3953
434.33	2557
436.83	2511
439.33	1565
441.83	2310
444.33	2936
446.83	3041
449.33	2544
451.83	1925
454.33	3862
456.83	3369
459.33	3187
461.83	2757
464.33	2412
466.83	2052
469.33	3161
471.83	3436
474.33	2959
476.83	2392
479.33	2447
481.83	2756
484.33	2254
486.83	2106
489.33	2460
491.83	2556
494.33	4307
496.83	3043
499.33	2636
501.83	1718
504.33	2755
506.83	3638
509.33	3721
511.83	4160
514.33	2849
516.83	2505
519.33	2651
521.83	2266
524.33	2394
526.83	3543
529.33	3220
531.83	1958
534.33	2224
536.83	2585
539.33	4023
541.83	4096
544.33	4402
546.83	2700
549.33	2587
551.83	2653
554.33	2288
556.83	3863

LB15-14	
Depth	Zr
559.33	3202
561.83	4193
564.33	3342
566.83	2345
569.33	3209
571.83	2980
574.33	2923
576.83	3867
579.33	3260
581.83	2699
584.33	2306
586.83	3606
589.33	4718
591.83	2752
594.33	2564
596.83	2490
599.33	4533
601.83	3633
604.33	2333
606.83	3872
609.33	2339
611.83	3757
614.33	3050
616.83	2821
619.33	2839
621.83	3297
624.33	4566
626.83	3806
629.33	4767
631.83	4647
634.33	4748
636.83	3549
639.33	2505
641.83	3237
644.33	2891
646.83	2970
649.33	3397
651.83	4519
654.33	4175
656.83	4593
659.33	4569
661.83	4079
664.33	3012
666.83	4089
669.33	5895
671.83	8234
674.33	3027
676.83	3182
679.33	2322
681.83	3507
684.33	2798
686.83	3468
689.33	3483
691.83	3351
694.33	3319
696.83	4405
699.33	9890
701.83	13853
704.33	7476
706.83	4633
709.33	3846
711.83	2895
714.33	4525
716.83	3245

Table A.2.2 Zirconium (Zr) profile for LB15-18

LB15-8

LB15-8	
Depth	Zr
0	3346
2.5	6296
5	7920
7.5	5875
10	2356
12.5	2837
15	2436
17.5	2505
20	1989
22.5	1291
25	2367
27.5	1935
30	2284
32.5	2435
35	1813
37.5	2671
40	3761
42.5	5121
45	6056
47.5	4884
50	4700
52.5	3392
55	2080
57.5	1401
60	1382
62.5	2532
65	2834
67.5	2995
70	4718
72.5	4749
75	3265
77.5	3428
80	2199
82.5	1536
85	2397
87.5	1616
90	1584
92.5	1866
95	2211
97.5	2123
100	2229
102.5	3411
105	2911
107.5	3723
110	1917
112.5	1798
115	1720
117.5	2355
120	3138
122.5	2659
125	3175
127.5	3253
130	2020
132.5	2797
135	2189
137.5	2476
140	2374
142.5	3413
145	3481
147.5	3546
150	3394
152.5	4081
155	3676
157.5	5347
160	5740
162.5	5058
165	4101
167.5	3938
170	3805
172.5	3501
175	2710
177.5	2675

LB15-8	
Depth	Zr
180	2638
182.5	3045
185	3505
187.5	4699
190	4453
192.5	5514
195	4810
197.5	4329
200	5104
202.5	5180
205	5307
207.5	4182
210	1380
212.5	1451
215	2785
217.5	3046
220	2485
222.5	2416
225	3026
227.5	2595
230	1978
232.5	1497
235	1689
237.5	3301
240	2615
242.5	2887
245	2604
247.5	1750
250	2732
252.5	3209
255	3654
257.5	3331
260	3321
262.5	3905
265	5577
267.5	4681
270	2620
272.5	2770
275	2418
277.5	1114
280	1928
282.5	3358
285	1965
287.5	1904
290	2477
292.5	1662
295	1783
297.5	1975
300	1587
302.5	1094
305	2909
307.5	2688
310	2857
312.5	2862

Table A.2.3 Zirconium (Zr) profile for LB15-18

LB15-8

LB15-18	
Depth	Zr
1	2177
2	1867
3	2956
4	3217
5	3042
6	3273
7	3508
8	2974
9	3172
10	3252
11	3459
12	3012
13	2608
14	4461
15	3988
16	3885
17	3323
18	5165
19	4248
20	3644
21	5061
22	6316
23	3869
24	4318
25	4818
26	4530
27	3568
28	4884
29	5189
30	5400
31	3170
32	4438
33	5831
34	5114
35	5572
36	5039
37	4432
38	5432
39	6791
40	12104
41	4197
42	2517
43	2996
44	2201
45	2626
46	2886
47	2023
48	1637
49	3151
50	2466
51	2026
52	3035
53	2975
54	2783
55	2822
56	2562
57	2585
58	2729
59	3170
60	4097
61	3669
62	1735
63	2722
64	2617
65	3447
66	2553
67	2040
68	3299
69	2234
70	3349
71	5621
72	3216

LB15-18	
Depth	Zr
73	1919
74	2395
75	2328
76	3085
77	3111
78	3001
79	3442
80	3422
81	2782
82	3009
83	3885
84	3987
85	3480
86	5868
87	5446
88	4961
89	3451
90	2772
91	2044
92	3639
93	4990
94	4838
95	3797
96	3605
97	2276
98	3124
99	2200
100	2115
101	2648
102	3382
103	1593
104	2922
105	2130
106	2378
107	1570
108	1957
109	3436
110	2806
111	2744
112	2431
113	3725
114	2046
115	2268
116	1631
117	1982
118	4089
119	3750
120	2690
121	2859
122	1871
123	1571
124	3384
125	2804
126	2546
127	1697
128	3755
129	2898
130	5139
131	5006
132	4761
133	2641
134	2946
135	1501
136	1860
137	2569
138	1579
139	2582
140	2083
141	1902
142	2951
143	1564
144	2896

LB15-18	
Depth	Zr
145	3014
146	5021
147	3412
148	2920
149	2690
150	2922
151	2991
152	2375
153	2837
154	2394
155	1931
156	1356
157	2461
158	2902
159	3988
160	5983
161	3822
162	1486
163	3016
164	2108
165	1743
166	2981
167	5234
168	4226
169	5567
170	5233
171	3841
172	4380
173	5471
174	2808
175	2083
176	3347
177	3193
178	2143
179	2719
180	3049
181	2970
182	3154
183	2807
184	2625
185	2256
186	1738
187	1572
188	4415
189	8493
190	5681
191	2791
192	2281
193	2378
194	3134
195	3229
196	2377
197	2608
198	1939
199	2276
200	2838
201	1585
202	2987
203	2390
204	1504
205	1742
206	1821
207	2243
208	2078
209	1406
210	2018
211	3080
212	2182
213	2294
214	1815
215	3256
216	2565

LB15-18	
Depth	Zr
216	2565
217	2175
218	2142
219	1827
220	2695
221	1919
222	1855
223	2596
224	4484
225	2776
226	1773
227	2333
228	2396
229	3160
230	3945
231	3623
232	2262
233	3492
234	5628
235	3721
236	2806
237	2375
238	989
239	3491
240	2183
241	1934
242	2485
243	3166
244	2145
245	3434
246	2796
247	2929
248	2847
249	2084
250	3215
251	1824
252	2113
253	1881
254	545
255	2242
256	2927
257	4476
258	3669
259	4684
260	3466
261	3319
262	3718
263	3705
264	3424
265	4990
266	4434
267	8859
268	8712
269	4299
270	5255
271	6153
272	8836

Table A.2.4 Elements of Dataset 1 for LB15-14

	LB15-14											
	Elemental Profiles											
Depth (mm)	Fe	Mg	Al	K	Ca	Ti	Mn	Cu	Rb	Sr	Zr	Si
108	459486	67	335	16172	197367	11607	5770	1322	5812	15252	5996	2451
108.5	457426	57	293	17014	189094	11737	6091	1282	6285	15544	7139	2428
109	490888	0	291	19261	169023	11821	6391	1572	6050	15734	6358	2442
109.5	550924	54	390	20717	136093	13235	6925	1184	7292	14533	6121	2657
110	662580	62	337	23954	102222	14241	8203	1247	9811	12442	2804	2713
110.5	674568	79	422	25086	106680	13818	8579	1252	10311	11856	1804	2749
111	661366	43	434	24841	112609	14040	7954	1497	9844	12021	2086	2878
111.5	642388	87	434	25098	114157	13673	8203	1451	9725	12430	3013	2857
112	622631	72	408	24452	127306	14228	8065	1745	9526	12723	2555	2836
112.5	660199	28	393	25210	100158	13825	7660	1462	10061	12057	2583	2715
113	696666	102	467	26629	80611	14271	7679	1773	11316	10856	2356	2627
113.5	702445	75	420	27591	76518	14144	8174	1753	11327	11147	1559	2606
114	691238	6	417	26915	80234	14323	8042	1791	10607	11021	2027	2469
114.5	664672	32	320	25676	90086	14518	7868	1493	10108	12029	3059	2456
115	648512	65	458	25178	93385	14199	7394	1395	9744	12262	2329	2548
115.5	648496	116	438	25420	96620	14334	8495	1334	8595	12354	3139	2655
116	665060	29	393	25912	98896	14797	8053	1572	9306	12674	2938	2757
116.5	653221	46	384	24866	99576	14409	8149	1421	9549	12422	2816	2601
117	618690	28	376	23955	107995	13932	7931	1463	9576	13399	1779	2548
117.5	641929	73	375	25527	118603	14850	8262	1629	8912	13184	1965	2745
118	560120	45	384	21453	106810	13104	7184	1460	7896	12645	3034	2256
118.5	542596	0	348	19822	102949	11907	7096	1244	7202	12569	2514	2057
119	583231	78	313	22100	103639	13078	7263	1351	7924	12521	2488	2251
119.5	591969	87	337	23037	102120	13925	7187	1584	8288	12737	2187	2341
120	596562	41	426	22516	104371	14059	7197	1287	8968	13133	2942	2355
120.5	607600	45	404	23365	96069	14121	7360	1813	8342	13284	3090	2536
121	611305	37	410	23054	90621	14048	7003	1558	9030	12823	1852	2455
121.5	595223	0	394	22661	91474	14109	6731	1526	8834	12828	1468	2437
122	593440	122	428	22300	93861	13629	7204	1499	8256	12529	2798	2522
122.5	595425	76	309	22331	96449	14295	6858	1258	8116	12679	2059	2360
123	595988	0	324	22221	105278	14349	6679	1445	9136	13217	2758	2439
123.5	588719	72	391	21780	109261	14192	6953	1199	7977	13095	3184	2474
124	587319	71	384	21552	114062	14862	7368	1712	7865	13223	2411	2468
124.5	589519	7	390	21060	119207	14292	7828	1311	7917	13664	2871	2363
125	588317	0	301	20908	128443	14305	7749	1456	8989	13793	2834	2425
125.5	577008	68	345	20348	132743	14494	7637	1149	6651	14374	3309	2262
126	575811	24	382	20274	135003	15077	7229	1620	7225	14001	3343	2295
126.5	572006	49	392	19678	135716	14710	7466	1682	7242	14824	3392	2317
127	579883	0	333	19954	137779	15068	7192	1285	7074	14514	3123	2413
127.5	577766	59	365	19539	135690	15307	7349	1292	7351	13994	3910	2296
128	568861	53	348	19149	136607	15317	6850	1253	6950	14231	4118	2313
128.5	560793	49	340	18436	132384	14544	6828	1442	6779	14285	3526	2200
129	573758	45	371	19082	128901	13896	7747	1320	6718	14589	2987	2190
129.5	582431	0	387	19040	127190	14321	7378	1169	7362	14584	3321	2290
130	591044	24	288	19492	130618	14442	7588	1543	7476	14029	3823	2259
130.5	589699	75	355	19471	130285	14175	8237	1568	6568	13692	4082	2135
131	594983	52	369	19309	131903	14909	8179	1217	7239	14268	2990	2319
131.5	596973	33	348	19397	136119	14847	8108	1655	7470	14316	3122	2309
132	584900	67	370	18797	141094	14032	7670	1445	6532	14095	4417	2371
132.5	543506	23	376	17888	150865	13974	7444	1481	6910	14339	4041	2255
133	565789	0	283	18662	139833	14692	7304	1676	6016	14412	4378	2226
133.5	576854	89	355	18633	129147	14419	7894	1633	7088	13975	4962	2274
134	602386	76	330	18492	121068	15159	7464	1640	7360	14396	3871	2177
134.5	596631	90	314	18453	123495	15314	7585	1525	6559	14237	3882	2171
135	593412	5	373	18373	122225	15075	7592	1504	7110	13997	3787	2233
135.5	584791	71	327	18146	123541	15224	7277	1762	6341	13844	4221	2159
136	566943	35	296	17454	126637	14615	7010	1311	6902	13818	4968	2104
136.5	561234	49	312	17474	128428	14394	7017	1480	6919	14657	5297	2057
137	554942	38	320	17177	131323	14055	7218	1612	5813	14587	4757	2171
137.5	578254	63	352	18367	135541	14886	7246	1593	6731	15078	4599	2273
138	564759	51	349	18641	136571	15096	6861	1661	6227	14513	4984	2328
138.5	528908	0	251	17289	127607	14221	6367	1459	5492	14110	4884	2113
139	517035	66	307	16708	131364	14727	6481	1428	6492	14780	5455	2058
139.5	525675	42	314	16884	130328	13778	6594	1429	5771	14700	5476	2050
140	550707	54	343	18352	128822	13459	6806	1329	6774	14729	5138	2187
140.5	561834	82	332	19059	130215	13372	6684	1166	7297	14694	4631	2286
141	560653	0	325	19112	132383	13539	7951	1548	7012	15141	4022	2257
141.5	554593	30	266	18834	136113	13246	7515	1382	6901	15357	3976	2295
142	539058	0	277	18401	133667	13590	6698	1476	6867	15309	4026	2187
142.5	529386	58	313	17947	129308	13314	6971	1418	6527	14906	4238	2117
143	534391	91	347	17903	127492	13043	7121	1388	7490	14329	4086	2043
143.5	553918	47	314	19370	128903	12994	7500	1376	7192	14853	3323	2207
144	562282	91	343	18831	130589	13427	7837	1439	7219	14736	4754	2180
144.5	569928	58	305	19503	133615	13600	7671	1509	6871	15078	2577	2263
145	578904	6	342	19447	136526	13783	7696	1347	7411	15236	3526	2227
145.5	577497	76	370	19288	131407	14083	7591	1435	6364	14592	3511	2221
146	591014	45	347	18625	125673	14458	7824	1616	7387	14405	2972	2058

Table A.2.5 Elements of Dataset 1for LB15-14

	LB15-14											
	Elemental Profiles											
Depth (mm)	Fe	Mg	Al	K	Ca	Ti	Mn	Cu	Rb	Sr	Zr	Si
147	620917	0	339	19699	123106	14722	8055	1734	6528	14268	3796	2190
147.5	633933	59	358	20167	120671	15318	8609	1801	6484	13568	3573	2140
148	613170	40	302	19164	114663	13937	8103	1673	7661	13109	3522	2132
148.5	614409	79	330	18773	112395	14242	7800	1688	7726	12855	3930	1904
149	627149	51	286	19112	116325	14488	8247	1788	7419	12903	3175	1927
149.5	601191	58	272	18415	113725	13642	7489	1495	7166	12782	3905	1844
150	585016	99	294	17434	114902	13896	7148	1606	6626	12503	3681	1926
150.5	581562	60	303	17278	116620	14485	7430	1386	7226	13053	2990	2021
151	571799	112	311	16458	121608	13785	6887	1655	6484	12973	4162	1935
151.5	565958	12	285	16171	130368	14510	7356	1598	7479	13711	3522	2063
152	562467	92	337	16589	144916	14980	6849	1614	6703	13712	4436	2179
152.5	525264	23	273	15672	153379	14569	6109	1501	6777	14578	5214	2141
153	485395	15	307	15126	148420	14281	5635	1315	6328	14442	6798	2005
153.5	470539	8	284	15015	150032	13758	5565	1351	6164	15103	4990	1923
154	486523	64	354	15213	152695	14215	5612	1269	5914	14589	4607	1988
154.5	481210	29	261	15562	166482	14376	5785	1302	5323	14640	5170	1976
155	467991	0	327	15336	170782	14034	5841	1406	5629	15075	5207	2067
155.5	469975	56	300	15584	182096	13147	6430	1438	6125	14049	5189	1873
156	471395	37	279	16720	194229	11774	6803	1471	5450	14439	5203	1823
156.5	477501	0	302	18288	197068	12048	6591	1535	4971	14616	4682	2107
157	523482	55	347	20499	170957	12564	7695	1327	5763	14261	3749	2128
157.5	562125	75	315	21319	146800	13163	8550	1116	6774	12831	3166	2179
158	585796	33	310	22547	143581	13368	8412	1496	7179	11272	2246	2293
158.5	599277	34	415	23855	141372	13847	7939	1324	7736	11635	3356	2461
159	601091	94	391	24539	147310	14161	8142	1317	8253	12120	2720	2625
159.5	629929	44	395	24865	128175	14109	8606	1458	7877	11559	2054	2504
160	597756	26	352	23794	142742	13308	8280	1131	7556	11747	1925	2470
160.5	566036	84	422	23057	158839	13436	8328	1365	7562	12920	2434	2536
161	540790	41	405	22070	166685	12811	8548	1184	8111	14255	3177	2391
161.5	528695	53	398	21679	166033	12874	8014	1313	8200	15088	2138	2496
162	503522	42	401	20867	170374	12427	6972	1375	8546	16439	2092	2478
162.5	478846	0	306	19395	182523	11840	7057	945	7198	17343	2697	2488
163	455150	8	285	18238	177238	12147	6541	895	6544	20377	3096	2470
163.5	362019	35	292	14844	227991	11004	6307	3469	4690	24572	2736	2220
164	370326	60	366	15378	211966	12362	5834	1403	5021	25746	4025	2324
164.5	419618	63	334	18152	175305	11785	5569	1114	5687	25467	3650	2373
165	514766	26	373	21418	148385	12387	6655	1033	6636	22440	3958	2397
165.5	569867	60	369	22370	136729	13989	7420	1244	7245	16522	4916	2313
166	583678	93	390	22510	140647	13481	7729	1278	8129	13807	3793	2320
166.5	608566	98	336	21783	149161	12736	8166	1172	7820	11541	3102	2297

Table A.2.6 Elements of Dataset 2 for LB15-14

	LB15-14							
	Elemental Ratios							
epth (mm)	Ti/Ca	Rb/Sr	Zr/Rb	Zr/K	Mn/Ca	K/Ti	Ca/Ti	Ca/Rb
108	0.059	0.381	1.032	0.371	0.029	1.393	17.004	33.959
108.5	0.062	0.404	1.136	0.420	0.032	1.450	16.111	30.087
109	0.070	0.385	1.051	0.330	0.038	1.629	14.299	27.938
109.5	0.097	0.502	0.839	0.295	0.051	1.565	10.283	18.663
110	0.139	0.789	0.286	0.117	0.080	1.682	7.178	10.419
110.5	0.130	0.870	0.175	0.072	0.080	1.815	7.720	10.346
111	0.125	0.819	0.212	0.084	0.071	1.769	8.021	11.439
111.5	0.120	0.782	0.310	0.120	0.072	1.836	8.349	11.739
112	0.112	0.749	0.268	0.104	0.063	1.719	8.948	13.364
112.5	0.138	0.834	0.257	0.102	0.076	1.824	7.245	9.955
113	0.177	1.042	0.208	0.088	0.095	1.866	5.649	7.124
113.5	0.185	1.016	0.138	0.057	0.107	1.951	5.410	6.755
114	0.179	0.962	0.191	0.075	0.100	1.879	5.602	7.564
114.5	0.161	0.840	0.303	0.119	0.087	1.769	6.205	8.912
115	0.152	0.795	0.239	0.093	0.079	1.773	6.577	9.584
115.5	0.148	0.696	0.365	0.123	0.088	1.773	6.741	11.241
116	0.150	0.734	0.316	0.113	0.081	1.751	6.684	10.627
116.5	0.145	0.769	0.295	0.113	0.082	1.726	6.911	10.428
117	0.129	0.715	0.186	0.074	0.073	1.719	7.752	11.278
117.5	0.125	0.676	0.220	0.077	0.070	1.719	7.987	13.308
118	0.123	0.624	0.384	0.141	0.067	1.637	8.151	13.527
118.5	0.116	0.573	0.349	0.127	0.069	1.665	8.646	14.295
119	0.126	0.633	0.314	0.113	0.070	1.690	7.925	13.079
119.5	0.136	0.651	0.264	0.095	0.070	1.654	7.334	12.321
120	0.135	0.683	0.328	0.131	0.069	1.602	7.424	11.638
120.5	0.147	0.628	0.370	0.132	0.077	1.655	6.803	11.516
121	0.155	0.704	0.205	0.080	0.077	1.641	6.451	10.036
121.5	0.154	0.689	0.166	0.065	0.074	1.606	6.483	10.355
122	0.145	0.659	0.339	0.125	0.077	1.636	6.887	11.369
122.5	0.148	0.640	0.254	0.092	0.071	1.562	6.747	11.884
123	0.136	0.691	0.302	0.124	0.063	1.549	7.337	11.523
123.5	0.130	0.609	0.399	0.146	0.064	1.535	7.699	13.697
124	0.130	0.595	0.307	0.112	0.065	1.450	7.675	14.502
124.5	0.120	0.579	0.363	0.136	0.066	1.474	8.341	15.057
125	0.111	0.652	0.315	0.136	0.060	1.462	8.979	14.289
125.5	0.109	0.463	0.498	0.163	0.058	1.404	9.158	19.958
126	0.112	0.516	0.463	0.165	0.054	1.345	8.954	18.686
126.5	0.108	0.489	0.468	0.172	0.055	1.338	9.226	18.740
127	0.109	0.487	0.441	0.157	0.052	1.324	9.144	19.477
127.5	0.113	0.525	0.532	0.200	0.054	1.276	8.865	18.459
128	0.112	0.488	0.593	0.215	0.050	1.250	8.919	19.656
128.5	0.110	0.475	0.520	0.191	0.052	1.268	9.102	19.529
129	0.108	0.460	0.445	0.157	0.060	1.373	9.276	19.187
129.5	0.113	0.505	0.451	0.174	0.058	1.330	8.881	17.277
130	0.111	0.533	0.511	0.196	0.058	1.350	9.044	17.472
130.5	0.109	0.480	0.621	0.210	0.063	1.374	9.191	19.836
131	0.113	0.507	0.413	0.155	0.062	1.295	8.847	18.221
131.5	0.109	0.522	0.418	0.161	0.060	1.306	9.168	18.222
132	0.099	0.463	0.676	0.235	0.054	1.340	10.055	21.600
132.5	0.093	0.482	0.585	0.226	0.049	1.280	10.796	21.833
133	0.105	0.417	0.728	0.235	0.052	1.270	9.518	23.244
133.5	0.112	0.507	0.700	0.266	0.061	1.292	8.957	18.221
134	0.125	0.511	0.526	0.209	0.062	1.220	7.987	16.449
134.5	0.124	0.461	0.592	0.210	0.061	1.205	8.064	18.828
135	0.123	0.508	0.533	0.206	0.062	1.219	8.108	17.191
135.5	0.123	0.458	0.666	0.233	0.059	1.192	8.115	19.483
136	0.115	0.499	0.720	0.285	0.055	1.194	8.665	18.348
136.5	0.112	0.472	0.766	0.303	0.055	1.214	8.922	18.562
137	0.107	0.399	0.818	0.277	0.055	1.222	9.344	22.591
137.5	0.110	0.446	0.683	0.250	0.053	1.234	9.105	20.137
138	0.111	0.429	0.800	0.267	0.050	1.235	9.047	21.932
138.5	0.111	0.389	0.889	0.282	0.050	1.216	8.973	23.235
139	0.112	0.439	0.840	0.326	0.049	1.135	8.920	20.235
139.5	0.106	0.393	0.949	0.324	0.051	1.225	9.459	22.583
140	0.104	0.460	0.758	0.280	0.053	1.364	9.571	19.017
140.5	0.103	0.497	0.635	0.243	0.051	1.425	9.738	17.845
141	0.102	0.463	0.574	0.210	0.060	1.412	9.778	18.879
141.5	0.097	0.449	0.576	0.211	0.055	1.422	10.276	19.724
142	0.102	0.449	0.586	0.219	0.050	1.354	9.836	19.465
142.5	0.103	0.438	0.649	0.236	0.054	1.348	9.712	19.811
143	0.102	0.523	0.546	0.228	0.056	1.373	9.775	17.022
143.5	0.101	0.484	0.462	0.172	0.058	1.491	9.920	17.923

Table A.2.7 Elements of Dataset 2 for LB15-14

	LB15-14							
	Elemental Ratios							
Depth (mm)	Ti/Ca	Rb/Sr	Zr/Rb	Zr/K	Mn/Ca	K/Ti	Ca/Ti	Ca/Rb
144	0.103	0.490	0.659	0.252	0.060	1.402	9.726	18.090
144.5	0.102	0.456	0.375	0.132	0.057	1.434	9.825	19.446
145	0.101	0.486	0.476	0.181	0.056	1.411	9.905	18.422
145.5	0.107	0.436	0.552	0.182	0.058	1.370	9.331	20.648
146	0.115	0.513	0.402	0.160	0.062	1.288	8.692	17.013
146.5	0.117	0.460	0.514	0.176	0.063	1.329	8.519	18.757
147	0.120	0.458	0.581	0.193	0.065	1.338	8.362	18.858
147.5	0.127	0.478	0.551	0.177	0.071	1.317	7.878	18.611
148	0.122	0.584	0.460	0.184	0.071	1.375	8.227	14.967
148.5	0.127	0.601	0.509	0.209	0.069	1.318	7.892	14.548
149	0.125	0.575	0.428	0.166	0.071	1.319	8.029	15.679
149.5	0.120	0.561	0.545	0.212	0.066	1.350	8.336	15.870
150	0.121	0.530	0.556	0.211	0.062	1.255	8.269	17.341
150.5	0.124	0.554	0.414	0.173	0.064	1.193	8.051	16.139
151	0.113	0.500	0.642	0.253	0.057	1.194	8.822	18.755
151.5	0.111	0.545	0.471	0.218	0.056	1.114	8.985	17.431
152	0.103	0.489	0.662	0.267	0.047	1.107	9.674	21.620
152.5	0.095	0.465	0.769	0.333	0.040	1.076	10.528	22.632
153	0.096	0.438	1.074	0.449	0.038	1.059	10.393	23.454
153.5	0.092	0.408	0.810	0.332	0.037	1.091	10.905	24.340
154	0.093	0.405	0.779	0.303	0.037	1.070	10.742	25.819
154.5	0.086	0.364	0.971	0.332	0.035	1.082	11.581	31.276
155	0.082	0.373	0.925	0.340	0.034	1.093	12.169	30.340
155.5	0.072	0.436	0.847	0.333	0.035	1.185	13.851	29.730
156	0.061	0.377	0.955	0.311	0.035	1.420	16.496	35.638
156.5	0.061	0.340	0.942	0.256	0.033	1.518	16.357	39.644
157	0.073	0.404	0.651	0.183	0.045	1.632	13.607	29.665
157.5	0.090	0.528	0.467	0.149	0.058	1.620	11.152	21.671
158	0.093	0.637	0.313	0.100	0.059	1.687	10.741	20.000
158.5	0.098	0.665	0.434	0.141	0.056	1.723	10.210	18.275
159	0.096	0.681	0.330	0.111	0.055	1.733	10.403	17.849
159.5	0.110	0.681	0.261	0.083	0.067	1.762	9.085	16.272
160	0.093	0.643	0.255	0.081	0.058	1.788	10.726	18.891
160.5	0.085	0.585	0.322	0.106	0.052	1.716	11.822	21.005
161	0.077	0.569	0.392	0.144	0.051	1.723	13.011	20.550
161.5	0.078	0.543	0.261	0.099	0.048	1.684	12.897	20.248
162	0.073	0.520	0.245	0.100	0.041	1.679	13.710	19.936
162.5	0.065	0.415	0.375	0.139	0.039	1.638	15.416	25.357
163	0.069	0.321	0.473	0.170	0.037	1.501	14.591	27.084
163.5	0.048	0.191	0.583	0.184	0.028	1.349	20.719	48.612
164	0.058	0.195	0.802	0.262	0.028	1.244	17.147	42.216
164.5	0.067	0.223	0.642	0.201	0.032	1.540	14.875	30.826
165	0.083	0.296	0.596	0.185	0.045	1.729	11.979	22.361
165.5	0.102	0.439	0.679	0.220	0.054	1.599	9.774	18.872
166	0.096	0.589	0.467	0.169	0.055	1.670	10.433	17.302
166.5	0.085	0.678	0.397	0.142	0.055	1.710	11.712	19.074

Table A.2.8 Elements of Dataset 1 for LB15-8

LB15-8												
	Elemental Profiles											
Depth	Fe	Mg	Al	K	Ca	Ti	Mn	Cu	Rb	Sr	Zr	Si
182	627852	82	361	23624	142121	14022	8691	1604	10304	12998	1877	2233
182.5	490114	45	318	18410	150278	11593	7459	1544	7211	16199	3005	1853
183	455784	71	255	17203	147943	11265	7142	1267	6630	18866	2135	1951
183.5	437675	23	262	16534	137134	10915	7359	1107	7037	19529	3421	1805
184	486616	84	323	17081	121626	11437	7970	1136	7250	18757	3379	1776
184.5	501246	65	290	16662	105527	10747	7612	1186	7544	15696	2456	1583
185	560055	78	354	16802	79728	11240	7980	1323	8371	12547	3024	1494
185.5	654187	92	249	18041	62835	11771	8929	1404	9878	10464	2419	1444
186	722652	46	258	21648	63014	13147	9906	1469	10178	9556	2166	1599
186.5	745757	97	323	23288	60951	13652	9469	1850	10720	9534	2436	1979
187	722252	96	249	23657	67090	13856	8967	1375	11093	10270	2883	2028
187.5	689598	65	296	23030	71215	13436	9546	1537	10115	10235	2640	2023
188	680184	79	271	24549	87060	14228	9023	1795	9750	11276	2852	2325
188.5	665269	56	380	25398	97225	14434	8624	1569	9001	11482	2127	2408
189	589845	65	311	21043	90847	12492	7724	1439	8735	11272	2168	1991
189.5	490555	85	253	15905	84942	10439	6880	1051	8437	10883	2040	1466
190	438674	30	271	12535	83490	9182	6940	1408	7037	12203	3033	1170
190.5	504370	41	258	16249	89623	10751	6922	1621	8075	12590	3740	1591
191	545583	51	254	17540	85130	11977	7294	1709	9133	11972	3606	1629
191.5	524554	56	269	15818	72044	11746	7113	1957	7515	11644	4153	1554
192	500208	43	232	14766	66533	10858	6298	1346	7121	11495	4298	1398
192.5	477715	36	244	13988	63834	10119	6480	1574	6377	10604	4989	1379
193	486499	96	259	14509	66644	10553	7096	1777	7105	10830	4455	1288
193.5	477919	39	200	13930	61493	10481	6581	1448	7108	11115	5175	1237
194	449436	0	198	12196	54848	9541	6284	1398	6693	10540	4213	1101
194.5	445762	62	215	12048	56640	8843	6299	1561	7199	10246	5382	1108
195	487474	81	245	13304	59960	9961	6647	1850	7670	10942	5305	1264
195.5	550380	61	270	15022	64551	11735	7070	1306	7658	11380	3215	1352
196	582341	57	218	17181	71578	12680	7585	1602	8253	11771	3519	1670
196.5	602353	75	281	17796	75506	12873	7643	2038	8162	11654	4365	1696
197	591525	0	279	17067	73642	12396	7584	1803	9198	11781	5149	1512
197.5	599163	0	276	17531	74642	12791	8187	1693	8527	11335	5521	1604
198	602087	36	283	18375	79881	13434	8630	1737	9034	12233	4759	1771
198.5	589988	71	282	18277	78930	12644	8364	1500	8043	11419	5105	1748
199	566544	61	301	16801	76006	12443	8291	1455	8610	11928	4898	1512
199.5	528598	59	259	15345	68469	11226	7669	1304	8713	11680	4121	1458
200	539792	16	304	15683	67544	11765	7601	1599	7891	11363	4668	1415
200.5	541307	31	230	14768	64421	11547	7822	1483	7459	11217	4194	1282
201	534447	22	249	14443	62793	11284	7775	1516	8318	11306	4565	1288
201.5	522284	41	251	14197	64451	11146	6807	1621	7713	11500	3923	1319
202	548537	91	327	15252	68839	11745	7071	1612	8224	11141	5369	1346
202.5	577685	57	269	17260	74863	12536	8009	1541	7471	11443	4442	1487
203	586637	69	297	17210	78721	12751	7729	1511	7804	11526	4206	1523
203.5	586269	49	309	17477	78190	12774	7779	1818	7841	11715	4424	1560
204	586114	54	232	17851	77444	13241	7884	1358	8350	11685	4328	1631
204.5	577268	118	228	17209	77576	12145	7458	1409	7306	11348	4816	1488
205	583323	21	252	17606	80193	12884	7523	1463	8125	11532	4748	1587
205.5	572773	69	231	16982	80612	12459	7814	1461	8132	11726	4317	1597
206	570048	33	242	16554	80902	11932	7519	1478	9124	11872	5453	1564
206.5	576508	41	263	17244	81678	12303	7672	1831	7721	11558	5380	1716
207	582100	33	294	16924	81829	12500	7686	1568	8908	11269	4370	1561
207.5	577954	50	219	16468	78314	12729	8008	1567	7450	11234	4877	1434
208	535252	42	256	15284	71804	11597	7542	1645	7689	11479	5142	1401
208.5	542468	75	224	15421	66457	11814	8195	1790	7401	12004	5485	1163
209	548929	83	225	15753	70715	12957	7115	1631	7824	11576	5824	1295
209.5	557457	75	244	15184	72236	12397	7866	1527	7657	11442	4402	1343
210	553706	25	202	15233	71408	12751	7564	1669	6100	12168	5079	1185
210.5	556745	74	196	15052	70311	12755	7772	1292	7828	12076	5922	1234
211	554206	22	269	15593	73175	13017	7400	1207	8839	12247	5842	1527
211.5	523479	70	228	15272	70219	12396	6835	1140	7012	12877	6122	1578

Table A.2.9 Elements of Dataset 2 for LB15-8

	LB15-8							
	Elemental Ratios							
Depth (mm)	Rb/Sr	Zr/Rb	Zr/K	K/Ti	Ca/Ti	Ca/Rb	Ca/Ti	Rb/Sr
182	0.793	0.182	0.079	1.685	10.136	13.793	10.136	0.793
182.5	0.445	0.417	0.163	1.588	12.963	20.840	12.963	0.445
183	0.351	0.322	0.124	1.527	13.133	22.314	13.133	0.351
183.5	0.360	0.486	0.207	1.515	12.564	19.488	12.564	0.360
184	0.387	0.466	0.198	1.493	10.634	16.776	10.634	0.387
184.5	0.481	0.326	0.147	1.550	9.819	13.988	9.819	0.481
185	0.667	0.361	0.180	1.495	7.093	9.524	7.093	0.667
185.5	0.944	0.245	0.134	1.533	5.338	6.361	5.338	0.944
186	1.065	0.213	0.100	1.647	4.793	6.191	4.793	1.065
186.5	1.124	0.227	0.105	1.706	4.465	5.686	4.465	1.124
187	1.080	0.260	0.122	1.707	4.842	6.048	4.842	1.080
187.5	0.988	0.261	0.115	1.714	5.300	7.041	5.300	0.988
188	0.865	0.293	0.116	1.725	6.119	8.929	6.119	0.865
188.5	0.784	0.236	0.084	1.760	6.736	10.802	6.736	0.784
189	0.775	0.248	0.103	1.685	7.272	10.400	7.272	0.775
189.5	0.775	0.242	0.128	1.524	8.137	10.068	8.137	0.775
190	0.577	0.431	0.242	1.365	9.093	11.864	9.093	0.577
190.5	0.641	0.463	0.230	1.511	8.336	11.099	8.336	0.641
191	0.763	0.395	0.206	1.464	7.108	9.321	7.108	0.763
191.5	0.645	0.553	0.263	1.347	6.133	9.587	6.133	0.645
192	0.619	0.604	0.291	1.360	6.128	9.343	6.128	0.619
192.5	0.601	0.782	0.357	1.382	6.308	10.010	6.308	0.601
193	0.656	0.627	0.307	1.375	6.315	9.380	6.315	0.656
193.5	0.639	0.728	0.372	1.329	5.867	8.651	5.867	0.639
194	0.635	0.629	0.345	1.278	5.749	8.195	5.749	0.635
194.5	0.703	0.748	0.447	1.362	6.405	7.868	6.405	0.703
195	0.701	0.692	0.399	1.336	6.019	7.817	6.019	0.701
195.5	0.673	0.420	0.214	1.280	5.501	8.429	5.501	0.673
196	0.701	0.426	0.205	1.355	5.645	8.673	5.645	0.701
196.5	0.700	0.535	0.245	1.382	5.865	9.251	5.865	0.700
197	0.781	0.560	0.302	1.377	5.941	8.006	5.941	0.781
197.5	0.752	0.647	0.315	1.371	5.836	8.754	5.836	0.752
198	0.738	0.527	0.259	1.368	5.946	8.842	5.946	0.738
198.5	0.704	0.635	0.279	1.446	6.242	9.814	6.242	0.704
199	0.722	0.569	0.292	1.350	6.108	8.828	6.108	0.722
199.5	0.746	0.473	0.269	1.367	6.099	7.858	6.099	0.746
200	0.694	0.592	0.298	1.333	5.741	8.560	5.741	0.694
200.5	0.665	0.562	0.284	1.279	5.579	8.637	5.579	0.665
201	0.736	0.549	0.316	1.280	5.565	7.549	5.565	0.736
201.5	0.671	0.509	0.276	1.274	5.782	8.356	5.782	0.671
202	0.738	0.653	0.352	1.299	5.861	8.371	5.861	0.738
202.5	0.653	0.595	0.257	1.377	5.972	10.020	5.972	0.653
203	0.677	0.539	0.244	1.350	6.174	10.087	6.174	0.677
203.5	0.669	0.564	0.253	1.368	6.121	9.972	6.121	0.669
204	0.715	0.518	0.242	1.348	5.849	9.275	5.849	0.715
204.5	0.644	0.659	0.280	1.417	6.387	10.618	6.387	0.644
205	0.705	0.584	0.270	1.367	6.224	9.870	6.224	0.705
205.5	0.694	0.531	0.254	1.363	6.470	9.913	6.470	0.694
206	0.769	0.598	0.329	1.387	6.780	8.867	6.780	0.769
206.5	0.668	0.697	0.312	1.402	6.639	10.579	6.639	0.668
207	0.790	0.491	0.258	1.354	6.546	9.186	6.546	0.790
207.5	0.663	0.655	0.296	1.294	6.152	10.512	6.152	0.663
208	0.670	0.669	0.336	1.318	6.192	9.339	6.192	0.670
208.5	0.617	0.741	0.356	1.305	5.625	8.979	5.625	0.617
209	0.676	0.744	0.370	1.216	5.458	9.038	5.458	0.676
209.5	0.669	0.575	0.290	1.225	5.827	9.434	5.827	0.669
210	0.501	0.833	0.333	1.195	5.600	11.706	5.600	0.501

Table A.2.10 Ratios of Dataset 2 for LB15-8

	LB15-8							
	Elemental Ratios							
Depth (mm)	Rb/Sr	Zr/Rb	Zr/K	K/Ti	Ca/Ti	Ca/Rb	Ca/Ti	Rb/Sr
210.5	0.648	0.757	0.393	1.180	5.512	8.982	5.512	0.648
211	0.722	0.661	0.375	1.198	5.621	8.279	5.621	0.722
211.5	0.545	0.873	0.401	1.232	5.665	10.014	5.665	0.545
212	0.597	1.002	0.453	1.310	6.000	10.124	6.000	0.597
212.5	0.589	0.661	0.339	1.282	5.797	8.813	5.797	0.589
213	0.853	0.313	0.199	1.346	6.063	7.078	6.063	0.853
213.5	0.851	0.241	0.104	1.630	5.095	7.248	5.095	0.851
214	0.812	0.225	0.088	1.722	5.060	7.533	5.060	0.812
214.5	0.899	0.222	0.100	1.666	5.788	7.741	5.788	0.899
215	1.179	0.150	0.073	1.663	4.082	5.066	4.082	1.179
215.5	1.053	0.226	0.094	1.784	3.558	4.779	3.558	1.053
216	1.003	0.257	0.100	1.870	3.812	5.251	3.812	1.003
216.5	1.154	0.153	0.057	1.937	3.024	4.188	3.024	1.154
217	1.315	0.156	0.062	1.907	3.235	4.239	3.235	1.315
217.5	1.192	0.128	0.051	1.860	3.702	5.004	3.702	1.192
218	1.061	0.191	0.070	1.825	4.134	6.177	4.134	1.061
218.5	1.019	0.279	0.098	1.829	5.047	7.882	5.047	1.019
219	0.736	0.277	0.088	1.793	9.607	16.939	9.607	0.736
219.5	0.495	0.535	0.154	1.700	15.649	32.021	15.649	0.495
220	0.575	0.297	0.118	1.595	19.163	30.270	19.163	0.575
220.5	0.773	0.309	0.129	1.714	15.041	21.009	15.041	0.773
221	0.805	0.228	0.100	1.722	8.432	11.220	8.432	0.805
221.5	0.489	0.391	0.157	1.656	9.244	13.868	9.244	0.489

Table A.2.11 Elements of Dataset 1 for LB15-15

	LB15-15												
	Elemental Profiles												
Depth	Fe	Mg	Al	K	Fe	Ca	Ti	Mn	Cu	Rb	Sr	Zr	Si
108.48	551601	43	362	19707	551601	106147	12344	7472	986	7873	12087	1845	2005
108.98	587247	28	388	20626	587247	106237	13289	7647	1094	8741	12551	2586	2333
109.48	640076	45	328	23251	640076	99120	14261	8543	1200	9948	12272	2418	2386
109.98	643187	63	356	22774	643187	103768	13899	8260	1230	9242	12262	2825	2414
110.48	611256	40	332	21010	611256	105009	13828	8177	1047	9262	13543	2672	1929
110.98	581629	52	395	20716	581629	132085	13863	8049	1238	6967	13652	3684	2230
111.48	559133	36	305	19237	559133	166620	14486	8360	1152	6230	12888	4140	2219
111.98	539838	61	297	18803	539838	161541	13701	7883	1118	6062	12639	3702	1883
112.48	597116	0	260	19031	597116	127044	12510	7840	1054	7952	10903	2522	1816
112.98	638470	0	280	20008	638470	100931	14136	7862	1289	8725	11730	2810	1794
113.48	604622	26	327	19199	604622	91101	12416	7477	1253	10273	12492	2950	1602
113.98	655052	39	310	21060	655052	73607	12410	7721	1457	10456	11655	2456	1736
114.48	664011	69	300	22023	664011	69248	13105	7704	1207	9732	11042	1960	1755
114.98	610408	77	301	20446	610408	80822	12968	7329	1453	9697	11396	1742	1731
115.48	616611	15	348	19976	616611	93888	13779	7291	1121	9756	12257	2134	1837
115.98	627992	49	323	20048	627992	100852	13912	7795	1054	9751	12554	1936	1808
116.48	599889	71	328	19324	599889	101815	13588	8003	1167	9664	12708	975	1819
116.98	593732	56	334	19058	593732	106674	13463	7337	1044	9292	12589	1996	1963
117.48	601675	71	289	19099	601675	107785	14344	8010	1440	8515	13271	2331	1852
117.98	588067	67	299	19141	588067	110191	13427	7543	1228	8699	13906	1931	2052
118.48	590888	112	295	19414	590888	112516	14292	7611	1311	8989	15259	3049	2123
118.98	606367	17	275	19261	606367	116856	14374	7682	1214	9451	14923	2757	2007
119.48	521166	40	300	16617	521166	104114	12845	6871	1358	7921	13858	3051	1671
119.98	463188	43	252	14614	463188	99201	11372	6066	1384	6813	13591	2159	1676
120.48	443657	87	280	13815	443657	95778	10930	5564	915	5930	12789	3144	1515
120.98	420841	102	311	13022	420841	85328	10203	5184	989	6213	12327	2568	1379
121.48	421537	0	266	12901	421537	86175	9972	5284	838	6682	12479	2896	1318
121.98	451356	0	177	14292	451356	94776	11125	5673	906	5608	12367	2725	1547
122.48	472140	36	260	14635	472140	102050	11304	5531	1021	5499	12161	2372	1583
122.98	489517	52	259	15461	489517	107793	11904	6137	839	6752	13097	2780	1726
123.48	525000	29	244	16600	525000	118686	12919	6663	1112	5953	13151	2940	1964
123.98	563072	0	255	17709	563072	127346	13939	7273	1204	6287	14294	3548	1976
124.48	570518	12	312	18022	570518	132060	14269	7405	1121	6568	14499	3518	2066
124.98	559647	51	333	16960	559647	126177	13698	6995	1045	6597	14318	3630	1959
125.48	578816	73	313	17332	578816	126980	14549	7137	1183	7448	14398	4218	1847
125.98	558063	0	273	17024	558063	125130	14175	6972	1388	6068	13901	3943	1921
126.48	525223	0	278	15613	525223	125463	13531	6508	961	5492	14463	4984	1844
126.98	519067	28	258	15612	519067	120674	13735	6819	1415	7076	14166	4683	1772
127.48	514535	76	297	15701	514535	118172	12999	6769	1428	6789	14130	4805	1844
127.98	547211	25	282	17471	547211	124787	13678	7339	1293	6996	14634	3934	1971
128.48	569895	127	274	18390	569895	128638	13724	8253	1336	7137	14961	2595	2035
128.98	575038	61	383	18784	575038	130294	13569	8072	1098	7522	15066	3765	2144
129.48	586586	68	297	19299	586586	124541	14079	8216	1176	7757	14020	3656	2205
129.98	576954	15	346	19269	576954	127029	14265	8206	1157	6996	14663	3033	2171
130.48	557904	0	276	19018	557904	135099	13772	7782	1080	7220	15467	3868	2185
130.98	546581	0	242	19530	546581	145060	13920	6997	1667	6915	16175	3050	2204
131.48	540718	50	317	19442	540718	147585	13200	7647	1100	7324	16025	3631	2280
131.98	541852	0	319	19269	541852	145528	13736	8287	1280	6300	16029	3558	2320
132.48	553138	41	349	19030	553138	145083	13635	8177	1096	7779	16044	3939	2159
132.98	551033	81	357	18896	551033	144441	13633	7838	1300	7076	15795	3654	2135
133.48	551899	68	345	19054	551899	140716	13333	8106	1202	7184	15583	4008	2099
133.98	555706	58	307	18913	555706	132191	13840	7865	1058	6340	14951	3594	2032
134.48	588152	37	320	19259	588152	123870	13453	8247	1520	6519	14080	4051	2149
134.98	597502	63	300	19059	597502	123658	13688	7578	1388	7679	14032	4336	1923
135.48	604145	9	298	18643	604145	118812	13908	7754	1292	7551	13779	3498	1973
135.98	585687	106	271	18202	585687	116649	14222	7477	1470	7367	13550	4556	1974
136.48	573418	5	291	16836	573418	116006	14246	8432	1310	7646	13933	4060	1879
136.98	550460	32	261	16079	550460	109172	13642	7765	1164	6664	14107	4392	1734
137.48	543782	38	284	15637	543782	111620	14326	7529	1424	6250	14162	5472	1827
137.98	516434	95	297	14267	516434	110379	13949	6863	1256	6615	14295	5488	1693
138.48	482422	147	314	13474	482422	109599	13675	6532	1179	5455	14753	6817	1541
138.98	486871	75	374	13132	486871	114858	13771	6013	1198	5740	14343	5743	1509
139.48	502283	49	225	13368	502283	114097	14151	6196	1375	5097	13960	5810	1506
139.98	469253	61	286	13401	469253	123290	13754	5380	940	5763	15547	5888	1583
140.48	484168	88	268	13656	484168	132149	13151	5383	1376	5784	14990	6388	1654
140.98	418181	16	262	11761	418181	111130	11718	4647	1281	4841	13543	4296	1467
141.48	376840	25	259	10523	376840	98299	9957	4761	1334	4021	11585	4805	1300
141.98	423516	55	249	12568	423516	121102	11740	5456	1188	4001	12561	5441	1429
142.48	452333	73	282	13285	452333	137705	12904	6091	1005	5662	14398	5451	1612
142.98	479570	109	280	15097	479570	169666	13275	7027	927	5764	15074	5491	1713
143.48	489354	58	317	16862	489354	182376	12710	7556	1161	5457	14749	3934	1993
143.98	552106	38	294	19888	552106	152041	12885	8839	1273	7551	13274	2872	2077
144.48	653225	71	403	24744	653225	111846	13642	8851	975	9171	11908	1644	2365
144.98	663448	23	381	25539	663448	92431	13490	8674	1185	10564	11699	1235	2559
145.48	633925	47	374	24732	633925	107972	12959	8639	1175	9062	11833	1804	2381
145.98	607036	36	355	23921	607036	121567	13161	8234	1214	8955	13010	2084	2451
146.48	568678	49	347	22600	568678	139162	12965	8558	1400	9096	14388	1788	2408
146.98	559967	31	358	22074	559967	127120	12750	8035	1002	8264	16048	2255	2473
147.48	550165	31	300	21916	550165	109787	12630	7326	1045	8515	15821	1687	2610

Table A.2.12 Elements of Dataset 2 for LB15-15

	LB15-15							
	Elemental Ratios							
Depth (mm)	Rb/Sr	Zr/Rb	Zr/K	K/Ti	Ca/Ti	Ca/Rb	Ca/Ti	Rb/Sr
108.48	0.651	0.234	0.094	1.596	8.599	13.482	8.599	0.651
108.98	0.696	0.296	0.125	1.552	7.994	12.154	7.994	0.696
109.48	0.811	0.243	0.104	1.630	6.950	9.964	6.950	0.811
109.98	0.754	0.306	0.124	1.639	7.466	11.228	7.466	0.754
110.48	0.684	0.288	0.127	1.519	7.594	11.338	7.594	0.684
110.98	0.510	0.529	0.178	1.494	9.528	18.959	9.528	0.510
111.48	0.483	0.665	0.215	1.328	11.502	26.745	11.502	0.483
111.98	0.480	0.611	0.197	1.372	11.790	26.648	11.790	0.480
112.48	0.729	0.317	0.133	1.521	10.155	15.976	10.155	0.729
112.98	0.744	0.322	0.140	1.415	7.140	11.568	7.140	0.744
113.48	0.822	0.287	0.154	1.546	7.337	8.868	7.337	0.822
113.98	0.897	0.235	0.117	1.697	5.931	7.040	5.931	0.897
114.48	0.881	0.201	0.089	1.681	5.284	7.115	5.284	0.881
114.98	0.851	0.180	0.085	1.577	6.232	8.335	6.232	0.851
115.48	0.796	0.219	0.107	1.450	6.814	9.624	6.814	0.796
115.98	0.777	0.199	0.097	1.441	7.249	10.343	7.249	0.777
116.48	0.760	0.101	0.050	1.422	7.493	10.535	7.493	0.760
116.98	0.738	0.215	0.105	1.416	7.923	11.480	7.923	0.738
117.48	0.642	0.274	0.122	1.331	7.514	12.658	7.514	0.642
117.98	0.626	0.222	0.101	1.426	8.207	12.667	8.207	0.626
118.48	0.589	0.339	0.157	1.358	7.873	12.517	7.873	0.589
118.98	0.633	0.292	0.143	1.340	8.130	12.364	8.130	0.633
119.48	0.572	0.385	0.184	1.294	8.105	13.144	8.105	0.572
119.98	0.501	0.317	0.148	1.285	8.723	14.561	8.723	0.501
120.48	0.464	0.530	0.228	1.264	8.763	16.151	8.763	0.464
120.98	0.504	0.413	0.197	1.276	8.363	13.734	8.363	0.504
121.48	0.535	0.433	0.224	1.294	8.642	12.897	8.642	0.535
121.98	0.453	0.486	0.191	1.285	8.519	16.900	8.519	0.453
122.48	0.452	0.431	0.162	1.295	9.028	18.558	9.028	0.452
122.98	0.516	0.412	0.180	1.299	9.055	15.965	9.055	0.516
123.48	0.453	0.494	0.177	1.285	9.187	19.937	9.187	0.453
123.98	0.440	0.564	0.200	1.270	9.136	20.255	9.136	0.440
124.48	0.453	0.536	0.195	1.263	9.255	20.107	9.255	0.453
124.98	0.461	0.550	0.214	1.238	9.211	19.126	9.211	0.461
125.48	0.517	0.566	0.243	1.191	8.728	17.049	8.728	0.517
125.98	0.437	0.650	0.232	1.201	8.828	20.621	8.828	0.437
126.48	0.380	0.908	0.319	1.154	9.272	22.845	9.272	0.380
126.98	0.500	0.662	0.300	1.137	8.786	17.054	8.786	0.500
127.48	0.480	0.708	0.306	1.208	9.091	17.406	9.091	0.480
127.98	0.478	0.562	0.225	1.277	9.123	17.837	9.123	0.478
128.48	0.477	0.364	0.141	1.340	9.373	18.024	9.373	0.477
128.98	0.499	0.501	0.200	1.384	9.602	17.322	9.602	0.499
129.48	0.553	0.471	0.189	1.371	8.846	16.055	8.846	0.553
129.98	0.477	0.434	0.157	1.351	8.905	18.157	8.905	0.477
130.48	0.467	0.536	0.203	1.381	9.810	18.712	9.810	0.467
130.98	0.428	0.441	0.156	1.403	10.421	20.978	10.421	0.428
131.48	0.457	0.496	0.187	1.473	11.181	20.151	11.181	0.457
131.98	0.393	0.565	0.185	1.403	10.595	23.100	10.595	0.393
132.48	0.485	0.506	0.207	1.396	10.640	18.651	10.640	0.485
132.98	0.448	0.516	0.193	1.386	10.595	20.413	10.595	0.448
133.48	0.461	0.558	0.210	1.429	10.554	19.587	10.554	0.461
133.98	0.424	0.567	0.190	1.367	9.551	20.850	9.551	0.424
134.48	0.463	0.621	0.210	1.432	9.208	19.001	9.208	0.463
134.98	0.547	0.565	0.228	1.392	9.034	16.103	9.034	0.547
135.48	0.548	0.463	0.188	1.340	8.543	15.735	8.543	0.548
135.98	0.544	0.618	0.250	1.280	8.202	15.834	8.202	0.544
136.48	0.549	0.531	0.241	1.182	8.143	15.172	8.143	0.549
136.98	0.472	0.659	0.273	1.179	8.003	16.382	8.003	0.472
137.48	0.441	0.876	0.350	1.092	7.791	17.859	7.791	0.441
137.98	0.463	0.830	0.385	1.023	7.913	16.686	7.913	0.463
138.48	0.370	1.250	0.506	0.985	8.015	20.091	8.015	0.370
138.98	0.400	1.001	0.437	0.954	8.341	20.010	8.341	0.400
139.48	0.365	1.140	0.435	0.945	8.063	22.385	8.063	0.365
139.98	0.371	1.022	0.439	0.974	8.964	21.393	8.964	0.371
140.48	0.386	1.104	0.468	1.038	10.049	22.847	10.049	0.386
140.98	0.357	0.887	0.365	1.004	9.484	22.956	9.484	0.357
141.48	0.347	1.195	0.457	1.057	9.872	24.446	9.872	0.347
141.98	0.319	1.360	0.433	1.071	10.315	30.268	10.315	0.319
142.48	0.393	0.963	0.410	1.030	10.671	24.321	10.671	0.393
142.98	0.382	0.953	0.364	1.137	12.781	29.435	12.781	0.382
143.48	0.370	0.721	0.233	1.327	14.349	33.421	14.349	0.370
143.98	0.569	0.380	0.144	1.544	11.800	20.135	11.800	0.569
144.48	0.770	0.179	0.066	1.814	8.199	12.196	8.199	0.770
144.98	0.903	0.117	0.048	1.893	6.852	8.750	6.852	0.903
145.48	0.766	0.199	0.073	1.908	8.332	11.915	8.332	0.766
145.98	0.688	0.233	0.087	1.818	9.237	13.575	9.237	0.688
146.48	0.632	0.197	0.079	1.743	10.734	15.299	10.734	0.632
146.98	0.515	0.273	0.102	1.731	9.970	15.382	9.970	0.515
147.48	0.538	0.198	0.077	1.735	8.693	12.893	8.693	0.538

Fig. A.2.1 Elemental ratios profile of LB15-15

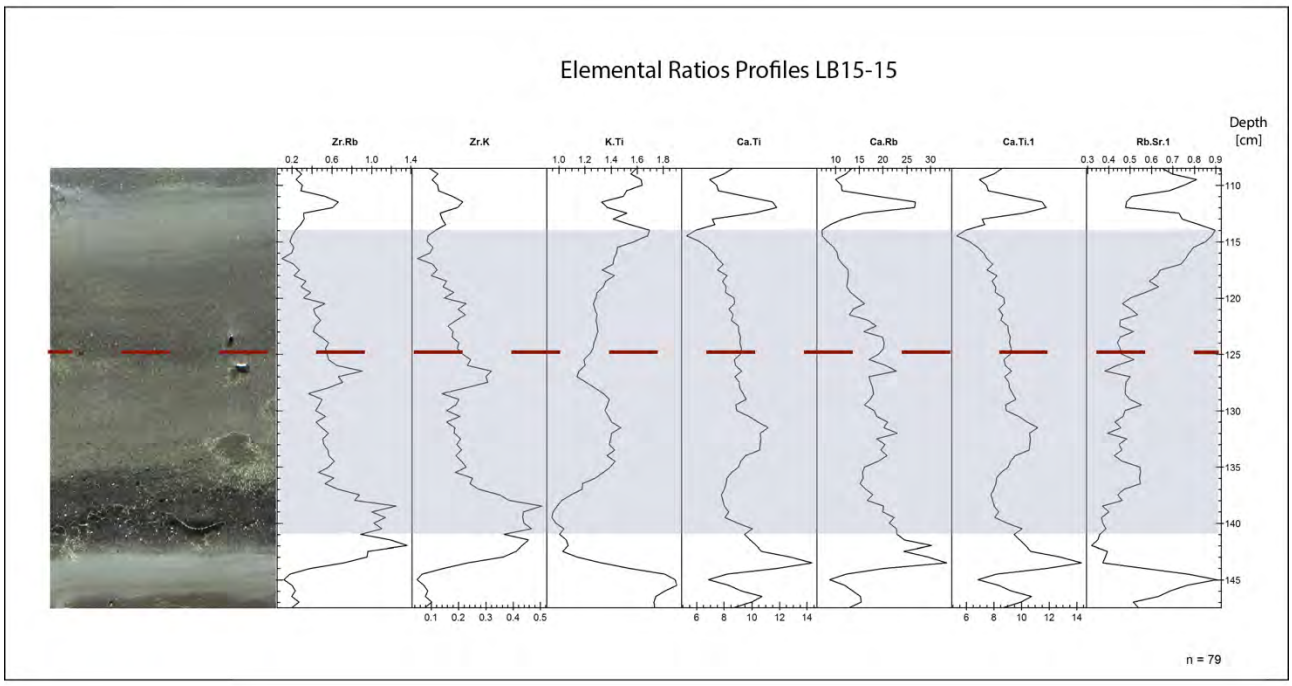

Fig. A.2.2 Broken-stick plot for LB15-14

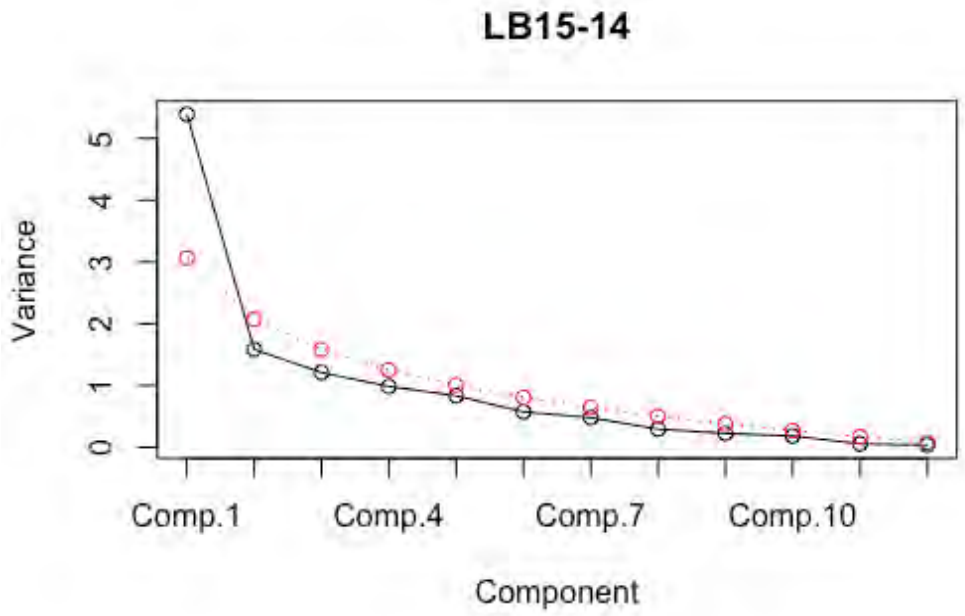

Fig. A.2.3 Broken-stick plot for LB15-15

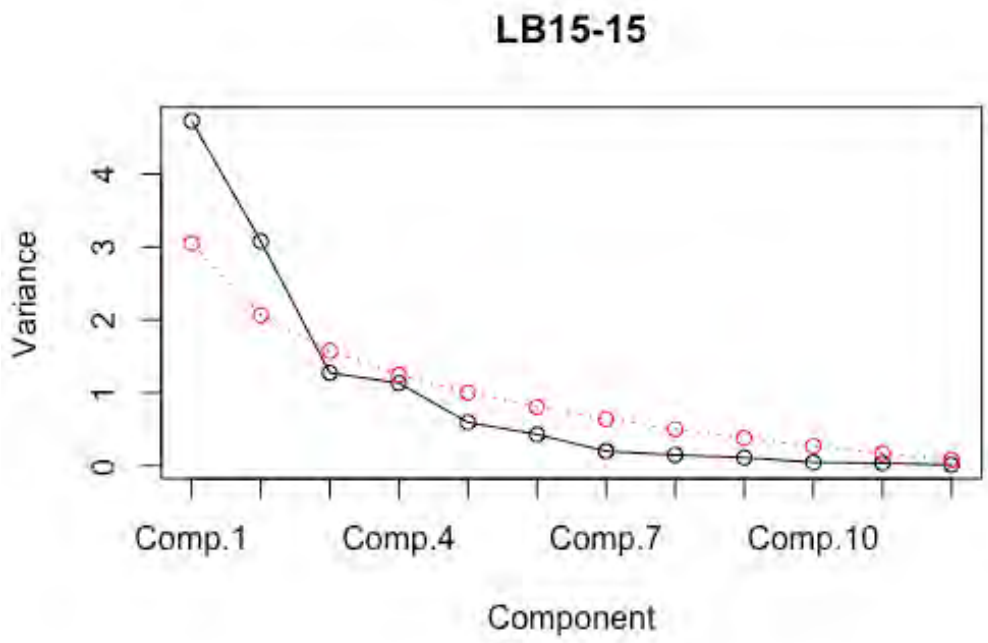

Fig. A.2.4 Biplot of PC1 and PC2 for LB15-14, sub-layer A

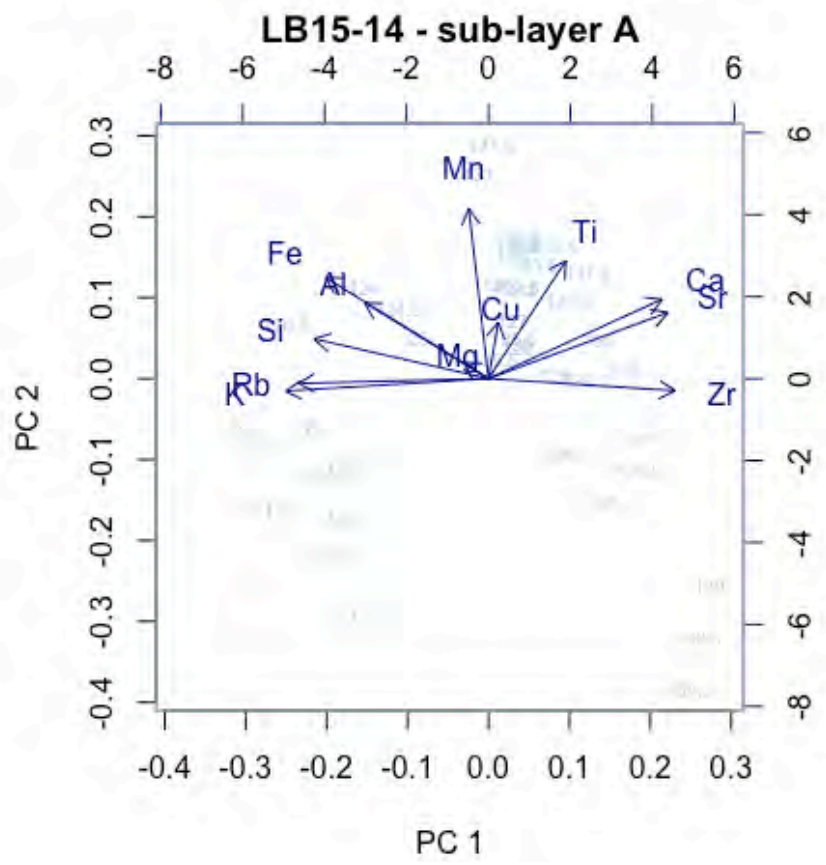

Fig. A.2.5 Biplot of PC1 and PC2 for LB15-14, sub-layer B

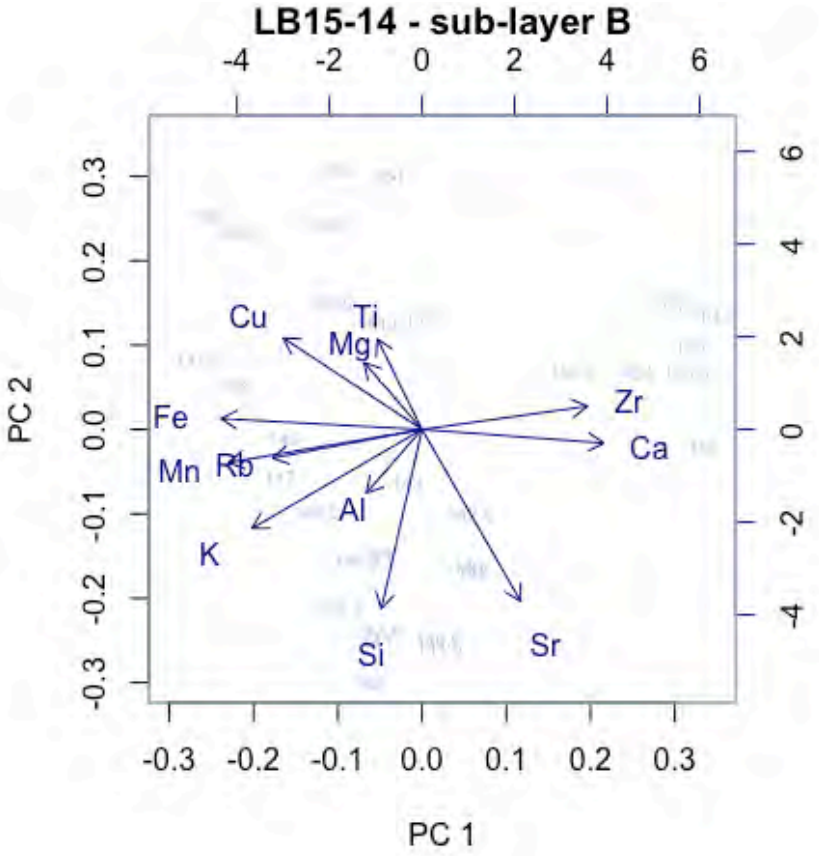

Fig. A.2.6 Biplot of PC1 and PC2 for LB15-15, sub-layer A

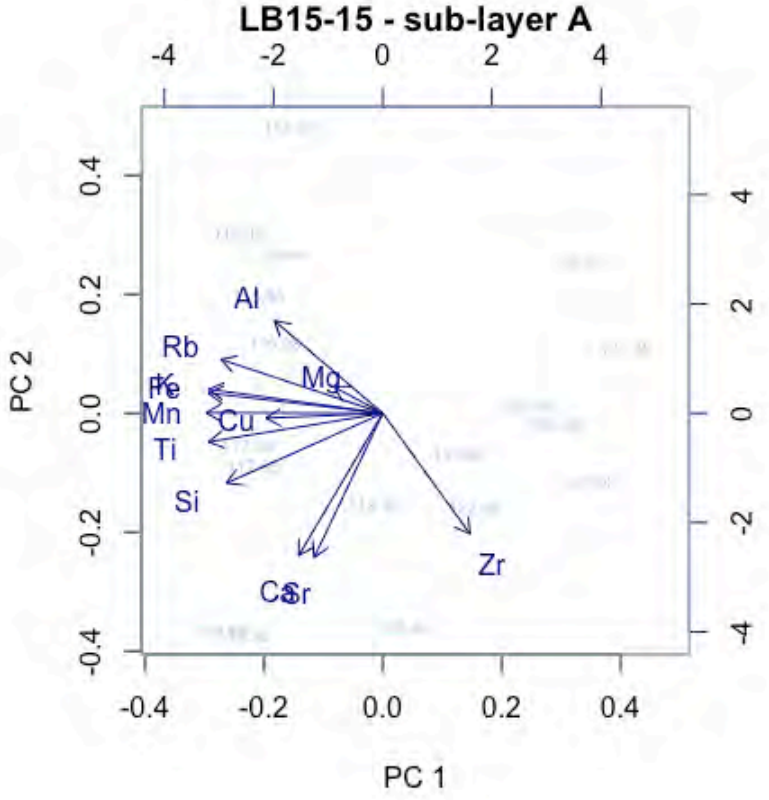

Fig. A.2.7 Biplot of PC1 and PC2 for LB15-15, sub-layer B

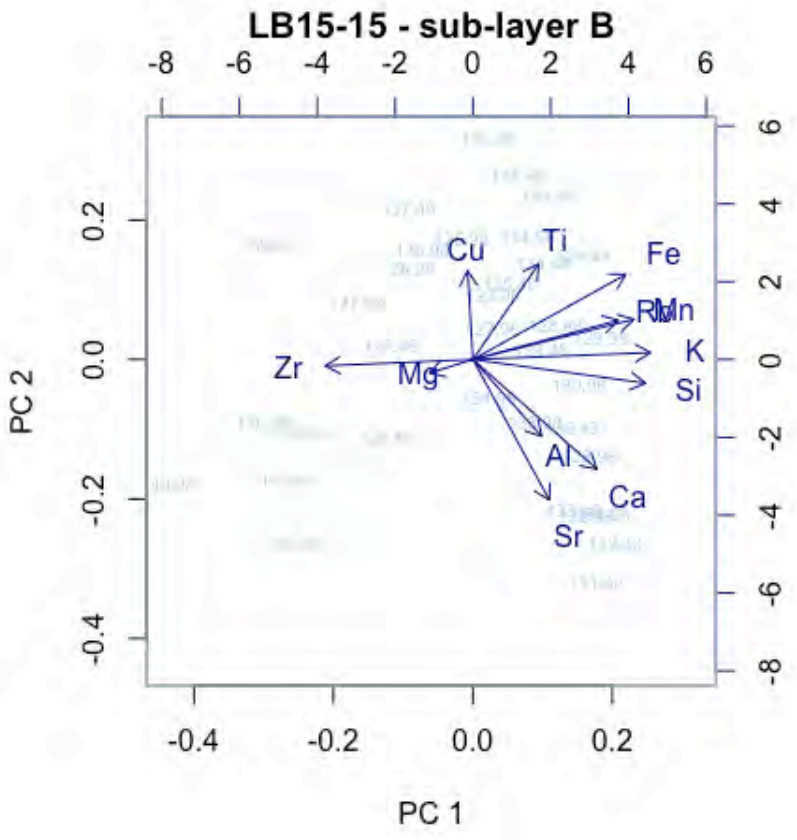

Fig. A.2.8 Broken-stick plot for LB15-8

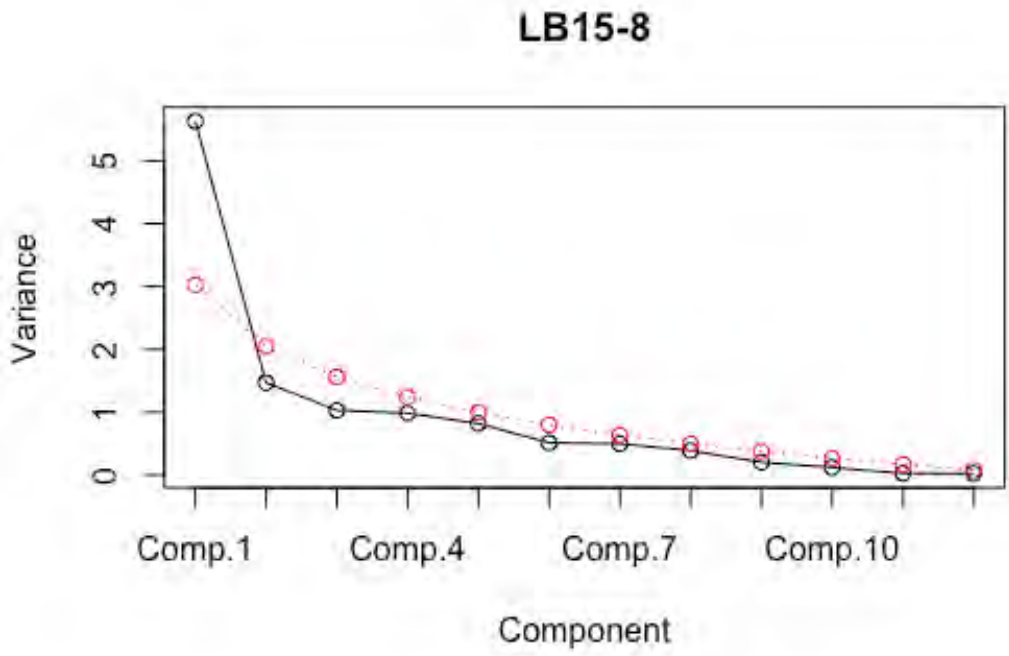

Table A.2.13 Grain size granulometric classes (clay, silt and sand) and mean grain size (microns) for LB15-2, LB15-14, LB15-15, LB15-3 and LB15-18

	Depth	Clay (0.02µm-2µm)	Silt (2.00µm-63µm)	Sand (63µm-2000µm)	Mean Grain Size
LB15-2	21	15.316	79.891	4.793	20.70
	21.25	12.611	84.781	2.608	21.70
	21.5	8.997	85.618	5.385	29.76
	21.75	7.582	84.988	7.429	34.83
	22	7.612	85.365	7.023	34.56
	22.25	7.692	84.863	7.445	34.78
	22.5	6.733	82.905	10.362	35.40
	22.75	5.627	76.425	17.948	49.19
	23	5.96	76.301	17.739	48.63
	23.25	6.491	79.617	13.892	59.56
	23.5	6.798	82.453	10.749	44.65
	23.75	6.537	80.991	12.472	40.32
	24	6.646	81.017	12.337	42.76
	24.25	7.571	80.347	12.082	43.31
	24.5	8.102	78.16	13.738	59.34
LB15-14	11.75	19.712	70.466	9.822	21.93
	12	17.88	77.379	4.741	19.56
	12.25	16.105	78.262	5.633	21.22
	12.5	15.868	81.915	2.216	18.25
	12.75	11.149	78.057	10.794	29.81
	13	9.414	82.244	8.342	31.82
	13.25	8.104	82.809	9.086	35.35
	13.5	7.664	82.422	9.914	36.64
	13.75	6.634	83.55	9.817	38.61
	14	5.825	76.587	17.589	48.56
	14.25	5.802	74.791	19.407	50.73
	14.5	6.806	77.67	15.524	44.60
	14.75	7.357	80.175	12.469	40.60
	15	6.864	79.44	13.696	42.46
	15.25	6.979	78.079	14.942	43.15
	15.5	5.014	70.182	24.805	59.03
	15.75	4.126	66.926	28.948	69.63
LB15-15	11.5	15.9	81.591	2.509	19.62
	11.75	10.03	84.976	4.994	28.06
	12	6.938	80.679	12.383	39.61
	12.25	6.634	82.495	10.87	39.95
	12.5	6.714	79.369	13.917	43.24
	12.75	7.306	81.732	10.961	39.80
	13	7.396	84.647	7.956	36.98
	13.25	6.141	77.434	16.425	46.71
	13.5	4.451	66.02	29.529	68.50
	13.75	2.801	56.294	40.904	95.82
	14	3.314	56.387	40.299	92.41
LB15-3	2.75	11.404	82.202	6.394	28.71
	3	8.705	83.374	7.922	33.88
	3.25	8.312	83.476	8.212	34.61
	3.5	7.603	82.562	9.835	37.41
	3.75	6.005	77.766	16.229	47.80
	4	5.509	75.681	18.81	54.15
	4.25	5.588	76.574	17.838	52.62
	4.5	3.697	60.309	35.994	79.15
	4.75	2.047	56.403	41.55	98.54
LB15-18	4.75	9.333	73.747	16.92	39.35
	5	4.241	57.334	38.425	74.73
	5.25	3.747	46.712	49.542	62.56
	5.5	2.269	31.786	65.945	52.18
	5.75	1.234	21.405	77.361	58.72
	6	4.284	40.724	54.992	77.43

Table A.2.14 Grain size granulometric classes (silt, clay and sand) and mean grain size (microns) for LB15-19, LB15-7, LB15-8 and LB15-20

	Depth	Clay (0.02µm-2µm)	Silt (2.00µm-63µm)	Sand (63µm-2000µm)	Mean Grain Size
LB15-19	10.75	5.567	67.735	26.699	58.95
	11	4.469	62.002	33.529	65.94
	11.25	3.495	47.718	48.787	62.78
	11.5	1.236	30.061	68.703	115.3
	11.75	1.078	28.568	70.354	151.7
	12	1.194	28.218	70.588	156.3
	12.25	10.915	66.227	22.858	37.42
	12.5	14.134	75.034	10.832	26.02
LB15-7	17.25	12.632	80.945	6.423	25.63
	17.5	6.436	75.425	18.139	48.25
	17.75	6.275	76.147	17.578	48.48
	18	5.885	74.349	19.765	51.26
	18.25	6.102	71.159	22.74	55.16
	18.5	5.285	65.222	29.493	66.11
	18.75	5.599	65.438	28.963	65.61
	19	4.715	55.618	39.667	86.58
LB15-8	19.25	7.623	76.291	16.086	41.88
	19.5	6.298	71.824	21.878	53.28
	19.75	6.195	76.283	17.522	48.65
	20	5.964	75.21	18.826	50.31
	20.25	5.27	64.474	30.256	66.54
	20.5	5.703	64.958	29.339	63.93
	20.75	5.232	62.193	32.574	71.06
	21	9.354	67.788	22.858	43.59
	21.25	18.062	77.826	4.113	18.30
LB15-20	14.5	10.786	80.22	8.993	29.67
	14.75	5.259	69.378	25.363	58.62
	15	4.511	62.598	32.891	69.36
	15.25	2.055	42.017	55.928	120.6
	15.5	2.125	40.573	57.302	118.6

Table A.2.15 Organic Matter and Calcite percentages for the 2005 layer in all the 9 cores

	Depth (cm)	TOC	TIC	OM (%)	Calcite (%)
LB15-2	21	0.716	2.806	1.217	23.374
	21.25	0.903	1.861	1.536	15.505
	21.5	1.212	2.178	2.060	18.147
	21.75	1.290	2.436	2.193	20.291
	22	1.216	2.469	2.068	20.566
	22.25	1.469	2.246	2.498	18.708
	22.5	1.389	2.176	2.362	18.122
	22.75	1.472	2.208	2.502	18.394
	23	1.274	2.357	2.165	19.636
	23.25	1.131	2.358	1.923	19.641
	23.5	1.206	3.289	2.050	27.399
	23.75	1.275	2.175	2.167	18.115
	24	1.368	2.079	2.326	17.322
	24.25	1.295	2.244	2.201	18.693
	24.5	1.204	2.338	2.047	19.473
LB15-14	11.75	1.144	1.231	1.945	10.257
	12	0.984	1.833	1.672	15.268
	12.25	1.142	1.870	1.941	15.573
	12.5	1.125	1.566	1.913	13.043
	12.75	1.190	1.666	2.024	13.874
	13	1.249	2.268	2.123	18.892
	13.25	1.317	2.427	2.239	20.217
	13.5	1.288	2.422	2.189	20.176
	13.75	1.494	2.176	2.540	18.123
	14	1.579	2.122	2.684	17.678
	14.25	1.522	2.164	2.587	18.023
	14.5	1.443	2.173	2.453	18.101
	14.75	1.368	2.118	2.325	17.642
	15	1.575	2.112	2.677	17.593
	15.25	1.502	2.256	2.554	18.793
	15.5	1.308	2.161	2.224	18.005
	15.75	1.212	3.024	2.061	25.190
LB15-15	11.5	0.924	1.716	1.571	14.293
	11.75	1.232	2.102	2.094	17.514
	12	1.298	2.442	2.207	20.345
	12.25	1.420	2.261	2.414	18.834
	12.5	1.258	2.427	2.138	20.220
	12.75	1.217	2.436	2.069	20.289
	13	1.119	2.501	1.902	20.836
	13.25	1.388	2.239	2.360	18.647
	13.5	1.919	2.246	3.263	18.705
	13.75	2.190	2.520	3.723	20.989
	14	2.234	2.431	3.797	20.247
LB15-3	2.75	1.098	1.970	1.867	16.412
	3	1.189	2.246	2.022	18.705
	3.25	1.085	2.179	1.844	18.149
	3.5	1.128	2.384	1.917	19.860
	3.75	1.159	2.327	1.970	19.380
	4	0.905	2.177	1.538	18.132
	4.25	0.896	1.418	1.523	11.808
	4.5	1.310	2.056	2.226	17.126
	4.75	1.156	2.448	1.965	20.390
LB15-18	4.75	1.426	1.533	2.424	12.767
	5	1.856	1.123	3.155	9.354
	5.25	3.299	1.540	5.608	12.831
	5.5	3.988	1.105	6.780	9.202
	5.75	5.181	2.578	8.808	21.473
	6	2.379	0.815	4.044	6.785

	Depth (cm)	TOC	TIC	OM (%)	Calcite (%)
LB15-19	10.75	1.208	1.5631976	2.053	13.021
	11	1.435	1.4103255	2.439	11.748
	11.25	1.244	1.4324642	2.115	11.932
	11.5	0.464	0.7559038	0.788	6.297
	11.75	0.932	0.956351	1.585	7.966
	12	0.355	0.9911123	0.603	8.256
	12.25	0.628	1.1454309	1.067	9.541
	12.5	0.873	1.2930888	1.483	10.771
LB15-7	17.25	1.069	1.655	1.818	13.789
	17.5	1.456	1.322	2.475	11.015
	17.75	1.512	1.134	2.570	9.449
	18	1.435	1.321	2.440	11.003
	18.25	1.555	1.421	2.643	11.833
	18.5	1.595	1.248	2.711	10.398
	18.75	1.958	1.149	3.329	9.569
	19	1.900	0.925	3.230	7.708
LB15-8	19.25	1.322	1.643	2.247	13.682
	19.5	1.756	1.136	2.985	9.467
	19.75	1.703	1.167	2.895	9.720
	20	1.589	1.182	2.701	9.843
	20.25	2.112	0.907	3.590	7.555
	20.5	2.233	1.116	3.797	9.293
	20.75	1.799	1.325	3.059	11.040
	21	1.097	1.134	1.865	9.449
	21.25	1.064	0.900	1.809	7.499
LB15-20	14.25	0.839	1.286	1.427	10.716
	14.5	0.853	1.662	1.450	13.848
	14.75	1.363	1.158	2.318	9.646
	15	1.137	0.975	1.934	8.123
	15.25	1.094	0.919	1.860	7.659
	15.5	1.039	0.752	1.767	6.265

Declaration of Consent

On the basis of Art. 28 Para. 2 RSL 05

Last, first name: Motta, Danae

Matriculation number: 11-417-706

Programme: Master in Climate Science

Bachelor ☐ Master ☐ Dissertation ☐

Thesis title: Signature of the 2005 Flood Event in the Sediments of Lake Brienz: Implications for Flood Reconstructions

Thesis supervisor: Prof. Flavio Anselmetti

I hereby declare that this submission is my own work and that, to the best of my knowledge and belief, it contains no material previously published or written by another person, except where due acknowledgement has been made in the text. In accordance with academic rules and ethical conduct, I have fully cited and referenced all material and results that are not original to this work. I am well aware of the fact that, on the basis of Article 36 Paragraph 1 Letter o of the University Law of 5 September 1996, the Senate is entitled to deny the title awarded on the basis of this work if proven otherwise. I grant inspection of my thesis.

…… ……

Place, date Signature